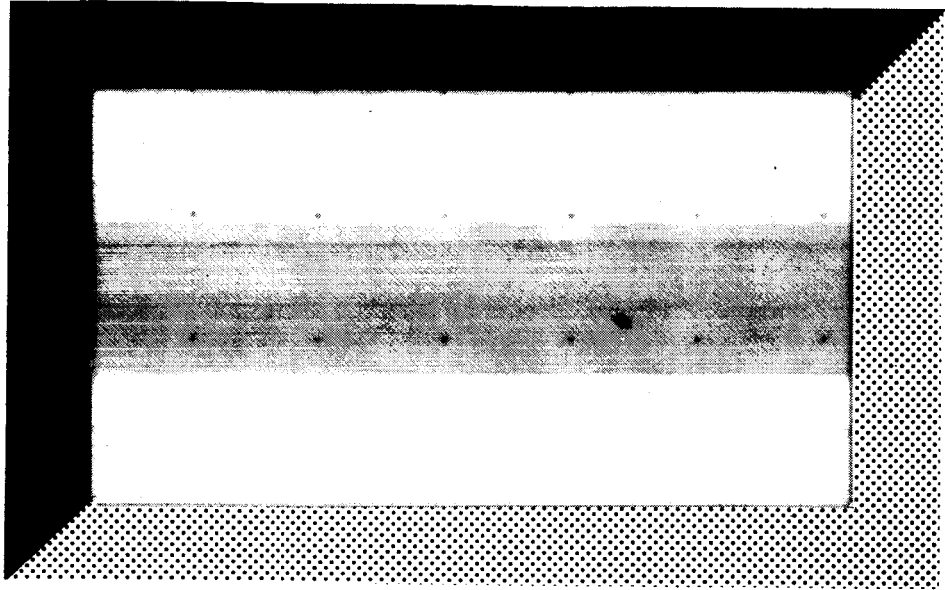


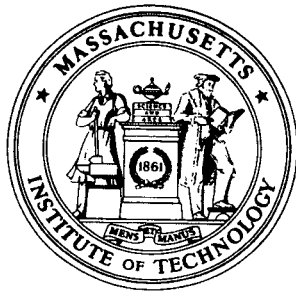
DRA AMES



(NASA-CR-177081) CALCULATIONS OF
AXISYMMETRIC VORTEX SHEET ROLL-UP USING A
PANEL AND A FILAMENT MODEL (Massachusetts
Inst. of Tech.) 182 p CSCL 01A

N86-29767

Unclass
G3/02 43221



**DEPARTMENT OF
AERONAUTICS AND ASTRONAUTICS**
MASSACHUSETTS INSTITUTE OF TECHNOLOGY
CAMBRIDGE, MASSACHUSETTS 02139

CALCULATIONS OF AXISYMMETRIC VORTEX
SHEET ROLL-UP
USING A PANEL AND A FILAMENT MODEL¹

by

John P. Kantelis and Sheila E. Widnall

FDRL Report No. 86-1

February, 1986

NASA/Ames Research Center contract NAG2-251

Fluid Dynamics Research Laboratory
Department of Aeronautics and Astronautics
Massachusetts Institute of Technology
Cambridge, MA 02139

A method for calculating the self-induced motion of a vortex sheet using discrete vortex elements is presented. Vortex panels and vortex filaments are used to simulate two-dimensional and axisymmetric vortex sheet roll-up. A straightforward application using vortex elements to simulate the motion of a disk of vorticity with an elliptic circulation distribution yields unsatisfactory results where the vortex elements move in a chaotic manner. The difficulty is assumed to be due to the inability of a finite number of discrete vortex elements to model the singularity at the sheet edge and due to large velocity calculation errors which result from uneven sheet stretching.

A model of the inner portion of the spiral is introduced to eliminate the difficulty with the sheet edge singularity. The model replaces the outermost portion of the sheet with a single vortex of equivalent circulation and a number of higher order terms which account for the asymmetry of the spiral. The effect of the uneven sheet stretching is minimized by periodic discretization of the sheet.

The resulting discrete vortex model is applied to both two-dimensional and axisymmetric sheets. The two-dimensional roll-up is compared to the solution for a semi-infinite sheet with good results. The axisymmetric cases show a smooth roll-up with none of the chaotic behavior seen in the straightforward approach.

¹Adapted from the S.M. Thesis by John P. Kantelis, "Calculations of Axisymmetric Vortex Sheet Roll-Up Using a Panel and a Filament Model", M.I.T., February, 1986.

Contents

1	Introduction	13
1.1	Vortex Sheet Modelling	14
1.2	Previous Work	15
1.3	Motivation for this Study	17
2	Problem Statement and Discrete Model	19
2.1	Introduction	19
2.2	Vortex Panel Model	22
2.3	Vortex Filament Model	24
3	Numerical Solution of the Evolution Equations	29
3.1	Euler Time Step Procedure	29
3.2	Runge-Kutta Time Step Procedure	30
4	Straightforward Application of Discrete Model	32
4.1	Results	32
4.2	Effect of Time Stepping Procedure	32
4.3	Suspected Cause of Chaotic Motion	34
5	Special Models	41
5.1	Model of Singularity at Sheet Edge	41
5.1.1	Motivation for Special Model	41
5.1.2	Inner Spiral Model	42

5.1.3	Initial Representation of the Sheet	50
5.1.4	Tip Ring Amalgamation	51
5.2	Rediscretization to Alleviate Velocity Errors	52
5.2.1	Motivation for Rediscretization	52
5.2.2	Application to the Discrete Axisymmetric Model	53
6	Application of Discrete Vortex Model	63
6.1	Summary of Model	63
6.2	Results	64
6.2.1	Two-Dimensional Model Validation	64
6.2.2	Elliptic Loading Case	74
6.2.3	Helicopter Loading Case	79
7	Conclusions	118
A	Vortex Polygon Model	123
A.1	Cut-Off Method	123
A.2	Polygon Model	123
B	Computer Program ROLLUP	127
B.1	Description of Program	127
B.2	Program Listing	136

List of Figures

2.1	Vortex Panel and Coordinate Systems	28
4.1	Straightforward Application of Discrete Model	37
4.2	Fluid Impulse for the Euler Method	38
4.3	Fluid Impulse for the Runge-Kutta Method	38
4.4	Kinetic Energy for the Euler Method	39
4.5	Kinetic Energy for the Runge-Kutta Method	40
5.1	Inner Spiral Model	56
5.2	Time Dependency of the Inner Spiral Model	57
5.3	Numerical Integration over the Inner Spiral	58
5.4	Rotation of Inner Spiral Model to Match Actual Sheet Orientation . . .	58
5.5	Initial Representation of Sheet	59
5.6	Sheet Edge Filament Amalgamation Procedure	60
5.7	Cubic Spline for Sheet Rediscretization	61
5.8	Rediscretization at Outer Sheet Edge	62
6.1	Initial Filament Placement and Sheet Strength Distribution for the Two-Dimensional Sheet	84
6.2	Vertical Velocity Distribution at Time $t = t_0$ for the Panel and the Filament Models	85
6.3	Horizontal Velocity Distribution at Time $t = t_0$ for the Panel and the Filament Models	86
6.4	Sheet Roll-Up Before Amalgamation – Panel Model	87
6.5	Sheet Roll-Up Before Amalgamation – Filament Model	87

6.6	Enlargement of Spiral Region With Ten Turns – Panel Model	88
6.7	Enlargement of Spiral Region With Ten Turns – Filament Model	88
6.8	Sheet Strength Distribution to $t = 0.122$ – Panel Model	89
6.9	Sheet Strength Distribution to $t = 0.136$ – Filament Model	89
6.10	Vertical Velocity of the Spiral Center to $t = 0.122$ – Panel Model	90
6.11	Vertical Velocity of the Spiral Center to $t = 0.136$ – Filament Model	90
6.12	Effect of Inner Spiral Model on Tip Filament Vertical Velocity	91
6.13	Definition of Radial Circulation Distribution	92
6.14	Radial Distribution of Circulation to $t = 0.122$ – Panel Model	93
6.15	Radial Distribution of Circulation to $t = 0.136$ – Filament Model	93
6.16	Circulation Contained in Spiral to $t = 0.122$ – Panel Model	94
6.17	Circulation Contained in Spiral to $t = 0.136$ – Filament Model	94
6.18	Distance of Sheet From Spiral Center at $t = 0.122$ – Panel Model	95
6.19	Distance of Sheet From Spiral Center at $t = 0.136$ – Filament Model	95
6.20	Sheet Geometry to $t = 4.35$ – Panel Model	96
6.21	Sheet Geometry to $t = 4.31$ – Filament Model	96
6.22	Sheet Geometry to $t = 8.50$ – Panel Model	97
6.23	Sheet Geometry to $t = 8.45$ – Filament Model	98
6.24	Sheet Strength Distribution to $t = 8.50$ – Panel Model	99
6.25	Sheet Strength Distribution to $t = 8.45$ – Filament Model	99
6.26	Vertical Velocity of the Spiral Center Filament to $t = 8.50$ – Panel Model	100
6.27	Vertical Velocity of the Spiral Center Filament to $t = 8.45$ – Filament Model	100
6.28	Circulation Contained in Spiral to $t = 8.50$ – Panel Model	101
6.29	Circulation Contained in Spiral to $t = 8.45$ – Filament Model	101
6.30	Radial Distribution of Circulation to $t = 8.50$ – Panel Model	102

6.31	Radial Distribution of Circulation to $t = 8.45$ - Filament Model	102
6.32	Initial Panel Placement and Sheet Strength Distribution for the Axisymmetric Elliptically Loaded Disk	103
6.33	Axial and Radial Velocity Distributions at Time $t = t_0$ - Elliptic Loading	104
6.34	Sheet Roll-Up Before Amalgamation - Elliptic Loading	105
6.35	Detailed View of the Spiral Region with Ten Turns - Elliptic Loading .	105
6.36	Sheet Strength Distribution to $t = 0.126$ - Elliptic Loading	106
6.37	Axial Velocity of the Spiral Center Filament to $t = 0.126$ - Elliptic Loading	106
6.38	Radial Distribution of Circulation to $t = 0.126$ - Elliptic Loading	107
6.39	Circulation Contained in the Spiral to $t = 0.126$ - Elliptic Loading . . .	107
6.40	Distance of Sheet From Spiral Center at $t = 0.126$ - Elliptic Loading . .	108
6.41	Sheet Strength Distribution vs. θ at $t = 0.126$ - Elliptic Loading	108
6.42	Sheet Geometry to $t = 1.52$ - Elliptic Loading	109
6.43	Sheet Strength Distribution to $t = 1.52$ - Elliptic Loading	110
6.44	Axial Velocity of the Spiral Center Filament to $t = 1.52$ - Elliptic Loading	110
6.45	Circulation Contained in the Spiral to $t = 1.52$ - Elliptic Loading	111
6.46	Radial Distribution of Circulation to $t = 1.52$ - Elliptic Loading	111
6.47	Distance of Sheet From Spiral Center at $t = 1.52$ - Elliptic Loading . . .	112
6.48	Sheet Strength Distribution vs. θ at $t = 1.52$ - Elliptic Loading	112
6.49	Initial Panel Placement and Sheet Strength Distribution for the Axisymmetric Disk with a Helicopter Type Loading	113
6.50	Axial and Radial Velocity Distributions at Time $t = t_0$ - Helicopter Loading	114
6.51	Sheet Geometry to $t = 0.076$ - Helicopter Loading	115
6.52	Sheet Geometry to $t = 3.51$ - Helicopter Loading	115
6.53	Sheet Strength Distribution to $t = 0.076$ - Helicopter Loading	116

6.54	Sheet Strength Distribution to $t = 3.51$ - Helicopter Loading	116
6.55	Axial Velocity of the Spiral Center Filament - Helicopter Loading	117
6.56	Circulation Contained in the Spiral - Helicopter Loading	117
A.1	The Cut-Off Method	126
A.2	Construction of a Vortex Polygon from a Vortex Ring	126
B.1	Main Program of ROLLUP	131
B.2	Subroutine MOVEM	132
B.3	Subroutine VELOCY	133
B.4	Subroutine REDISC	134
B.5	Subroutine LUMPS	135

Nomenclature

Roman Letters

<i>A</i>	Material particle at junction of inner spiral and sheet
<i>a</i>	Scale factor for loading of a semi-infinite sheet
<i>a</i> ₀	Horizontal position of spiral center at time $t = t_0$
<i>b</i>	Semi-span of vortex sheet at time $t = 0$
<i>b</i> ₀	Vertical position of spiral center at time $t = t_0$
<i>c</i>	Radius of a vortex ring core section
<i>E</i>	Complete elliptic integral of the first kind
<i>f</i>	Interpolated function in cubic splining procedure
<i>g</i>	Intermediate function in cubic splining procedure
<i>K</i>	Complete elliptic integral of the second kind
<i>k</i> _{<i>i</i>}	Runge-Kutta coefficients
<i>l</i> _{<i>i</i>}	Runge-Kutta coefficients
<i>P</i>	Fluid impulse
<i>R</i>	Radius of a vortex ring or panel
<i>R</i> _{<i>A</i>}	Radius of boundary of inner spiral model
(r, z)	Inertial axisymmetric cylindrical coordinate system
$(\tilde{r}, \tilde{\theta})$	Polar coordinate system fixed to the inner spiral
\hat{r}	Distance measured from spiral center
<i>s</i>	Arc length or distance
<i>T</i>	Kinetic energy

t	Time
U_{ref}	Reference velocity
u	Axial component of velocity
\tilde{u}	Velocity component in the \tilde{x} direction
\vec{V}	Velocity vector
V_{max}	Maximum velocity of any vortex element
v	Radial component of velocity
\tilde{v}	Velocity component in the \tilde{y} direction
w	Panel half-width
\vec{x}	Position vector
(x, y)	Inertial cartesian coordinate system
(\tilde{x}, \tilde{y})	Cartesian coordinate system fixed to the inner spiral

Greek Letters

α	Arbitrary constant in Kaden's spiral
α_{rot}	Angle through which the inner spiral model is rotated to match the position of the sheet edge
$\hat{\alpha}$	Scaling factor in Kaden's spiral
Γ	Circulation
Γ_{sp}	Circulation contained in the spiral region
Γ_0	Reference circulation
γ	Sheet strength
ϵ	Arbitrary constant in Kaden's spiral
η	Imaginary part of Ω
θ	Angular coordinate measured from spiral center

κ	Strength of a vortex panel or filament
λ	Similarity parameter, argument of Ω
ν	Exponent on θ in Kaden's spiral
ξ	Real part of Ω
ρ	Density
τ	Similarity parameter, λ^{-3}
ϕ	Argument for elliptic integrals
Ψ	Stream function
Ω	Pullin's non-dimensional sheet shape function
Ω_v	Location of spiral center in Pullin's solution
ω	Vorticity

Subscripts

A	Value at the material particle A
i	Pertaining to the i^{th} vortex element
in	Inner flow solution
io	Inner/outer matching flow solution
out	Outer flow solution
ref	Reference quantity
tip	Pertaining to the spiral center vortex filament
0	Conditions at the initial time

Superscripts

n Pertaining to the n^{th} time step
' Dimensional quantity

Chapter 1

Introduction

A surface of discontinuity in the tangential component of the velocity field is called a vortex sheet. This three-dimensional surface, or sheet, can be thought of as a slip layer which is composed of vortex lines. A requirement for the existence of a vortex sheet is that the effect of viscous diffusion be very small, i.e., that the Reynolds number is very large. In the ideal case where the effect of viscosity is reduced to zero, the sheet is taken to be of zero thickness. In a real fluid the effect of viscosity is to immediately diffuse the vortex sheet into a shear layer of finite thickness, the rate of growth of the layer thickness being dependent on the fluid viscosity.

In real fluids, vortex layers of finite thickness may form whenever a body with a sharp trailing edge such as a wing, or other lifting surface, moves through the fluid. This is the result of the generation of vorticity along the surface of the body ahead of the trailing edge due to viscosity. In the ideal fluid model, this condition is simulated by imposing the Kutta condition artificially at the sharp edge and the result is a vortex sheet of zero thickness. In the ideal case, it is also convenient to think of vortex sheets as being formed by moving a thin object through a fluid and then dissolving the object. At that instant there exists a vortex sheet in the shape of the object. An example of this is found in a paper by Taylor [22].

The most common examples of vortex sheets (or finite shear layers) are those which are shed into the wake at the trailing edge of an aircraft wing or helicopter rotor. The ensuing motion of these sheets is characterized by a rapid rolling up of the edges of the

sheet into concentrated vortex structures. Knowledge of the behavior of these sheets is desirable since they can have important influences on the behavior of the aircraft itself, particularly rotary-wing aircraft, as well as on nearby aircraft. The introduction of very heavy aircraft in recent years has renewed interest in the study of vortex sheet roll-up. These aircraft can produce very powerful rolled-up wake regions known as wing tip vortices which can be very dangerous to smaller aircraft should they happen to fly through them. Helicopter rotor performance is also greatly effected by these vortical regions since the loading on a helicopter rotor is strongly coupled with the motion of the rolled-up vortices in its own wake.

This work is directed at developing a reliable and accurate method for calculating the motion of vortex sheets, particularly the motion and development of the sheet edge roll-up. Two-dimensional and axisymmetric sheets are studied with circulation distributions similar to that of the wake shed by an elliptically loaded wing or a helicopter rotor. The sheets are modelled using a discrete vortex element simulation where the continuous structure of the sheet is represented as a series of individual flat vortex panels or vortex filaments. The elements are followed in time in a Lagrangian manner with the velocities calculated numerically.

1.1 Vortex Sheet Modelling

Since the wake of an aircraft wing or helicopter rotor is characterized by very high local shear, it is a convenient and accurate approximation to model it as a vortex sheet immersed in a potential flow. Helmholtz' theorems require that regions of vorticity in an inviscid fluid convect through the fluid with the local flow velocity. In an ideal fluid, any fluid element retains its vorticity as it moves. This is a very useful property since only the fluid particles having vorticity, namely the vortex sheet, need to be tracked as the flow evolves in time. This approach is commonly referred to as a Lagrangian description

of the flowfield since individual fluid particles of fixed identity are being tracked. A significant advantage computationally is realized here since typically in these types of flows only a very small region of the flow is of non-zero vorticity.

The exact representation of the time evolution of a vortex sheet is given by a difficult singular integro-differential equation. For the general case the solution of this equation is not practical and a numerical approach is taken. Typically, the continuous sheet is divided into a finite number of discrete elements, e.g., vortex filaments or flat panels, and each of these elements is tracked individually based on its local velocity obtained by the Biot-Savart law or some other method.

1.2 Previous Work

The first attempt at a flow computation for the roll-up of a vortex sheet using these techniques was performed by Rosenhead [18] in 1931. Rosenhead modelled a two-dimensional vortex sheet using a number of point vortices whose motion was tracked by computing the mutual induced velocities of all of the other vortices. It is perhaps fortuitous that Rosenhead had no computer available to do the arithmetic, forcing the work to be done by hand because it appears now that the fairly good results he achieved were in part due to the artificial smoothing of the data introduced by the manual computations.

Later effort by Birkoff and Fisher [3] using a more refined computer analysis with more vortices than that used by Rosenhead resulted in much poorer results. The reason for this is thought to rest in the question of the existence and uniqueness of this initial value problem. It seems that an increasing number of point vortices to model the sheet does not yield a consistent solution of the original problem. It is not even clear that the inviscid problem is well-posed, as described by Saffman and Baker [20]. They indicate

that it is possible that smooth solutions may not exist for more than a finite amount of time.

Another difficulty in the analysis of vortex sheets is their inherent instability. A two-dimensional vortex sheet is known to be unstable to small disturbances, the classic Kelvin-Helmholtz instability. This complicates the matter of computations for the roll-up of vortex sheets in that there are other reasons, related to the numerical procedure, why the sheet may become unstable. This instability, however, may be suppressed by artificially smoothing the sheet between time steps. Moore [12] shows this for the case of a circular vortex sheet. Smoothing has been applied indirectly in a number of vortex methods in the form of rediscrretization of the sheet at regular intervals in time. This method was first used by Fink and Soh [7], [8] where their point-vortex model of the two-dimensional vortex sheet is rediscrretized at every time step to ensure that the point-vortices are equally spaced. The smoothing effect was a secondary consequence of the original motivation of Fink and Soh to rediscrretize the sheet to reduce the truncation error in their velocity calculation. A numerical solution technique presented by Pullin [16] avoids the stability issue by computing the roll-up of a semi-infinite parabolically loaded two-dimensional sheet as a similarity solution. Pullin writes the governing equation in a pseudo-time dependent similarity form which he solves iteratively for the sheet shape. The inner region of the resulting spiral agrees well with Kaden's similarity solution [10]. Pullin was also able to obtain the value of the arbitrary parameter inherent in Kaden's solution.

Additional two-dimensional models of vortex sheets have been presented including point-vortex models, vortex blob, cloud-in-cell, and panel methods. The vortex blob method [5] eliminates the singularity in the velocity field as the point-vortex is approached by smearing out the vortex into a small finite region. This method is effective although somewhat arbitrary. The cloud-in-cell method [1] computes the velocities at each of the point vortices by solving the Poisson equation for the streamfunction and

then differentiating to obtain the velocity. The principle advantage of this method is its greatly increased computational efficiency, allowing for a greater number of vortices to simulate the flow. A difficulty with the method is the appearance of small scale structure in the solution which appears to be grid dependent. The cloud-in-cell method has additional difficulties in axisymmetric flow where the self-induced velocities due to curvature are strongly grid dependent (Roberts and Murman [17]). Panel methods offer an advantage over point-vortex methods in that they yield a more accurate calculation of the induced velocity. Hoeijmakers and Vaatstra [9] presented a two-dimensional panel method which uses a splining technique for recomputing the sheet geometry at each time step.

1.3 Motivation for this Study

The purpose of this work is to extend the analysis of two-dimensional vortex sheets performed by authors such as Fink and Soh and Hoeijmakers into axisymmetric vortex sheets modelled with circular vortex panels and to compare the results with those obtained using circular vortex filaments. Axisymmetric sheets, being three-dimensional, have the added complexity of having additional self-induced velocity components. This arises from the well known fact that a curved vortex filament induces a velocity on itself. A combination of the methods developed for the two-dimensional sheets are employed and adapted for use on three-dimensional sheets.

The validity of the method is demonstrated by computing the roll-up of a two-dimensional vortex sheet similar to the one shed by an elliptically loaded wing and comparing the results to the similarity solution for the semi-infinite sheet given by Kaden.

The time evolution of two general configurations of axisymmetric sheet are studied,

the initially flat vortex disk resulting from a translating solid disk which suddenly disappears (i.e., Taylor's problem), and a disk of vorticity more closely resembling that which would be produced by a helicopter rotor in hover. The translating disk is a good starting point for a study of this type since it is the axisymmetric analogue of the two-dimensional wake shed by an elliptically loaded wing. This later flow is certainly one of the most widely studied configurations and as such has a large assortment of results for comparison from previous studies in two-dimensions. The helicopter rotor case has more practical value where several of the disks may be stacked on top of each other to simulate an evolving helicopter wake.

Chapter 2

Problem Statement and Discrete Model

2.1 Introduction

The problem addressed here is that of an infinitely thin shear layer in an inviscid and otherwise irrotational fluid. The shear layer, hereafter referred to as a vortex sheet, convects through the fluid with its own induced velocity. Flows of this type are governed by Helmholtz' vortex laws which state that the vorticity in the flow is conserved in time and that the vorticity is associated with material particles. That is, any fluid particle which had a certain amount of vorticity at the start of the flow will have the same vorticity for all time and any particle which was irrotational at the start will remain irrotational. Furthermore, it can be shown that the velocity field is uniquely determined by the distribution of vorticity.

This is used to advantage here in that in order to follow the motion of the entire flow, only the motion of those particles which are rotational need be followed. This is very useful in that the rotational part of the flow is confined to a sheet. So by tracking only the convection of vorticity, the entire flowfield may be reconstructed. This type of analysis of motion is generally referred to as a Lagrangian analysis.

The specific problem of interest is the motion of an axisymmetric vortex sheet, or disk. As shown by Batchelor [2], the velocity field, $\vec{V}(\vec{x})$, is given by

$$\vec{V}(\vec{x}) = -\frac{1}{4\pi} \int_{\sigma} \frac{\vec{s} \times \vec{\Gamma}'}{s^3} dA(\vec{x}') \quad (2.1)$$

where $\vec{s} = \vec{x} - \vec{x}'$, $\vec{\Gamma}'$ is the strength of the sheet at the point \vec{x}' , and σ extends over the entire sheet. The resulting motion is then given by the solution of the integro-differential equation formed from Equation 2.1 with $\vec{V}(\vec{x}) = d\vec{x}/dt$.

This study will examine the motion of two axisymmetric sheets in particular, a sheet with a distribution of vorticity similar to that in the wake of an elliptically loaded wing and a distribution more typical of that in the wake of a helicopter rotor in hover. The initial motion of each of these cases is approximately known from the results of Kaden's similarity solution [10] for a two-dimensional semi-infinite vortex sheet. This sheet has a vorticity distribution consistent with a parabolic loading which very strongly resembles the cases considered here near the edge. Therefore, in the initial time period the behavior should be similar. Kaden's solution shows that the sheet immediately rolls up into an infinitely long logarithmic spiral at the tip singularity. It will be seen that this singularity is a cause of many problems in this type of analysis, however, it must be dealt with rationally since this feature is the driving force of the phenomena.

The complexity of Equation 2.1 makes it unrealistic to expect an analytic solution for the vortex sheet roll-up, therefore a numerical approach is taken. The standard numerical method is to follow the motion of only a finite number of points along the sheet, each of which is assumed to represent the motion of an associated small piece of sheet, or, sheet segment. The problem is then to accurately calculate the induced velocities at these points, i.e., that which would result from evaluating Equation 2.1 over each of the sheet segments. Due to the singular nature of Equation 2.1 and due to the curvature of the sheet the self-induced component of a segment on itself must be treated with some care. Given the induced velocities the points are tracked as they convect through the fluid. The two general approaches to sheet discretization have been to model the segments using vortex panels or vortex filaments. This will be done for both two and three-dimensional flows.

The vortex panel method involves discretizing the sheet into a finite number of segments and then modelling each segment as a curved or straight panel of some predefined shape and strength distribution. The velocity field induced by an axisymmetric vortex panel is given by Sugioka [21] and is used here in a comparison with a filament model. The vortex filament method involves a further simplification in that all of the circulation contained in each segment is concentrated into a single vortex filament located at the center of the segment. The self-induced velocity of the segment is then taken to be that of the vortex filament.

At large distances from the sheet the induced velocities predicted by the panel and the filament models agree; however, as the sheet is approached, the flow field predicted by the panel model is smoother and more accurate. Both models display a large inaccuracy in the induced velocity field at close range due to the inherent "graininess" of the discrete models. Whereas the vortex sheet is a continuous structure, the models considered here are discrete in that a singularity in the velocity field is present at each vortex or panel edge.

Another method is to represent the circular vortex elements with sections of straight vortex filaments arranged into polygons. The velocity of each of the straight pieces is determined by evaluating the Biot-Savart integral over all of the remaining pieces. This is commonly known as the cut-off method. The advantage over axisymmetric panels or filaments is that the polygons will allow the sheet to develop in a fully three dimensional manner. The finite length of the elements introduces an effective core size with the representation of a vortex ring by a polygon. While not evaluated here, the relationship between a polygon and a ring is described in Appendix A. The polygon is the basis of free wake calculations that use vortex quadrilaterals. The equivalence of these methods for axisymmetric flows will be considered in a later portion of the study.

2.2 Vortex Panel Model

A detailed account of the induced velocity of a vortex panel is given by Sugioka [21] and is only outlined here.

In the vortex panel model, the axisymmetric vortex sheet is subdivided into a number of flat axisymmetric panels or bands. Each of the panels has a total strength equal to the circulation of the sheet segment which it represents and is considered to be uniformly distributed over the panel. A description of a vortex panel and the coordinate system used in what follows is presented in Figure 2.1. The axisymmetric sheet geometry is described by a cylindrical coordinate system with r as the radial coordinate and z as the axial coordinate. All of the results presented here are for symmetry in the azimuthal direction. For the inner solution analysis, a panel centered coordinate system with an origin at the panel center is more convenient. The velocity component in the x or r direction is u and the component in the y or z direction is v .

Sugioka obtained a uniformly valid expression for the induced velocity field of the panel by the method of matched asymptotic expansions. The solution approaches that of a circular vortex filament at large distances from the panel. Near the panel it closely resembles the two-dimensional solution for a vortex panel but includes (to first order) the effects of curvature. The velocity field is given as

$$u(x, y) = u_{in} + u_{out} - u_{io} \quad (2.2)$$

$$v(x, y) = v_{in} + v_{out} - v_{io} \quad (2.3)$$

where

$$u_{in} = \frac{-\kappa}{4\pi} \left(1 + \frac{x}{2R}\right) \left[-\sin \theta \log \frac{Q_2}{Q_1} + 2 \cos \theta \left(\arctan \frac{w - Q_3}{Q_4} + \arctan \frac{w + Q_3}{Q_4} \right) \right]$$

$$v_{in} = \frac{\kappa}{4\pi} \left(1 + \frac{x}{2R}\right) \left[-\cos \theta \log \frac{Q_2}{Q_1} - 2 \sin \theta \left(\arctan \frac{w - Q_3}{Q_4} + \arctan \frac{w + Q_3}{Q_4} \right) \right]$$

$$\begin{aligned}
& + \frac{1}{2R} [(w - Q_3) \log Q_2 + (w + Q_3) \log Q_1 - 4w \\
& \quad + 2Q_4 \arctan \frac{w - Q_3}{Q_4} + 2Q_4 \arctan \frac{w + Q_3}{Q_4}] \\
u_{out} &= \frac{\kappa w}{\pi(R+x)} \left[\left(\frac{y}{r_1} + \frac{y}{r_2} \right) (K - E) + (r_1 + r_2) \frac{\partial(K - E)}{\partial y} \right] \\
v_{out} &= \frac{-\kappa w}{\pi(R+x)} \left[\left(\frac{x}{r_1} + \frac{x+2R}{r_2} \right) (K - E) + (r_1 + r_2) \frac{\partial(K - E)}{\partial x} \right] \\
u_{io} &= \frac{-\kappa w}{\pi} \left(1 + \frac{x}{2R} \right) \frac{y}{r_1^2} \\
v_{io} &= \frac{\kappa w}{\pi} \left[\left(1 + \frac{x}{2R} \right) \frac{x}{r_1^2} + \frac{1}{2R} \log \frac{r_1}{8R} \right]
\end{aligned}$$

and

$$Q_1 = Q_5 + 2aQ_3 + w^2$$

$$Q_2 = Q_5 - 2aQ_3 + w^2$$

$$Q_3 = x \cos \theta + y \sin \theta$$

$$Q_4 = y \cos \theta - x \sin \theta$$

$$Q_5 = x^2 + y^2$$

r_1 = least distance from (x, y) to the panel center

r_2 = greatest distance from (x, y) to the panel center

where w is the half width of a panel, $2\kappa w$ is the panel circulation or strength, R is the radius of the panel center, and K and E are the complete elliptic integrals of the first and second kinds respectively.

The components u_{out} and v_{out} are the outer flow solution which is that of a single vortex ring. u_{in} and v_{in} are the inner solution components which are that for the two-dimensional panel including the effect of curvature and u_{io} and v_{io} are the components

which must be subtracted to complete the matching process. The primary advantage of the panel model over the filament model is that the resulting solution is uniformly valid in the entire domain including the panel itself (except near the edges) and is more accurate as the panel is approached. Additionally, the solution requires that w/R be much less than unity. This is violated as $R \rightarrow 0$ but since $\kappa \rightarrow 0$ as $R \rightarrow 0$ this does not seem to pose a problem in the numerical method.

The corresponding expressions for the induced velocity of a two-dimensional vortex panel are considerably simpler since the effect of curvature is not present. As given by Sugioka in the cartesian panel centered coordinate system of Figure 2.1, they are:

$$u = \frac{-\kappa}{4\pi} \left[-\sin \theta \log \frac{Q_2}{Q_1} + 2 \cos \theta \left(\arctan \frac{w - Q_3}{Q_4} + \arctan \frac{w + Q_3}{Q_4} \right) \right] \quad (2.4)$$

$$v = \frac{\kappa}{4\pi} \left[-\cos \theta \log \frac{Q_2}{Q_1} - 2 \sin \theta \left(\arctan \frac{w - Q_3}{Q_4} + \arctan \frac{w + Q_3}{Q_4} \right) \right] \quad (2.5)$$

where the Q_i , κ , and w are the same as for the axisymmetric case. These formulae are exact.

2.3 Vortex Filament Model

In the vortex filament model, the vorticity disk is modelled as a system of concentric circular vortex filaments, or vortex rings, which are initially evenly spaced along the disk. Each ring has a strength equal to the amount of circulation contained in the segment of the sheet which it represents.

As is well known, a curved vortex filament possesses an infinite self-induced velocity at all points where its curvature is non-zero. In order to eliminate this infinite velocity it is necessary to consider the vortex rings as having a core of finite thickness with distributed vorticity. The self-induced velocity is now finite, but also dependent on the assumed distribution of vorticity within the core, which, unfortunately, is arbitrary.

However, since the vortex ring is intended to simulate the action of a vortex panel, a vorticity distribution may be assigned such that the two models become in some way equivalent. For example, as demonstrated by Sugioka [21], for equally spaced filaments a distribution of uniform vorticity within a circular core of diameter equal to 0.52 times the panel width (i.e., the distance between filaments) will yield equivalent kinetic energy and velocity for the two models. This is used as a criterion for determining the vortex ring structure.

For a given core size, the associated velocity field of a vortex ring system may be determined by using the results presented in Lamb [11] for the induced velocity of a vortex ring.

In general, the stream function at a point (r, z) due to a circular vortex filament is given by

$$\Psi(r, z) = -\frac{\kappa}{2\pi}(r_1 + r_2)[K(\phi) - E(\phi)] \quad (2.6)$$

where:

- Ψ = Stokes stream function
- κ = filament strength
- r_1 = least distance from (r, z) to the ring
- r_2 = greatest distance from (r, z) to the ring
- ϕ = $(r_1 - r_2)/(r_1 + r_2)$
- K = complete elliptic integral of the first kind
- E = complete elliptic integral of the second kind

The velocity components in the axial and radial directions are then

$$v = -\frac{1}{r} \frac{\partial \Psi}{\partial r} \quad (2.7)$$

$$u = \frac{1}{r} \frac{\partial \Psi}{\partial z} \quad (2.8)$$

These are also applicable to the case of a vortex ring of finite core when the point (r, z) is not in or near the core. For (r, z) inside the core and at the center, the self-induced velocity of the single ring is

$$v = \frac{\kappa}{4\pi R} \left[\log \frac{8R}{c} - \frac{1}{4} \right] \quad (2.9)$$

$$u = 0 \quad (2.10)$$

where R is the radius of the ring, κ is its strength, and c is the radius of the core.

The two-dimensional form of the vortex filament is the familiar line or point vortex. In this case the velocity is given very simply as

$$u_{azimuthal} = -\frac{\kappa}{2\pi r} \quad (2.11)$$

$$u_{radial} = 0 \quad (2.12)$$

where κ is the strength of the filament and r is the distance from the filament. In the cartesian coordinate system of Figure 2.1 the (x, y) velocity components are

$$u = -\kappa \frac{y}{r^2} \quad (2.13)$$

$$v = \kappa \frac{x}{r^2} \quad (2.14)$$

Then for either the panel or the filament model, the induced velocity at any position i is the summation of the contributions from each of the other elements and its self-induced velocity. The equations of motion for each ring or panel i become

$$\frac{dr_i}{dt} = \sum_{j=1}^N u_{i,j} \quad (2.15)$$

$$\frac{dz_i}{dt} = \sum_{j=1}^N v_{i,j} \quad (2.16)$$

where for axisymmetric panels:

$$u_{i,j} = \text{Equation 2.2}$$

$$v_{i,j} = \text{Equation 2.3}$$

or for axisymmetric filaments:

$$u_{i,j} = \text{Equation 2.8} \quad \text{when } i \neq j$$

$$= 0 \quad \text{when } i = j$$

$$v_{i,j} = \text{Equation 2.7} \quad \text{when } i \neq j$$

$$= \text{Equation 2.9} \quad \text{when } i = j$$

and for two-dimensional panels:

$$u_{i,j} = \text{Equation 2.4}$$

$$v_{i,j} = \text{Equation 2.5}$$

or for two-dimensional filaments:

$$u_{i,j} = \text{Equation 2.13} \quad \text{when } i \neq j$$

$$= 0 \quad \text{when } i = j$$

$$v_{i,j} = \text{Equation 2.14} \quad \text{when } i \neq j$$

$$= 0 \quad \text{when } i = j$$

The motion of the sheet is given by the solution of the system of non-linear ordinary differential equations 2.15 and 2.16.

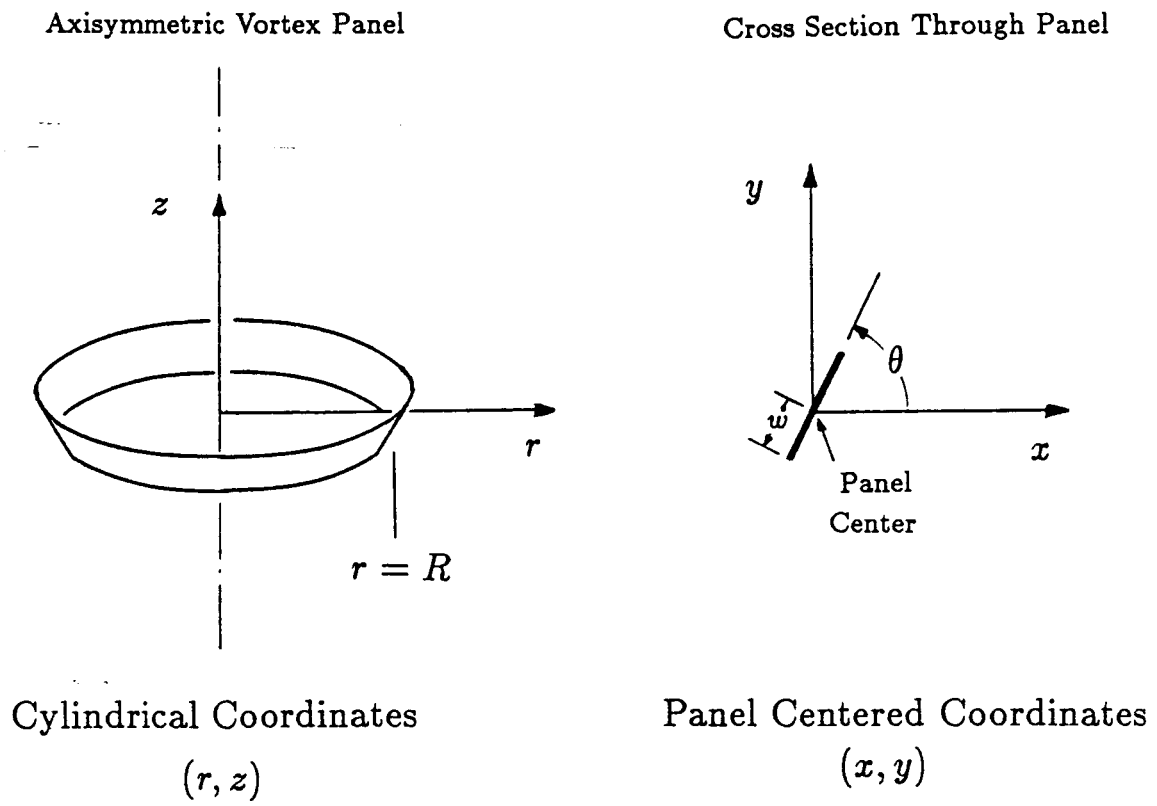


Figure 2.1: Vortex Panel and Coordinate Systems

Chapter 3

Numerical Solution of the Evolution Equations

The system of ordinary differential equations 2.15 and 2.16 governing the motion of the vortex filaments may be solved with a variety of numerical procedures. Considered here are the Euler method and a fourth-order Runge-Kutta method. Although generally more accurate, the Runge-Kutta method is much slower computationally than the Euler method, therefore, both methods will be evaluated to determine which has the best overall performance for this application.

3.1 Euler Time Step Procedure

The Euler method results from expressing the system 2.15 and 2.16 as the first order approximation to a Taylor Series.

$$r_i^{n+1} = r_i^n + \Delta t \dot{r}_i^n \quad (3.1)$$

$$z_i^{n+1} = z_i^n + \Delta t \dot{z}_i^n \quad (3.2)$$

where the superscripts refer to the time step level, i is the vortex element index, Δt is the time step, and \dot{r}_i and \dot{z}_i are given by Equations 2.15 and 2.16. This method is easy to program and therefore suited to initial concept exploration runs, but it suffers from lack of accuracy unless the time step is very small.

3.2 Runge-Kutta Time Step Procedure

The Runge-Kutta method results from modelling the solution over a time step as a polynomial rather than as a linear function as in the Euler model and is therefore more accurate for a given step size. However, the method requires the evaluation of the right-hand-side of the differential equations four times within each time step rather than once as in the Euler method. Therefore, for the Runge-Kutta method to be preferable over the Euler, the Runge-Kutta method needs to achieve accuracy greater than the Euler method for time steps that are four times larger.

The Runge-Kutta method applied to Equations 2.15 and 2.16 yield the following set of algebraic equations to be evaluated at each time step:

$$r_i^{n+1} = r_i^n + \frac{k_0 + 2k_1 + 2k_2 + k_3}{6} \quad (3.3)$$

$$z_i^{n+1} = z_i^n + \frac{l_0 + 2l_1 + 2l_2 + l_3}{6} \quad (3.4)$$

where

$$k_0 = \Delta t \dot{r}_i(r_i^n, z_i^n)$$

$$k_1 = \Delta t \dot{r}_i(r_i^n + k_0/2, z_i^n + l_0/2)$$

$$k_2 = \Delta t \dot{r}_i(r_i^n + k_1/2, z_i^n + l_1/2)$$

$$k_3 = \Delta t \dot{r}_i(r_i^n + k_2, z_i^n + l_2)$$

and

$$l_0 = \Delta t \dot{z}_i(r_i^n, z_i^n)$$

$$l_1 = \Delta t \dot{z}_i(r_i^n + k_0/2, z_i^n + l_0/2)$$

$$l_2 = \Delta t \dot{z}_i(r_i^n + k_1/2, z_i^n + l_1/2)$$

$$l_3 = \Delta t \dot{z}_i(r_i^n + k_2, z_i^n + l_2)$$

where \dot{r}_i and \dot{z}_i are given by Equations 2.15 and 2.16.

The value of the time step, Δt , is determined such that the maximum distance moved by any vortex element is limited to a specified value, Δx_{max} . Within each time step, after the velocities of all elements on the sheet have been calculated, the time step is computed as $\Delta t = \Delta x_{max}/V_{max}$ where V_{max} is the maximum velocity on the sheet.

The relative merits of the two time step methods will be evaluated in Chapter 4 where the vortex filament model is tested in a straightforward roll-up calculation. The time step procedures are evaluated based on their ability to conserve certain integral invariants of the flow; fluid impulse and kinetic energy.

Chapter 4

Straightforward Application of Discrete Model

4.1 Results

A straightforward application of the vortex filament model to a vortex disk where the vortex filaments retained their identity throughout the calculation yields disappointing, although not unexpected, results. Similar to results for two-dimensional cases, the vortex rings begin to roll-up as expected, but then cease to define a sheet as smooth lines connecting the vortex rings begin to cross over each other. A typical example of this for the vorticity sheet generated by the translating disk described earlier and modelled by 20 rings is presented in Figure 4.1. This case was run with the Runge-Kutta time stepping procedure with $\Delta t = 0.005$. The diameter of each filament core was chosen to be 0.52 times the width of the section of disk which it represents as discussed in Section 2.3. Note that the sheet initially moves as expected but quickly the motion becomes chaotic with the sheet crossing itself. As discussed for similar cases in two-dimensions by, for example, Saffman and Baker [20], increasing the number of vortex rings results in no improvement.

4.2 Effect of Time Stepping Procedure

To eliminate the possibility of the chaotic motion being merely the result of inaccurate time stepping, the integral quantities mentioned in Section 3.2 may be evaluated

and checked for invariance. These invariants, impulse and kinetic energy, should remain constant in time.

The total fluid impulse, given by $P/\rho = \pi \sum \kappa r^2$ summed over all of the vortex rings, is presented for the duration of the simulation in Figure 4.2 for the Euler method and in Figure 4.3 for the Runge-Kutta method. Each method was run with step sizes ranging from $\Delta t = 0.1$ to $\Delta t = 0.0001$. As expected, the Runge-Kutta procedure is far more accurate than the Euler procedure. A step size of $\Delta t = 0.05$ yields a nearly constant impulse for the Runge-Kutta method while the Euler method does not achieve constant impulse for even the smallest step size used.

The total kinetic energy of the flow is given by Lamb [11] as

$$T = -\pi\rho \int_0^\infty \int_{-\infty}^\infty \Psi\omega dzdr \quad (4.1)$$

where ω is the vorticity, Ψ is the streamfunction, and ρ is the fluid density. Since this flow is irrotational everywhere except in the interior of the vortex ring, the energy can be expressed simply as a summation over each of the rings

$$T = -\pi\rho \sum_{i=1}^N \iint \Psi_i\omega_i dzdr \quad (4.2)$$

where N is the number of vortex rings and the integration is performed only over the filament core sections. For each core section i , the streamfunction is written as the sum of the contributions of all of the vortex rings including that of ring i itself.

$$\Psi_i = \sum_{j=1}^N \Psi_{i,j} \quad (4.3)$$

where $\Psi_{i,j}$ is the streamfunction at ring i due to ring j . With this the kinetic energy becomes

$$T = -\pi\rho \sum_{i=1}^N \left[\iint \Psi_{i,i}\omega_i dzdr + \iint \sum_{j=1, j \neq i}^N \Psi_{i,j}\omega_i dzdr \right] \quad (4.4)$$

where $\Psi_{i,i}$ is the streamfunction at ring i due to ring i . The first term in the brackets is given by Lamb as

$$\iint \Psi_{i,i} \omega_i dz dr = -\frac{\kappa_i^2 R_i}{2\pi} \left[\log \frac{8R_i}{c_i} - \frac{7}{4} \right] \quad (4.5)$$

where κ_i is the strength of ring i , R_i is the radius, and c_i is the radius of the core section. The second term is evaluated numerically by assuming that $\Psi_{i,j}$, given by Equation 2.6, is constant over the core section of the ring.

The resulting kinetic energy for the straightforward case is shown in Figure 4.4 for the Euler method and in Figure 4.5 for the Runge-Kutta runs. This shows similar results although smaller time steps are needed to achieve constant energy. The kinetic energy is not constant for the Runge-Kutta method until the step size is reduced to about $\Delta t = 0.01$, while again it doesn't become constant at all for the Euler method.

These results indicate that the Runge-Kutta time step procedure is not the cause of the observed chaotic motion.

4.3 Suspected Cause of Chaotic Motion

The reason for this chaotic behavior and lack of smooth roll-up is not known with certainty. The two usual arguments are (1) Kelvin-Helmholtz instability and (2) velocity calculation error.

For the two-dimensional vortex sheet it is shown by Moore [13] that the sheet is unstable to small disturbances of any wavelength unless the sheet is rapidly stretching. That the sheet is most unstable to shortest wavelengths suggests that the initial value problem of two-dimensional sheet roll-up is not well posed. However, Saffman [19] explains in a heuristic argument that the extension of the sheet due to stretching also extends the disturbances and, hence, their wavelengths. Since the rate of growth of the

disturbance decreases with increasing wavelength, the stretching can have a stabilizing effect on the motion. Moore and Griffith-Jones [15] and Moore [14] confirm this argument, quantitatively, by determining that if the sheet stretches fast enough, such that the sheet strength drops off faster than $time^{-1/2}$, then the sheet is stable. Moore then applies the result to the tightly wound portion of a two-dimensional roll-up spiral with a parabolic distribution of circulation and finds that the condition is met for stability.

For parts of the sheet where rapid stretching does not occur Moore [12] shows that a discrete form of Kelvin-Helmholtz instability can ruin the calculations by amplifying the round-off and truncation errors inherent in the numerical procedures.

The calculations presented for the straightforward case show that the calculations break down in the region of the spiral roll-up where the stretching is greatest and, hence, the sheet is most stable. In addition, the region where the sheet is still nearly flat shows no sign of Kelvin-Helmholtz instability. Therefore, it is assumed that the cause of the chaotic motion is not due to Kelvin-Helmholtz instability.

Fink and Soh [7],[8] have demonstrated for the two-dimensional sheet that large errors are introduced into the velocity calculations as the vortices move away from the centers of their segments. This situation occurs very quickly at the outer edge of the sheet where the roll-up takes place. The high concentration of vorticity in this region induces very high rates of stretching and moves the vortices away from the centers of their segments. Fink and Soh suggest that this is the cause of the chaotic motion observed so quickly during the roll-up process. It is assumed that the same type of velocity errors are present in the three-dimensional sheet calculations and that this is the immediate cause of the error in the roll-up calculations presented in Figure 4.1.

A second major source of error in the straightforward approach is in the inability of a finite number of discrete elements to model the more tightly wound regions of the spiral. As can be seen from Kaden's similarity solution for the roll-up of a semi-infinite

two-dimensional vortex sheet with a parabolic circulation distribution, the inner part of the core assumes a logarithmic spiral shape:

$$r = \hat{\alpha}\theta^\nu \tag{4.6}$$

where r and θ are polar coordinates with origin at the center of the spiral, $\hat{\alpha}$ is a scaling factor, and $\nu \rightarrow -2/3$ as $\theta \rightarrow \infty$. At any time after the start of the motion the sheet is infinitely long and is rolled into loops of rapidly decreasing spacing. It seems doubtful that any discrete model could successfully represent this region of the flow.

In summary, the straightforward approach has two major areas of difficulty:

1. Arbitrarily large velocity errors result from stretching.
2. Tip region not modelled correctly by a finite number of discrete elements.

These problems are discussed in the next sections.

These curves have been displaced vertically by the amount indicated for clarity

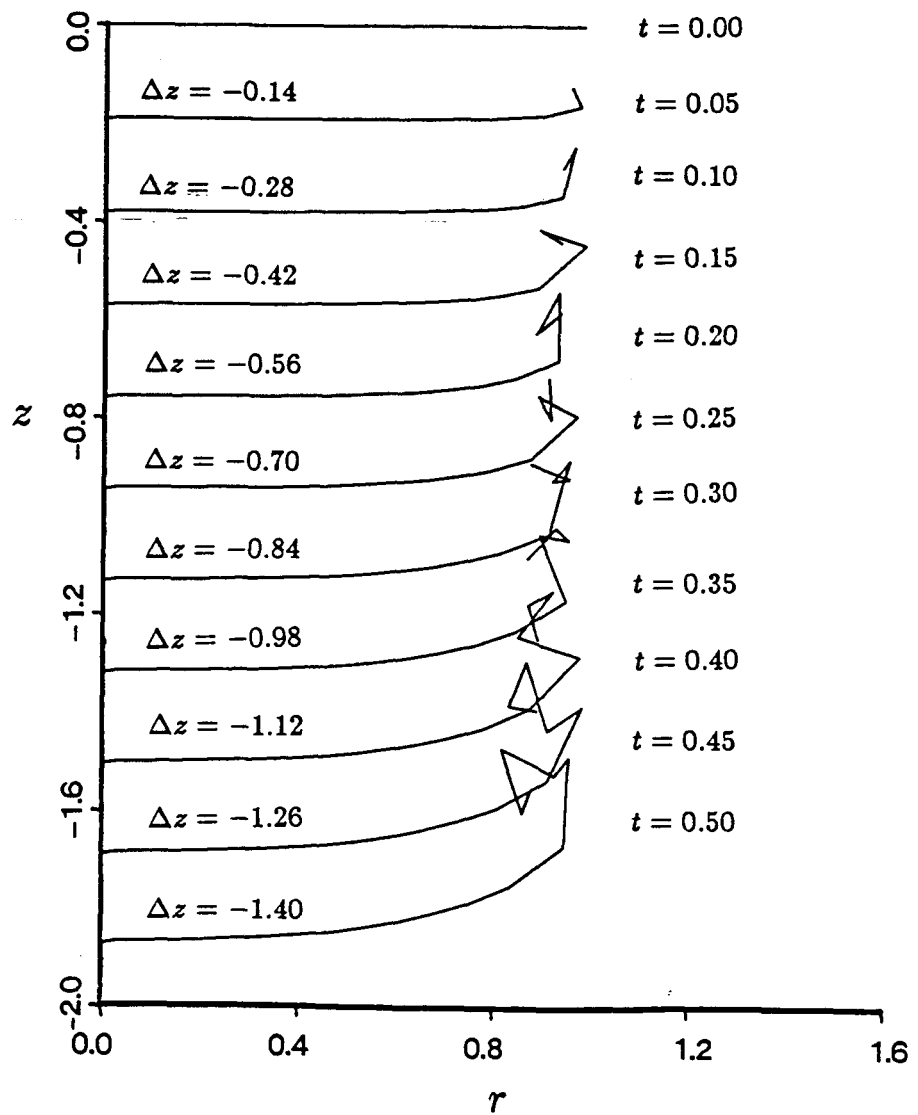


Figure 4.1: Straightforward Application of Discrete Model

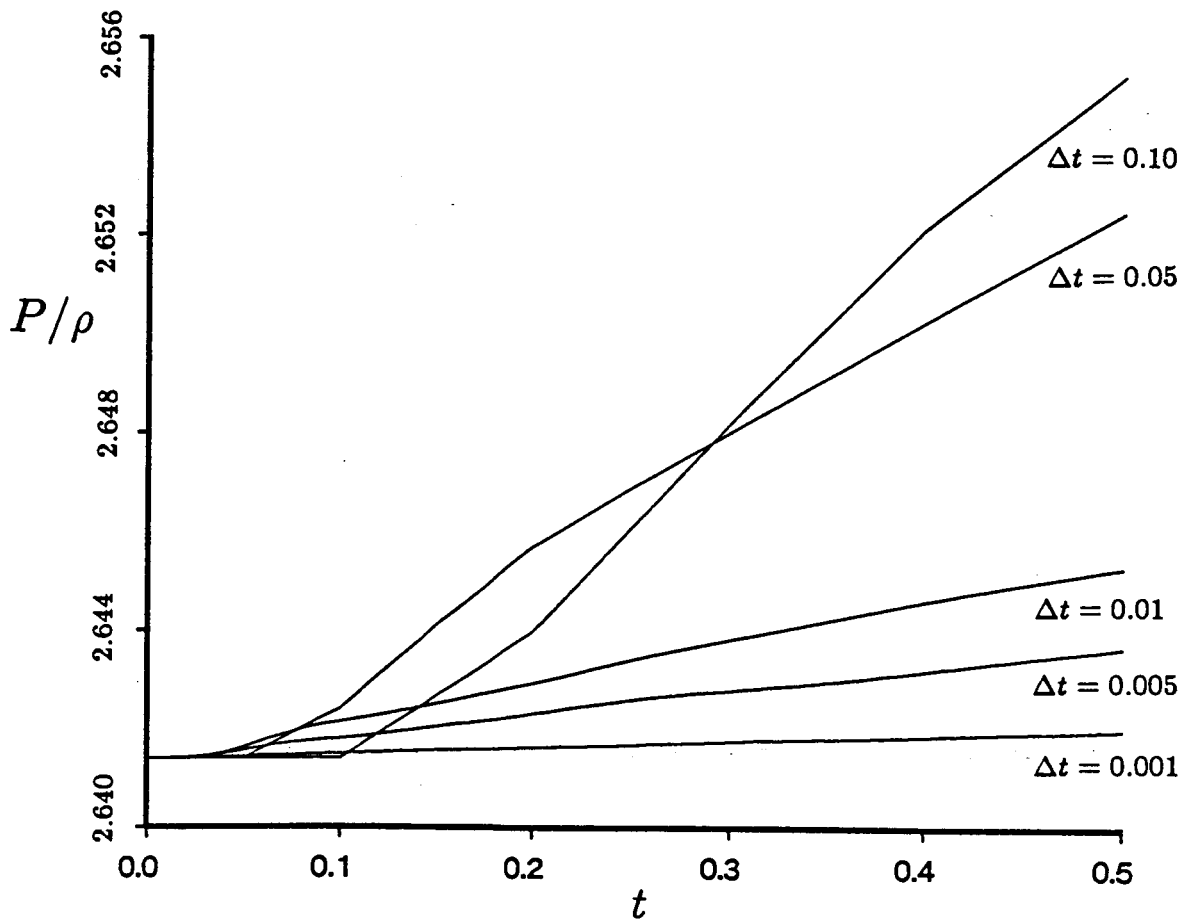


Figure 4.2: Fluid Impulse for the Euler Method

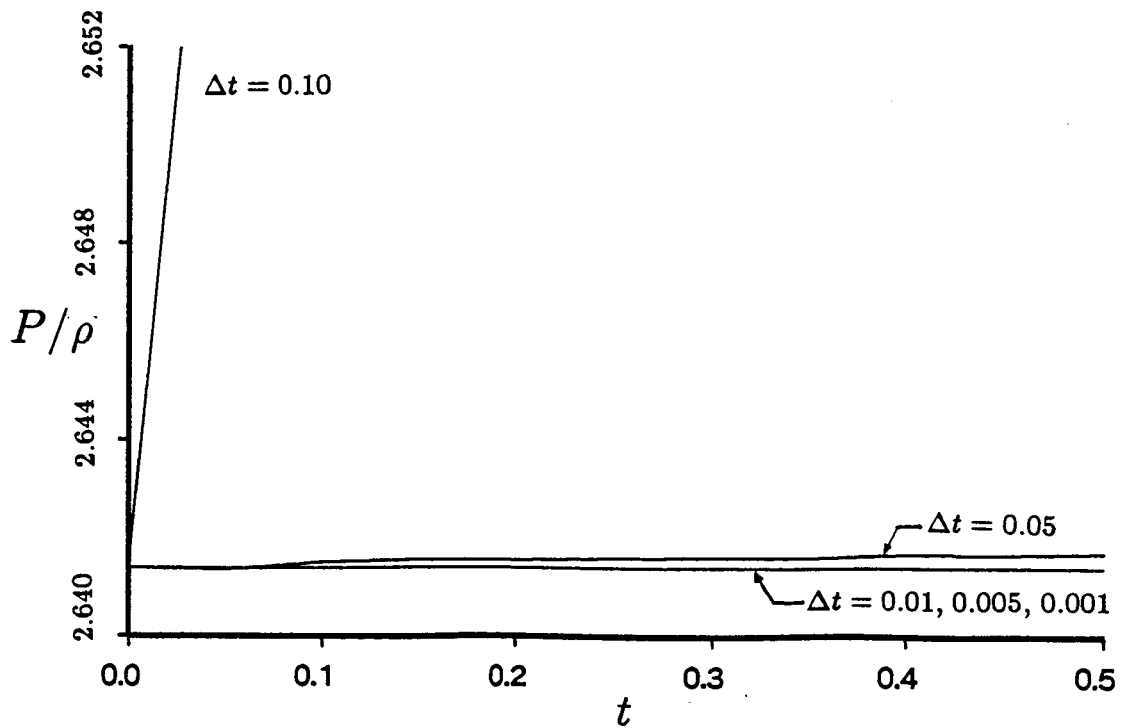


Figure 4.3: Fluid Impulse for the Runge-Kutta Method

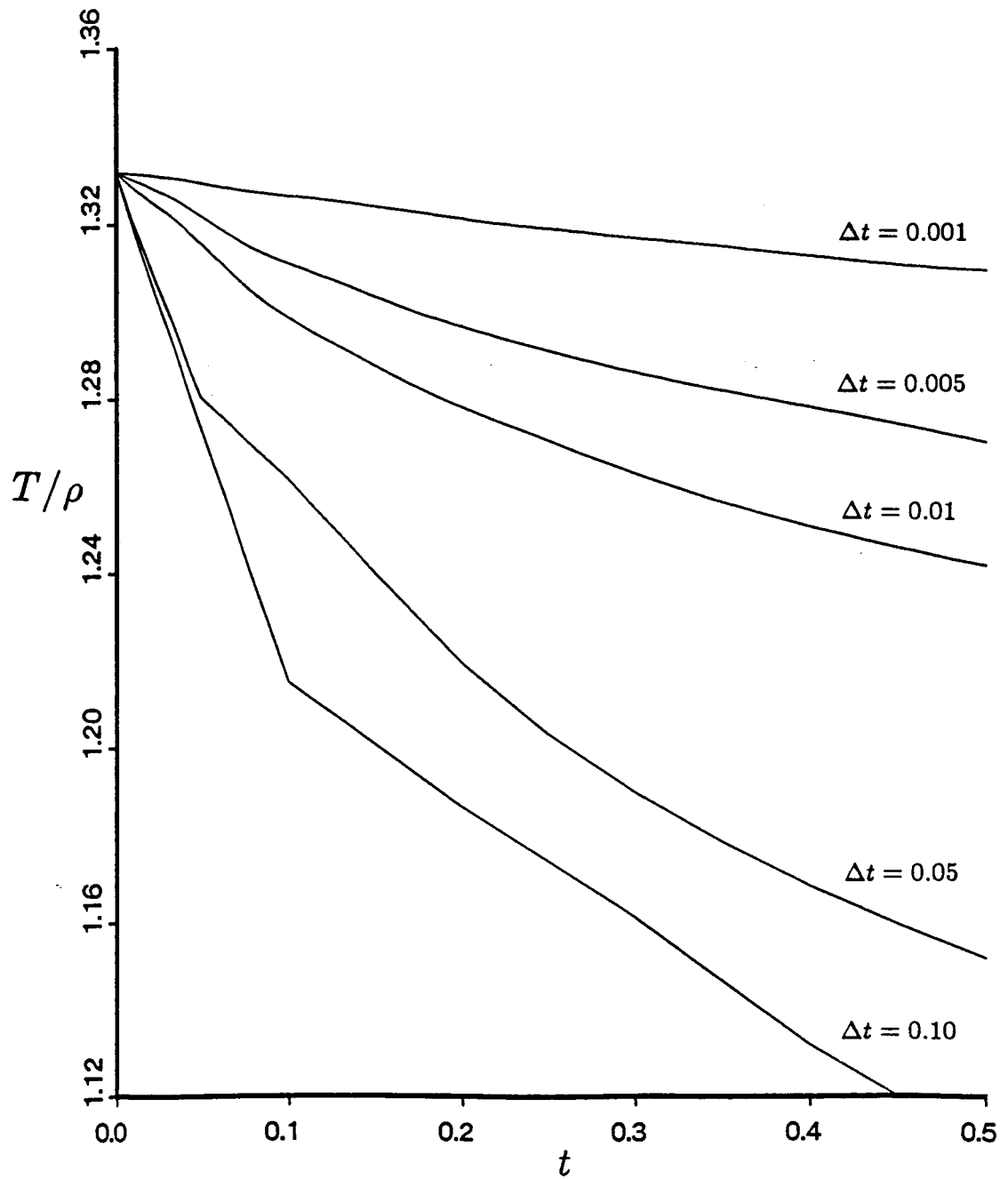


Figure 4.4: Kinetic Energy for the Euler Method

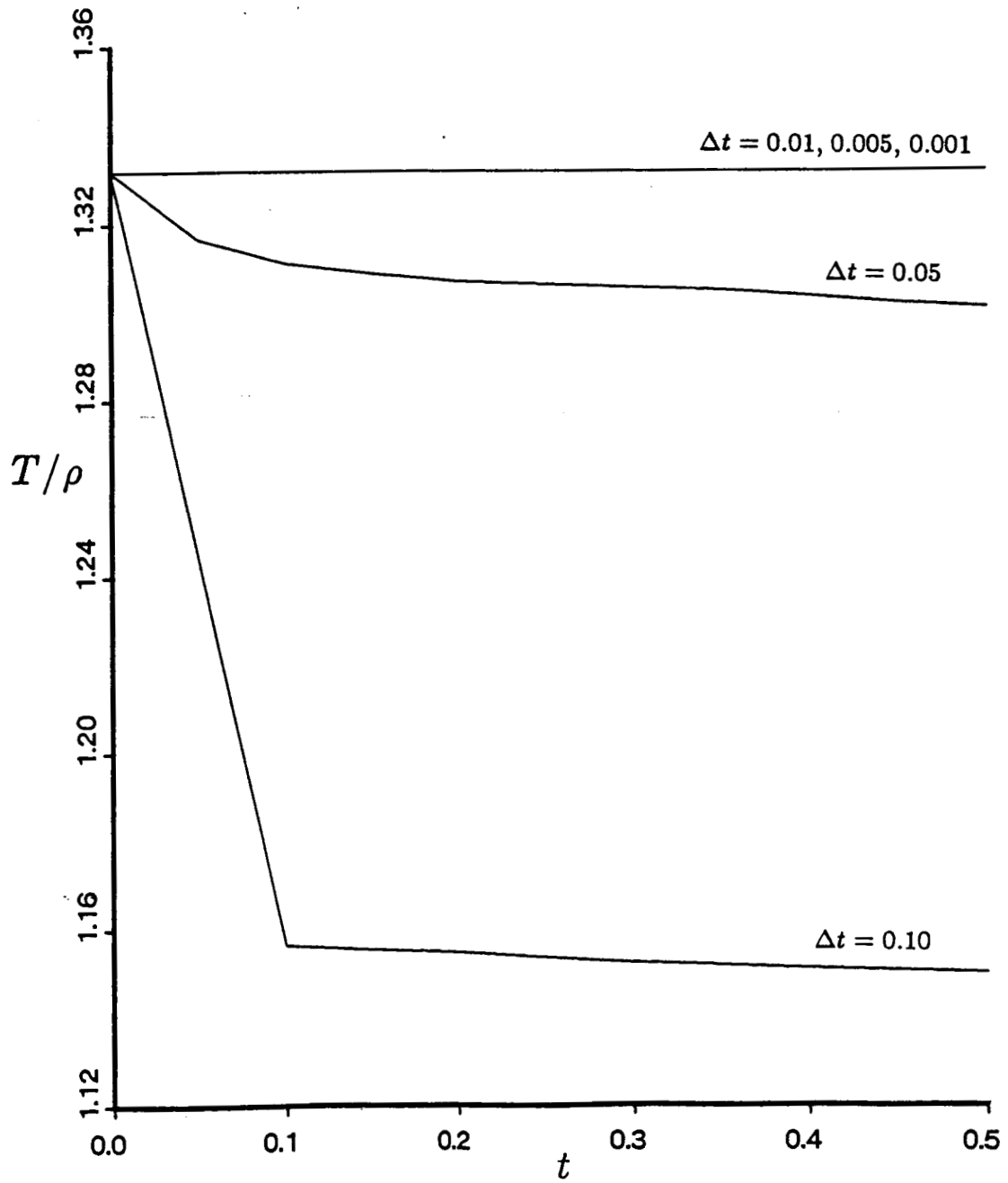


Figure 4.5: Kinetic Energy for the Runge-Kutta Method

Chapter 5

Special Models

5.1 Model of Singularity at Sheet Edge

5.1.1 Motivation for Special Model

A method for reducing the severity of the errors realized in modelling the tightly wound portion of the sheet edge in a discrete manner that has been used with some success by, for example, Hoeijmakers and Vaatstra [9] is to replace the inner portion of the spiral with a single filament of equal strength. As the inner layers of the sheet become more closely spaced, they are amalgamated into a single tip vortex ring such that the total strength and centroid of the system is preserved. This process is generally referred to as core dumping. Criteria for dumping that have been used include: restricting the spiral to a maximum number of loops, requiring a minimum number of vortices per loop, and amalgamating when the spiral layers move too closely to each other.

Another motivation for replacing the outer portion of the sheet with a single ring is more fundamental. It is doubtful that a finite number of discrete elements would ever be able to accurately model the singularity in the flowfield at the tip. This singularity is responsible for the initiation of the roll-up at the disk edge. In fact, the roll-up may be considered to be the initial condition for the motion of the sheet. The infinite velocity singularity at the sheet edge is resolved by the sheet assuming the shape of a spiral of infinite arc length placed at the sheet edge at time $t = 0^+$. The discrete model discussed

here, i.e., a series of equally spaced panels or filaments, does not in any way treat this aspect of the flowfield. In fact it may be questioned how any discrete model of a finite vortex sheet could show the proper type of roll-up behavior.

5.1.2 Inner Spiral Model

The asymmetry of the spiral cross section is neglected when using only a single vortex filament to represent the inner part of the spiral. A more accurate representation of the sheet edge and inner spiral may be obtained by replacing it with a numerical model of the Kaden [10] similarity solution for the roll-up of a parabolically loaded semi-infinite two-dimensional sheet. The asymmetric component included by the Kaden model has an effect on the flow at all points outside of the inner spiral and on the central vortex filament itself. Therefore, there are two additional velocity components to be modelled when using a single vortex filament to represent the circulation of the inner spiral, (1) that of the inner spiral asymmetry on the outer flow, and (2) that of the inner spiral asymmetry on the central vortex filament.

The inner spiral model is illustrated in Figure 5.1. The inner part of the spiral, i.e., the portion of the sheet contained within the circle of radius R'_A , is considered to be replaced with an equivalent flow system consisting of a single vortex filament of equal strength, κ' , and a number of higher order flow elements. The filament, located at the center of the spiral, accounts for all of the circulation in the circle R'_A and is also used to track the motion of the spiral center itself. The higher order elements model the asymmetry of the spiral and have no circulation. These act on both the sheet outside of the circle R'_A and on the central vortex filament.

The additional asymmetric velocity components are time dependent. As the roll-up progresses, the inner layers of the spiral move more closely together reducing the asymmetry and its effect on the flow. This may be seen by considering the sheet at

two different times, t_1 and t_2 where $t_2 > t_1$ as shown in Figure 5.2. The solid lines indicate the part of the sheet that is modelled using vortex panels or filaments while the broken lines indicate the part that is modelled by the inner spiral model. Since the points on the sheet are material particles, the edge of the sheet is always identified by the same fluid particle. In Figure 5.2 this particle is indicated as point A . The nature of the roll-up requires that point A always remain at the same distance from the spiral center, although it revolves around it. This constant distance, R'_A , is used as a reference parameter. Observe that the two inner spirals have the same diameter but that the configuration at time $t = t_2$ shows the spiral layers much closer together. This trend toward symmetry demonstrates the time dependency of the inner spiral model. As time increases and more turns are formed in the spiral, the contribution of the asymmetric components approaches zero.

The flow components due to the asymmetry of the inner spiral may be found by using the results of Pullin [16] for the roll-up of a parabolically loaded two-dimensional semi-infinite sheet. Pullin studied the roll-up by transforming the unsteady-time dependent problem into an integro-differential form using a similarity parameter involving time and circulation. This eliminated the need to study the problem in an unsteady manner along with the associated instabilities.

The initial condition for the semi-infinite problem is a flat sheet with a circulation distribution given as $\Gamma = 2a\sqrt{x}$ where x is the distance from the edge to a point on the sheet and a is an arbitrary scaling factor. Pullin describes the position of the sheet with the complex function $z_0(\Gamma, t)$ where t is time and Γ is the circulation which also identifies a particular fluid particle. Based on a dimensional analysis, the solution is written in the form

$$z_0(\Gamma, t) = (at)^{2/3}\Omega(\lambda) \quad (5.1)$$

where $\Omega(\lambda) = \xi(\lambda) + i\eta(\lambda)$ is the non-dimensional sheet shape and λ is the similarity

parameter,

$$\lambda = \frac{\Gamma}{(\alpha^4 t)^{1/3}} \quad (5.2)$$

Pullin solves for the sheet shape function $\Omega(\lambda)$ numerically using an iterative method which yields a similarity solution for the roll-up.

He then goes on to write Kaden's similarity solution in a form consistent with his notation as

$$\Omega - \Omega_0 = \alpha r^{-2/3} \exp \left[i \left(\frac{\tau}{2\pi\alpha^2} + \epsilon \right) \right] \quad (5.3)$$

where

$$r = \lambda^{-3} \quad (5.4)$$

Ω_0 is the location of the spiral center, and α and ϵ are arbitrary constants. The values of α and ϵ are determined by matching the numerical results to Equation 5.3 at a point in the inner spiral. The values found by Pullin are $\alpha = 0.124$ and $\epsilon = 2.69$.

Pullin's results are used to find the asymmetric velocity components by numerically integrating over the sheet inside the circle R'_A . For example, the velocity at the central vortex filament is found directly by integrating over the inner spiral for both the x and y cartesian velocity components. The flow external to the circle is determined somewhat less directly. An integration is performed over the sheet to yield the streamfunction on the circle. From this is subtracted the streamfunction of a point vortex of strength equal to that of the sheet yielding the streamfunction of only the asymmetric part. The streamfunction in the flowfield is then given as the solution to $\nabla^2 \Psi = 0$ with the value on the circle as the boundary condition.

Once these solutions have been found, it is necessary to express them in a rotating frame of reference since the integrations are performed with the point A on the negative \tilde{y} axis as shown in Figure 5.3, but its true orientation will vary with the rotation of the inner spiral during the roll-up. This is one aspect of the time dependency of the problem mentioned earlier. The other is that the sheet inside of point A becomes more

symmetric as the roll-up progresses. Therefore, the numerical integrations must be performed over a range of stages in the roll-up to determine the time dependency.

The numerical integration on the inner spiral is performed as follows. The sheet inside the circle of radius R'_A is divided into a number of straight segments, as shown in Figure 5.3, which are modelled as individual point vortices for the purposes of this integration. Associated with each point vortex i is a streamfunction and velocity components given by

$$\Psi'_i = -\frac{\kappa'_i}{2\pi} \log \frac{r'}{R'_A} \quad (5.5)$$

$$V'_{\theta_i} = \frac{\kappa'_i}{2\pi r'} \quad (5.6)$$

$$V'_{r_i} = 0 \quad (5.7)$$

where the primes indicate dimensional quantities, κ'_i is the strength of the filament, R'_A is the radius of the circle enclosing the spiral, and r' is the distance from the filament to the point where the integration is performed. The strength, κ'_i , is obtained from Pullin's similarity parameter as

$$\kappa'_i = \Gamma'_{i_2} - \Gamma'_{i_1} \quad (5.8)$$

where Γ'_{i_1} and Γ'_{i_2} are the values of the circulation at the end points of sheet segment i . Then from Equations 5.2 and 5.4

$$\kappa'_i = (a^4 t)^{1/3} (\tau_{i_2}^{-1/3} - \tau_{i_1}^{-1/3}) \quad (5.9)$$

which when substituted into Equations 5.5, 5.6, and 5.7 yields the contribution of segment i to the non-dimensional streamfunction, Ψ ,

$$\Psi_i = \frac{\Psi'_i}{(a^4 t)^{1/3}} = -\frac{\tau_{i_2}^{-1/3} - \tau_{i_1}^{-1/3}}{2\pi} \log r \quad (5.10)$$

and to the non-dimensional velocity components

$$V_{\theta_i} = V'_{\theta_i} \frac{R'_A}{(a^4 t)^{1/3}} = \frac{\tau_{i_2}^{-1/3} - \tau_{i_1}^{-1/3}}{2\pi r} \quad (5.11)$$

$$V_{r_i} = 0 \quad (5.12)$$

The velocity components are rotated to yield the non-dimensional components in the (\tilde{x}, \tilde{y}) system

$$\tilde{u}_i = -\frac{\tau_{i_2}^{-1/3} - \tau_{i_1}^{-1/3}}{2\pi r} \frac{y_c - y_i}{r} \quad (5.13)$$

$$\tilde{v}_i = \frac{\tau_{i_2}^{-1/3} - \tau_{i_1}^{-1/3}}{2\pi r} \frac{x_c - x_i}{r} \quad (5.14)$$

where $r = r'/R'_A$ and is expressed in Pullin's non-dimensional coordinates as

$$r = \sqrt{(\xi_i - \xi_c)^2 + (\eta_i - \eta_c)^2} \quad (5.15)$$

In this expression, the subscript i refers to the i^{th} segment of the sheet and the subscript c refers to the location of the point at which the streamfunction or velocity is calculated. ξ_i and η_i are obtained from Equation 5.3 as

$$\xi_i - \xi_v = \alpha \tau_i^{-2/3} \cos\left(\frac{\tau_i}{2\pi\alpha^2} + \epsilon\right) \quad (5.16)$$

$$\eta_i - \eta_v = \alpha \tau_i^{-2/3} \sin\left(\frac{\tau_i}{2\pi\alpha^2} + \epsilon\right) \quad (5.17)$$

where ξ_v and η_v are the positions of the spiral center and τ_i is the value of τ at the center of segment i .

In the numerical integration, each sheet segment, i , is chosen such that it subtends an angle $\Delta\tilde{\theta}$ along the sheet. The values of τ_i , τ_{i_1} , and τ_{i_2} are then obtained by noting from Equation 5.3 that r is proportional to the angle $\tilde{\theta}$, in fact, $\Delta\tau = 2\pi\alpha^2\Delta\tilde{\theta}$.

The radius of the circle, R'_A , is constant and is given by $R'_A = R(at)^{2/3}$ where R is the non-dimensional radius at time t . In an actual roll-up calculation, this may be evaluated once at time t_0 when the simulation begins where R_0 is given by $R_0 = \sqrt{(\xi_0 - \xi_v)^2 + (\eta_0 - \eta_v)^2}$. ξ_0 and η_0 are the positions of the edge of the inner spiral sheet at time t_0 which are obtained from Equations 5.16 and 5.17 with $\tau_0 = 0.24$, the value at the bottom of the spiral.

Equation 5.10 is used to calculate the contribution to the streamfunction at a point on the circle R'_A due to one segment of the spiral and Equations 5.13 and 5.14 to calculate the velocity at the spiral center. The total effect due to the spiral is obtained by integrating over the entire sheet inside the circle. However, since the sheet is infinitely long, the calculations are ended as soon as the solution converges. The entire numerical integration over the inner spiral is written

$$\Psi = - \sum_{\tau=\tau_A}^{\infty} \frac{\tau_{i_2}^{-1/3} - \tau_{i_1}^{-1/3}}{2\pi} \log r \quad (5.18)$$

$$\tilde{u} = - \sum_{\tau=\tau_A}^{\infty} \frac{\tau_{i_2}^{-1/3} - \tau_{i_1}^{-1/3}}{2\pi r} \frac{y_c - y_i}{r} \quad (5.19)$$

$$\tilde{v} = \sum_{\tau=\tau_A}^{\infty} \frac{\tau_{i_2}^{-1/3} - \tau_{i_1}^{-1/3}}{2\pi r} \frac{x_c - x_i}{r} \quad (5.20)$$

The dependency of the problem on time becomes apparent at this point. The limits on the integration of Equations 5.18 through 5.20 are from the outer edge of the sheet, $\tau = \tau_A$, to the center of the spiral, $\tau \rightarrow \infty$. As time advances and the roll-up progresses the value of τ_A changes since $\tau_A = a^4 t / \Gamma_A^3$ and Γ_A is constant. To determine the effect of increasing time (and symmetry) the calculations of Equations 5.18 through 5.20 are repeated over a range of values of τ_A , from the smallest expected to a very large value to determine the asymptotic behavior.

The resulting calculations for the non-dimensional velocity components at the central tip filament are found to very closely fit the forms

$$\tilde{u} = -0.000332 \tau_A^{-2.383} \quad (5.21)$$

$$\tilde{v} = -0.004885 \tau_A^{-1.543} \quad (5.22)$$

where (\tilde{x}, \tilde{y}) is the rotating coordinate system fixed to the sheet center. The dimensional components in the usual cartesian coordinate system are obtained by rotating Equations

5.21 and 5.22 through the angle α_{rot} and multiplying by $(a^4t)^{1/3}/R'_A$

$$u' = (\tilde{u} \cos \alpha_{rot} - \tilde{v} \sin \alpha_{rot}) \frac{(a^4t)^{1/3}}{R'_A} \quad (5.23)$$

$$v' = (\tilde{u} \sin \alpha_{rot} + \tilde{v} \cos \alpha_{rot}) \frac{(a^4t)^{1/3}}{R'_A} \quad (5.24)$$

The angle α_{rot} is dependent on time and is the angle through which the (\tilde{x}, \tilde{y}) coordinate system must be rotated in order to match the point A on the inner spiral to the point A on the actual sheet (i.e., the edge of the actual sheet). This is illustrated in Figure 5.4. The sheet edge position A is determined during the roll-up calculations.

The flowfield external to the circle is handled somewhat differently. Equation 5.18 is used to compute the asymmetric component of the streamfunction on the boundary of circle R'_A , denoted as $\Psi_{boundary}$. The flow exterior to the circle is then obtained as the solution to $\nabla^2\Psi = 0$ with $\Psi_{boundary}$ as the boundary condition. The solution may be written as

$$\Psi = \sum_{n=1}^{\infty} \left[B_n(\tau_A) \frac{\sin n\tilde{\theta}}{r^n} + D_n(\tau_A) \frac{\cos n\tilde{\theta}}{r^n} \right] \quad (5.25)$$

where B_n and D_n are written to emphasize their dependence on time. As shown in Figure 5.4 $\tilde{\theta}$ is measured from the negative \tilde{y} axis in the rotating (\tilde{x}, \tilde{y}) coordinate system. $B_n(\tau_A)$ and $D_n(\tau_A)$ are given by

$$B_n = \frac{r^n}{\pi} \int_0^{2\pi} \Psi_{boundary} \sin n\tilde{\theta} d\tilde{\theta}$$

$$D_n = \frac{r^n}{\pi} \int_0^{2\pi} \Psi_{boundary} \cos n\tilde{\theta} d\tilde{\theta}$$

where $\Psi_{boundary}$ is also dependent on τ_A . $B_n(\tau_A)$ and $D_n(\tau_A)$ are found to be fit closely by the forms

$$B_n = b_n \tau^{m_n}$$

$$D_n = d_n \tau^{l_n}$$

where

n	b_n	m_n	d_n	l_n
1	0.005301	-1.386	0.0010070	-2.373
2	0.001310	-1.363	0.0001550	-2.282
3	0.000575	-1.345	0.0000657	-2.409
4	0.000319	-1.330	0.0000312	-2.361
5	0.000202	-1.316	0.0000157	-2.173
6	0.000139	-1.301	0.0000102	-2.221
7	0.000100	-1.283	0.0000115	-2.807

are the first seven sets of coefficients.

Although the numerical computations yield decimal numbers for the time behavior of the spiral solution, in reality these should be rational numbers. Based on the results obtained, possible rational exponents are $-4/3$ for the m_n and $-7/3$ for the l_n .

The non-dimensional velocity components in the flow field are then given by

$$V_{\tilde{\theta}} = -\frac{\partial \Psi}{\partial \tilde{r}} + \frac{\kappa}{2\pi \tilde{r}} \quad (5.26)$$

$$V_{\tilde{r}} = \frac{1}{r} \frac{\partial \Psi}{\partial \tilde{\theta}} \quad (5.27)$$

where $(\tilde{r}, \tilde{\theta})$ is the coordinate system fixed to the center of the spiral as shown in Figure 5.4. The dimensional components in the usual cartesian coordinate system are given by

$$u' = (V_{\tilde{r}} \cos \theta_s - V_{\tilde{\theta}} \sin \theta_s) \frac{(a^4 t)^{1/3}}{R_A'} \quad (5.28)$$

$$v' = (V_{\tilde{r}} \sin \theta_s + V_{\tilde{\theta}} \cos \theta_s) \frac{(a^4 t)^{1/3}}{R_A'} \quad (5.29)$$

where $\theta_s = \tilde{\theta} - \pi/2 + \alpha_{rot}$ and is taken positive in the usual sense with $\theta_s = 0$ on the positive x axis.

5.1.3 Initial Representation of the Sheet

The Pullin solution may also be used as an initial condition so that the numerical simulation may be started at some time, $t = t_0$, where $t_0 > 0$. The outer most portion of the sheet will have already rolled up into an infinitely long logarithmic spiral which can be approximated using the Pullin model described in the previous section. This approach eliminates the problem of attempting to model the initial motion of the tip singularity in a discrete manner with a series of vortex elements.

The state of the sheet at time $t = t_0$ may be obtained from Pullin's results as follows. The outer portion of the sheet will have assumed the configuration shown in Figure 5.5. At time t_0 , point Λ_0 has convected to position Λ on the curved sheet and the location of the spiral center is at a_0, b_0 relative to the original location of the sheet edge. Pullin's results yield the location as $a_0 = 0.308(at_0)^{2/3}$ and $b_0 = 0.489(at_0)^{2/3}$ where t_0 is the initial time and a is a measure of the total sheet strength as given in Section 5.1.2 for the parabolically loaded sheet as $\Gamma = 2a\sqrt{x}$.

The approach taken here is to start the simulation at time $t = t_0$ with the outer portion of the sheet from the edge to point Λ_0 , and its associated circulation, represented as a single vortex filament and higher order components centered at location a_0, b_0 . The radius of the core section of this circular filament is determined by preserving the total kinetic energy of the system. Also, for simplicity, the inner portion of the sheet at time $t = t_0$, i.e., from point Λ to the central axis, is modelled as a flat sheet that is stretched uniformly from point Λ to point Λ_0 . This stretching procedure does not precisely conserve the fluid impulse but for the small values of t_0 used in the simulations the impulse is nevertheless correct typically to within less than 1%.

5.1.4 Tip Ring Amalgamation

As the sheet rolls up and the individual layers of the spiral come close together there will be large errors in the induced velocity calculated at the vortex elements. As a concentrated vortex is already present at the center of the spiral from the initial condition it is natural to use core amalgamation to lump together the inner portion of the spiral as the layers move too close together.

Core amalgamation may be accomplished in between time steps by requiring the before amalgamation and after amalgamation systems to be equivalent. The strength and location of the resulting single ring may be determined by conserving the circulation and centroid of vorticity of the group.

It is also necessary for the self-induced velocity of the centroid of the group and that of the amalgamated single ring to be equal. Bernardinis, Graham, and Parker [6] have expressed doubts about the amalgamation process when applied to three-dimensional flows unless this velocity can be maintained through the amalgamation process. In their work with vortex rings they do not explicitly require the velocities to be equal but instead determine the core radius (and hence the self-induced velocity) based on the conservation of the volume of the rotational fluid of the group of vortices. The approach taken here for the determination of the core radius is to conserve the kinetic energy of the flow across the amalgamation by adjusting the core radius of the resulting tip ring. In this way the three primary invariants of the flow, circulation, impulse, and kinetic energy are conserved throughout the simulation. The amalgamation process is summarized in Figure 5.6.

Limiting the spiral portion of the sheet to a fixed number of loops is the amalgamation criteria used here. Another method would be to check for a minimum distance between loops since this is the reason that amalgamation is used, but it is assumed that

simply counting loops provides a good enough approximation.

Another reason for limiting the number of loops is in consideration of the total length of the sheet. As more loops are allowed to form around the tip vortex ring core the sheet becomes excessively long requiring very many discrete vortex elements for sufficient resolution. The number of vortex elements, in turn, is limited by the computational resources available.

5.2 Rediscretization to Alleviate Velocity Errors

5.2.1 Motivation for Rediscretization

Fink and Soh [7], [8] show that the error in calculating the induced velocity at a point on a two-dimensional vortex sheet can become arbitrarily large if the point is not in the center of the segment. This is the result of the neglect of a logarithmic term in the solution of the Cauchy principle value integral representing the velocity. When the vortex is centered in the segment, the logarithmic term vanishes. As the vortex approaches the edges of the segment, however, the contribution of the logarithmic term becomes large and cannot be neglected. Even if the sheet is initially discretized into equal length segments, the ensuing stretching and deformation of the sheet results in their movement off center.

Fink and Soh eliminate this error by rediscretizing the vortex sheet at every time step and achieve good results. This involves constructing a new smooth sheet geometry through the convected positions of the point vortices using a curve fitting procedure and then counting off equally spaced intervals along the new sheet to form the (equal sized) sheet segments for the next time step. The point vortices are then put at the centers of each segment.

Moore [12] examines this discretization technique as applied to the case of a uniform circular vortex sheet in two-dimensions which has a known solution. For this flow, where there is no sheet stretching, the major concern is Kelvin-Helmholtz instability. Moore shows that the straightforward point vortex model experiences a discrete form of Kelvin-Helmholtz instability where the observed growth rate is that of the most unstable mode. He then shows that the discretization technique of Fink and Soh acts as a smoothing mechanism which reduces the instability and delays the onset of the chaotic motion (but does not eliminate it).

While these remarks on the error in the velocity are strictly applicable only to the two-dimensional sheet, it is assumed that the same general situation holds true for the three-dimensional axisymmetric sheets being considered here. The axisymmetric vortex segments behave locally as though they are two-dimensional, therefore, they should experience similar errors. To eliminate this error the discretization approach will be used for the three-dimensional axisymmetric sheet also.

5.2.2 Application to the Discrete Axisymmetric Model

Following Fink and Soh, after each time step a continuous model of the sheet is reconstructed by passing a smooth curve through all of the vortex elements in sequence along a cut through the sheet in a plane passing through the central axis. Simultaneously, a functional representation of the circulation distribution along the sheet is obtained. Given these, the total arc length is determined from the center to the outer edge of the sheet which when divided by the number of vortex elements yields a new sheet segment length. Vortex elements are then placed at the centers of each of the sheet segments and their strengths are determined from the sheet strength distribution. If the element is a vortex filament then it is simply placed on the curve in the center of the segment. If vortex panels are being used then the panel center is positioned to coincide

with the point on the curve in the center of the segment and the orientation of the panel is set such that the panel is tangent to the curve at the panel center. The panel width is set equal to the arc length of the segment. Observe that this method does not yield a model of the sheet where the panel edges are joined into a continuous structure except in the limit as the panel width approaches zero. The sheet is not considered to be composed of panels but, rather, the flat panels are used as approximations to the smoothly curved sheet segments for purposes of velocity calculation. Since the panel velocity is calculated at its center, which lies on the sheet, this method yields velocities on the sheet itself.

Once the sheet has formed a roll-up of about one and one half loops a different discretization technique is used in the spiral region. Rather than counting off equal length pieces of arc for the new segments, the segment lengths are chosen such that the individual vortex elements will line up with each other on successive layers in the radial direction. This is done in an attempt to minimize the effect of the artificial singularities associated with each of the vortex elements. By arranging the elements in this manner, the effect of the singularities nearly cancels and the segment lengths of neighboring elements will still be very nearly equal. The remaining sheet segments in the flat part of the sheet are discretized with equal spacing as described before.

The geometry and circulation of each portion of the sheet between any two vortex filaments or panel centers is described parametrically by an arc length parameter. For each ring interval i , the sheet is modelled as

$$r_i = r_i(s) \tag{5.30}$$

$$z_i = z_i(s) \tag{5.31}$$

$$\Gamma_i = \Gamma_i(s) \tag{5.32}$$

where r_i and z_i represent the radial and axial components of geometry respectively, Γ_i is the circulation, and s is the arc length along the sheet along the cut starting from

the central axis.

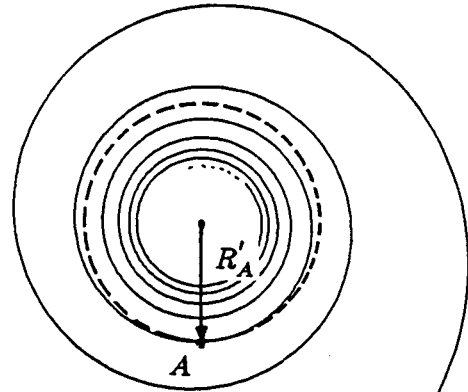
The functions for r_i , z_i , and Γ_i are a type of cubic spline that have the desirable property of bounding the interpolated curve which reduces the appearance of wiggles seen in other types of splines. The spline is constructed for a sheet segment between vortex elements i and $i + 1$ as shown in Figure 5.7. The first step is to construct a parabola, $g_i(s)$, through points $i - 2$, $i - 1$, and i and another parabola, $g_{i+1}(s)$, through the points $i - 1$, i , and $i + 1$. The interpolated function, $f_i(s)$, is then obtained as the following linear weighted average of $g_i(s)$ and $g_{i+1}(s)$

$$f_i(s) = g_i(s) \frac{s_{i+1} - s}{s_{i+1} - s_i} + g_{i+1}(s) \frac{s - s_i}{s_{i+1} - s_i} \quad (5.33)$$

where s_i and s_{i+1} are the values of arc length at points i and $i + 1$ respectively. This yields a cubic function for f_i which has a slope at the end points that matches that of the two generating parabolas. Repeated over all of the sheet segments, this process yields a continuous function from one end of the sheet to the other that has continuous first derivatives and is relatively free of the extraneous curvature seen in some other types of splines.

The only exception to this scheme occurs at the outer edge of the sheet. As shown in Figure 5.8, the location of the outer edge of the sheet is not known. The known positions are at the vortex rings or panel centers, but the outer most ring or panel center is not placed at the outer edge of the sheet, it is at or near the middle of the final segment. For purposes of rediscrretization the outer edge point of the sheet must be located. It is found by assuming that the final portion of the sheet has the shape of Kaden's spiral, i.e., $r = \hat{\alpha}\theta^{-2/3}$, where r and θ are referenced to the position of the center of the rolled-up tip vortex ring and $\hat{\alpha}$ is chosen to match the Kaden spiral to the last known point on the sheet. As shown in Figure 5.8, the origin for θ is taken as the horizontal axis through the spiral center and computed such that $r(\theta)$ is not multivalued.

Actual sheet



Sheet with
inner spiral model

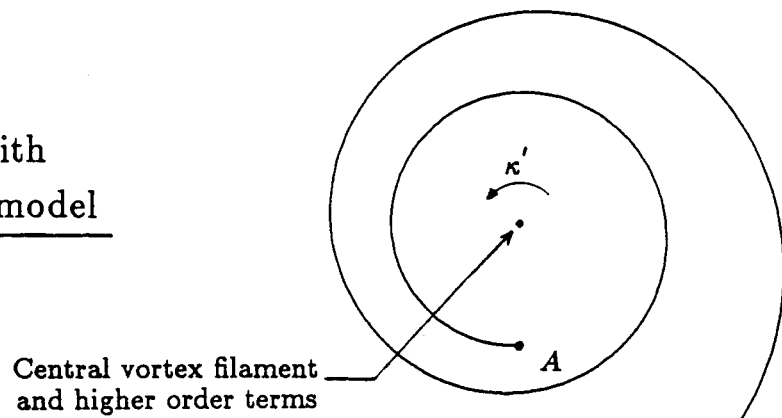
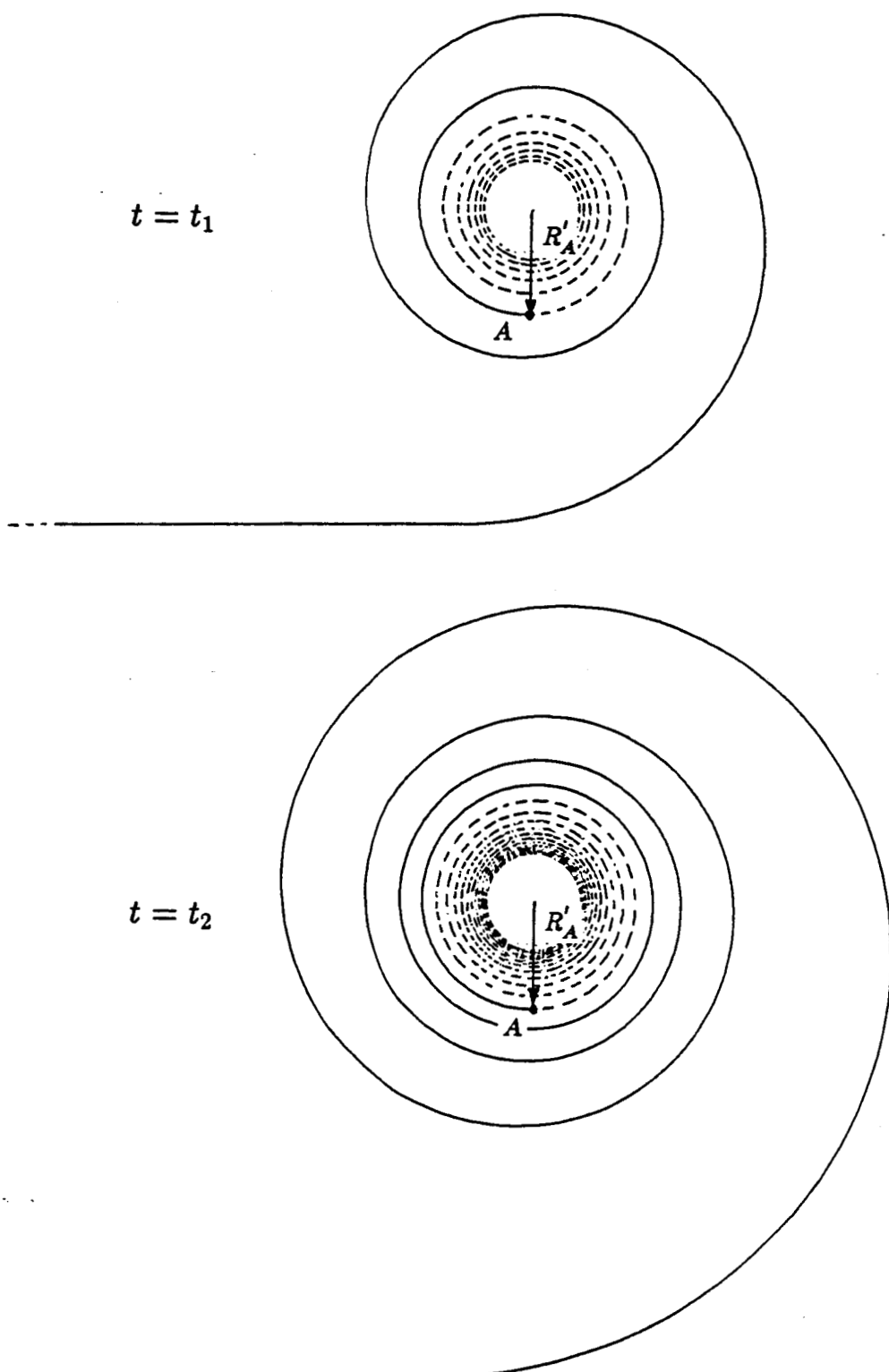


Figure 5.1: Inner Spiral Model



where:

- = portion of sheet modelled by discrete elements
- - - - - = portion of sheet replaced by the inner spiral model

Figure 5.2: Time Dependency of the Inner Spiral Model

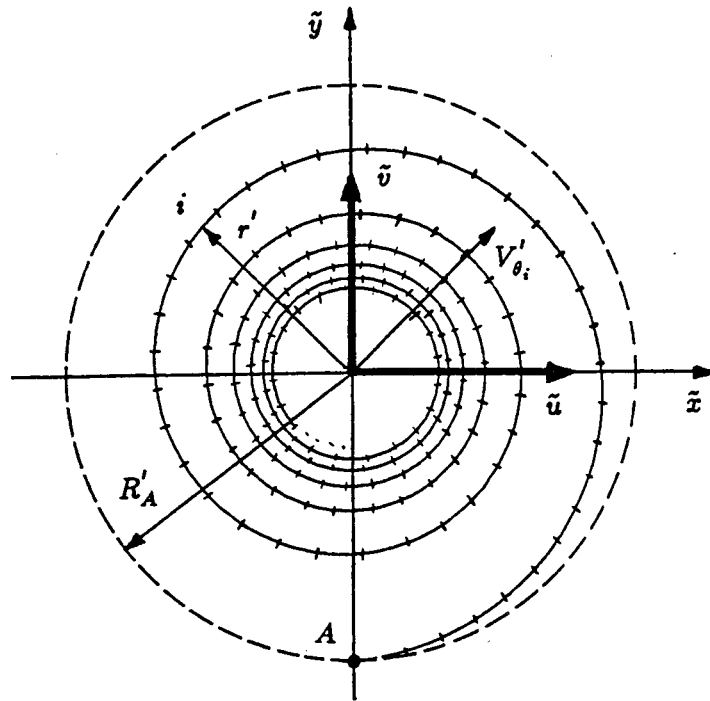


Figure 5.3: Numerical Integration over the Inner Spiral

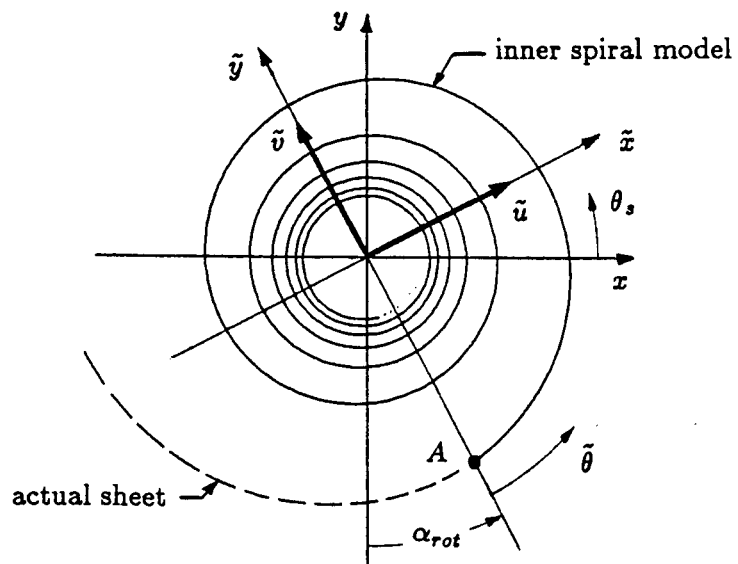
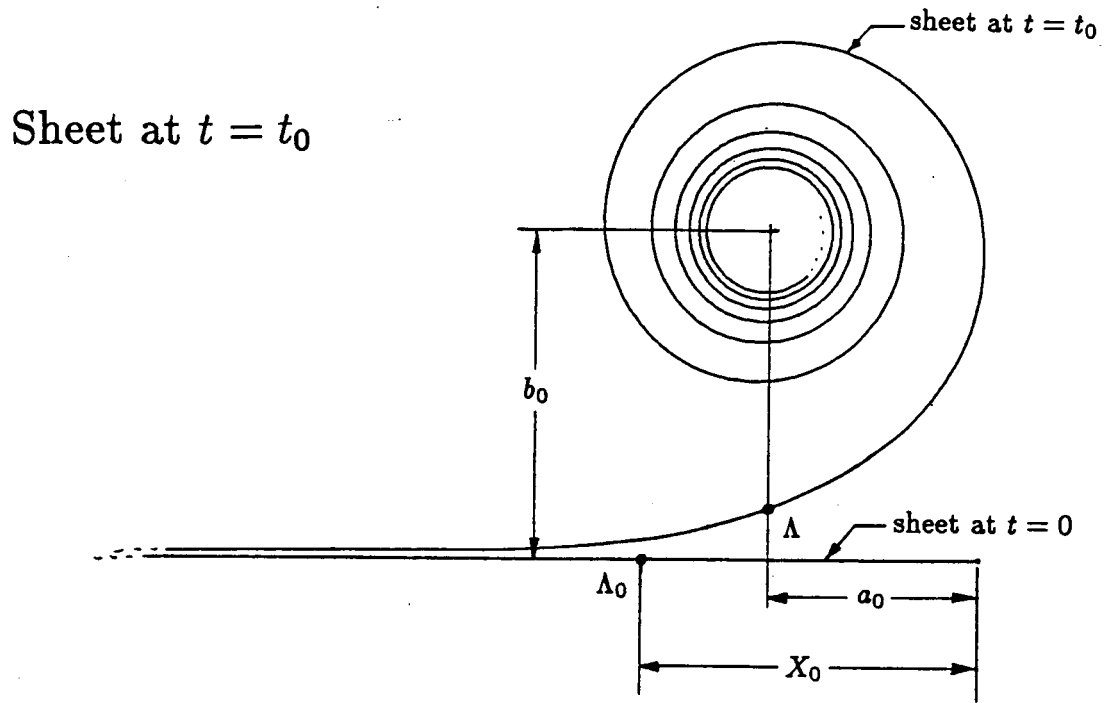


Figure 5.4: Rotation of Inner Spiral Model to Match Actual Sheet Orientation



is modelled as:

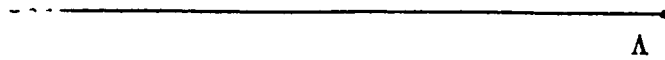
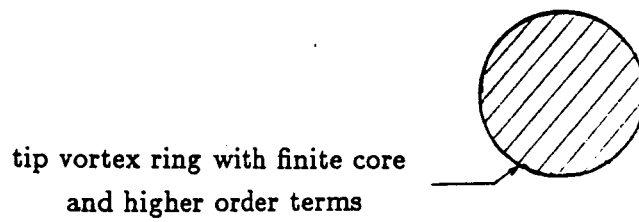
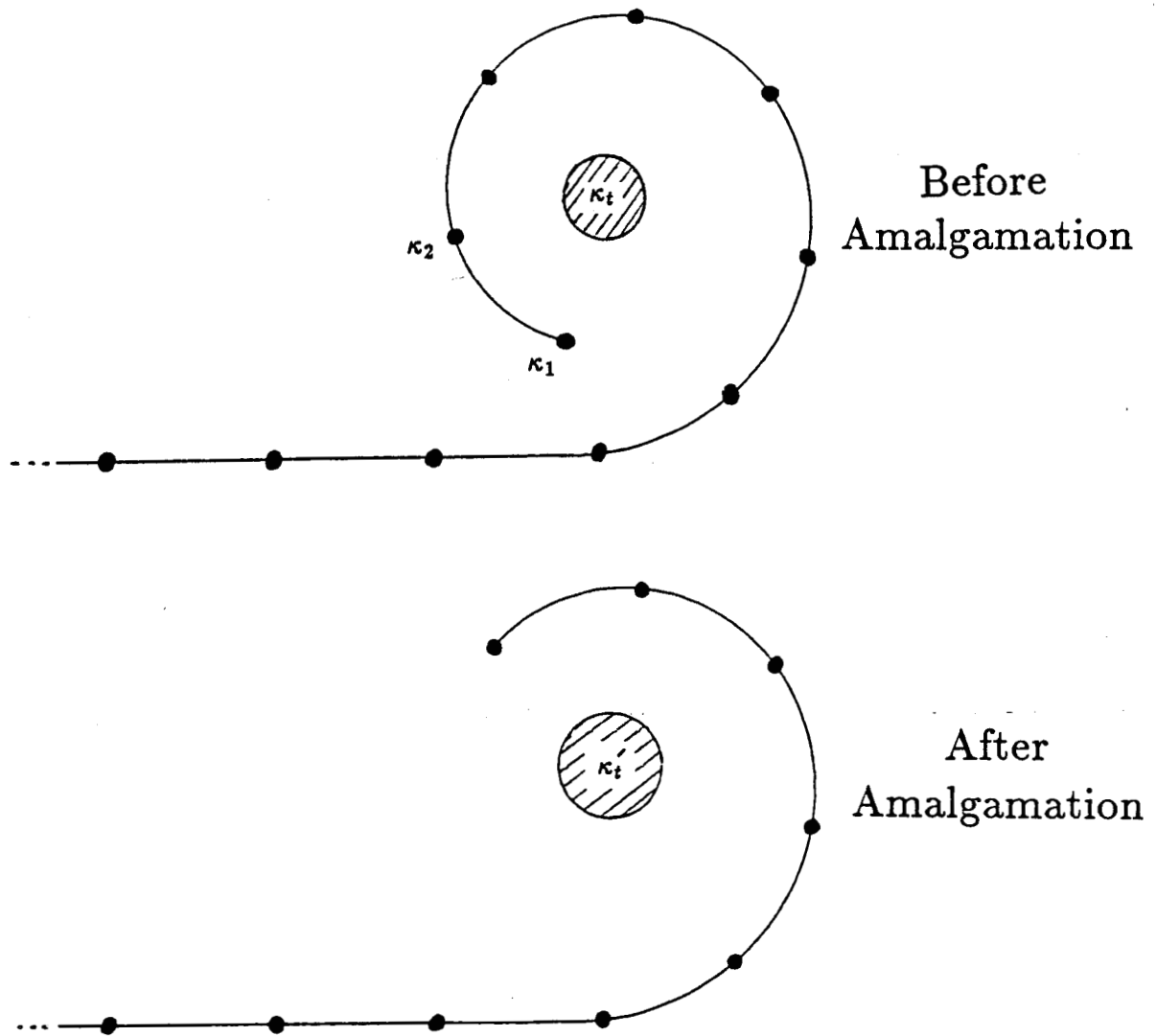


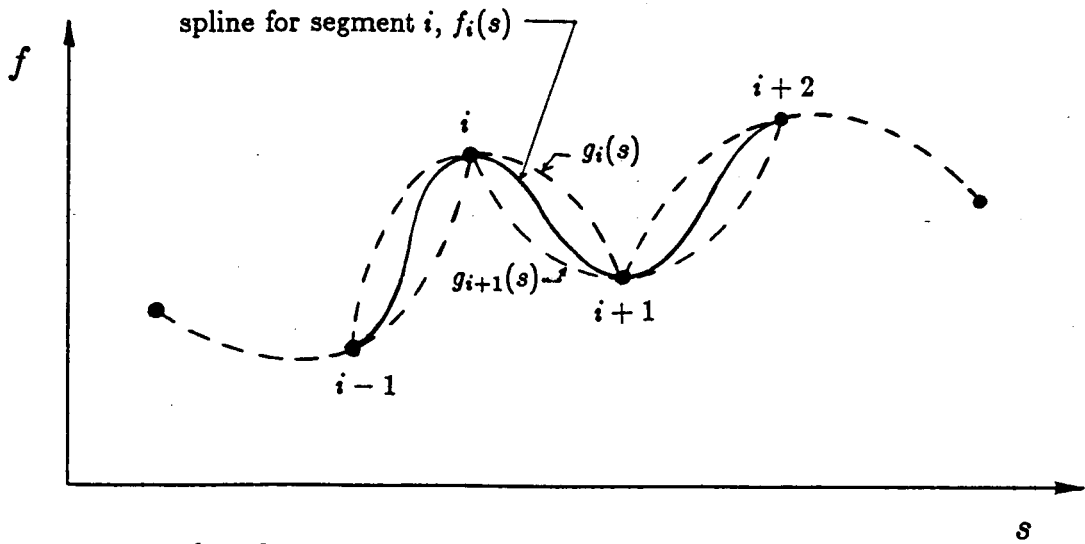
Figure 5.5: Initial Representation of Sheet



κ_1 , κ_2 , and κ_t are amalgamated to form κ_t'

1. Strength of tip filament found by conserving circulation
2. Location of tip filament found by conserving impulse
3. Tip filament core radius found by conserving kinetic energy

Figure 5.6: Sheet Edge Filament Amalgamation Procedure



$s = \text{arc length}$

$f_i = \text{function being splined, either } r_i, z_i, \text{ or } \Gamma_i$

$$f_i(s) = g_i(s) \frac{s_{i+1} - s}{s_{i+1} - s_i} + g_{i+1}(s) \frac{s - s_i}{s_{i+1} - s_i}$$

$$\begin{aligned} g_i(s) &= \text{parabola through points } i-1, i, i+1 \\ &= a_0 + a_1(s - s_i) + a_2(s - s_i)^2 \end{aligned}$$

$$\begin{aligned} g_{i+1}(s) &= \text{parabola through points } i, i+1, i+2 \\ &= b_0 + b_1(s - s_{i+1}) + b_2(s - s_{i+1})^2 \end{aligned}$$

Figure 5.7: Cubic Spline for Sheet Rediscretization

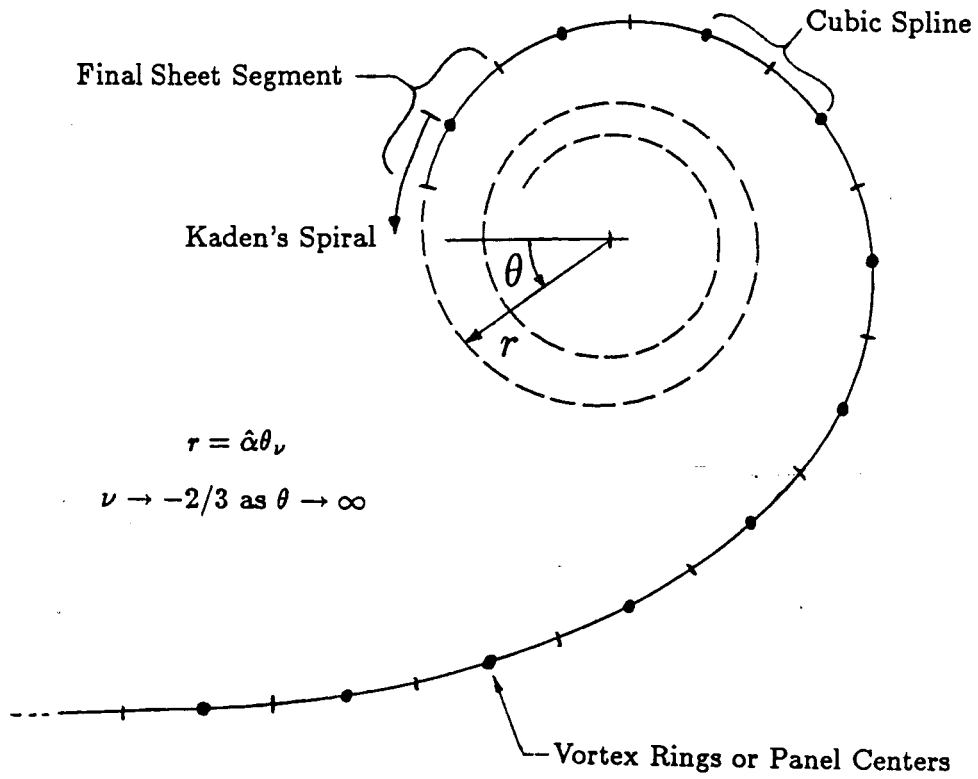


Figure 5.8: Rediscretization at Outer Sheet Edge

Chapter 6

Application of Discrete Vortex Model

6.1 Summary of Model

1. An axisymmetric sheet is modelled as a series of equally spaced concentric vortex rings or panels. For vortex rings, the core diameter is chosen to be one half of the distance between consecutive filaments, this choice of core diameter conserves kinetic energy.
2. The simulation starts at time $t = t_0$ with the spiral portion of the tip replaced with the inner spiral model consisting of an equivalent single vortex filament and higher order terms. Strength, location, and core radius of the tip ring are determined from conservation of circulation, centroid of vorticity, and kinetic energy respectively. A typical non-dimensional value of t_0 is 0.0075.
3. The induced velocities are calculated using Equations 2.15, 2.16, and the inner spiral model of Section 5.1.2 and the positions of the elements are updated using a fourth order Runge-Kutta time step method.
4. After each time step the sheet is rediscritized so that the vortex elements will remain equally spaced or along rays in the spiral region.
5. Excess spiral loops are amalgamated into the tip ring vortex as they form. Strength, location, and core radius of the new tip ring are determined from conservation of circulation, centroid of vorticity, and kinetic energy.

6.2 Results

The validity of the method is demonstrated by computing the roll-up of a two-dimensional sheet similar to that shed by an elliptically loaded wing. The results are compared to the similarity solution given by Kaden for the inner part of the roll-up of a semi-infinite sheet. This case is also used to compare and contrast the panel and filament models. Both are used to compute the two-dimensional roll-up and the results are compared.

The panel model is then applied to vortex disks of two vorticity distributions, an elliptic distribution produced by a disk which translates through a fluid at constant speed and then suddenly dissolves, i.e., the three-dimensional analogue of the elliptic wing problem, and a distribution more typical of that for a helicopter rotor blade with the load increasing towards the tip.

In all of the results that follow, t , Γ , length, and all velocities have been non-dimensionalized by t_{ref} , Γ_0 , b , and U_{ref} respectively, where, $t_{ref} = b^2/\Gamma_0$, b is the half-width of the sheet at time $t = 0$, Γ_0 is defined in the loading equations that follow, and U_{ref} is the magnitude of the velocity on the sheet at time $t = 0$. For comparison, it is recalled that Pullin's non-dimensional time is given in terms of his similarity variable as $\tau = \lambda^{-3} = a^4 t / \Gamma^3$.

6.2.1 Two-Dimensional Model Validation

The validity of the model may be evaluated by using it to compute the roll-up of a two-dimensional vortex sheet with an elliptic circulation distribution

$$\Gamma = \Gamma_0 \sqrt{1 - r^2}$$

which yields a value for the uniform downwash of $U_{ref} = \Gamma_0/2b$ and a corresponding sheet strength

$$\gamma = \Gamma_0 \frac{-r}{\sqrt{1-r^2}}$$

where r is the distance along the sheet. This is perhaps the most widely used test case for new methods because it is a good approximation to the three-dimensional roll-up of an elliptically loaded wing. Additionally, for very small values of time, an exact solution is available for the inner part of the spiral region in the form of a similarity solution. In the limit, as the center of the spiral is approached, the similarity solution becomes exact. Both the two-dimensional panel and filament models of Chapter 2 are used and the results are compared.

Simulation Parameters

The parameters used in this simulation are as follows:

Number of panels or filaments:	240
Portion of sheet edge initially rolled:	2.5%
Time step method:	Runge-Kutta
Δx_{max} :	0.003
Number of time steps:	3000
Maximum number of loops in spiral:	10

Initial Model of Sheet

The initial sheet geometry and sheet strength distribution are shown in Figure 6.1. The same initial condition applies to both the panel and the filament models. Two and one half percent of the outer portion of the sheet rolled into the tip vortex filament results

in a tip filament strength of about 22% of the total sheet strength. The large value is the result of the high concentration of vorticity in the outer portion of the sheet. As determined using the methods of Section 5.1.3, the location of the tip vortex filament is found to be $r = 0.987$ and $z = 0.021$ and the corresponding initial time is found to be $t_0 = 0.0123$. As mentioned earlier, the vortex elements which represent the sheet initially lie flat horizontally and are stretched out as indicated in Figure 5.5. The initial slight curvature of the sheet is ignored. The corresponding sheet circulation is also linearly stretched along with the filaments.

The initial vertical velocity distribution, v , is shown for the panel and filament models in Figure 6.2 and the initial horizontal velocity distribution, u , is shown for the two models in Figure 6.3. The exact initial condition for the vertical velocity on the sheet at time $t = 0$ is a uniform downwash from the center of the sheet to the outer edge and is equal to -1.0 . The horizontal velocity should be zero everywhere except at the outer edge where both velocity components are undefined. The velocity profiles of Figures 6.2 and 6.3 are not expected to agree exactly with the true initial condition at time $t = 0$ since the initial condition for the numerical simulation is at a short time later, i.e., at $t = t_0$ after a spiral has formed at the tip. However, t_0 being small implies that the initial velocity profiles should be very similar to those at $t = 0$. For both panels and filaments the vertical velocity agrees very closely with the expected value of -1.0 over most of the sheet. The large values realized at the outer edge are attributed to the inability of either the panel or the filament models to accurately compute the induced velocity in a region where the vorticity gradients are very large, however, the panel model shows less error than the filament model. The initial horizontal velocity distributions for both panel and filament models are identical from the sheet center to the outer edge where the effect of the tip filament becomes apparent. Over most of the sheet, the horizontal velocity is zero but at the outer edge it increases sharply in the outward sense due to the tip vortex producing great stretching in this region of the sheet.

Roll-Up Before Amalgamation

The resulting sheet roll-up computed using the inner spiral model of Section 5.1.2 is presented at several times up to the point when the first ten turns of the spiral are formed in Figure 6.4 for the panel model and in Figure 6.5 for the filament model. Note that in the figures some of the curves have been displaced vertically from their true positions in order to separate them for clarity. In general the models yield a very smooth roll-up with no sign of instability or other commonly observed chaotic behavior. The only noticeable difference between the panel and filament models at this point is that the panel model appears to roll-up slightly faster. Ten turns are achieved for the panel model at a time of $t = 0.122$ while for the filament model ten turns have not formed until $t = 0.136$. This difference is due to the retarding effect of the concentrated vortex at the control point on the neighboring turn.

An enlargement of the spiral region at the time when ten turns have formed is given in Figure 6.6 for the panel model and in Figure 6.7 for the filament model. Aside from the slight difference in size due to the difference in time, there is very little observable difference between the models. The use of the equi-angular discretization scheme is apparent in the inner part of the spirals but note that the outer most turn is composed of segments of equal length rather than equal angles. It was found necessary during the course of the calculations to discretize the outer turn of the spiral with equal length segments because the equi-angular method, together with the rapidly increasing radial distance of the sheet from the spiral center, resulted in sheet segments that were too unevenly spaced on this final turn. Unequal spacing of the vortex elements has been established as one of the causes of the breakdown in these methods due to the associated large errors in the velocity calculations. Therefore the equi-angular discretization could only be used on the inner part of the spiral where the distance of the sheet from the spiral center increases only slowly.

The sheet strength distributions plotted against arc length, s , measured from the sheet center are presented in Figures 6.8 for the panel model and in Figure 6.9 for the filament model. The stretching of the outer edge of the sheet is reflected in the sudden reduction in sheet strength as the edge is approached. In comparing panels and filaments, the results are very similar with, perhaps, the sheet strength distribution for the panel model slightly smoother near the end of the sheet. It is not clear if the wiggles are real or if they are due to numerical inaccuracy. Some waviness is expected in that the spiral is immersed in a strain field imposed by the remainder of the sheet.

The vertical velocity of the vortex filament which represents the spiral center, v_{tip} , is given in Figure 6.10 for the panel model and in Figure 6.11 for the filament model along with the value obtained from Pullin's results for the semi-infinite sheet. Pullin presents the position of the tip in terms of the similarity variable from which the tip vertical velocity may be obtained as

$$v_{tip} = \frac{d}{dt} [0.489(at)^{2/3}] - 1.0 \quad (6.1)$$

where the constant -1.0 is included to yield the velocity of the tip in the absolute reference frame used in the simulations and a is the sheet strength constant presented in Section 5.1.2. For the two-dimensional elliptically loaded sheet, $a = \Gamma_0/\sqrt{2}$.

The oscillations between times $t = t_0$ and $t = 0.065$ are not believed to be real but only a result of the inexact nature of the initial representation of the sheet. They are caused by the uneven distribution of vorticity around the tip filament as the sheet rolls up around it during the first few turns of the motion. The slightly faster roll-up of the panel model is reflected in the higher frequency of the oscillations in Figure 6.10 as compared to Figure 6.11.

The inner spiral model introduced in Section 5.1.2 could conceivably remove all of the oscillation but apparently the inexact nature of the initial representation of the sheet is enough to introduce the errors realized here. The model acts to considerably

lessen the amplitude of the oscillations but does not completely eliminate them. The effect of the model on the oscillations may be evaluated by comparing the simulation with the model in place (i.e., Figure 6.10) to the same simulation without the model. The tip filament vertical velocity for the first few turns of the roll-up using panels is compared with and without the inner spiral model in Figure 6.12. The effect of the model is to reduce the amplitude of the oscillations by 50% or more and to increase the rate of roll-up, as is seen indirectly from the frequency of the oscillations.

The distribution of circulation as a function of radius from the spiral center is evaluated by summing the strengths of the vortex elements enclosed by circles of increasing radius centered at the tip vortex filament. This process is illustrated in Figure 6.13. As the radius increases, eventually all of the vortex elements of the spiral are included by the radius \hat{r} . Further increase includes the unrolled part of the sheet as well.

The radial distribution of circulation for the discrete models is presented along with Pullin's result in Figure 6.14 for the panel model and in Figure 6.15 for the filament model. Consistent with the result for the semi-infinite sheet for small values of time, the circulation, once rolled up, remains at a constant radius from the spiral center. This is indicated by the clustering of lines for different values of time. Pullin's results yield a value of circulation about 5% smaller than those obtained here at the smaller values of radius, i.e., both discrete models predict that the circulation distribution for the elliptic loading is slightly more concentrated in the inner part of the spiral than that for the semi-infinite sheet. At larger values of \hat{r} the nearly parallel curves correspond to the part of the sheet which has not yet become rolled up. Since a point vortex is used to represent the center of the spiral, the curve of $\Gamma(\hat{r})$ begins at a non-zero value and is constant until the turns of the spiral are encountered.

The total circulation contained in the spiral region, Γ_{sp} , (somewhat arbitrarily defined as where the sheet first becomes vertical) is presented in Figure 6.16 for the panel

model and in Figure 6.17 for the filament model along with Pullin's results. The panel and filament models yield very similar results and both are very close to Pullin's result. This is to be expected since for small values of time when only the outermost portion of the sheet is rolled up, the loading for the semi-infinite sheet and the finite sheet are similar. By the time ten turns have formed, approximately 42% of the total circulation is contained in the spiral

The distance of the sheet from the spiral center plotted against angle, $r(\theta)$, is given in Figure 6.18 for the panel model and in Figure 6.19 for the filament model at the time just before the first amalgamation. Also given is Kaden's similarity solution using Pullin's constants for the inner part of the spiral. The distance for the panel model is everywhere smaller than the values obtained from Pullin's results while for the filament model the opposite is true. The small oscillations seen in both the panel and filament results indicate the slight ellipticity of the sheet due to the imposed strain field.

Roll-Up After Amalgamation

The roll-up continues after the time when ten turns have formed to about time $t = 8.5$ with the amalgamation procedure being used to limit the spiral to ten turns. Ten turns was selected as the cut-off for the spiral after several trial runs indicated that errors would be introduced into the solution (detected by tracking the total fluid impulse) after this point if the turns were allowed to continue to accumulate. This is thought to be due to lack of resolution and the close spacing of the inner layers of the spiral. However, in some cases, when the roll-up was continued without any amalgamation and without regard for the errors, spirals of considerably more turns were obtained before the sheet crossed over on itself. In addition, the panel model would allow for, typically, one or two more turns than the filament model.

The sheet geometry for the panel model is presented in Figures 6.20 and 6.22 and

for the filament model in Figure 6.21 and 6.23 for a series of times between $t = 1.09$ and $t = 8.5$, i.e, between the first amalgamation and the end of the simulation. The corresponding sheet strength distributions are given in Figure 6.24 for the panel model and in Figure 6.25 for the filament model. The roll-up continues smoothly, still with no sign of Kelvin-Helmholtz instability. At time about time $t = 6.8$ the spiral center (not the centroid of vorticity) has moved its greatest distance inward to $r = 0.778$ which is very near the expected asymptotic value of $r = 0.785$. The effect of the amalgamation is clear from the figures as the inner parts of the spiral gradually disappear, being absorbed by the tip filament. The sheet strength distributions have more of the small bumps seen earlier indicating the presence of the strain field due to the rest of the sheet. At this later stage in the roll-up, there is very little difference in the results between the panel and the filament models although there are some slight differences in the sheet strength distributions.

The vertical velocity of the tip filament has approached the correct asymptotic value for this flow of $v = -0.205$ at about time $t = 1.3$ as shown in Figure 6.26 for the panel model and in Figure 6.27 for the filament model. The total circulation contained in the spiral is shown in Figures 6.28 and 6.29 against time for the two cases. Also shown is Pullin's result for the semi-infinite sheet. By the end of the simulation, about 96% of the circulation has become rolled up, as the spiral has been defined.

The radial distribution of circulation in the spiral is presented in Figure 6.30 for panels and in Figure 6.31 for filaments along with Pullin's result. For larger values of time, in contradiction to the results observed for small values of time, the circulation distribution is not completely constant. As the sheet rolls up, the vorticity in the spiral layers is slowly drawn in towards the center increasing the concentration of vorticity in the spiral core. This indicates that kinetic energy is not being conserved in the calculation and this was confirmed by numerical calculations.

A measure of the accuracy of the numerical simulation may be obtained by checking for the constancy of the total fluid impulse and kinetic energy. Since these are invariants, any deviation indicates numerical errors. For the panel model, the impulse increased by about 0.19% over the duration of the simulation or by about 0.000063% per time step. The corresponding values for the filament model are an increase of about 0.25% for the entire simulation and 0.000083% per time step indicating the greater accuracy of the panel model. A detailed analysis of the simulations revealed that about half of the increase in impulse is due to inaccuracy in time stepping and the other half is due to the discretization procedure. As was observed in the discussion on the radial distribution of circulation, kinetic energy was not conserved as well as impulse. As shown by Batchelor [2], the part of the kinetic energy which depends on the positions of the vortices is given by

$$T = -\frac{1}{4\pi} \sum_j \sum_i \kappa_i \kappa_j \log r_{ij}$$

where the summation is over all combinations of i and j except when $i = j$. Over the course of the simulation to $t = 8.5$ the kinetic energy decreased by about 6.0% for each of the discrete models, or by about 0.002% per time step.

Validity of Model

These results indicate that the model performs acceptably, both with panels and filaments, allowing for the roll-up of a good number of turns in the spiral and over a long period of time. The small change in impulse indicates that the time stepping and discretization procedures perform reasonably well although there is some error, noticeably in the kinetic energy which should be corrected in future work. The agreement with Pullin's results for the semi-infinite sheet is in most cases good with the exception of the initial motion of the spiral center. Perhaps a better initial definition of the unrolled part of the sheet would eliminate the oscillations noted in Figures 6.10 and 6.11 for

the vertical velocity of the spiral center. The results show that the model can be used to discern the slight ellipticity in the sheet shape due to the imposed strain field and to give useful information on the rate of roll-up and circulation distribution for other vortex sheets undergoing roll-up.

Comparison of Panels to Filaments

The primary advantage of panels over filaments is to moderately increase the accuracy of the calculations and to slightly increase the length of time that the spiral can roll-up, i.e., the number of turns that can form around the core. In trial runs, typically one or two additional turns could form in the spiral with panels before the sheet would cross over on itself. These benefits are attributed to the more accurate velocity calculation provided by the panel formulas, especially when the panels approach each other closely. However, because the distance between the spiral turns decreases rapidly as the center of the spiral is approached, the improvement seen with panels is small in terms of the number of additional turns that can form. In addition, some of the potential improvement of panels over filaments is not realized because of the sheet segment line up process that is used in the discretization procedure (Section 5.2.2). The line up feature eliminates much of the difficulty with the singularities associated with the vortex filaments because of cancellation due to the symmetry which is introduced. Therefore the potential advantage of using panels is not fully realized.

Axisymmetric Configurations

The following calculations are performed on axisymmetric vortex sheets. The panel model is applied to vortex disks of two vorticity distributions, an elliptic distribution produced by a disk which translates through a fluid at constant speed and then suddenly dissolves, i.e., the three-dimensional analogue of the elliptic wing problem, and a

distribution more typical of that for a helicopter rotor blade with the load increasing towards the tip.

6.2.2 Elliptic Loading Case

The vortex panel model is used to compute the roll-up of a circular disk of vorticity with an elliptic circulation distribution. This is a convenient test case for two reasons. First, it is the axisymmetric analogy of the frequently studied two-dimensional elliptic wake that was discussed in the previous section. Second, some features of the final rolled-up geometry are known. As described in Section 5.1, the edge of the vortex sheet is modelled as a single vortex ring of uniform vorticity which will eventually acquire all of the vorticity in the sheet due to the amalgamation process. The final characteristics of the ring may be determined by equating the strength, impulse, and kinetic energy of the ring to those of the initial disk as shown by Taylor [22]. This, of course, is not intended to imply that a single vortex ring of uniform vorticity is the correct final state of the roll-up process. Taylor finds that for the disk of elliptic loading with radius b , translating at a speed U_{ref} , the corresponding vortex ring would have a radius of $0.816b$ and a translation velocity of $0.436U_{ref}$. These values should provide a useful check towards the asymptotic limit of the simulation.

Simulation Parameters

The parameters used in this simulation are as follows:

Number of panels:	200
Portion of sheet edge initially rolled:	2.5%
Time step method:	Runge-Kutta
Δx_{maz} :	0.003

Number of time steps:	1100
Maximum number of loops in spiral:	10

Initial Model of Sheet

The initial configuration of the sheet is that which would be obtained from a circular disk translating normally to its axis which suddenly dissolves leaving a circular vortex sheet. The resulting circulation distribution is the same as that for the previous two-dimensional case

$$\Gamma = \Gamma_0 \sqrt{1 - r^2}$$

which yields a value for the uniform downwash of $U_{ref} = \pi\Gamma_0/4b$. The vorticity distribution across the sheet, obtained from the circulation as

$$\Gamma = \Gamma_0 \frac{-r}{\sqrt{1 - r^2}}$$

is illustrated in Figure 6.32 along with the initial positions of the vortex panel centers. Again, the two-dimensional tip model is used to define the initial conditions for the axisymmetric roll-up since for small values of time the axisymmetric sheet edge behaves similarly to the two-dimensional sheet. As for the two-dimensional case, the initial conditions yield an equivalent initial time of $t_0 = 0.0123$ and a tip filament containing 22% of the total strength of the sheet. The location of the tip vortex filament is $r = 0.987$ and $z = 0.021$ above the flat part of the sheet. The corresponding initial axial and radial velocity distributions, v and u , are given in Figure 6.33.

Roll-Up Before Amalgamation

The sheet roll-up computed by the vortex panel model prior to the point when 10 turns have formed in the spiral is presented in Figure 6.34 for times $t = 0.039, 0.077$, and

0.126. The sheet has formed 10 turns around the core at time $t = 0.126$ at which point the amalgamation process begins. As for the two-dimensional case, the sheet rolls up very smoothly exhibiting none of the typical chaotic behavior discussed earlier. A detailed view of the spiral region at time $t = 0.126$ is given in Figure 6.35. Comparison with Figure 6.6 reveals very little qualitative difference in the roll-up between the two-dimensional and axisymmetric sheets at this early stage. Note that the non-dimensionalization used allows for direct comparison between the two-dimensional and axisymmetric results in the non-dimensional time variable t .

The corresponding sheet strength distributions are given in Figure 6.36. As for the geometry, a comparison with the two-dimensional results show no notable differences. It is interesting to note the sharply defined location of the maximum sheet strength. The sheet inboard of this point shows very little stretching while outboard the sheet is stretched by a great amount due to the proximity of the spiral. The distance of this point from the edge of the sheet is found to vary approximately as \sqrt{t} .

The axial velocity of the tip vortex ring is found to experience the same slight oscillations during the time when the first few turns are forming as did the two-dimensional sheet, presumably for the same reasons. As can be seen in Figure 6.37 the oscillations subside after the first 3 or 4 loops but then reappear at time $t = 0.095$. The cause of the second set of oscillations is unknown, but as will be seen, they die out quickly.

The distribution of circulation within the spiral region during this period is presented in Figure 6.38 along with Pullin's result for the semi-infinite sheet. The constancy of the distribution with time is less for the axisymmetric case than it was for the two-dimensional sheet. At least part of this is due to the slightly irregular motion of the tip vortex filament since the distance plotted in the figure is measured from the tip. As for the two-dimensional case, Pullin's results indicate a slightly less concentrated spiral core than that obtained here for the axisymmetric sheet.

The total circulation in the spiral region as a function of time is presented in Figure 6.39 along with Pullin's results. The spiral region is defined to start where the sheet first becomes vertical. For the initial part of the roll-up, the agreement is very close between Pullin's results and the axisymmetric discrete model indicating that the initial roll-up is very nearly two-dimensional.

The distance of the sheet from the spiral center, \hat{r} , as a function of the angular position θ at time $t = 0.126$ is given in Figure 6.40 along with Pullin's results applied to Kaden's spiral. The small oscillations of the numerical results about the Pullin value indicate a slight ellipticity in the sheet shape. This is assumed to be caused by the strain field imposed on the spiral from the rest of the sheet. The sheet strength distribution as a function of θ is given in Figure 6.41 at time $t = 0.126$.

Roll-Up After Amalgamation

The roll-up calculations are continued past time $t = 0.126$ by using the amalgamation procedure to limit the number of turns in the spiral to 10. As for the two-dimensional case, 10 turns was selected as a compromise between achieving good resolution in the spiral and suffering from numerical inaccuracy due to the vortex elements approaching each other too closely in the inner turns. The sheet geometry and strength distributions are presented in Figures 6.42 and 6.43 respectively for times $t = 0.32$, 0.65 , and 1.52 when the calculation was stopped. The results are characterized by smooth roll-ups with no chaotic behavior. A feature of the axisymmetric roll-up that is not present in the two-dimensional case is the development of the asymmetry in the spiral which becomes apparent by time $t = 1.52$. The spiral has taken on a distinctly lopsided appearance with the outer most turn expanding inward and upward. Examination of the sheet strength distributions reveals the development of a local concentration of circulation in that part of the sheet. This is undoubtedly a function of the axisymmetric nature of

the sheet since it is not present at all in the two-dimensional case.

The axial velocity of the tip ring, v_{tip} , is shown in Figure 6.44 along with the asymptotic value given by Taylor of $v = -0.436$. After the previously mentioned second set of oscillations dies out, the asymptotic value is approximately reached at time $t = 1.02$. At this point, about 73% of the circulation has been rolled into the spiral as can be seen in Figure 6.45, where the spiral circulation is plotted against time. By the end of the simulation at time $t = 1.52$, about 80% of the circulation has been absorbed by the spiral.

The circulation distribution in the spiral as a function of radius is presented in Figure 6.46. The lack of symmetry in the spiral at large values of time is responsible for the jagged appearance of the curves. However, the inner turns of the spiral are more uniform and show a similar concentration of vorticity as time increases as was seen for the two-dimensional case.

The distance of the sheet from the spiral center, \hat{r} , and the sheet strength distribution, γ , as functions of θ are presented in Figures 6.47 and 6.48 respectively. The oscillations in the plot of $\hat{r}(\theta)$ are much larger compared to the earlier time indicating that the spiral turns are becoming more elliptic, especially the outermost turns.

The fluid impulse is seen to vary by about 1% over the duration of the simulation, or, about 0.001% per time step. This is about 5 times larger than the error realized in the two-dimensional case and is attributed to the approximations made in the derivation of the velocity formulas for the vortex panels.

6.2.3 Helicopter Loading Case

Configuration Description

A vortex disk similar qualitatively to that which would be produced by a single helicopter rotor blade with the load increasing towards the tip is modelled as an example of a more complex vorticity distribution. The rotor blade loading and resulting vorticity distribution across the sheet are given by

$$\Gamma(r) = \Gamma_0 r^2 \sqrt{1 - r^2} \quad (6.2)$$

$$\gamma(r) = \Gamma_0 \frac{d}{dr} (r^2 \sqrt{1 - r^2}) \quad (6.3)$$

Note that inboard of $r = 0.82$, the sheet strength is positive and outboard of $r = 0.82$ it is negative with the total circulation of the sheet equal to zero. In a gross sense, this is equivalent to two coplanar vortex rings of equal but opposite strength at different radii. As will be seen, the resulting sheet motion agrees with this interpretation.

The nature of the roll-up for this case is fundamentally different from that of the elliptic loading case in that there are two regions on the sheet of high vorticity concentration. The first is at the edge of the sheet as for the elliptic loading and the second is inboard at a radius of about $r = 0.52$. Apparently these differences in sheet strength distributions have resulted in some undesirable effects in the roll-up calculations. The sheet repeatedly experienced instabilities at the inner point of maximum sheet strength. These were characterized by an oscillation in the sheet strength distribution near the point of maximum strength with a period of about 9 or 10 panel widths. A similar phenomenon was observed by Sugioka [21] where the period of oscillation was about 11 panel widths. It was found that the instability could be delayed significantly by replacing the cubic fit of the circulation in the rediscrretization procedure with a linear function. In addition, increasing the number of vortex panels tends to aggravate the problem. For example, using 200 panels to model the sheet results in the sheet becoming

unstable before the secondary inner vortex can begin to form. Since this is one of the more interesting features of the flow, it was necessary to reduce the number of panels from that for the elliptic loading case to increase the length of time that a valid roll-up could be observed. For this reason, the calculation was limited to 160 panels. Also, because of the much greater lengthening of the sheet due to the stretching realized in this case, only four spiral loops are allowed to form around the tip ring in order to minimize the total sheet length and maximize the panel density along the sheet.

Simulation Parameters

The parameters used in this simulation are as follows:

Number of panels:	160
Portion of sheet edge initially rolled:	2.5%
Time step method:	Runge-Kutta
Δx_{max} :	0.003
Number of time steps:	1900
Maximum number of loops in spiral:	4

Initial Model of Sheet

The initial sheet geometry and sheet strength distributions are shown in Figure 6.49. Two and one half percent of the outer portion of the sheet accounts for about 55% of the negative vorticity leaving the sheet itself to be of mostly positive vorticity. The location of the tip ring is determined as for the previous case, by applying Kaden's solution to the outer part of the sheet, although its validity is somewhat more questionable here since the helicopter circulation distribution is even further removed from the parabolic one of

the semi-infinite sheet than that of the elliptic loading. The radial and axial location of the tip vortex ring are the same as for the elliptic case, $r = 0.987$ and $z = 0.021$ above the plane of the flat part of the sheet which is taken as $z = 0$ at $t = t_0$. The initial time is also the same, $t_0 = 0.0123$.

The initial axial and radial velocity distributions, v and u , are shown in Figure 6.50. Although a simple analytic expression for the initial downwash distribution is not available in this case, the computed results at least appear as would be expected with the interpretation of the sheet mentioned before as two coplanar vortex rings. The inner part of the sheet is moving upward and the outer part is moving downward. The initial radial velocity of the sheet is very similar to that of the previous case as is expected since the properties of the tip ring for the two cases are nearly the same.

Sheet Roll-Up

The sheet geometry for a series of times to $t = 3.51$ is presented in Figures 6.51 and 6.52 and the corresponding sheet strength distribution in Figures 6.53 and 6.54. The resulting sheet motion yields two distinct regions on the sheet. The outer region shows a roll-up very similar to that for the elliptically loaded disk especially up to a time of $t = 0.66$. This is not unexpected in that the sheet strength is very similar for the two cases near the edge. Four spiral turns, the maximum, are formed at time $t = 0.076$ after which the amalgamation procedure lumps any additional turns into the tip filament. The inner region of the sheet initially shows a smooth upward motion opposite that of the outer part of the sheet. This is due to the oppositely signed vorticity in this region.

As the roll-up progresses, the part of the sheet with the positively signed vorticity begins to move into the outer layers of the spiral. This is made evident by the swelling of the outer turn starting at time $t = 0.66$. By the end of the simulation the oppositely signed vorticity has caused the outer turn to move away from the spiral considerably,

especially in the inboard upper quarter. The amalgamation process resulted in the tip vortex filament absorbing about 95% of the negative vorticity in the sheet.

The most interesting feature of the flow is the development of the secondary concentrated inner vortex structure seen to be forming at a radius of about $r = 0.45$ and a height of $z = -0.15$ at time $t = 1.94$. Comparison with the sheet strength distributions indicates that the location of the inner vortex corresponds to the very strong maximum observed at an arc length of $s = 0.95$. As time increases the maximum becomes more and more sharply defined until it consists of only a few of the vortex panels. This maximum is a remnant of the original peak in the positive vorticity distribution at time $t = 0$ and occurs at very nearly the same material particle. The position of the material particle which was at the peak at time $t = 0$ is indicated in the sheet strength figures by the large solid dot. By the end of the simulation, this particle has moved away from the peak by only two or three panel widths. Although it seems clear that the inner vortex structure would assume the configuration of a double branched spiral if the simulation could be run for long enough, it would take a very long time, i.e., the inner and outer roll-up proceed at very different rates. By the end of the simulation, the inner vortex structure has formed about one half of a spiral turn.

The calculations invariably break down shortly after this point as the sheet crosses over itself in the region of the inboard secondary vortex. This is assumed to be caused by the very high strength of a few of the panels as is seen in Figure 6.54 at time $t = 3.51$. The very high concentration of vorticity that is forming in the secondary vortex spiral would perhaps be best handled by another concentrated filament as was done by Hoeijmakers and Vastra [9].

Examination of the sheet strength at times $t = 2.57$ and $t = 3.51$ in Figure 6.54 reveals the development of a potential instability in the sheet at a point just inboard of the sharp maximum coinciding with the inner vortex. The fluctuations of strength,

which become larger with time, are characteristic of the instability that has resulted in unsuccessful runs with larger numbers of panels. However, in this case the disturbance grew slowly enough so that the simulation was able to continue to the point when the secondary inboard vortex could develop.

The axial velocity of the tip filament, v_{tip} , is given in Figure 6.55. The inset in the Figure details the motion for early times. Initially the motion is very similar to that for the elliptic loading case but for later times the increase in speed is less due to the lesser total negative circulation in the spiral. This case shows more of the erratic behavior of the tip filament as the first few turns are formed than was seen in the elliptic loading case. This may be partly because the inner spiral model is based on a parabolic circulation distribution which is not very accurate away from the sheet edge in the helicopter loading case. Therefore for larger values of time the entrainment of the increasingly non-parabolic circulation distribution into the spiral is likely to have an effect on the inner spiral characteristics which is not accounted for in this model.

The total circulation of the edge roll-up is shown in Figure 6.56 against time. The different nature of the loading for the helicopter case is apparent when comparing this Figure against the corresponding one for the elliptic loading case. Initially, the results are consistent with Pullin's for the semi-infinite sheet as they should be considering that the sheet edges are similar. However, at time $t = 0.83$ the circulation in the spiral reaches a maximum at which point it contains all of the negative vorticity in the sheet and then begins rolling up the positive vorticity resulting in the total spiral strength being reduced. The spiral strength is reduced by about 12% from time $t = 0.83$ to $t = 3.51$ at the end of the simulation due to the addition of the positive vorticity.

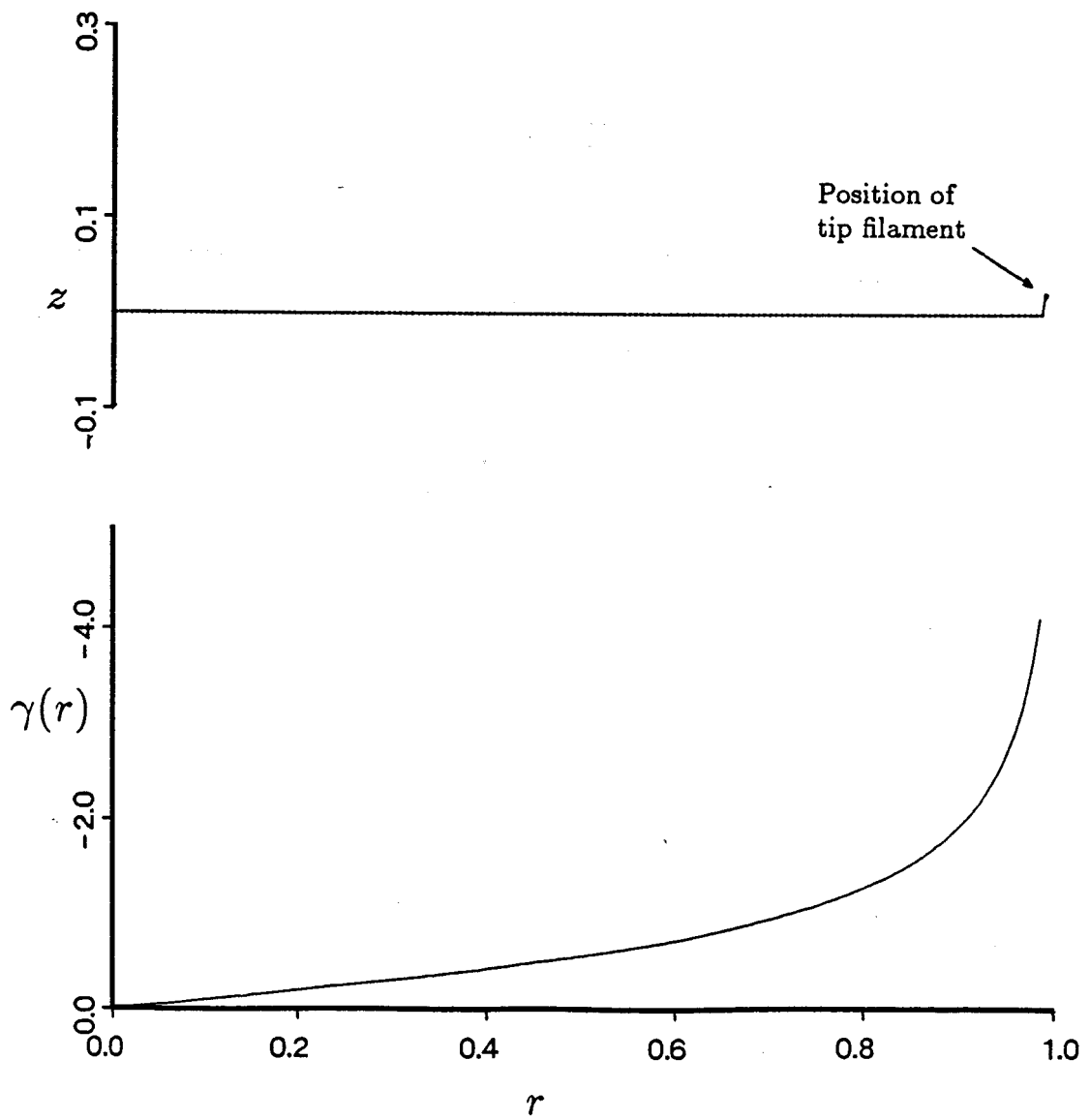


Figure 6.1: Initial Filament Placement and Sheet Strength Distribution for the Two-Dimensional Sheet

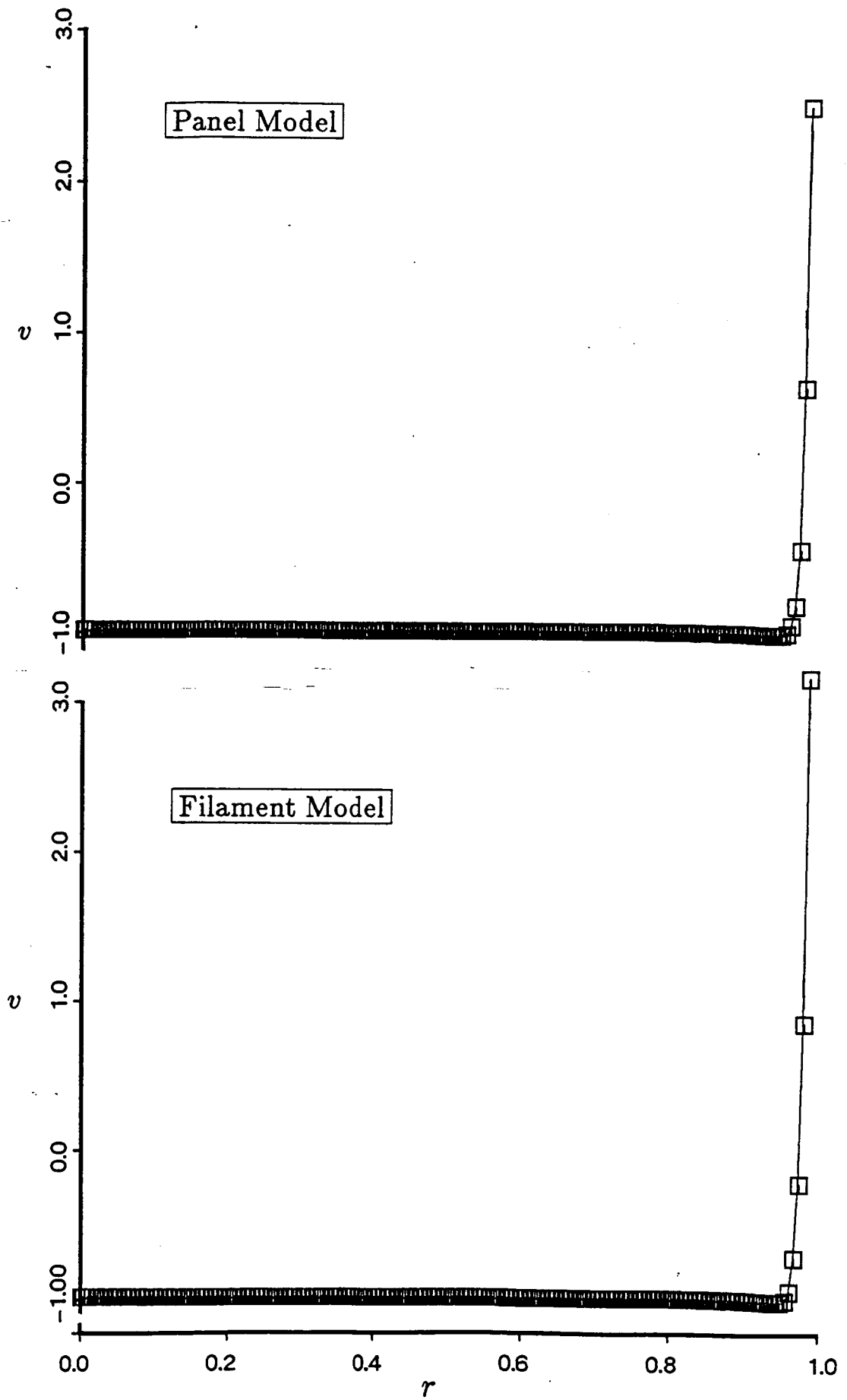


Figure 6.2: Vertical Velocity Distribution at Time $t = t_0$ for the Panel and the Filament Models

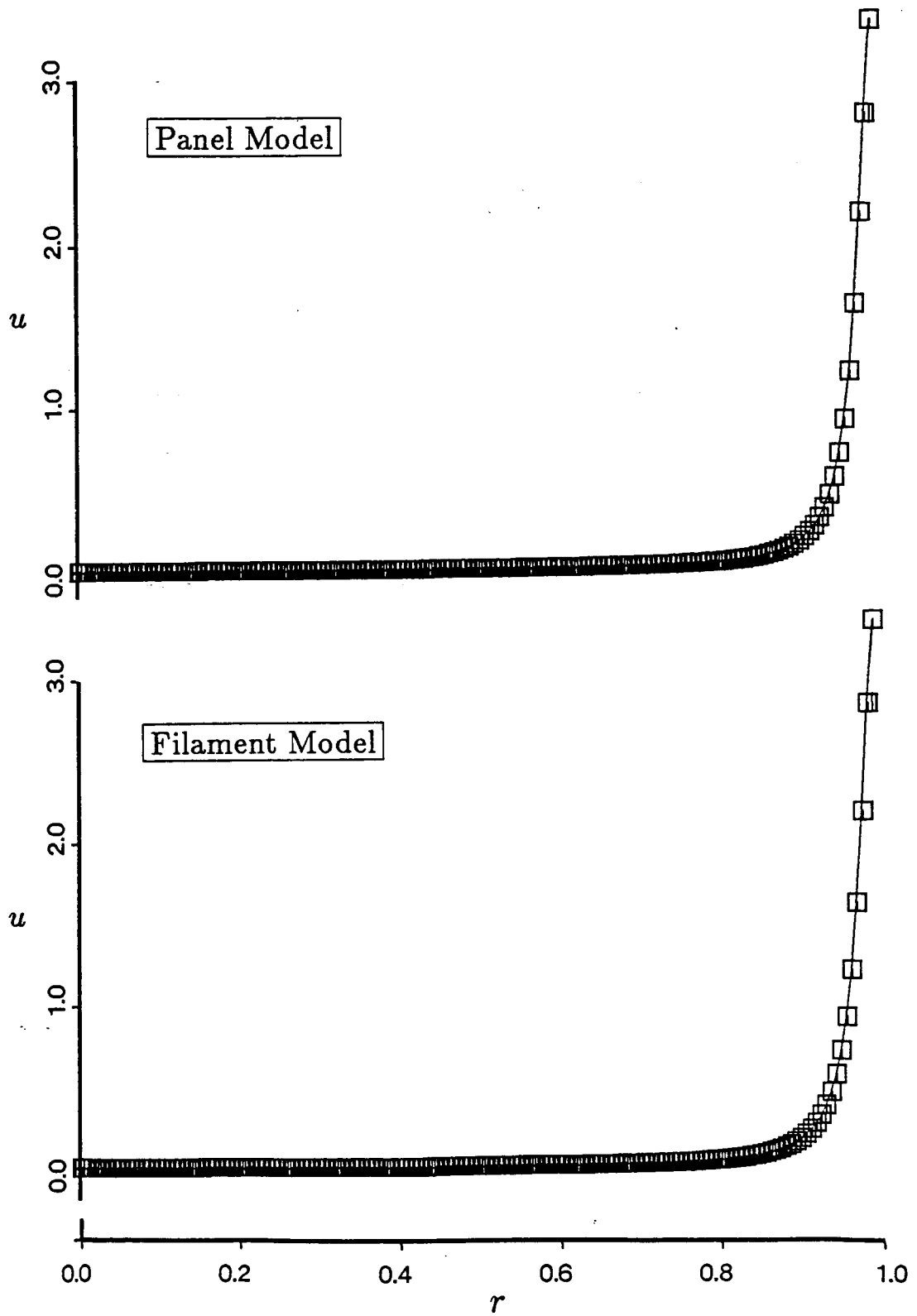


Figure 6.3: Horizontal Velocity Distribution at Time $t = t_0$ for the Panel and the Filament Models

These curves have been displaced vertically
by the amount indicated for clarity

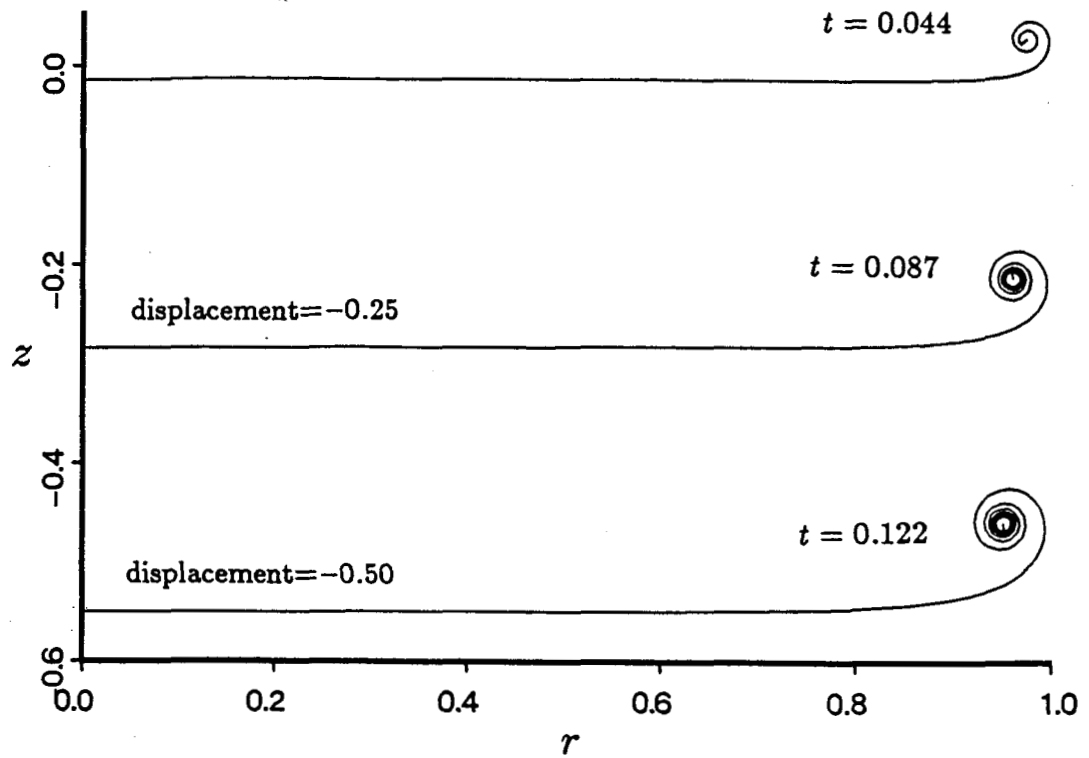


Figure 6.4: Sheet Roll-Up Before Amalgamation - Panel Model
Two-Dimensional Sheet

These curves have been displaced vertically
by the amount indicated for clarity

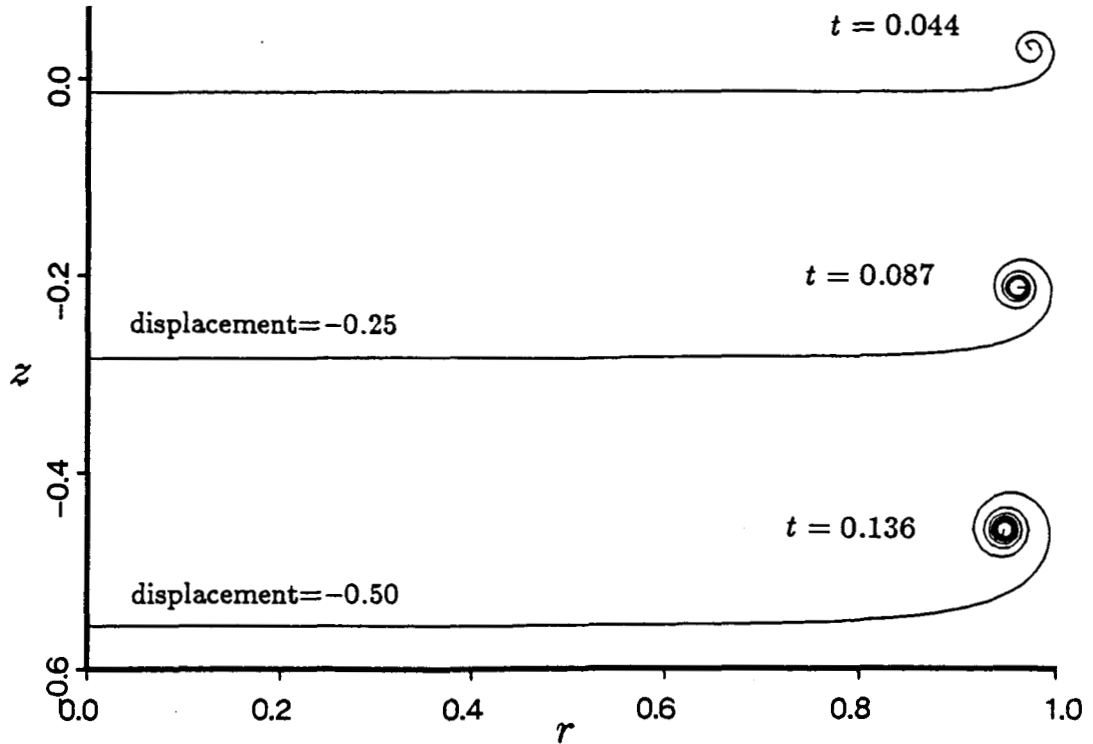


Figure 6.5: Sheet Roll-Up Before Amalgamation - Filament Model
Two-Dimensional Sheet

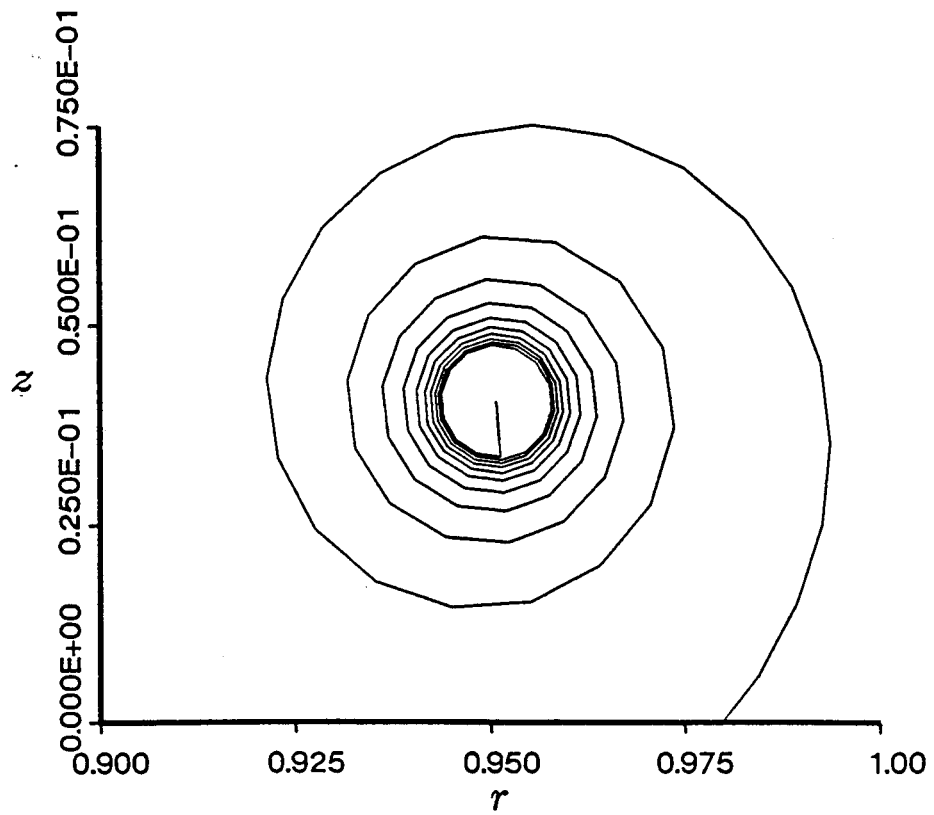


Figure 6.6: Enlargement of Spiral Region With Ten Turns – Panel Model
Two-Dimensional Sheet

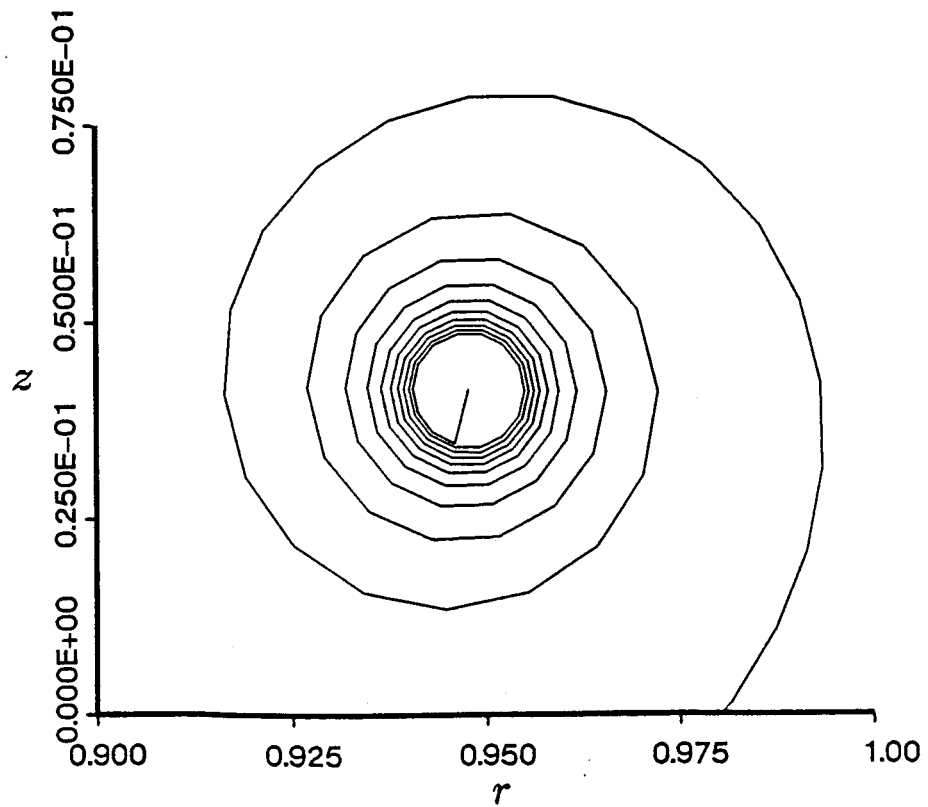


Figure 6.7: Enlargement of Spiral Region With Ten Turns – Filament Model
Two-Dimensional Sheet

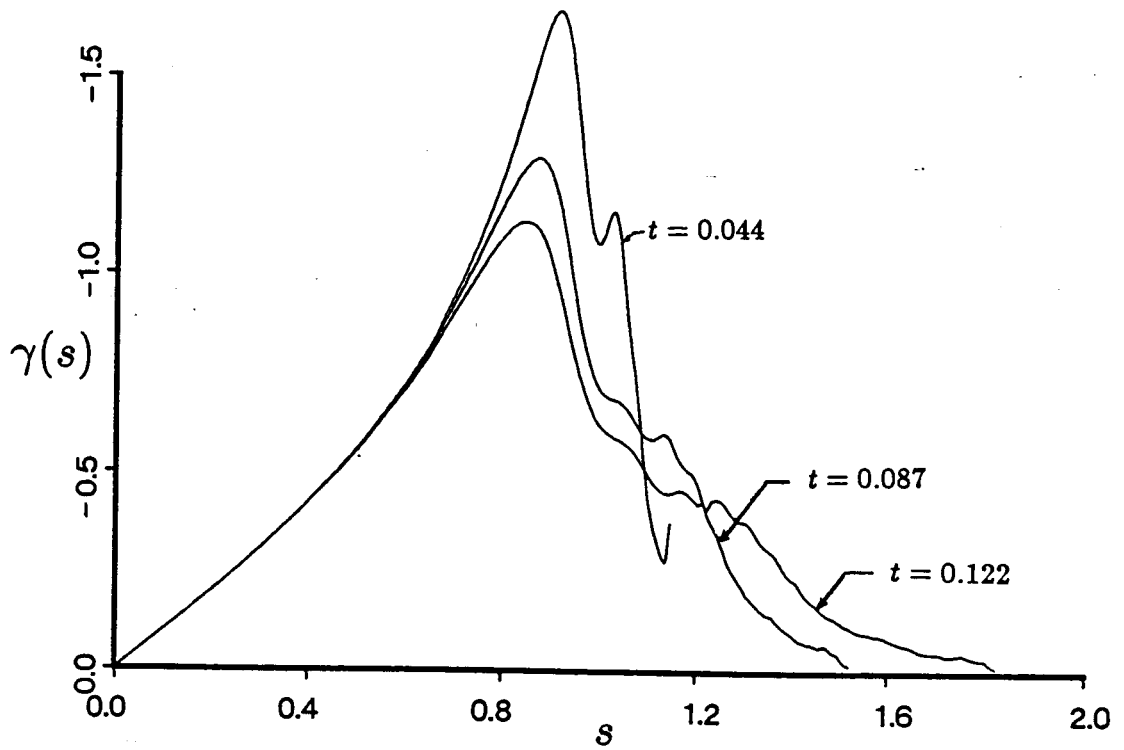


Figure 6.8: Sheet Strength Distribution to $t = 0.122$ - Panel Model
Two-Dimensional Sheet

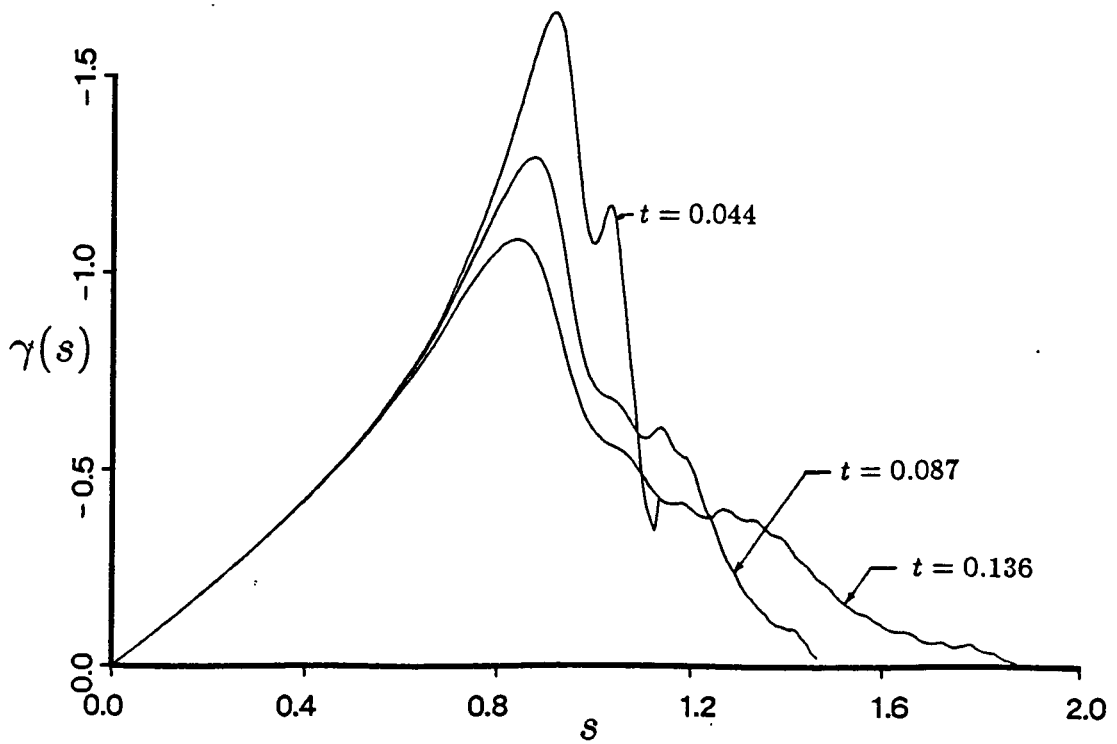


Figure 6.9: Sheet Strength Distribution to $t = 0.136$ - Filament Model
Two-Dimensional Sheet

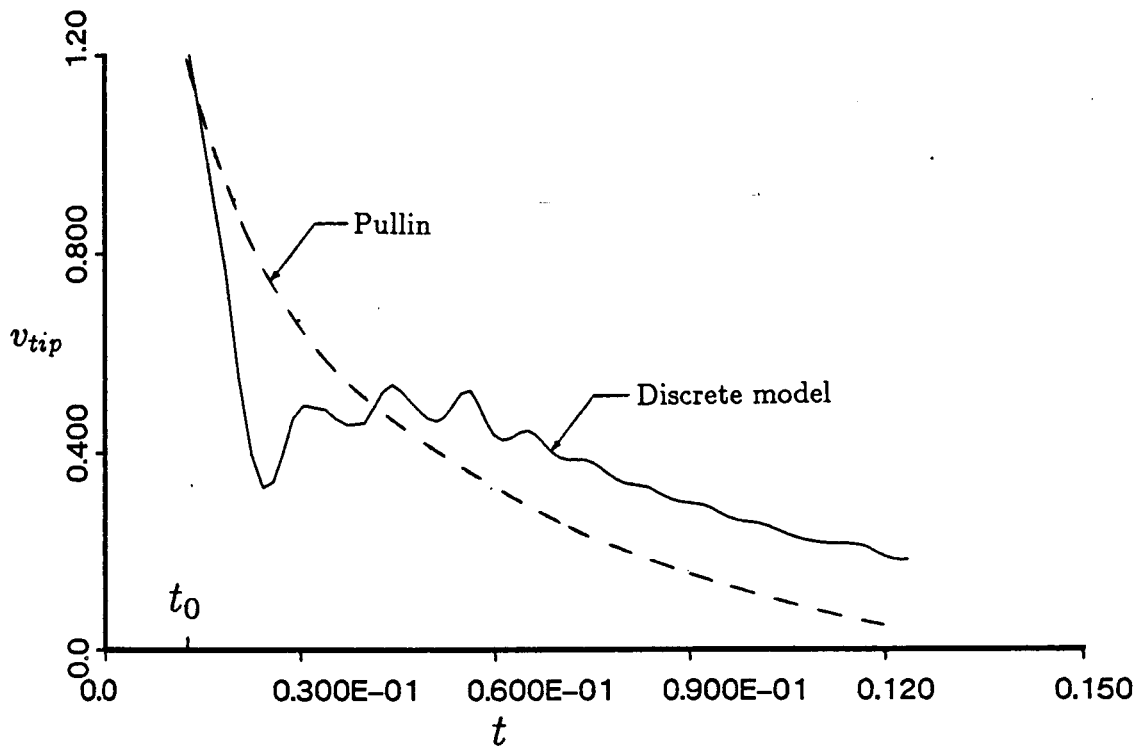


Figure 6.10: Vertical Velocity of the Spiral Center to $t = 0.122$ - Panel Model
Two-Dimensional Sheet

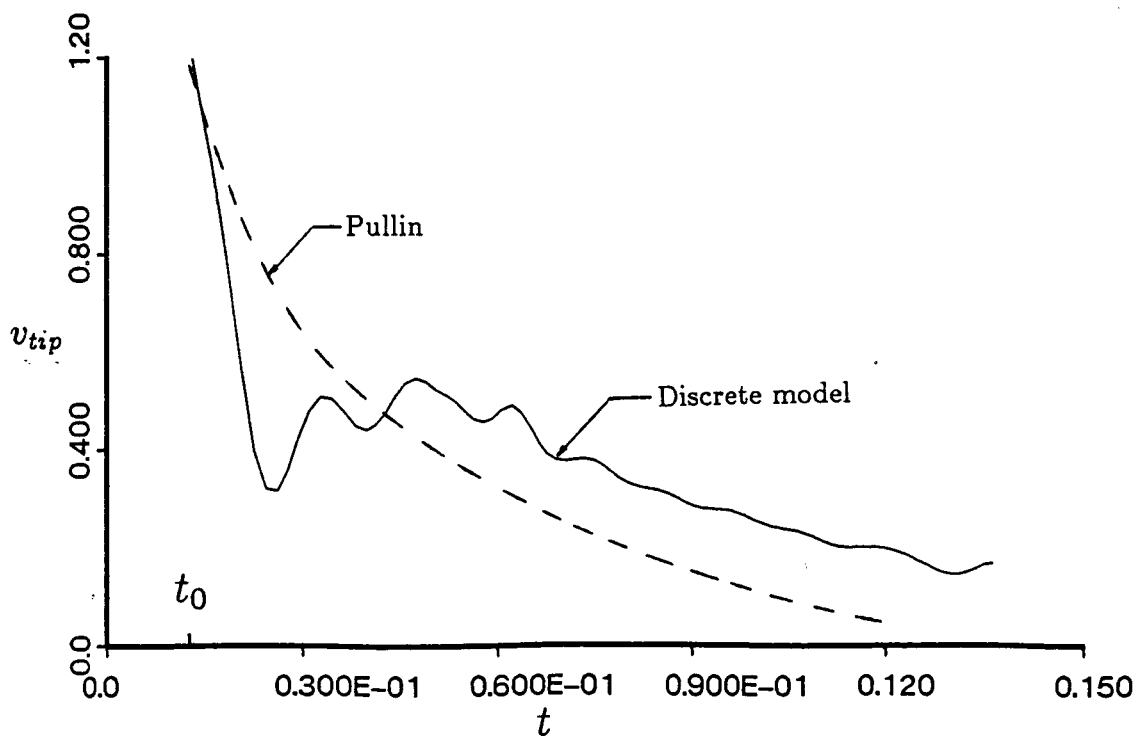


Figure 6.11: Vertical Velocity of the Spiral Center to $t = 0.136$ - Filament Model
Two-Dimensional Sheet

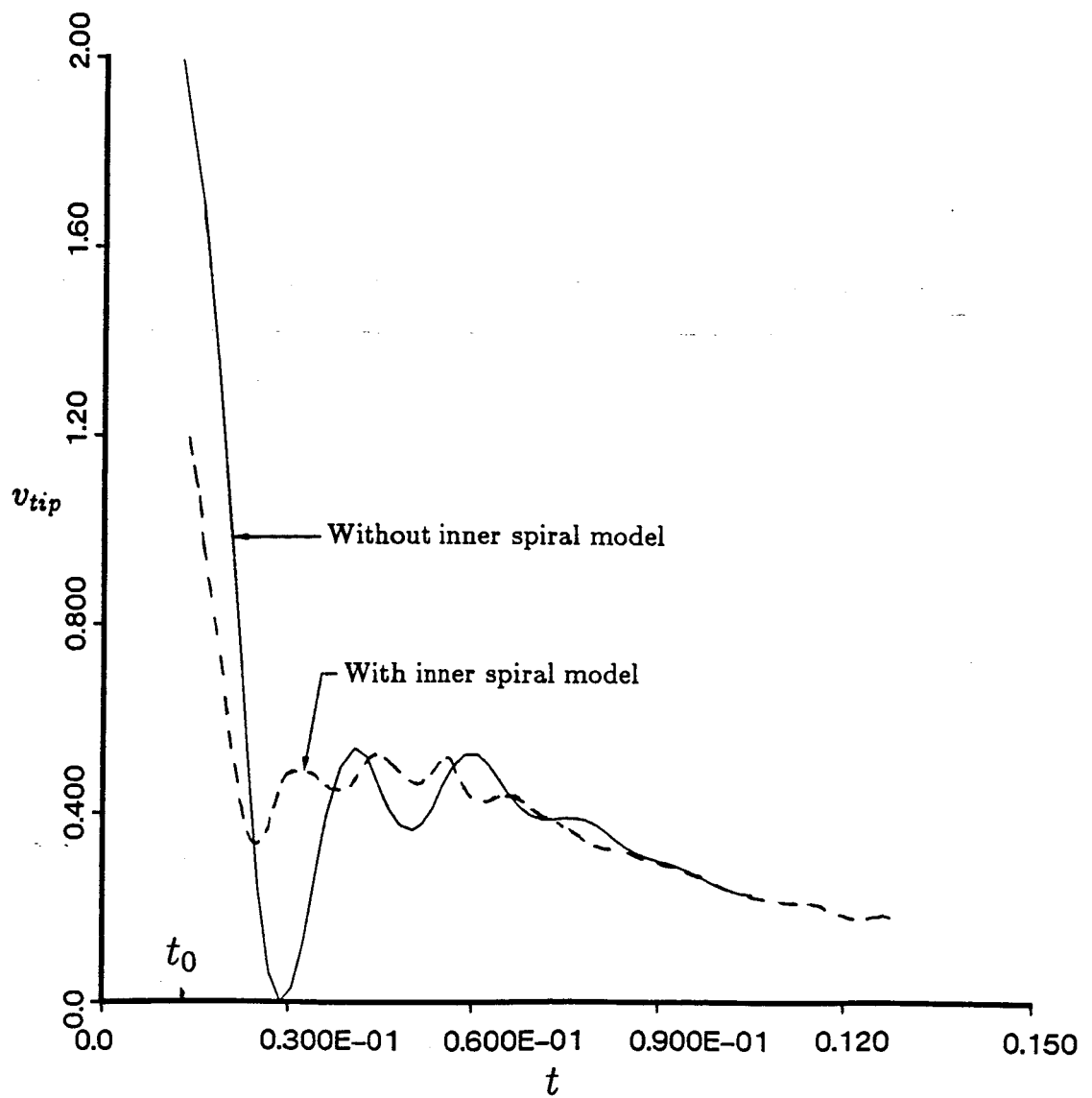


Figure 6.12: Effect of Inner Spiral Model on Tip Filament Vertical Velocity

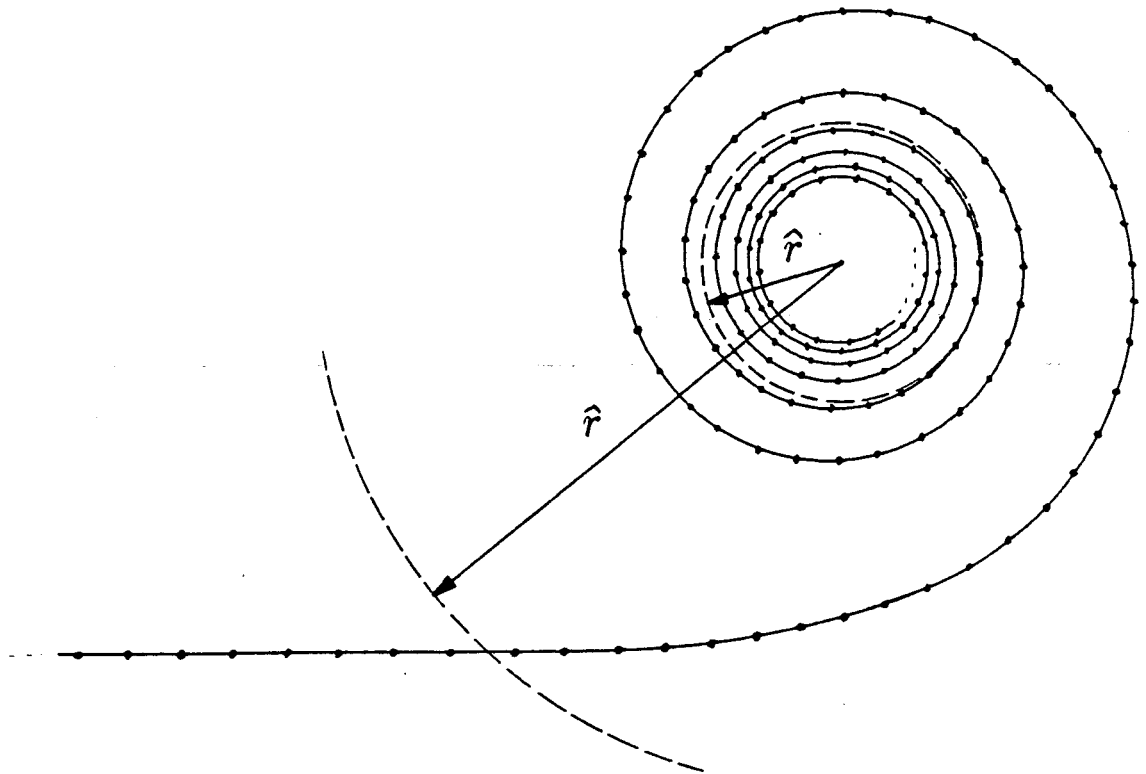


Figure 6.13: Definition of Radial Circulation Distribution

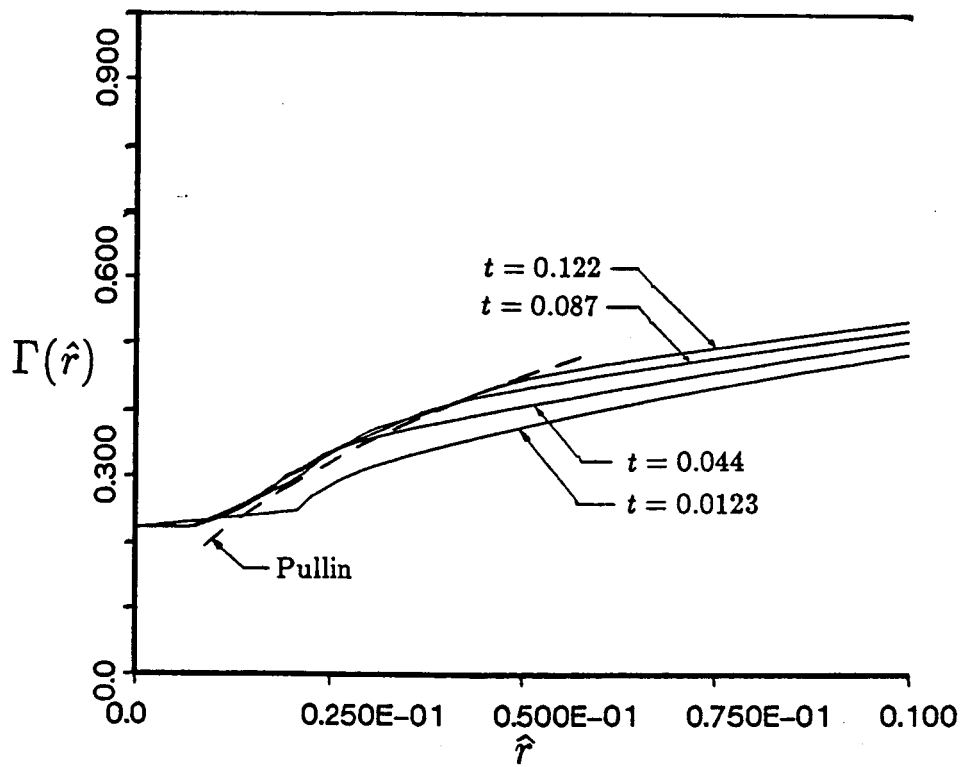


Figure 6.14: Radial Distribution of Circulation to $t = 0.122$ - Panel Model Two-Dimensional Sheet

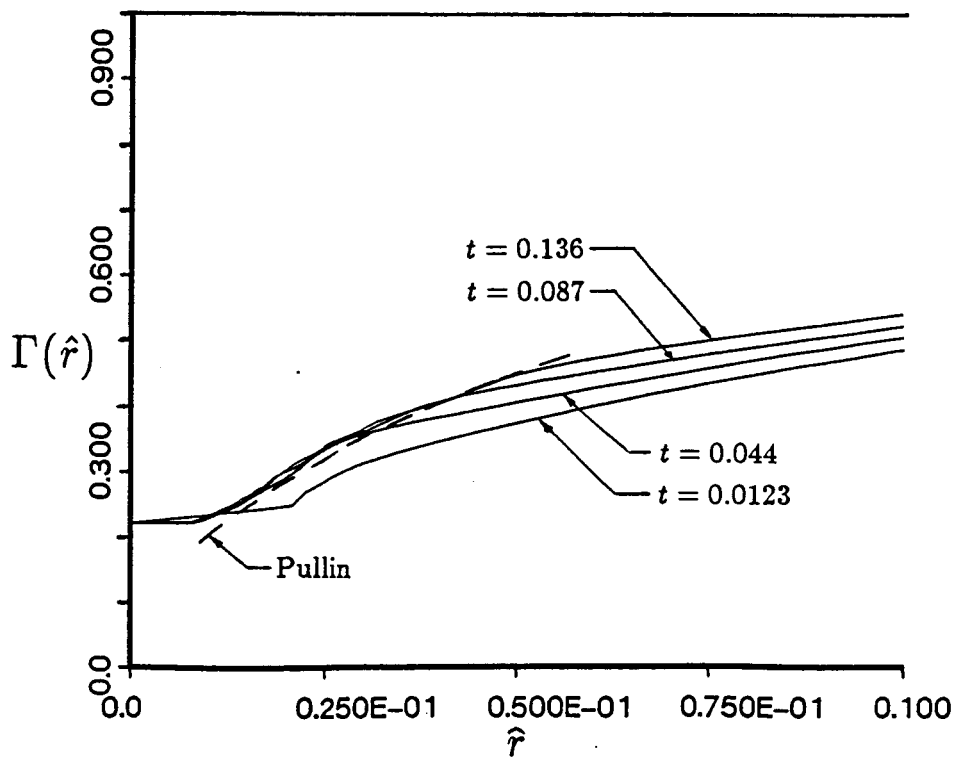


Figure 6.15: Radial Distribution of Circulation to $t = 0.136$ - Filament Model Two-Dimensional Sheet

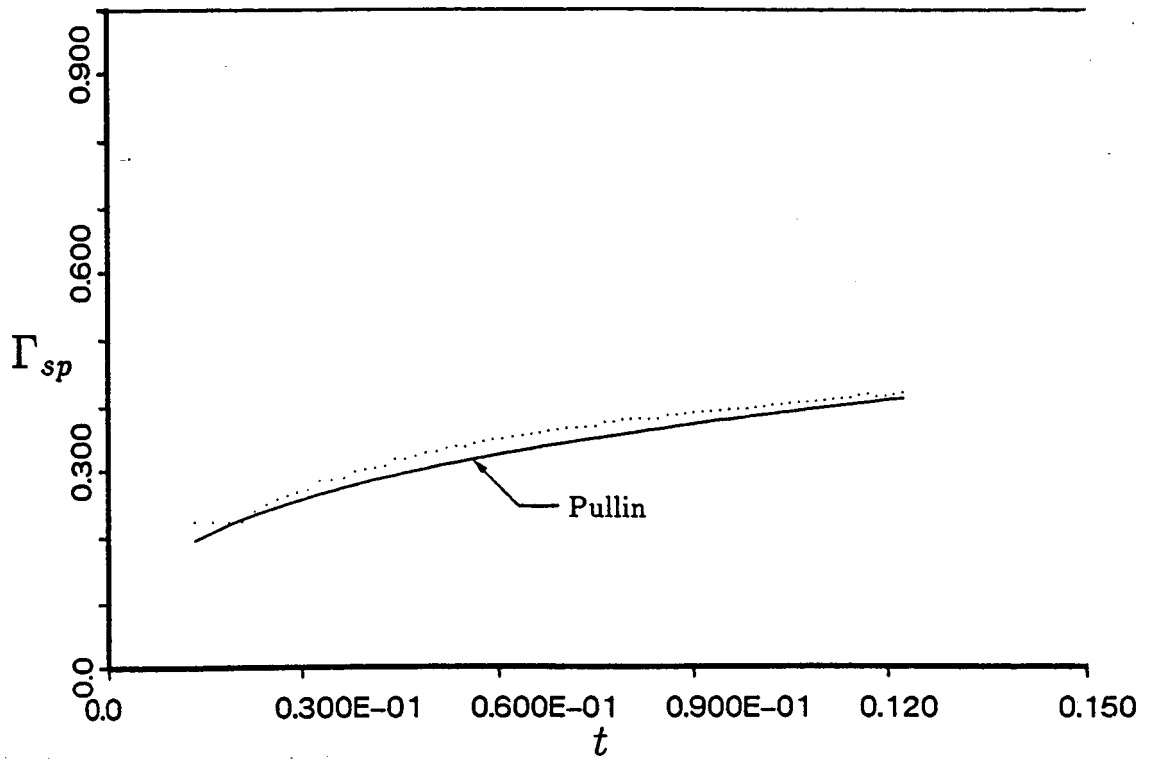


Figure 6.16: Circulation Contained in Spiral to $t = 0.122$ - Panel Model Two-Dimensional Sheet

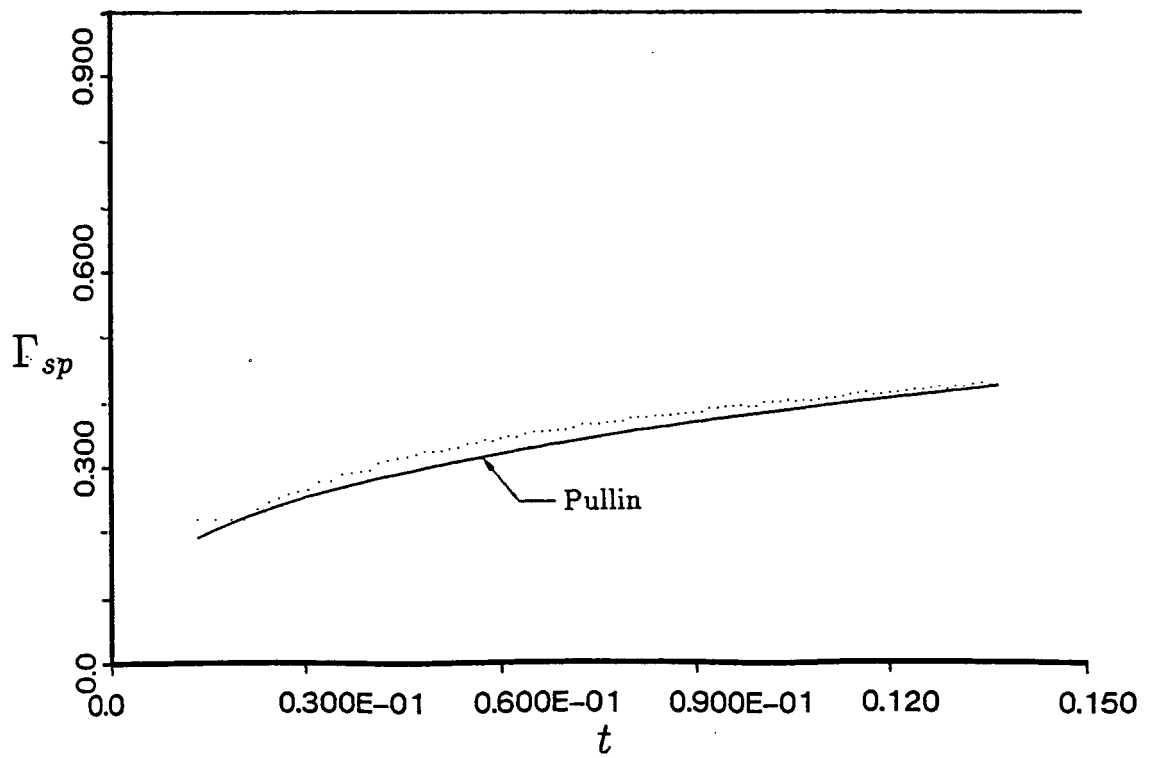


Figure 6.17: Circulation Contained in Spiral to $t = 0.136$ - Filament Model Two-Dimensional Sheet

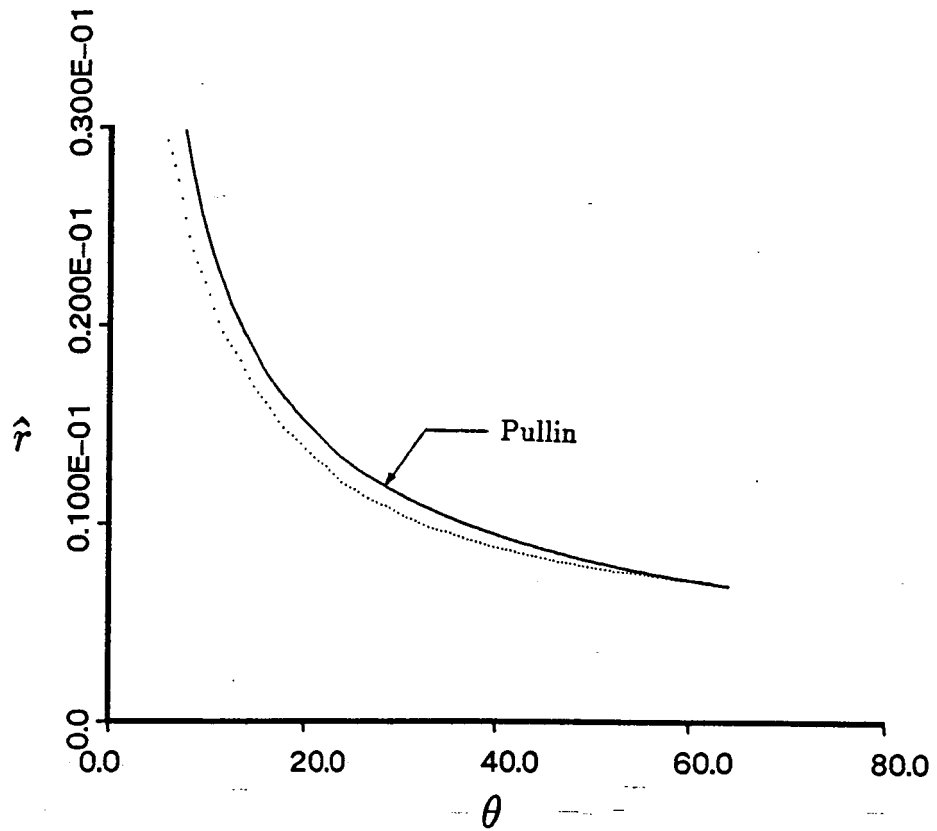


Figure 6.18: Distance of Sheet From Spiral Center at $t = 0.122$ - Panel Model Two-Dimensional Sheet

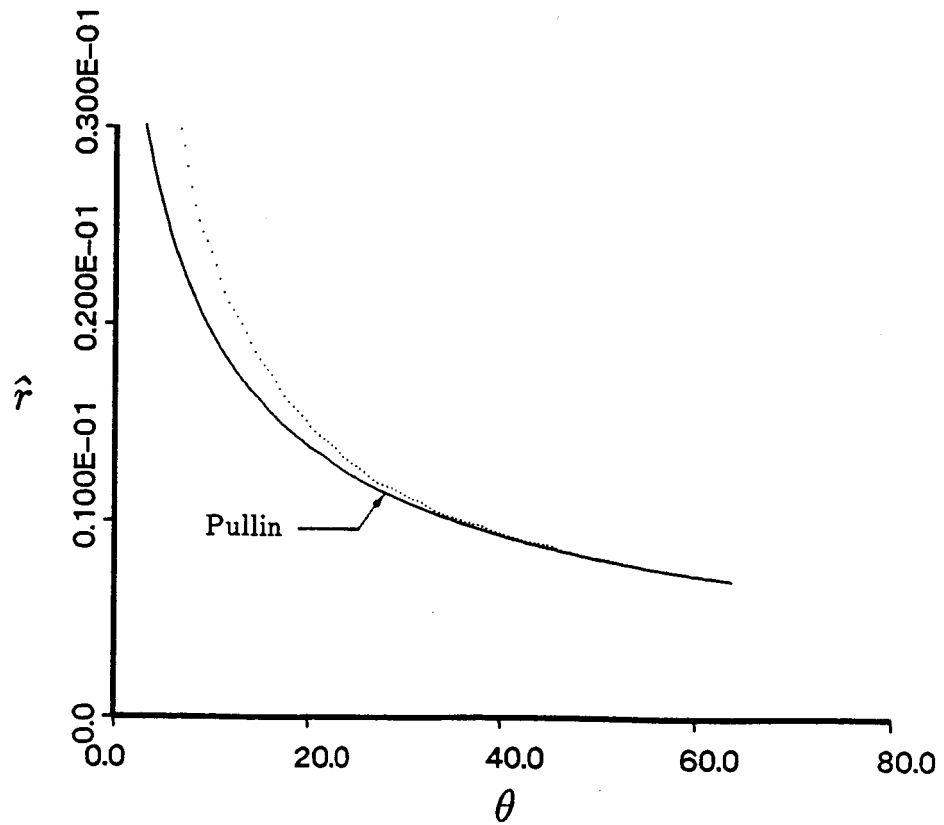


Figure 6.19: Distance of Sheet From Spiral Center at $t = 0.136$ - Filament Model Two-Dimensional Sheet

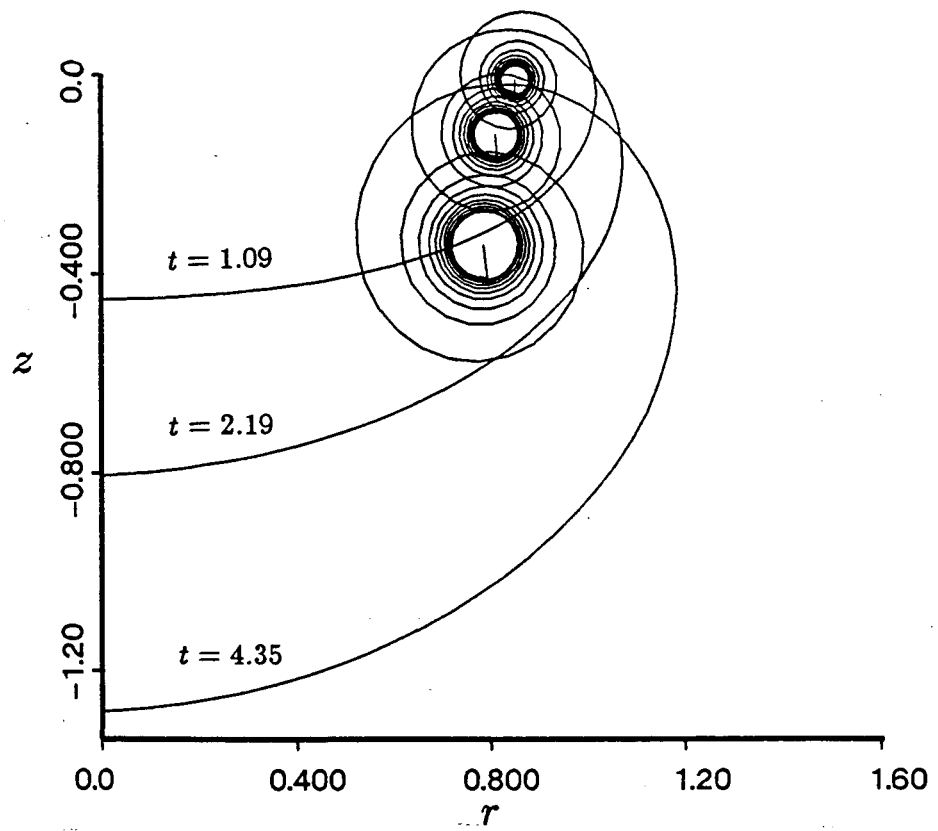


Figure 6.20: Sheet Geometry to $t = 4.35$ - Panel Model
Two-Dimensional Sheet

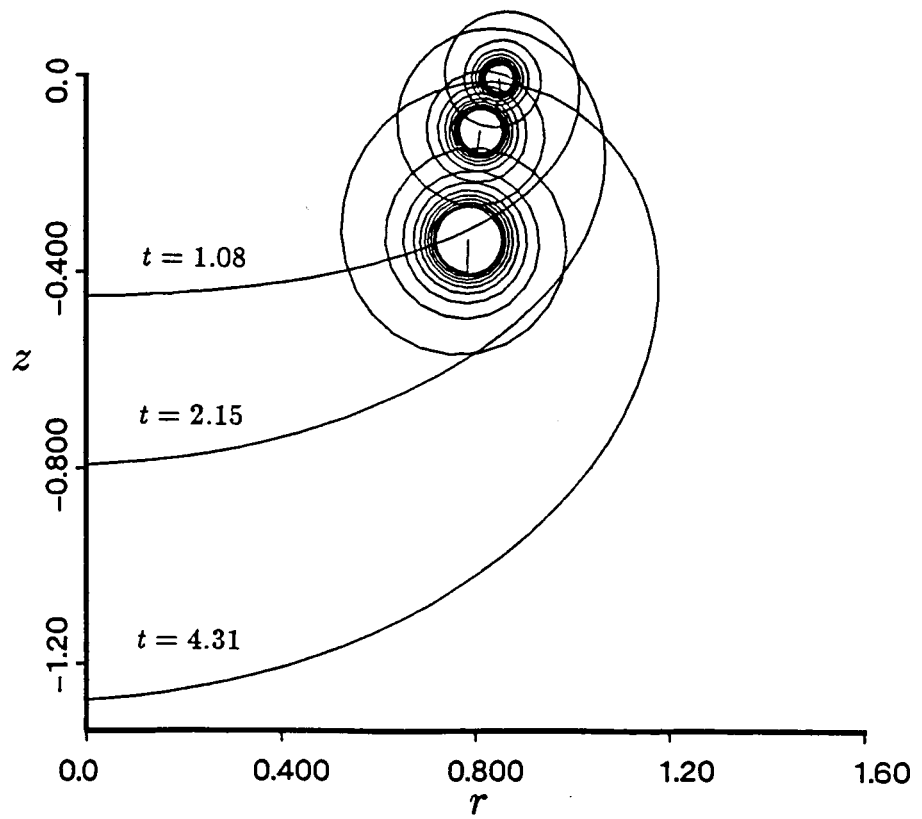


Figure 6.21: Sheet Geometry to $t = 4.31$ - Filament Model
Two-Dimensional Sheet

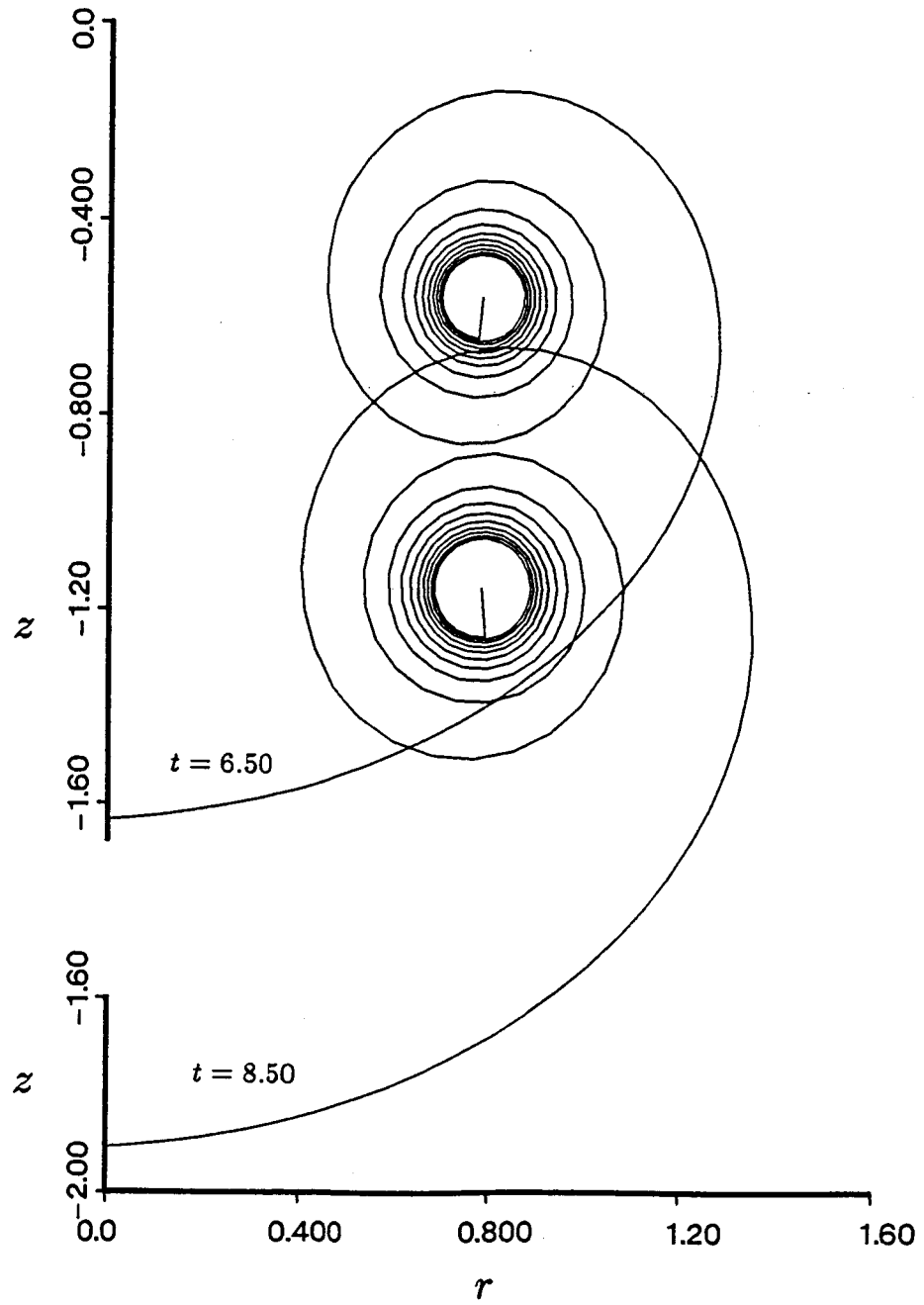


Figure 6.22: Sheet Geometry to $t = 8.50$ – Panel Model
Two-Dimensional Sheet

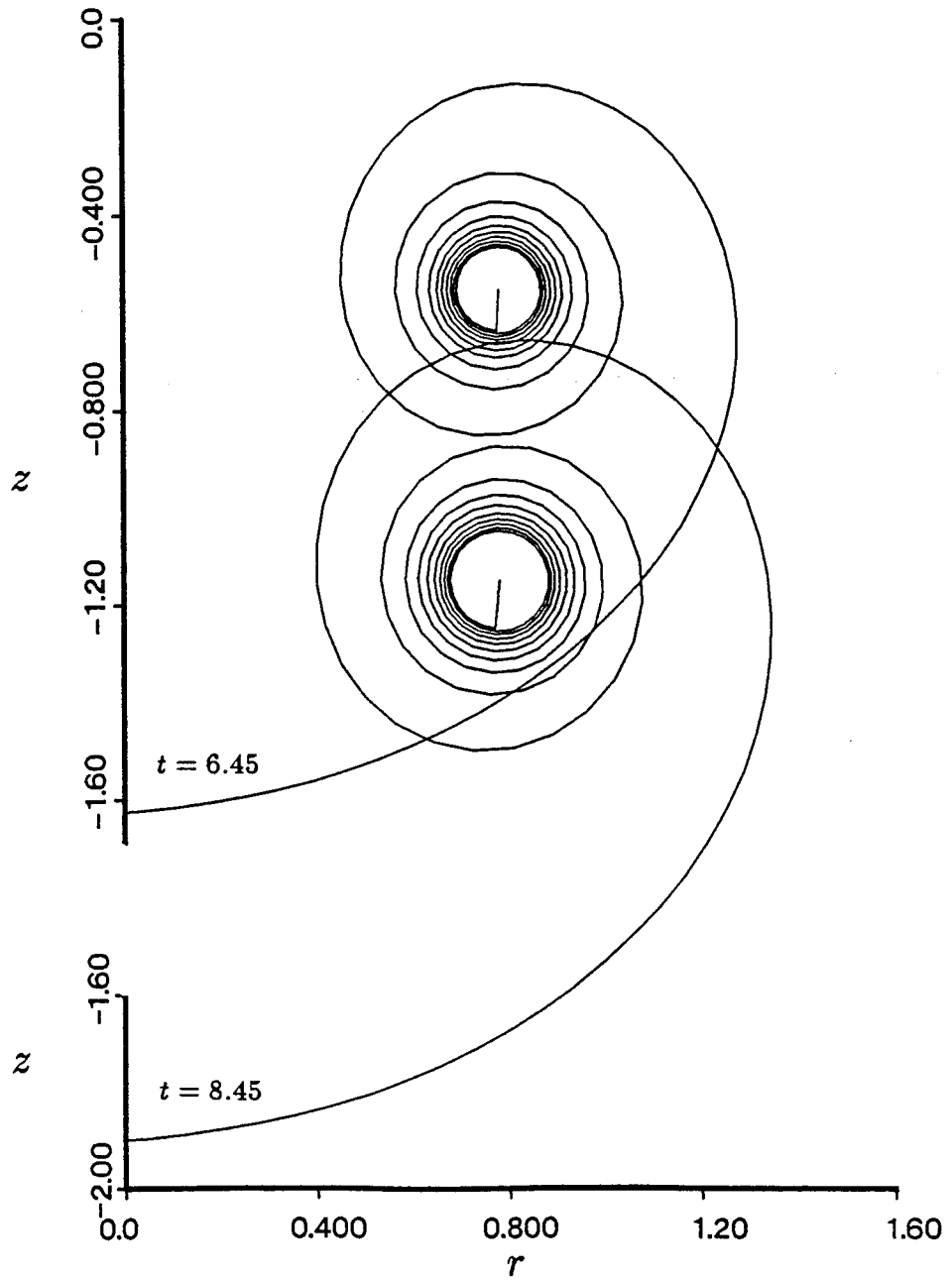


Figure 6.23: Sheet Geometry to $t = 8.45$ - Filament Model
Two-Dimensional Sheet

C. 2

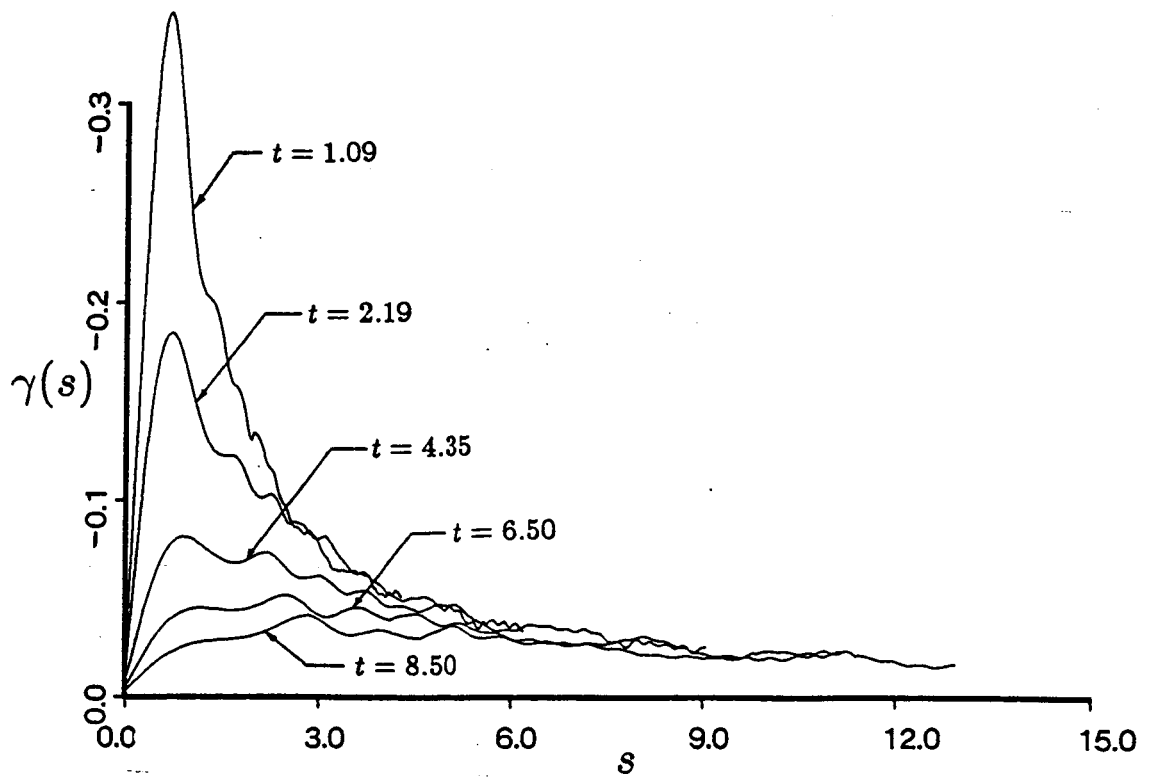


Figure 6.24: Sheet Strength Distribution to $t = 8.50$ - Panel Model Two-Dimensional Sheet

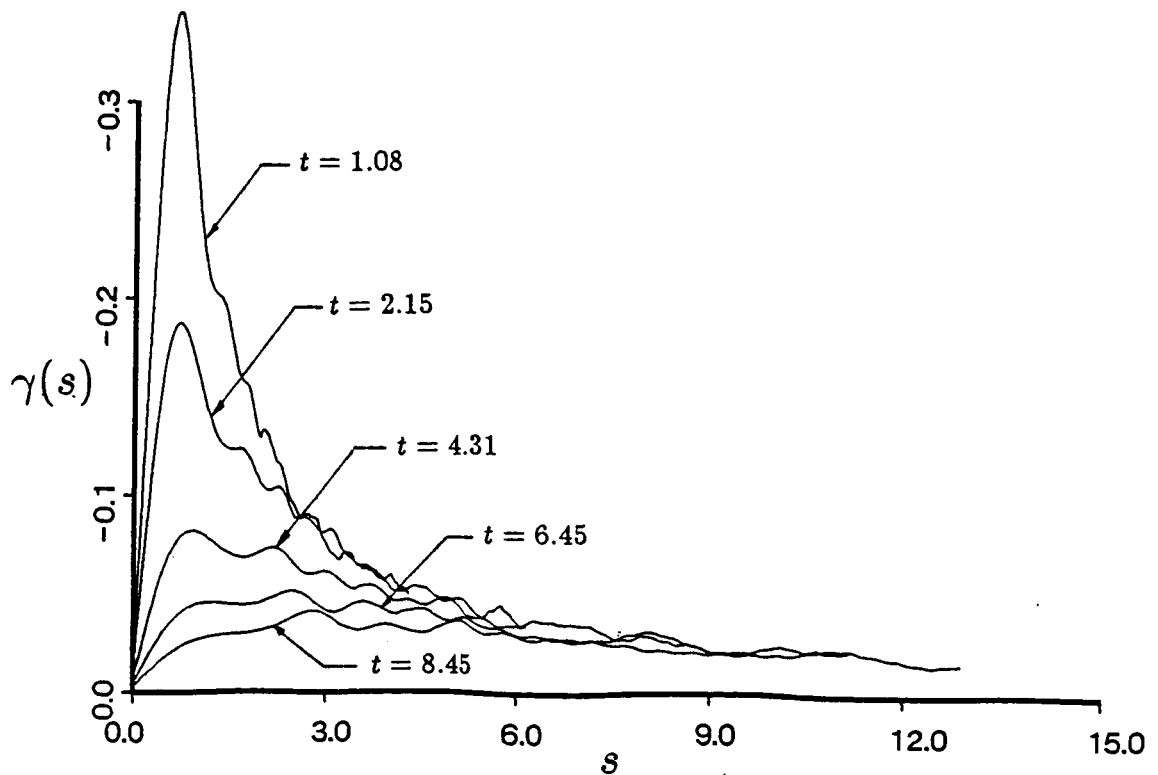


Figure 6.25: Sheet Strength Distribution to $t = 8.45$ - Filament Model Two-Dimensional Sheet

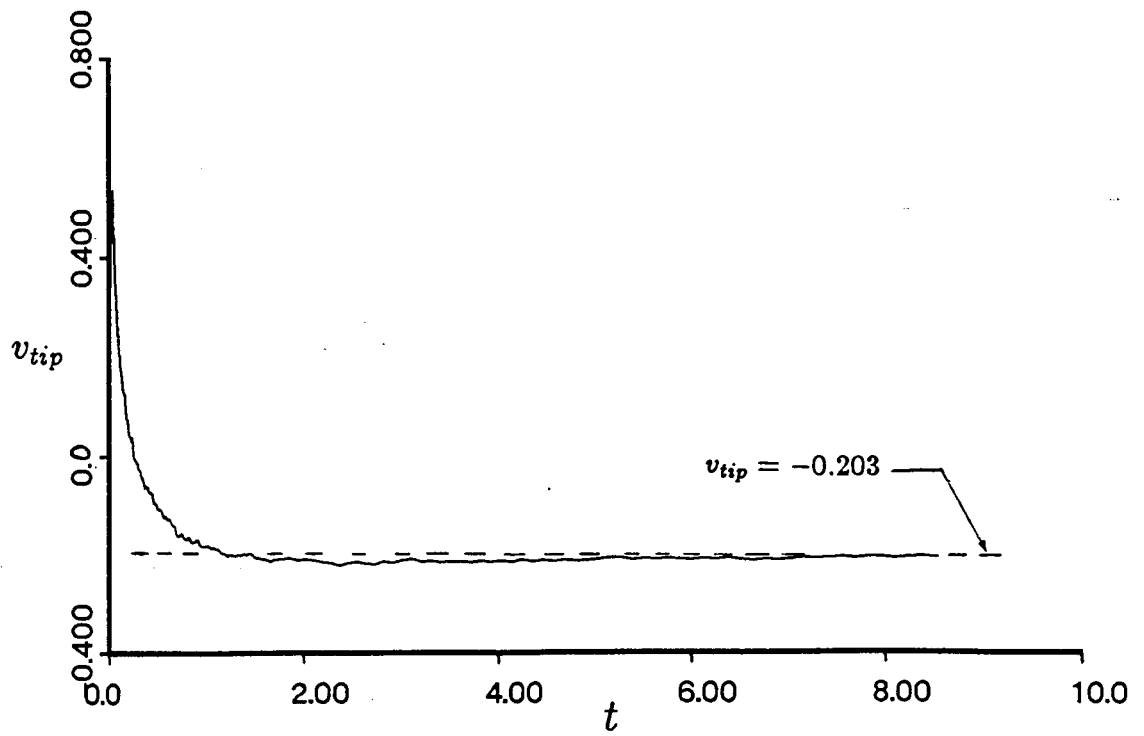


Figure 6.26: Vertical Velocity of the Spiral Center Filament to $t = 8.50$ - Panel Model
Two-Dimensional Sheet

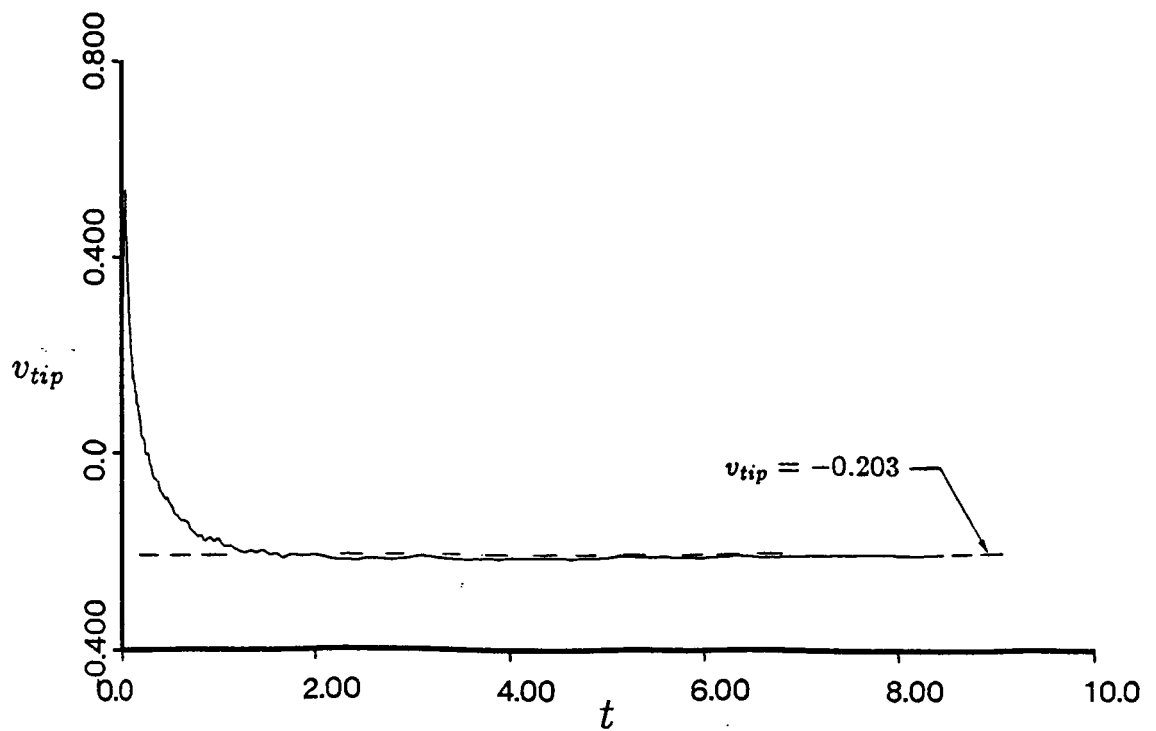


Figure 6.27: Vertical Velocity of the Spiral Center Filament to $t = 8.45$ - Filament Model
Two-Dimensional Sheet

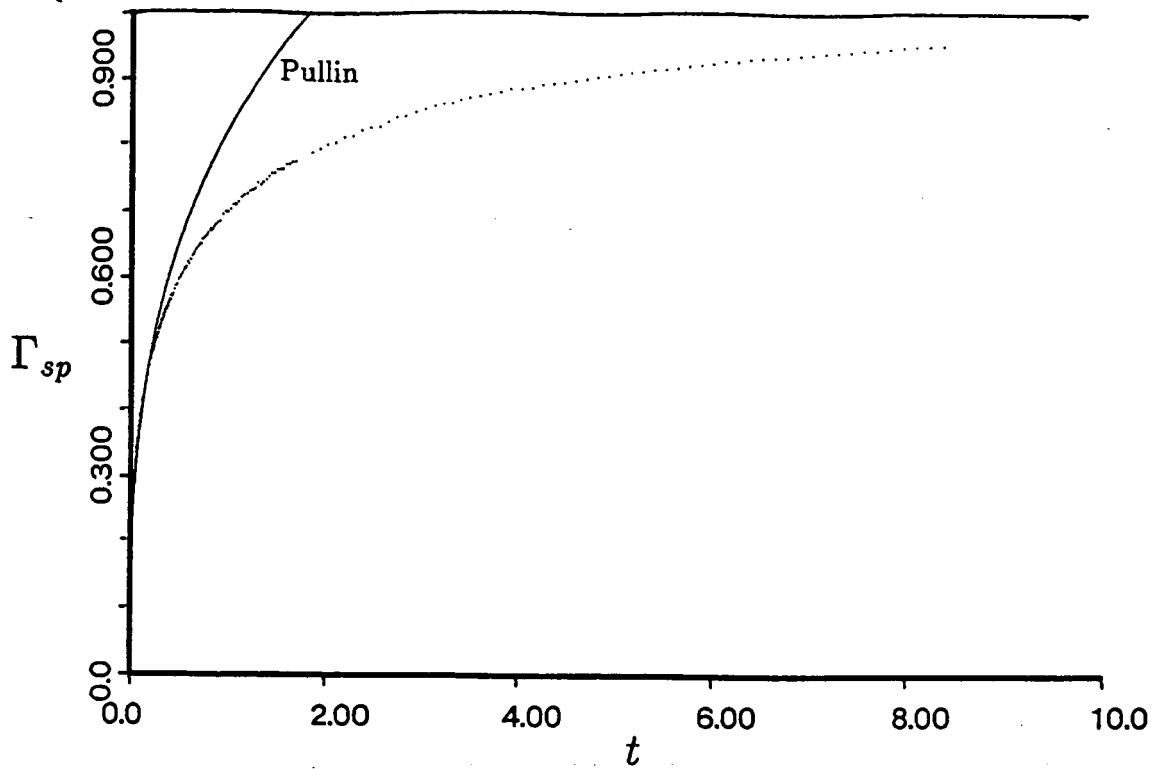


Figure 6.28: Circulation Contained in Spiral to $t = 8.50$ - Panel Model
Two-Dimensional Sheet

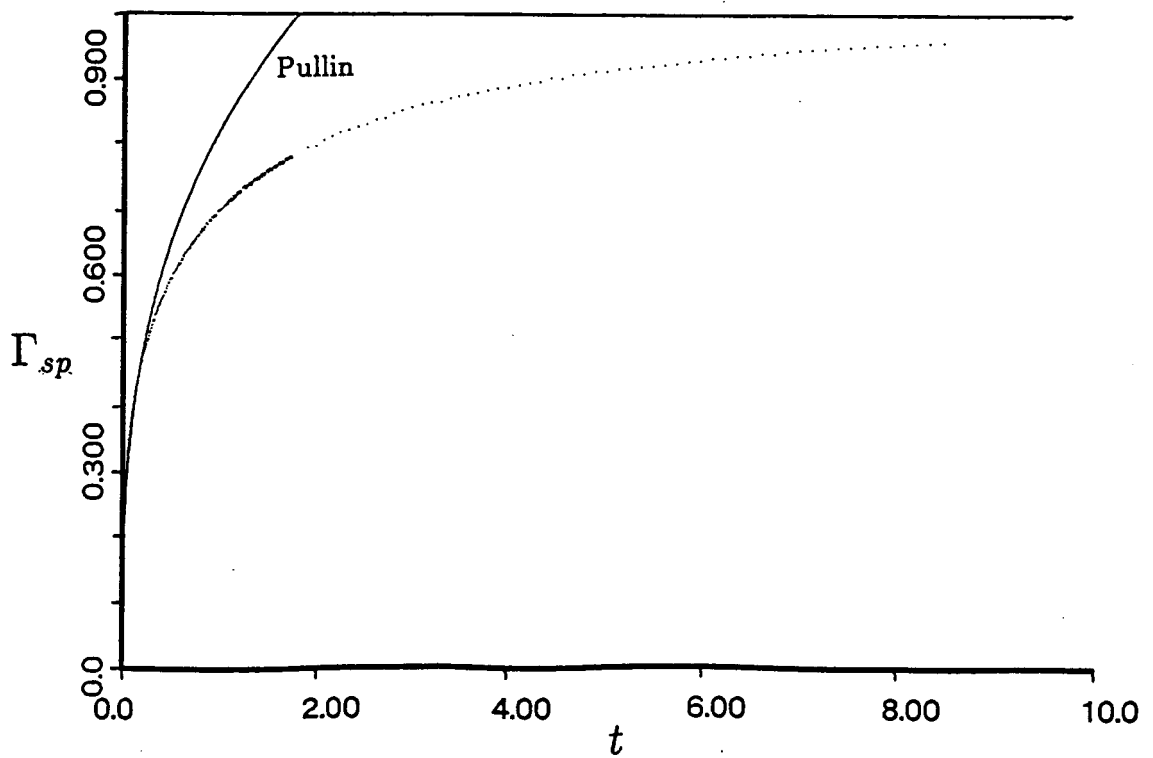


Figure 6.29: Circulation Contained in Spiral to $t = 8.45$ - Filament Model
Two-Dimensional Sheet

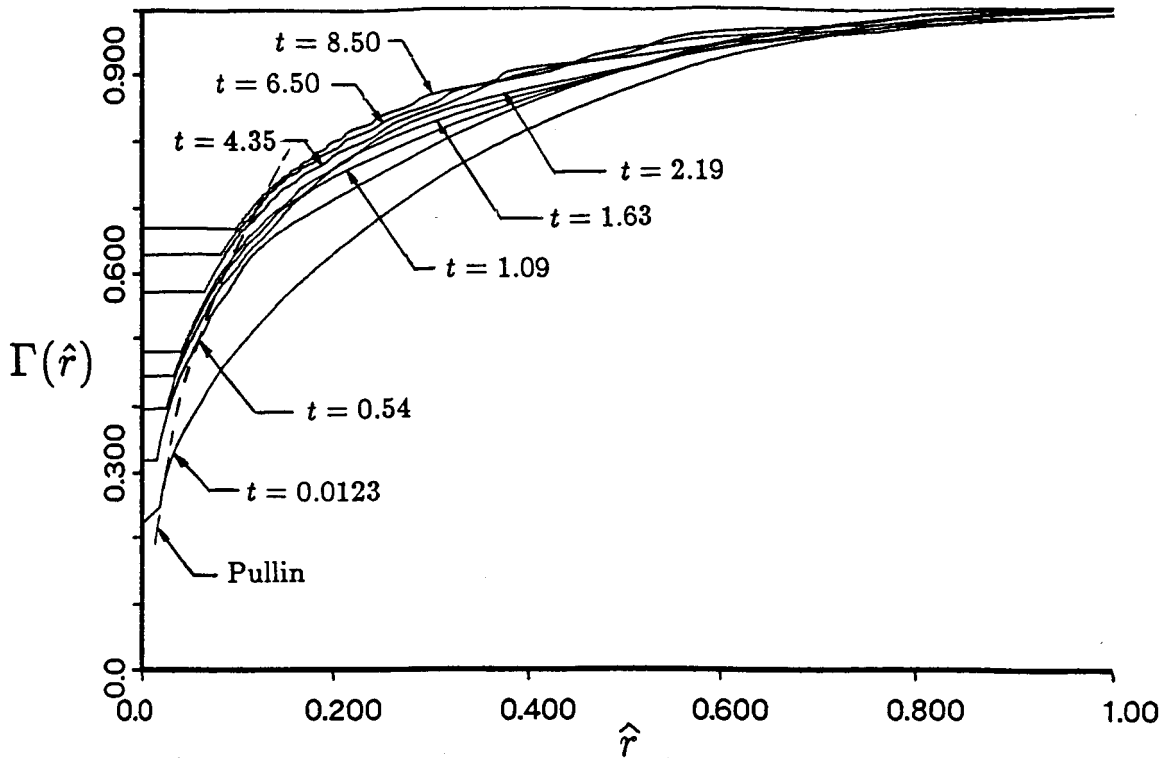


Figure 6.30: Radial Distribution of Circulation to $t = 8.50$ - Panel Model Two-Dimensional Sheet

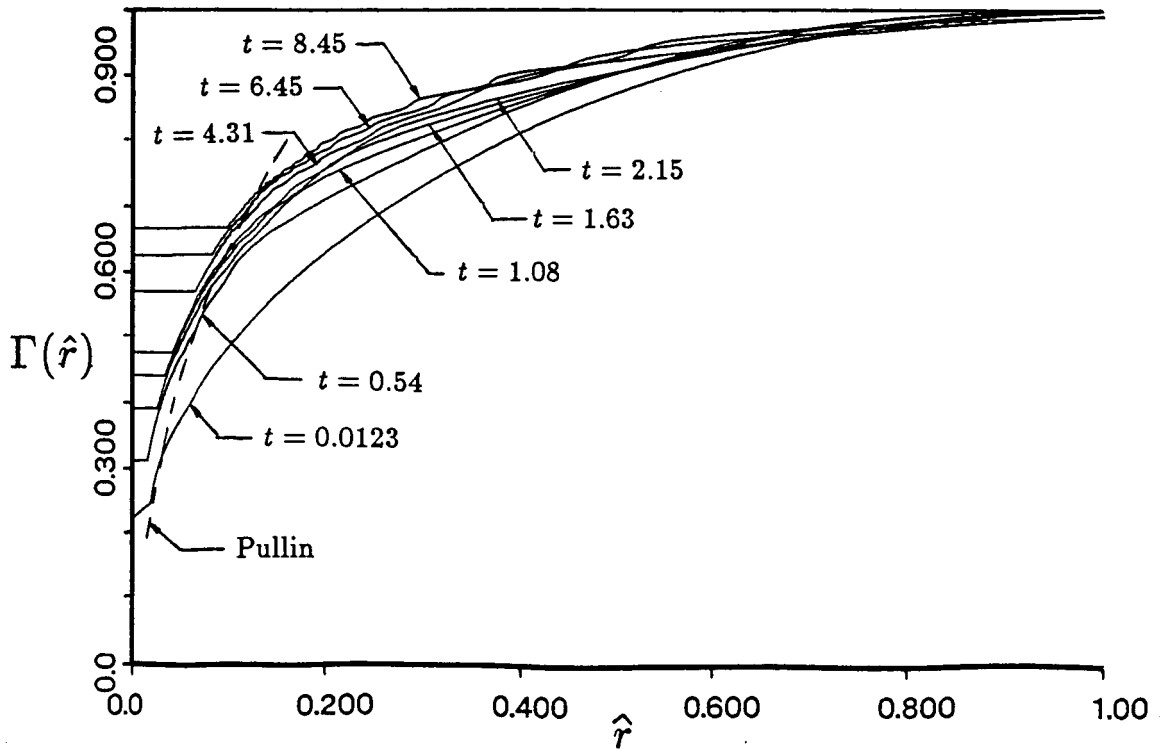


Figure 6.31: Radial Distribution of Circulation to $t = 8.45$ - Filament Model Two-Dimensional Sheet

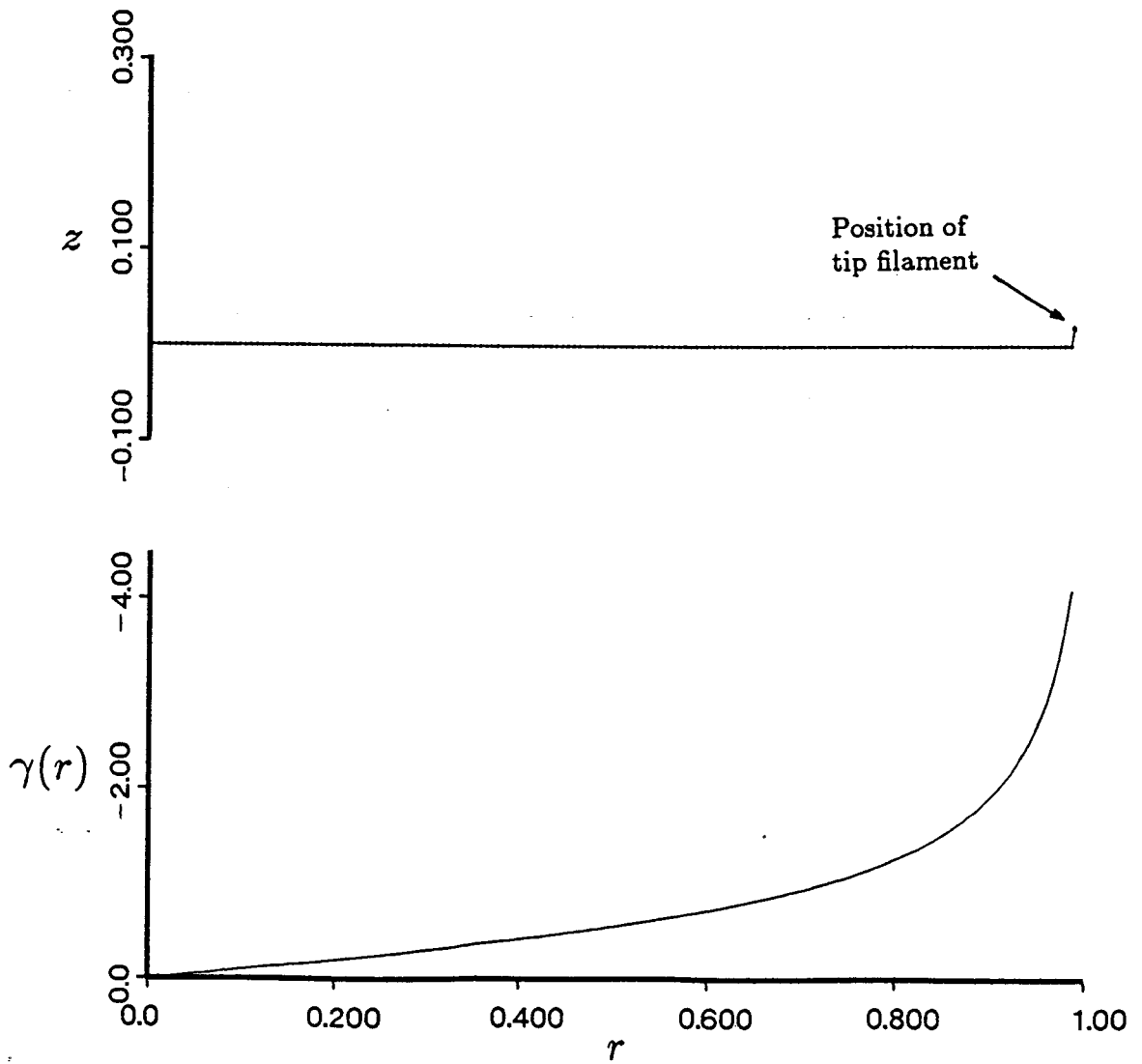


Figure 6.32: Initial Panel Placement and Sheet Strength Distribution for the Axisymmetric Elliptically Loaded Disk

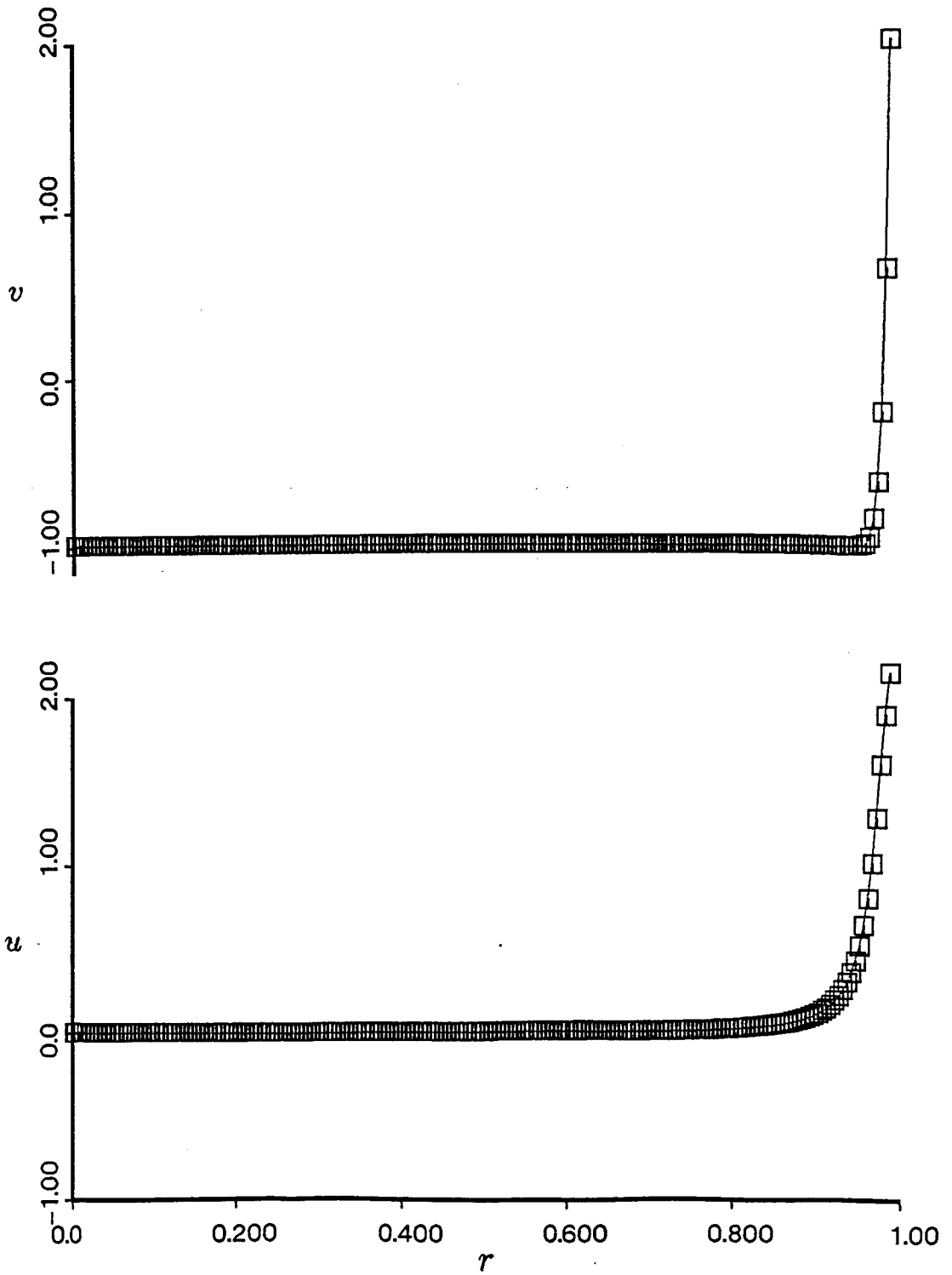


Figure 6.33: Axial and Radial Velocity Distributions at Time $t = t_0$ - Elliptic Loading Axisymmetric Sheet

These curves have been displaced vertically
by the amount indicated for clarity

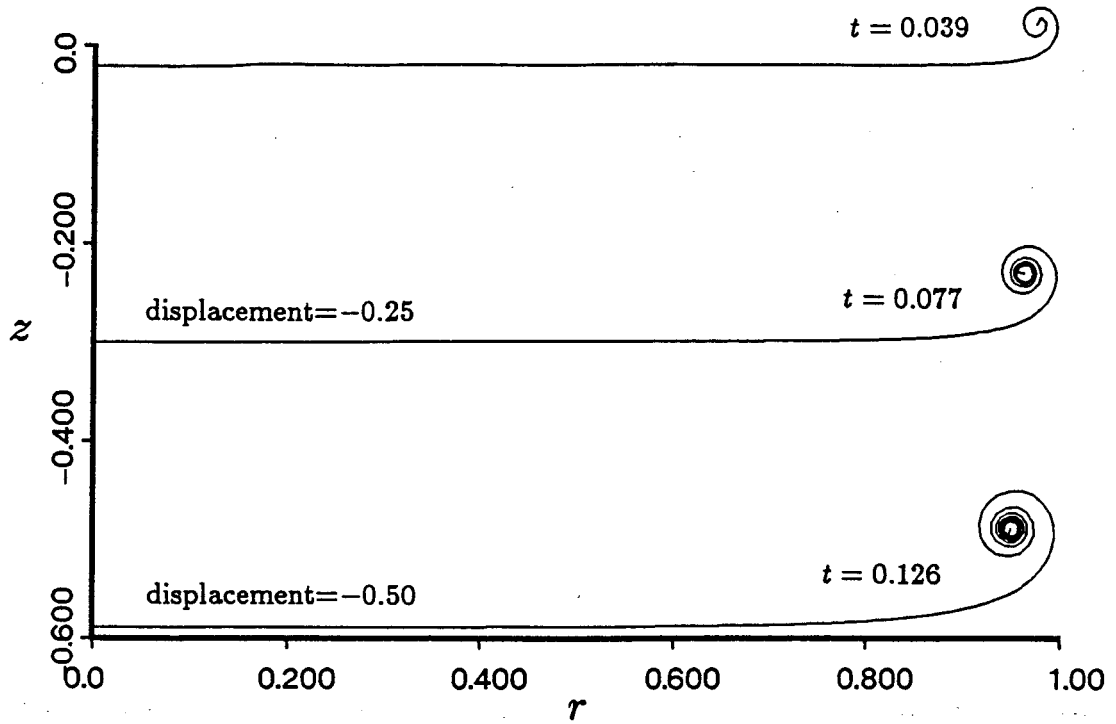


Figure 6.34: Sheet Roll-Up Before Amalgamation - Elliptic Loading
Axisymmetric Sheet

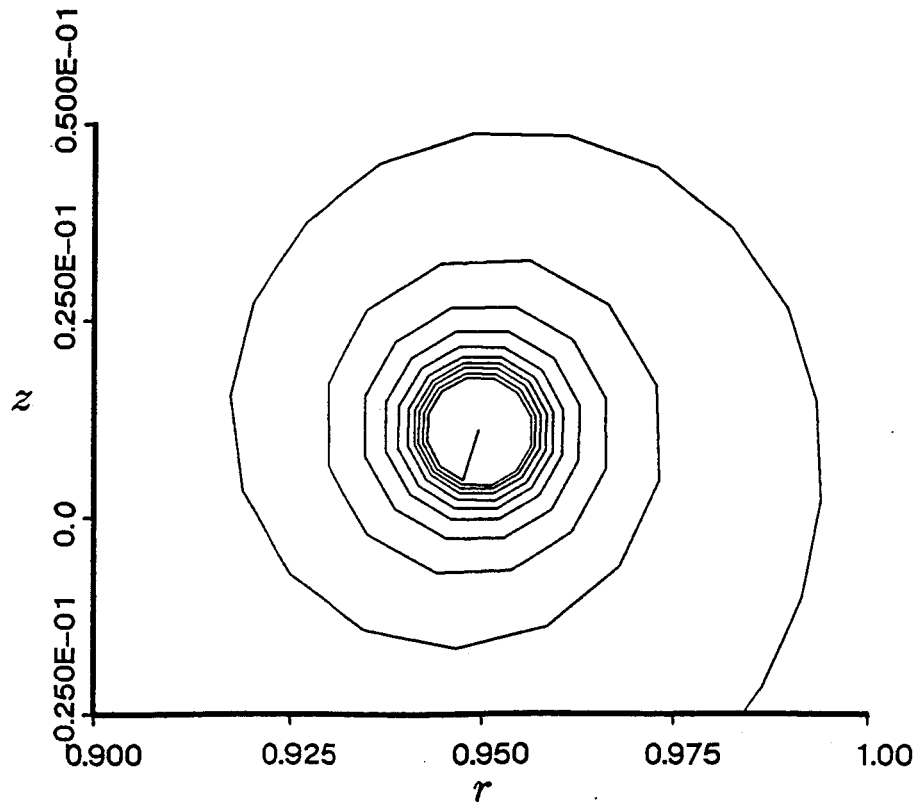


Figure 6.35: Detailed View of the Spiral Region with Ten Turns - Elliptic Loading
Axisymmetric Sheet

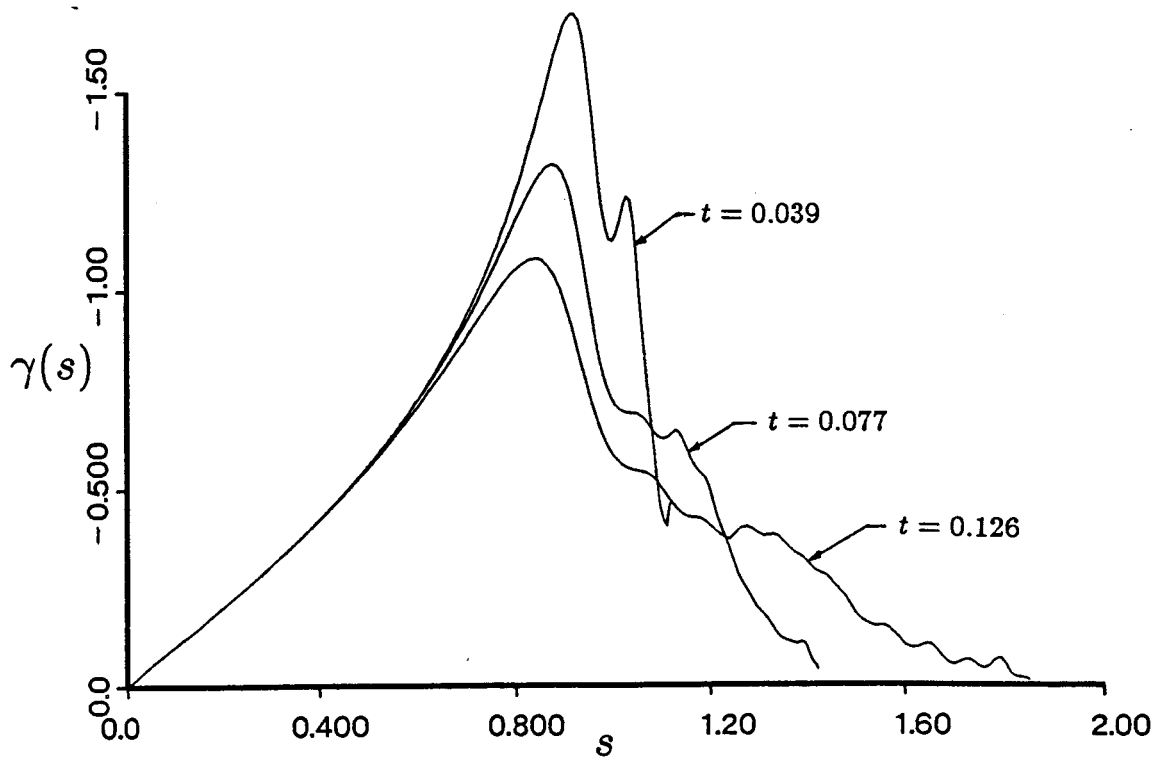


Figure 6.36: Sheet Strength Distribution to $t = 0.126$ - Elliptic Loading
Axisymmetric Sheet

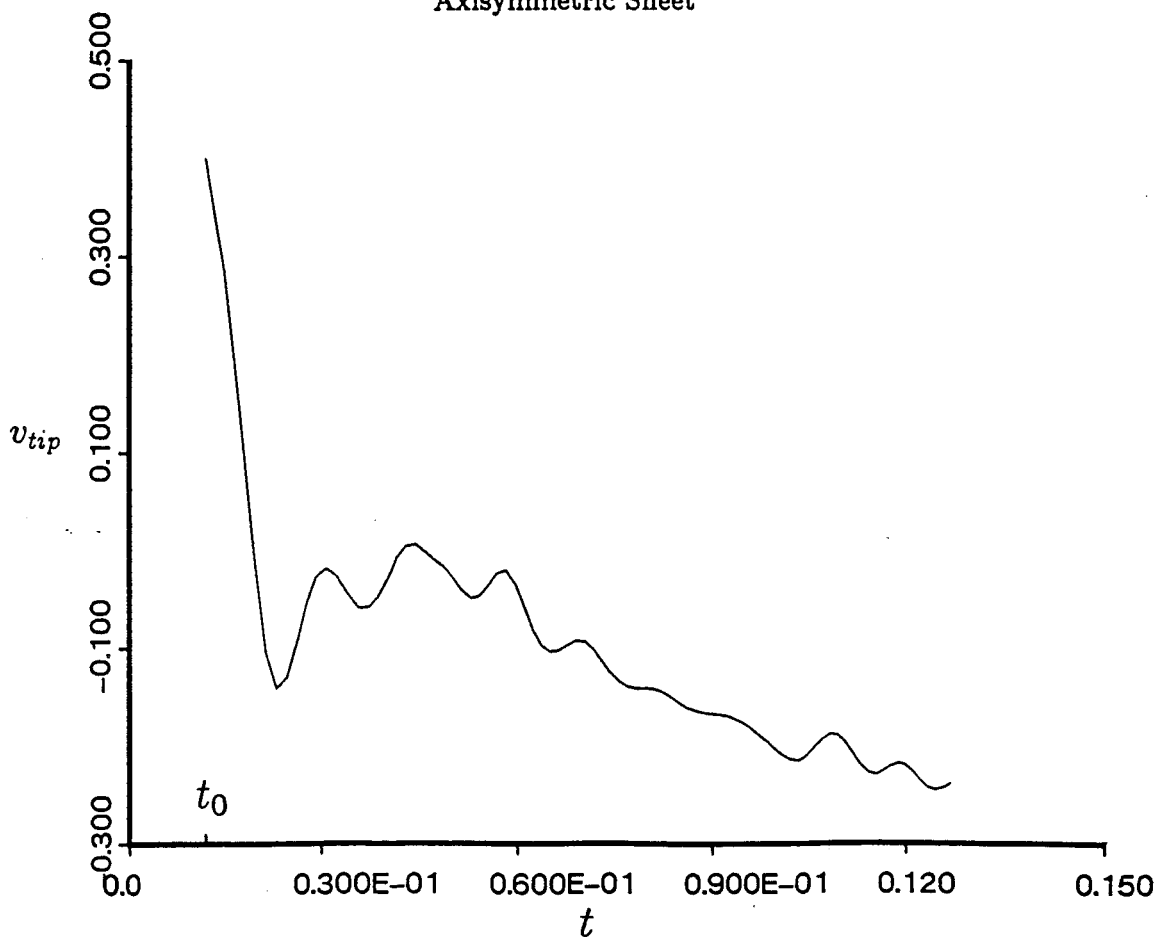


Figure 6.37: Axial Velocity of the Spiral Center Filament to $t = 0.126$ - Elliptic Loading
Axisymmetric Sheet

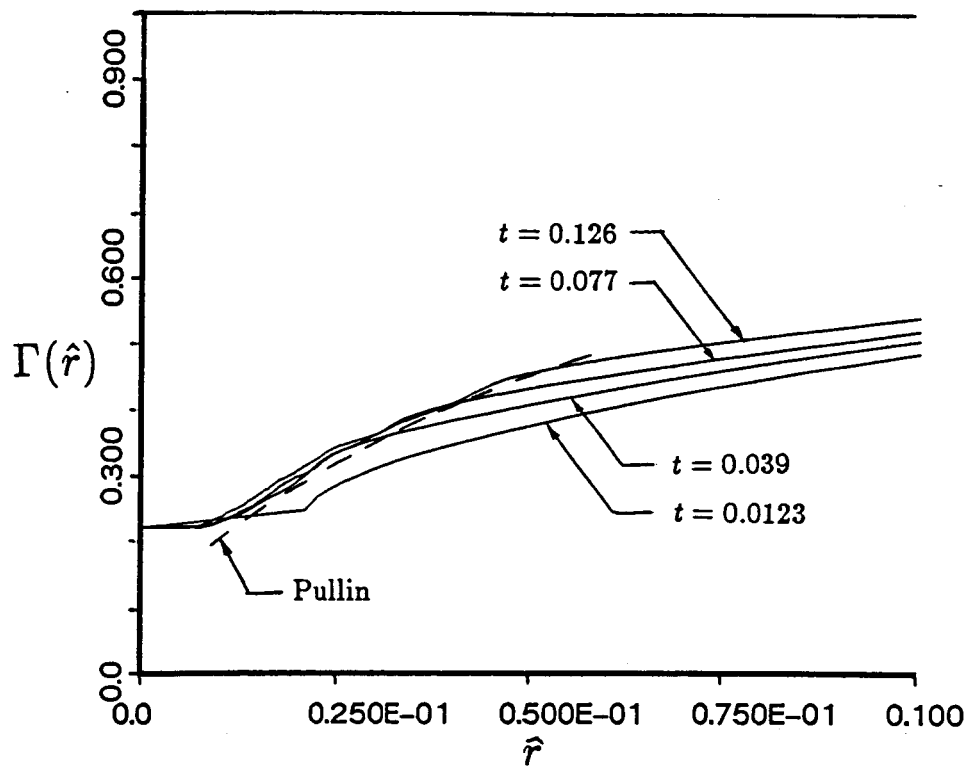


Figure 6.38: Radial Distribution of Circulation to $t = 0.126$ - Elliptic Loading Axisymmetric Sheet

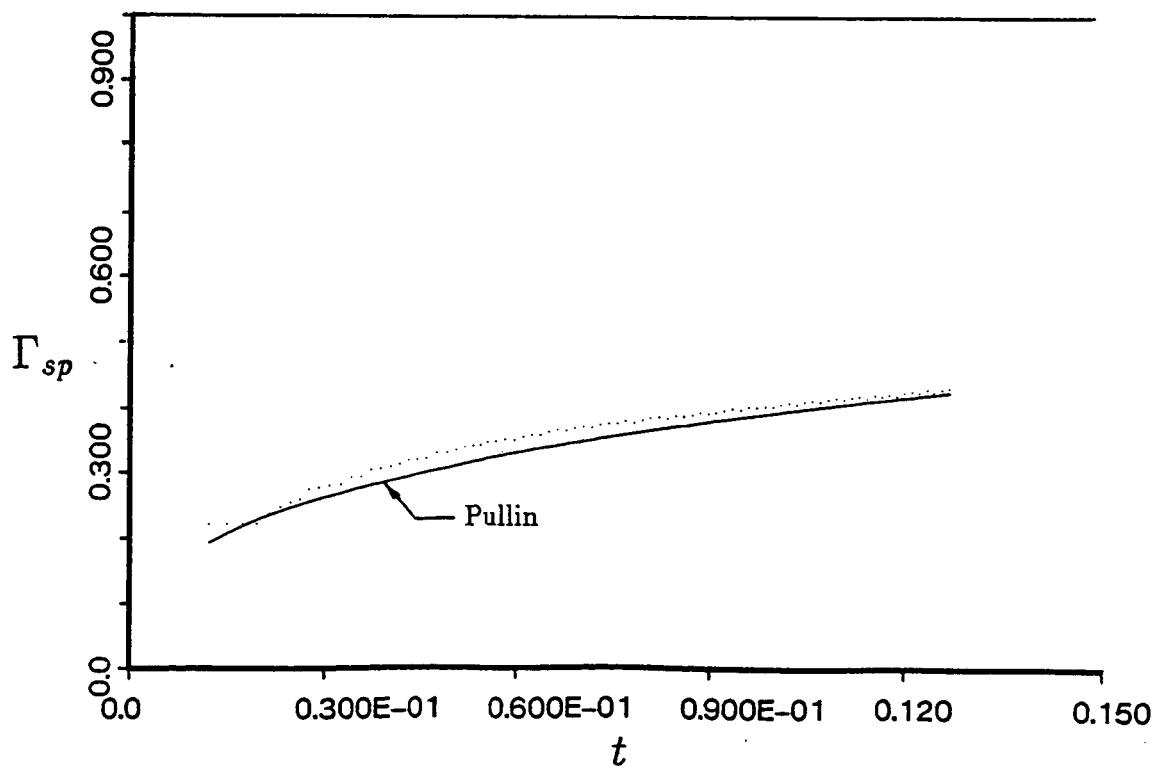


Figure 6.39: Circulation Contained in the Spiral to $t = 0.126$ - Elliptic Loading Axisymmetric Sheet

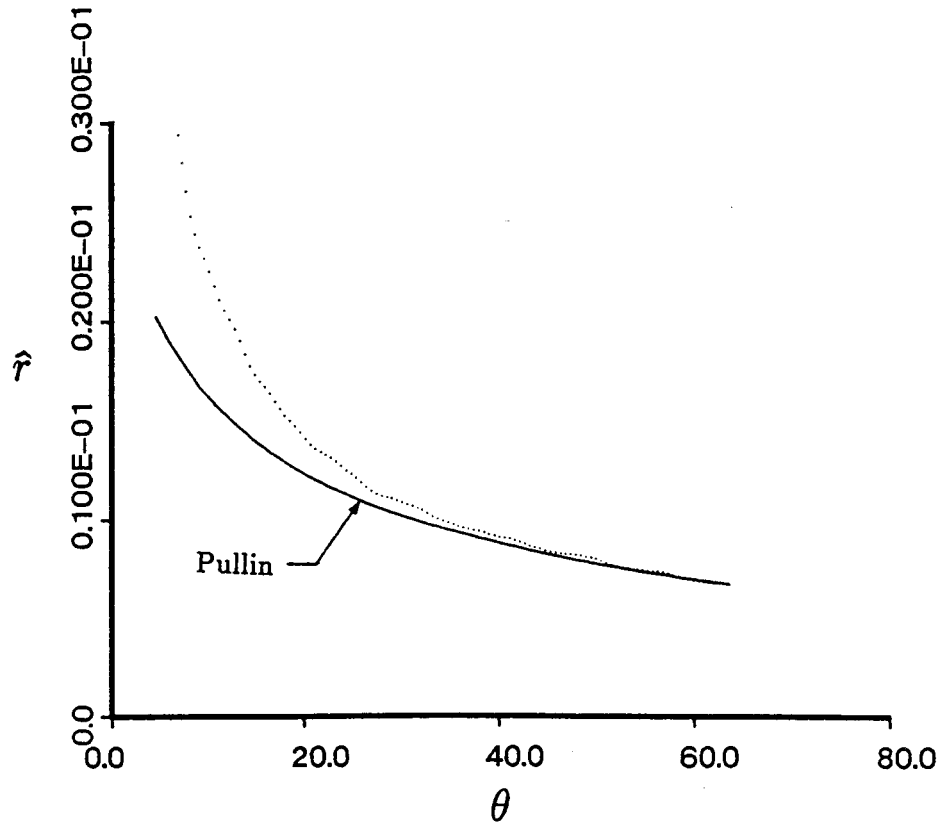


Figure 6.40: Distance of Sheet From Spiral Center at $t = 0.126$ - Elliptic Loading
Axisymmetric Sheet

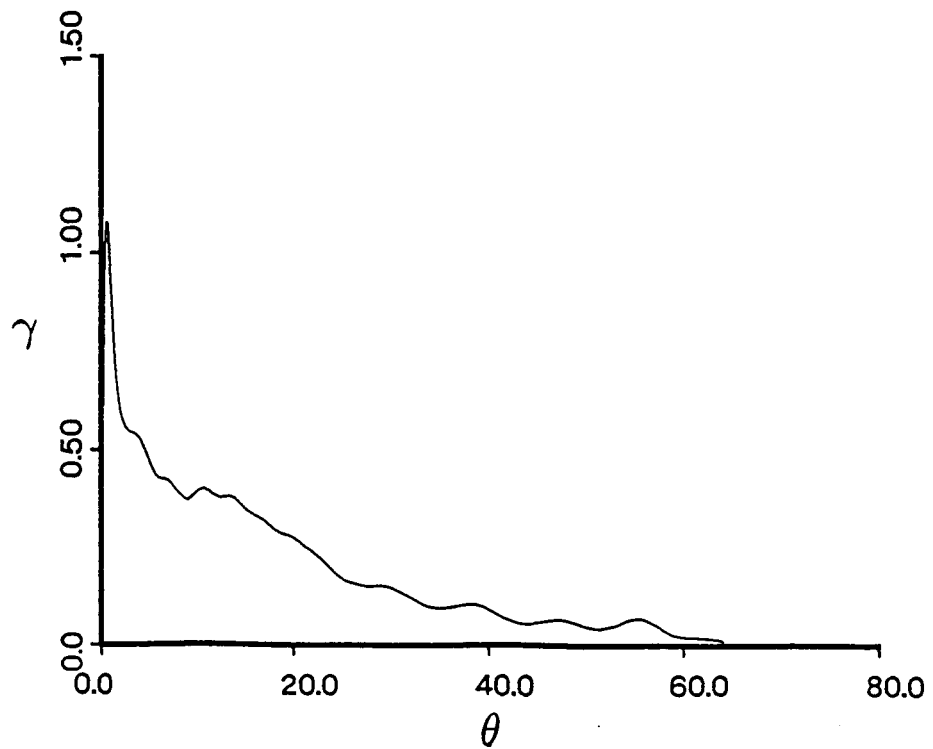


Figure 6.41: Sheet Strength Distribution vs. θ at $t = 0.126$ - Elliptic Loading
Axisymmetric Sheet

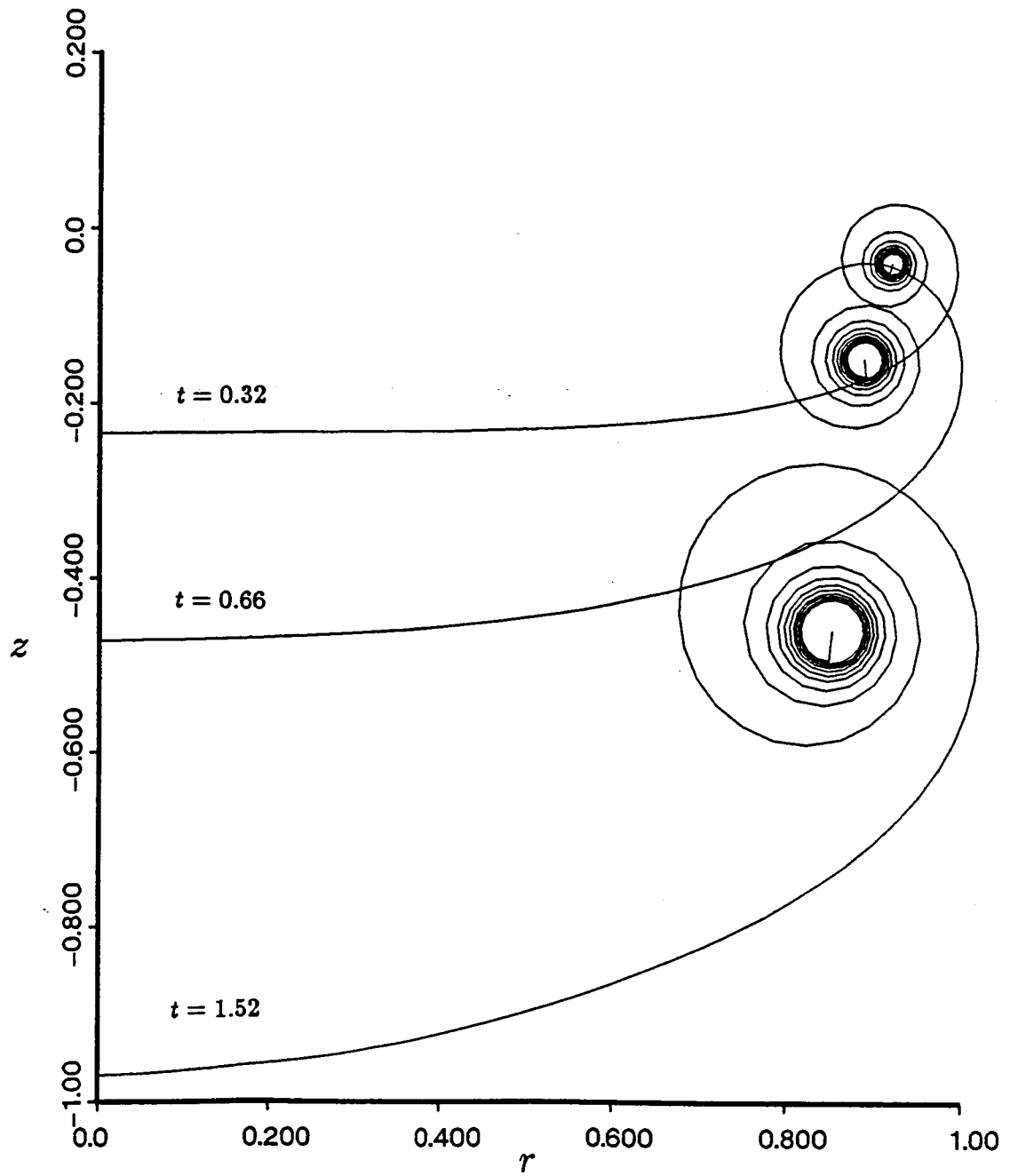


Figure 6.42: Sheet Geometry to $t = 1.52$ - Elliptic Loading
Axisymmetric Sheet

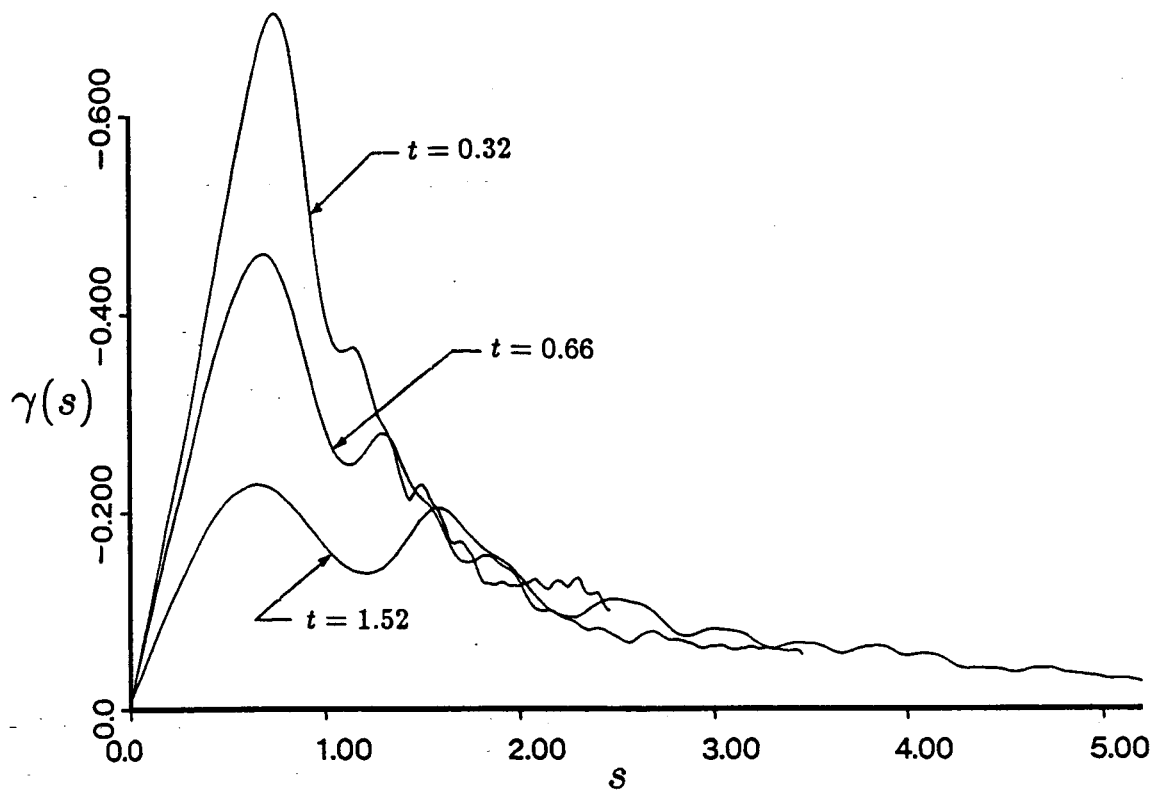


Figure 6.43: Sheet Strength Distribution to $t = 1.52$ - Elliptic Loading
Axisymmetric Sheet

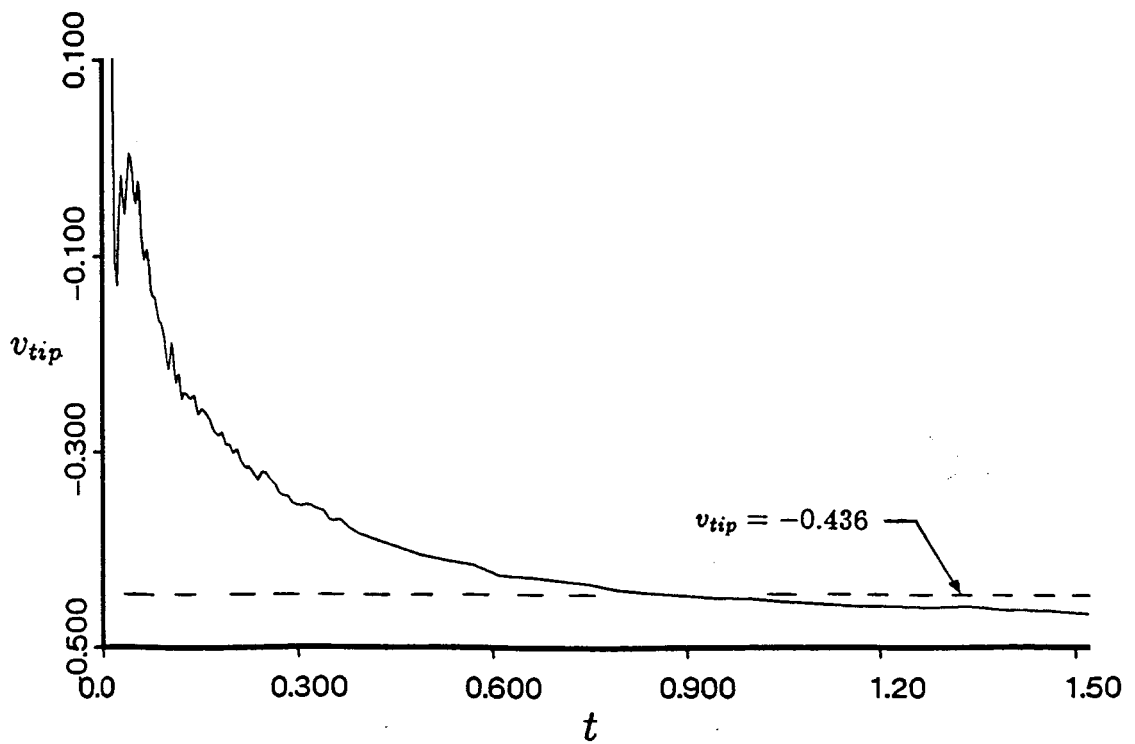


Figure 6.44: Axial Velocity of the Spiral Center Filament to $t = 1.52$ - Elliptic Loading
Axisymmetric Sheet

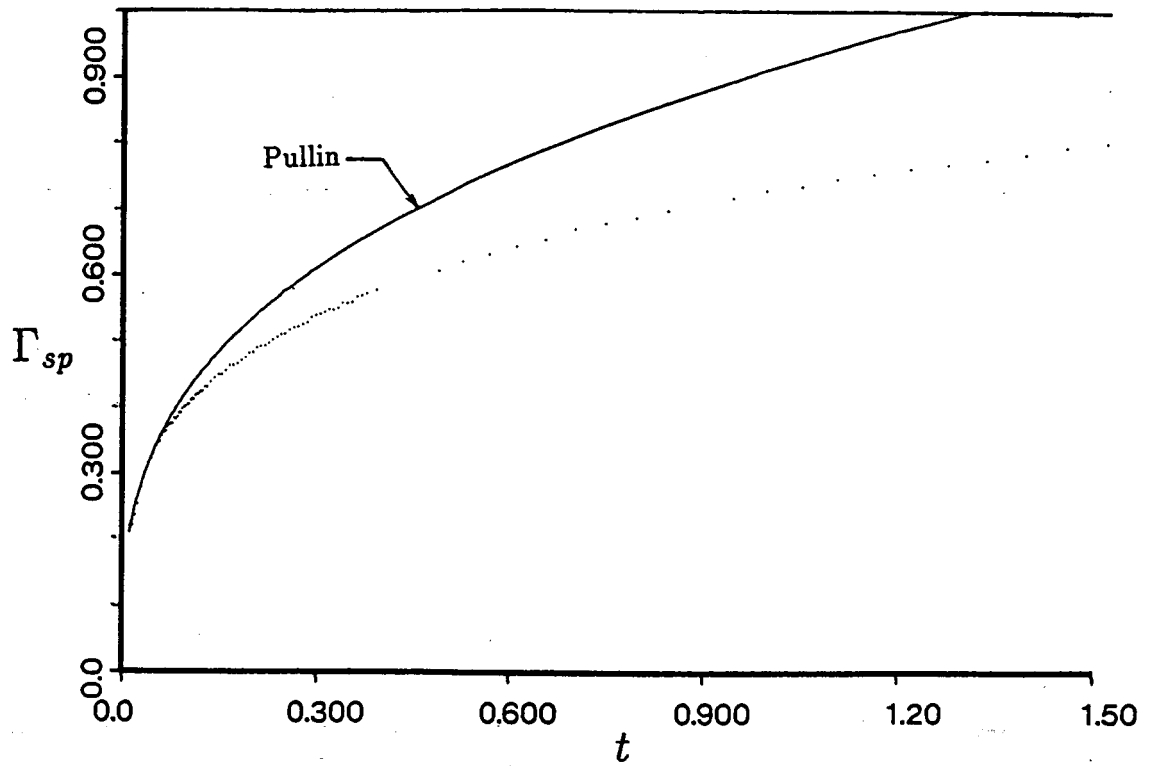


Figure 6.45: Circulation Contained in the Spiral to $t = 1.52$ - Elliptic Loading Axisymmetric Sheet

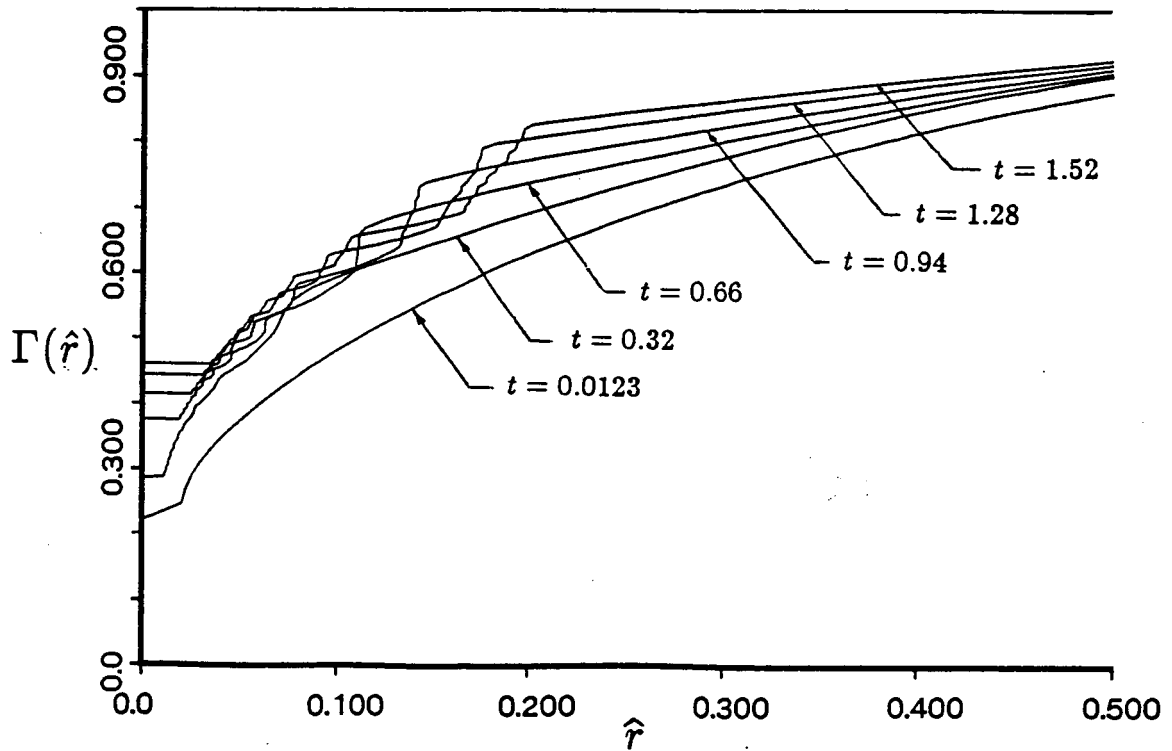


Figure 6.46: Radial Distribution of Circulation to $t = 1.52$ - Elliptic Loading Axisymmetric Sheet

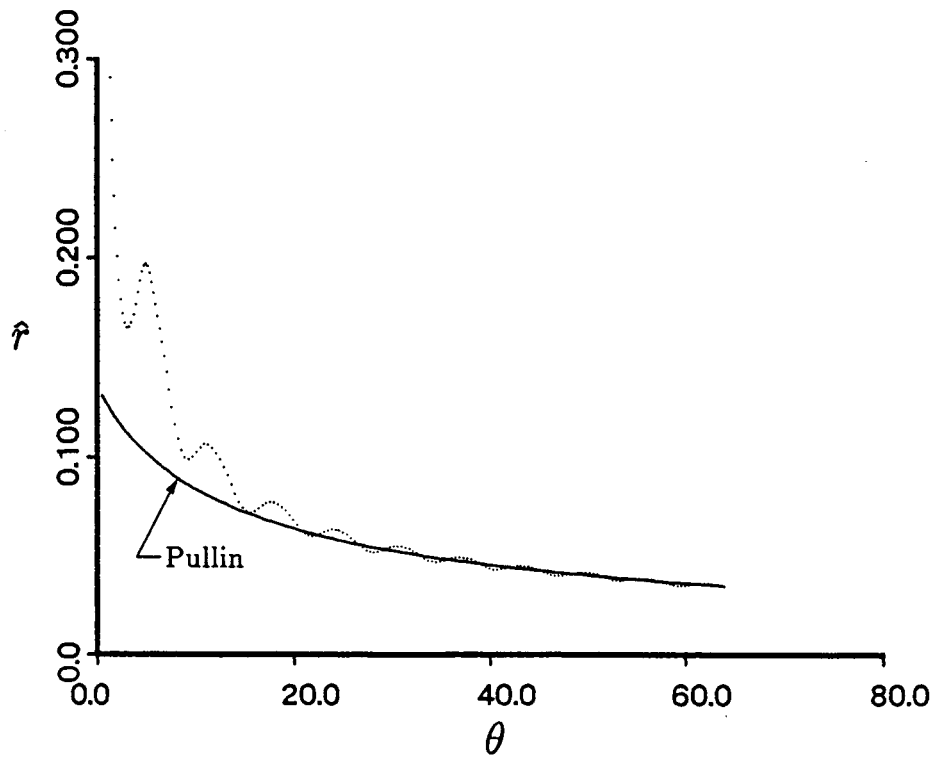


Figure 6.47: Distance of Sheet From Spiral Center at $t = 1.52$ - Elliptic Loading
Axisymmetric Sheet

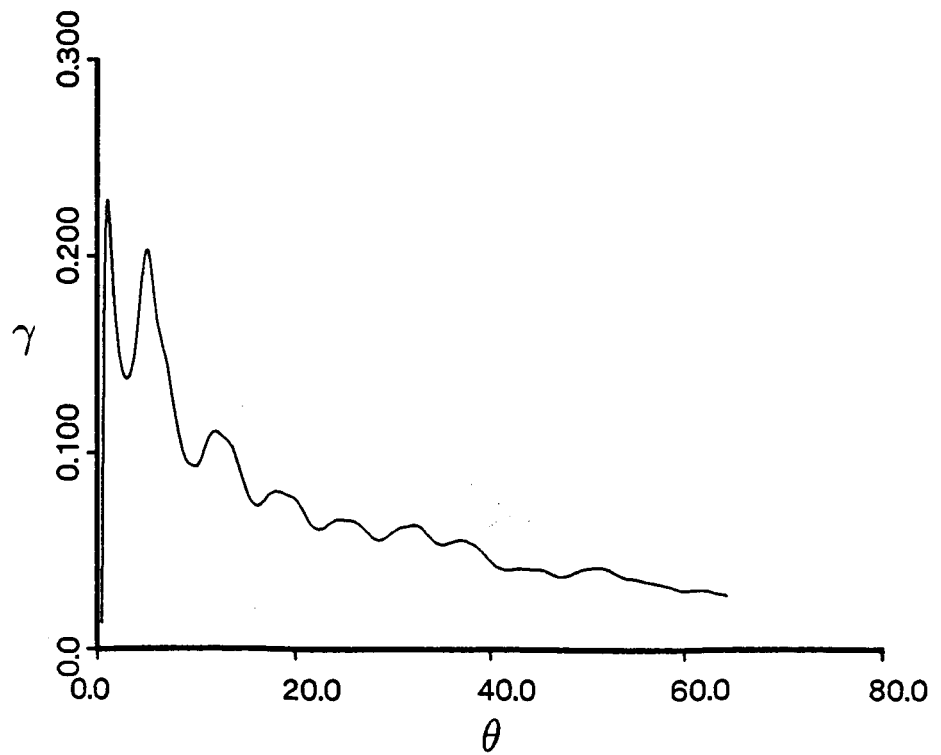


Figure 6.48: Sheet Strength Distribution vs. θ at $t = 1.52$ - Elliptic Loading
Axisymmetric Sheet

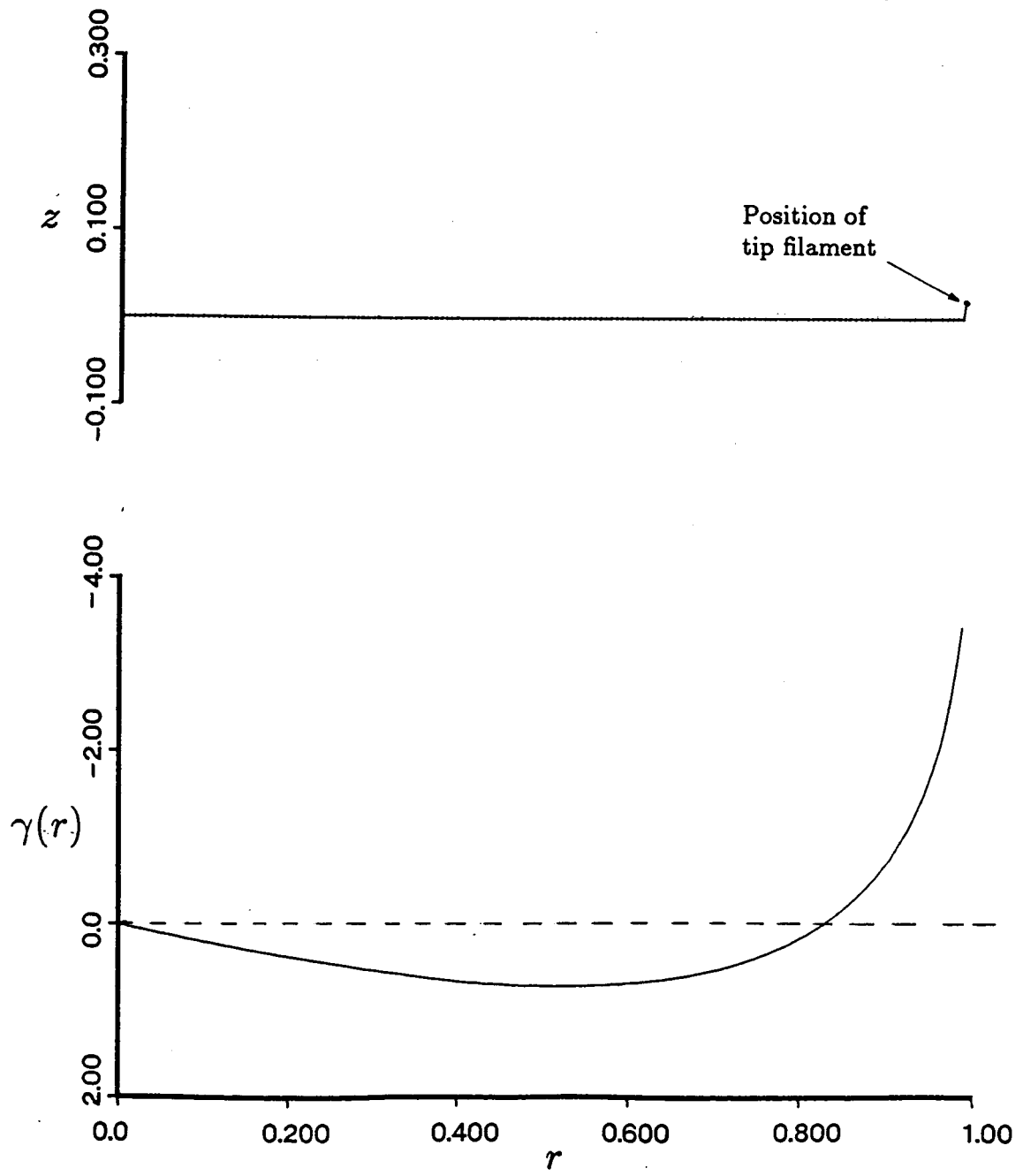


Figure 6.49: Initial Panel Placement and Sheet Strength Distribution for the Axisymmetric Disk with a Helicopter Type Loading

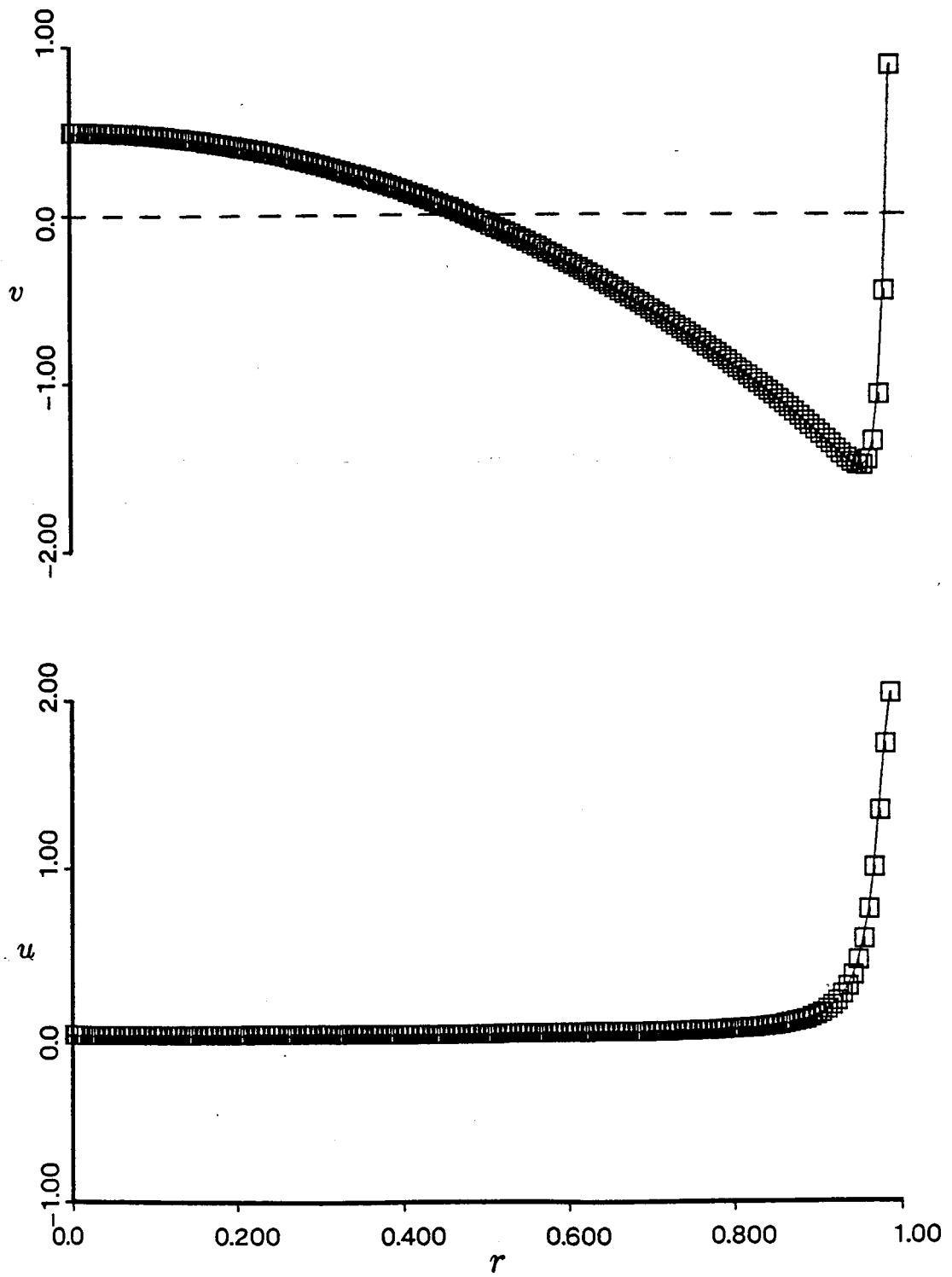


Figure 6.50: Axial and Radial Velocity Distributions at Time $t = t_0$ - Helicopter Loading Axisymmetric Sheet

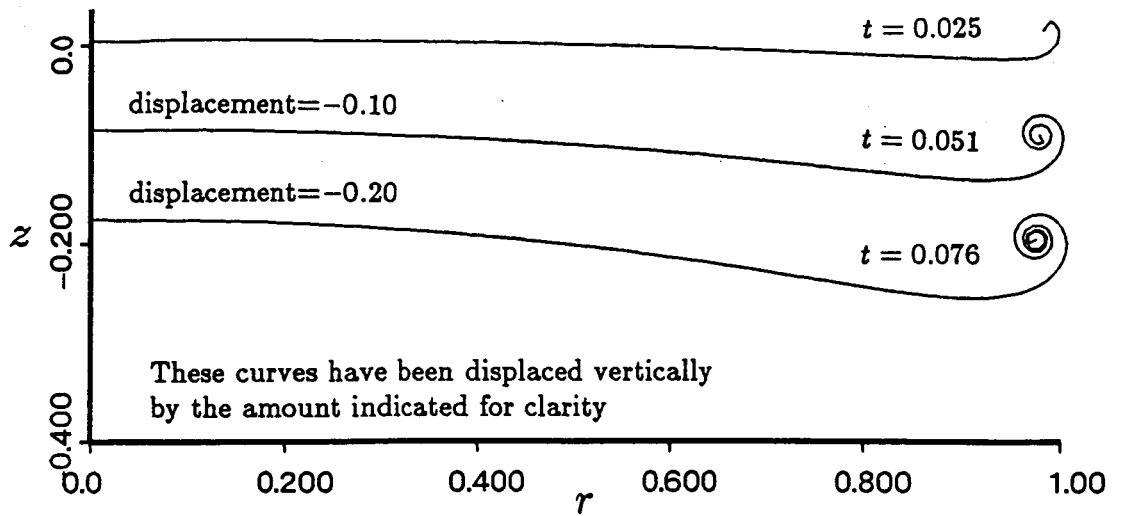


Figure 6.51: Sheet Geometry to $t = 0.076$ - Helicopter Loading
Axisymmetric Sheet

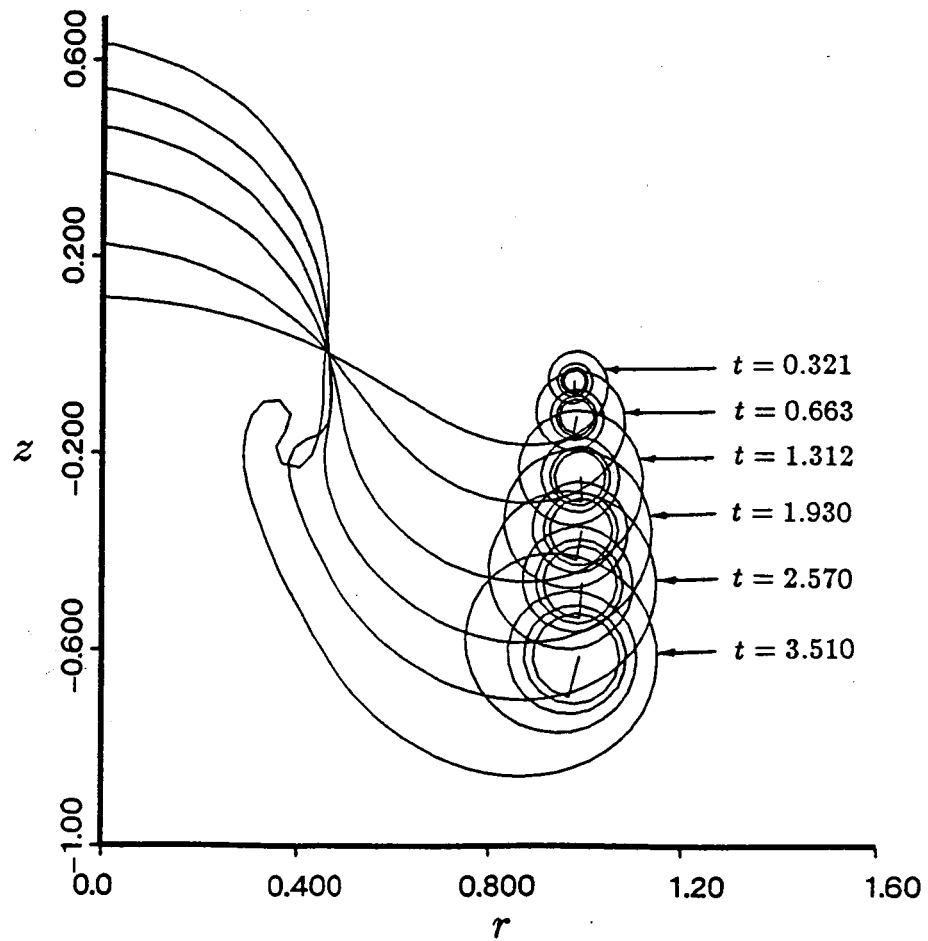


Figure 6.52: Sheet Geometry to $t = 3.51$ - Helicopter Loading
Axisymmetric Sheet

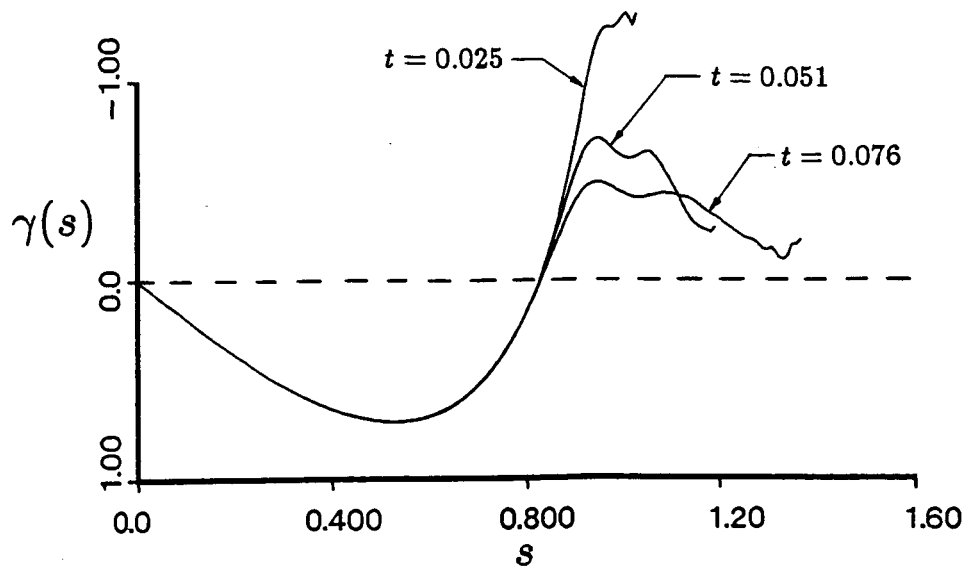


Figure 6.53: Sheet Strength Distribution to $t = 0.076$ - Helicopter Loading
Axisymmetric Sheet

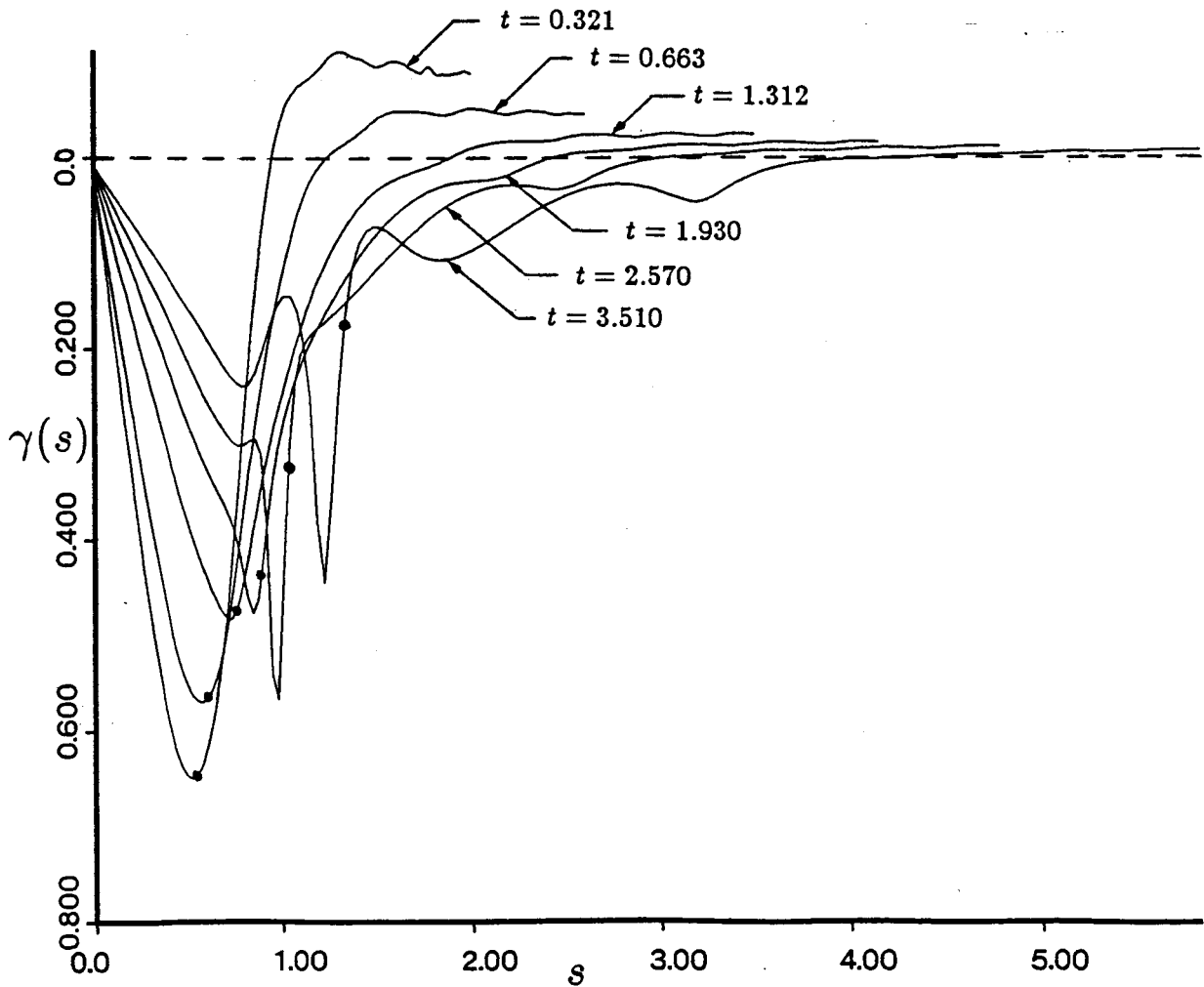


Figure 6.54: Sheet Strength Distribution to $t = 3.51$ - Helicopter Loading
Axisymmetric Sheet

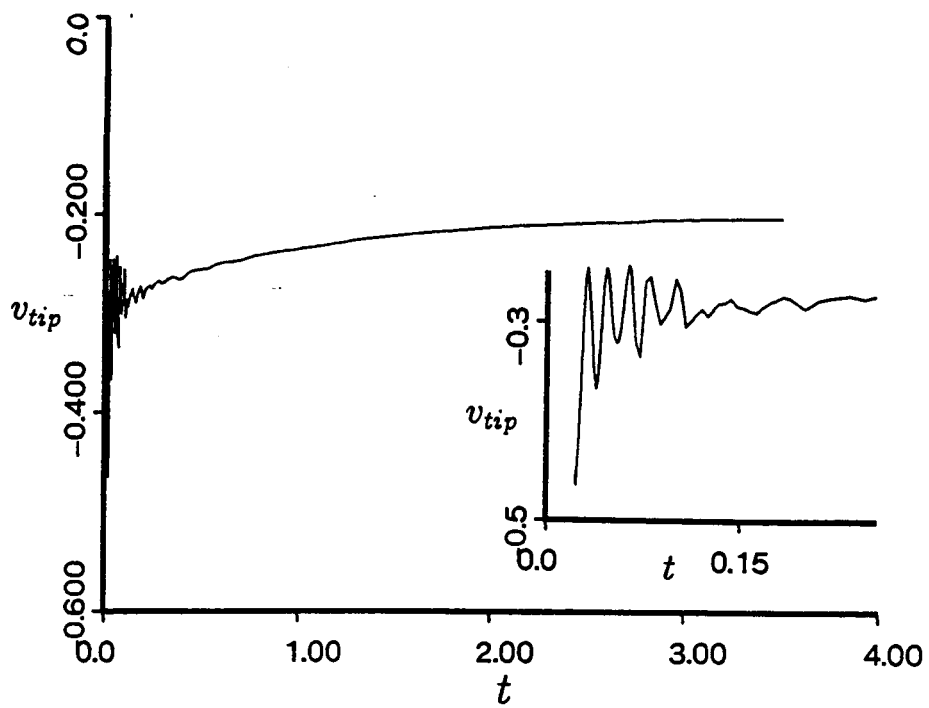


Figure 6.55: Axial Velocity of the Spiral Center Filament - Helicopter Loading Axisymmetric Sheet

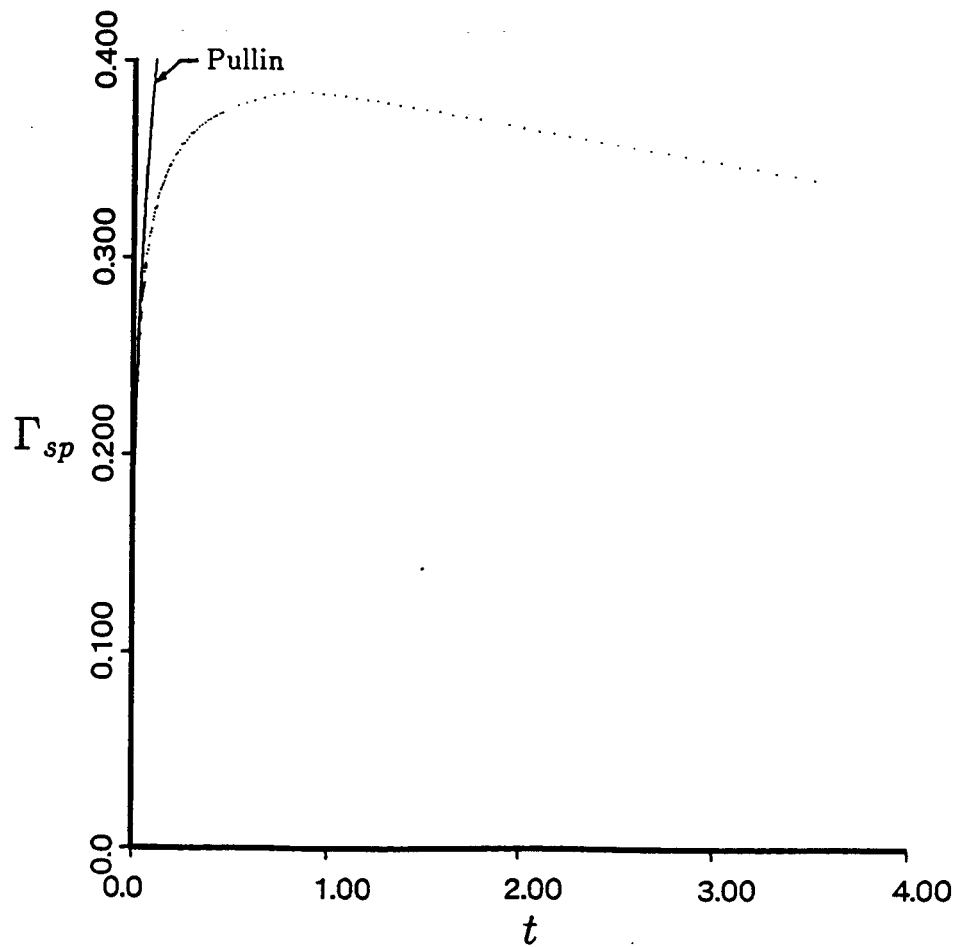


Figure 6.56: Circulation Contained in the Spiral - Helicopter Loading Axisymmetric Sheet

Chapter 7

Conclusions

Vortex sheet motion is an interesting and challenging subject. As an initial value problem it is ill-posed as the wavelength of disturbances approaches zero and is generally plagued with instabilities. However, it is possible through smoothing techniques to calculate the motion and determine useful information at moderate scales about the subsequent roll-up. This work was directed at developing a reliable and accurate method for calculating the motion of axisymmetric vortex sheets, especially the roll-up at the sheet edge. Knowledge of this type of motion is useful in the study and design of aircraft of various types including those of fixed and rotary wings.

The motion of the vortex sheet was studied in a Lagrangian manner, tracking individual material particles on the sheet. Both vortex panels and vortex filaments were used to represent the sheet. The material particles at which the velocities are calculated are located at the panel centers or at the filaments. A complete set of equations for the induced velocity was presented for both panel and filament models.

A comparison between the Euler and the Runge-Kutta time stepping procedures yielded the result that the Runge-Kutta procedure is far more accurate than the Euler procedure for equivalent step sizes in vortex motion calculations. Even considering the additional computations that must be performed at each time step for the Runge-Kutta method it still outperforms the Euler method by many times in vortex calculations.

The inherent difficulties in the calculation of vortex sheet motion were revealed in a straightforward calculation of the motion of an elliptically loaded disk of vorticity.

Shortly after starting, the vortex filaments used to model the sheet exhibited the classical chaotic behavior seen by many other investigators. It was determined that inaccurate time stepping was not the cause but that a variety of problems associated with the sheet itself and the sheet discretization procedure were responsible.

The largest single cause of the chaotic behavior observed very early in the simulation was determined to be due to the inability of a finite number of discrete vortex elements to model the singularity at the sheet edge. This was resolved with the introduction of a special model of the edge of the sheet. The model replaces the outermost portion of the sheet with a single vortex filament of equivalent strength and a number of higher order terms which account for the asymmetry of the spiral.

Another difficulty associated with representing the vortex sheet with a series of discrete vortex elements is the error associated with non-uniform element separation. As the sheet stretches unevenly, the initially equally spaced vortex elements become unevenly spaced which can introduce severe errors in the velocity calculations. The solution to this problem was to discretize the sheet at every time step to ensure that the vortex elements remain equally spaced.

The validity of the model was tested by computing the roll-up of a two-dimensional elliptically loaded sheet. A smooth roll-up was observed for the entire period of the simulation indicating that the method appears to have eliminated the primary causes of the chaotic motion observed earlier. Comparing the results to those obtained by Pullin for the similar semi-infinite sheet demonstrate that the model may be used successfully to simulate the roll-up of a vortex sheet, although the motion for very early times shows some error in the motion of the spiral center. Additionally, the two-dimensional test case was used to compare the panel and filament models. Few differences were observed in the results between the panel and filament models. The primary advantage of panels over filaments is their increased accuracy resulting in the ability to form more turns in

the spiral. However, the line up of the vortex elements in the spiral served to eliminate much of the problem of the singularity associated with the vortex filaments and so the potential advantage of panels was not fully realized.

The model was used to calculate the roll-up of two axisymmetric disks, one with an elliptic loading and one with a loading similar to that of a helicopter rotor in hover. For the elliptically loaded disk the method yielded a very smooth roll-up with none of the instability or chaotic behavior seen in the straightforward case. Fluid impulse was conserved to within about 1% indicating that the method is accurate. The helicopter loading case initially suffered some instability in the region of the inboard sheet strength maximum, but this was largely overcome by replacing the cubic fit of circulation with a simpler linear fit. The cubic function had introduced some extraneous curvature into the circulation distribution which became magnified by the differencing process used to obtain the strengths of the individual panels. The simulation of the helicopter rotor wake successfully captured the development of the secondary inboard vortex although it was not capable of fully simulating the double branch roll-up past the early stages. However, the addition of another isolated vortex at the inboard vortex position would likely allow the roll-up to continue.

References

- [1] G.R. Baker. The cloud-in-cell technique applied to the roll-up of vortex sheets. *J.Comp.Physics*, 31:76–95, (1979).
- [2] G.K. Batchelor. *Introduction to Fluid Dynamics*. Cambridge University, (1957).
- [3] G. Birkhoff and J. Fisher. Do vortex sheets roll up? *Circ.Mat.Palermo*, 8:77–90, (1959).
- [4] D. Bliss. *The Dynamics of Curved Rotational Vortex Lines*. Master's thesis, M.I.T., Aero/Astro, (1970).
- [5] A.J. Chorin and P.S. Bernard. Discretization of a vortex sheet with an example of roll-up. *J. Comp. Physics*, 13:423–429, (1973).
- [6] B. De Bernardinis, J.M.R. Graham, and K.H. Parker. Oscillatory flow around disks and through orifices. *Journal of Fluid Mechanics*, 102:279–299, (1981).
- [7] P.T. Fink and W.K. Soh. Calculation of vortex sheets in unsteady flow and applications in ship hydrodynamics. In *Proc. 10th Symp. Naval Hydrodynamics*, pages 463–488, Cambridge, Mass., (1974).
- [8] P.T. Fink and W.K. Soh. A new approach to roll-up calculations of vortex sheets. *Proc.R.Soc.London Ser.A*, 362:195–209, (1978).
- [9] H.W.M. Hoeijmakers and Vaatstra. A higher-order panel method applied to vortex sheet roll-up. *AIAA Paper*, (82-0096), (1982).
- [10] H. Kaden. *Ing. Arch.*, 2:140–168, (1931).
- [11] H. Lamb. *Hydrodynamics*. Dover, (1932).

- [12] D.W. Moore. On the point vortex method. *SIAM J.Sci.Stat.Comp.*, 2:65-84, (1981).
- [13] D.W. Moore. The spontaneous appearance of a singularity in the shape of an evolving vortex sheet. *Proc.R.Soc.London Ser.A*, 365:105-119, (1979).
- [14] D.W. Moore. The stability of an evolving two-dimensional vortex sheet. *Mathematika*, 23:35-44, (1976).
- [15] D.W. Moore and R. Griffith-Jones. The stability of an expanding circular vortex sheet. *Mathematika*, 21:128-133, (1974).
- [16] D.I. Pullin. On a generalization of kaden's problem. *J. Fluid Mech.*, 104:45-53, (1981).
- [17] T.W. Roberts and E.M. Murman. A computational method for helicopter vortex wakes. *AIAA Paper*, (84-1554), June (1984).
- [18] L. Rosenhead. The formation of vortices from a surface of discontinuity. *Proc.R.Soc.London Ser.A*, 134:170-92, (1931).
- [19] P.G. Saffman. The structure and decay of trailing vortices. *Archives of Mechanics*, 26:423-429, (1974).
- [20] P.G. Saffman and G.R. Baker. Vortex interactions. *Ann. Rev. Fluid Mech.*, 11:95-122, (1979).
- [21] I. Sugioka. *A Panel Method Study of Vortex Sheets with Special Emphasis on Sheets of Axisymmetric Geometry*. Master's thesis, M.I.T., Aero/Astro, (1985).
- [22] G.I. Taylor. Formation of a vortex ring by giving an impulse to a circular disk and then dissolving it away. *J. Appl. Phy.*, 24:104, (1953).

Appendix A

Vortex Polygon Model

A.1 Cut-Off Method

The self-induced velocity of a vortex filament is infinite at any point where the curvature is non-zero. A popular method to avoid this problem when attempting to calculate the velocity on the curved filament by means of Biot-Savart integration, is to remove a section of the filament around the point of calculation from the integration. This is commonly known as the cut-off method. As shown in Figure A.1, a segment of length l_c is removed from either side of the control point. Bliss [4] has shown that the correct self-induced velocity is obtained if the cut-off length satisfies

$$\log \frac{l_c}{c} = -\log 2 + \frac{1}{2} - A + C \quad (\text{A.1})$$

where c is the radius of the equivalent core section of uniform vorticity. A and C are constants which are determined by the axial velocity and the distribution of vorticity within the core respectively. For no axial velocity, $A = 0$, and for uniform vorticity, $C = 1/4$ which yields $l_c/c = 0.6420$.

A.2 Polygon Model

The approach considered in this appendix is to model a vortex ring as a vortex polygon consisting of N straight sides of equal length. A vortex polygon is constructed from a circular vortex ring as illustrated in Figure A.2. The ends of the straight segments

lie on the ring and the segments themselves lie inside the circular ring. The motion of the polygon may be tracked by computing the velocity at the centers of each of the segments due to all of the other segments and all of the other polygons. This naturally results in a type of cut-off procedure where the cut-off length, l_c , is half of the length of one of the polygon sides. The objective is to determine the appropriate cut-off length in order to model a vortex ring of a given core section radius.

For a vortex ring of radius R , and strength κ , the self-induced axial velocity is given by Lamb [11] as

$$V = \frac{\kappa}{4\pi R} \left[\log \frac{8}{\epsilon} - \frac{1}{4} \right] \quad (\text{A.2})$$

where $\epsilon = c/R$, the ratio of core radius to ring radius. Solving for ϵ yields

$$\epsilon = 8 \exp \left[\frac{1}{4} + V \frac{4\pi R}{\kappa} \right]^{-1} \quad (\text{A.3})$$

The idea is to numerically evaluate the velocity at the center of one of the straight segments by applying the Biot-Savart integral to all of the other segments. The resulting velocity is then substituted into equation A.3 to determine an effective ϵ for this cut-off length.

For large values of N (i.e., $N > 75$), the value obtained is $l_c/c = 1.387$. This is considerably larger than the cut-off length determined by Bliss because of the difference in the location of the control point. For Bliss the control point is located on the ring itself, while for the polygon method, the control point is located on the center of one of the segments which is further in towards the center.

The implication of this result is that the modelling of a vortex line by a set of straight filament sections in which the self-induced velocity of the straight filament section upon itself is zero is equivalent to a vortex core of radius $c = 1.387l_c$.

This result yields a method for determining the number of polygon segments to be used in a ring system to model a disk. Consider a circular vortex disk of radius b which

is subdivided into a number of equally spaced annuluses. At the center of each annulus a vortex polygon is placed having the same strength as the annulus which it represents. An effective core radius may be determined for the polygon using a result presented in Section 2.3, i.e., $c = w/4$ where w is the width of the annulus. If the cut-off length is indicated by l_c and the associated subtended angle by θ then for large values of N , i.e., small values of θ , l_c may be approximated by $l_c/R \approx \pi/N$ or with $\epsilon = c/R$ and $l_c/c = 1.387$ we get

$$N = 1.766 N_R \frac{r}{b} \quad (\text{A.4})$$

where N_R is the number of polygons used to model the disk. This expression yields the number of segments to use in each of the polygons from the center ($r/b = 0$) to the outer edge ($r/b = 1$). The number of polygon segments increases linearly with the distance from the center of the disk with the value at the center equal to zero. Clearly this would have to be approximated, but that is acceptable in that the strength of the rings in the center is very small so the error should also be small. Also, the number of polygon segments increases linearly with the number of polygons. This could represent difficulties computationally in that a very large number of polygon sides may be needed to model a vorticity disk and achieve good resolution.

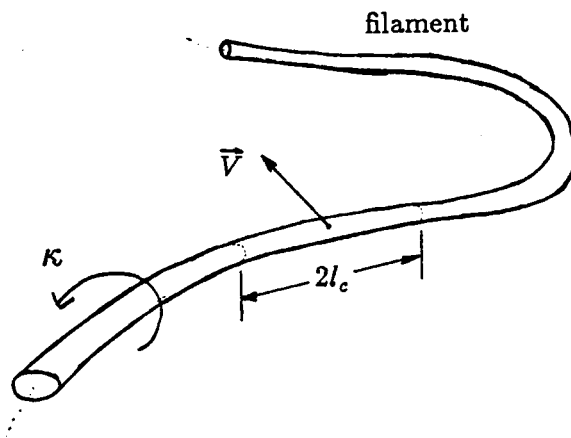


Figure A.1: The Cut-Off Method

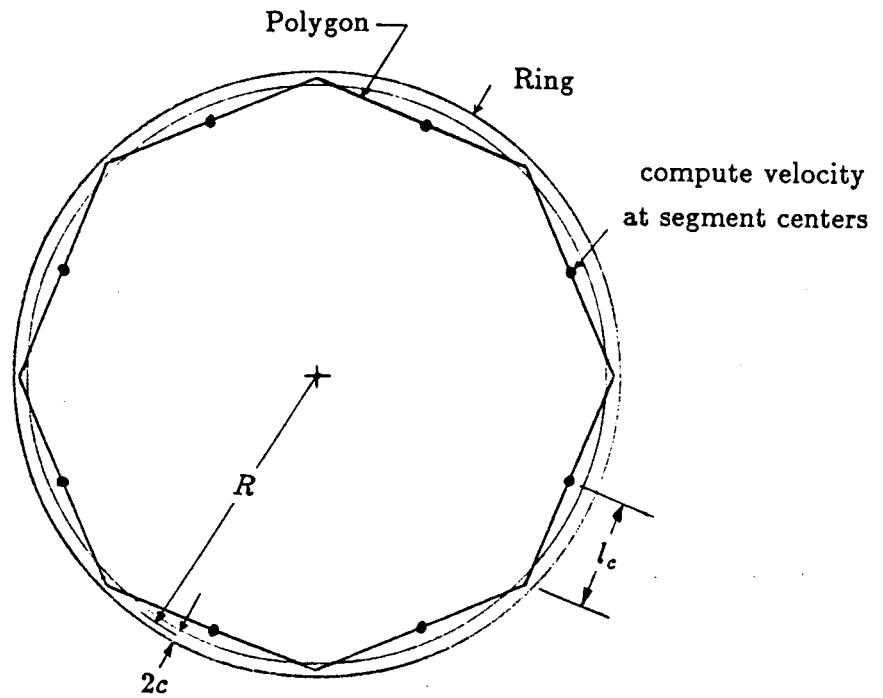


Figure A.2: Construction of a Vortex Polygon from a Vortex Ring

Appendix B

Computer Program ROLLUP

B.1 Description of Program

All of the results presented in Chapter 6 were calculated by the computer program ROLLUP. ROLLUP incorporates the vortex dynamics algorithm presented in Chapters 2 through 5 including the velocity calculations, the inner spiral model, and the rediscrretization procedure. The operation of the program is detailed in the series of flowcharts presented in Figures B.1 through B.5.

The user supplied input data to program ROLLUP is described in what follows and is read by ROLLUP from unit 5.

IWR	=	FORTRAN unit number for printed output.
NRING	=	Number of vortex elements to be used initially, the actual number used may vary according to the value supplied for MINSECT.
IAXI	=	0 for two-dimensional sheet. = 1 for axisymmetric sheet.
INTKOD	=	0 for Euler time stepping procedure. = 1 for Runge-Kutta time stepping procedure.
DXMAX	=	Δx_{max} from Section 3.1, the maximum distance moved by any vortex element within one time step.
NSTEP	=	Number of time steps.
THMAX	=	The maximum angle that the sheet may roll-up. Any roll-up

greater than THMAX is amalgamated into the tip filament.

FRAC = Fraction of the sheet initially rolled (see Section 5.1.3).

IWING = 0 for elliptic loading.
= 1 for helicopter loading.

IREDIS = Flag for allowing calls to subroutine REDISC.
= 0 for rediscrretization not performed.
= 1 for rediscrretization performed at every time step.

NU2 = Frequency of unformatted WRITES to unit 2 for plotting.

IPANEL = 0 for filaments.
= 1 for panels.

LINEUP = 0 to inhibit the spiral lineup option.
= 1 to use the spiral lineup option.

MINSECT = The minimum number of sheet segments to be used on each turn of the spiral during rediscrretization. The total number of vortex elements may be increased during execution, if necessary, to satisfy MINSECT. This parameter has no effect if LINEUP = 0.

MAXSEGS = The maximum number of vortex elements that the program is allowed to use when trying to satisfy MINSECT. This parameter also has no effect if LINEUP = 0.

The main program, Figure B.1, acts primarily as a controller, calling the principle subroutines inside of the time step loop. First the user supplied data is read from unit 5. This is followed by the program initialization. All variables are initialized including the vortex element positions and strengths and if panels are used, their orientations. The properties of the tip vortex filament are defined and the equivalent initial time is calculated. Next, all of the initial data, including the initial sheet velocities are written to unit 2. At this point the time step loop is entered where the three primary

subroutines, MOVEM, REDISC, and LUMPS are called. At the end of each time step, depending on the NU2 parameter, the resulting data is written to unit 2.

Subroutine MOVEM updates the positions of the vortex elements on the sheet and the tip vortex filament. As illustrated in Figure B.2, the first step is to decide between the Euler and the Runge-Kutta time step procedures based on the user input. If the Euler time step is used then Subroutine VELOCITY is called which calculates the total induced velocity at every vortex element. This is followed by a call to subroutine UPDATE which moves the vortex elements according to Equations 3.1 and 3.2. If the Runge-Kutta time step has been selected then a similar process is followed except that the Runge-Kutta coefficients of Equations 3.3 and 3.4 are calculated by subroutine GETK after the velocities are determined by subroutine VELOCITY. Then the vortex positions are updated according to the Runge-Kutta formulas and the process is repeated using the modified vortex positions. The cycle is completed four times to generate the four sets of Runge-Kutta coefficients. The final positions are then obtained using the four Runge-Kutta coefficients in Equations 3.3 and 3.4.

Subroutine VELOCITY, outlined in Figure B.3, acts as a switch to select from the four possible velocity calculation subroutines: axisymmetric panels in subroutine PANVEL, axisymmetric filaments in subroutine INDVEL, two-dimensional panels in subroutine PANVEL2D, and two-dimensional filaments in subroutine INDVEL2D.

Subroutine REDISC is responsible for rediscrctizing the sheet at every time step. As illustrated in Figure B.4, the first step is to fit the cubic splines of Equations 5.30 and 5.31 to the current vortex positions to reconstruct the sheet. From this, the total sheet length is calculated. If the lineup option is not being used, a new, constant, panel width for the entire sheet is found by dividing the total sheet length by the number of vortex elements. Then the sheet is rediscrctized by counting off equal length segments along the sheet, each of width equal to the new panel width. If the lineup option is being used

then first a test is made to determine if there is at least one and one half turns in the spiral. If not, then the sheet has not rolled up sufficiently to use the lineup option and the sheet is rediscrctized with the equal panel width method. If the spiral is sufficiently formed then the lineup process continues with the determination of the length of the sheet forming the turns of the spiral and the number of segments that can be put on each turn. If the MINSECT parameter is not satisfied then the program attempts to increase the total number of vortex elements in the sheet until it is. This, however, is subject to the MAXSEGS parameter which is an upper limit to the number of elements that may be used. The new vortex element positions are then found in the spiral such that the elements line up along rays emanating from the origin. The remaining part of the sheet is rediscrctized with equally spaced elements.

At this point, the sheet geometry has been rediscrctized and all that remains is to determine the strengths of the vortex elements. The vorticity distribution along the sheet is integrated from the center of the sheet to the edge to yield the circulation distribution. Equation 5.32 is used to spline fit the circulation which is then differenced to obtain the individual vortex element strengths.

Subroutine LUMPS performs the amalgamation procedure as illustrated in Figure B.5. First, the extent of the roll-up is calculated by measuring the angle of the final sheet panel to determine if amalgamation is necessary, if not, the subroutine is exited. If the sheet has formed enough turns then any element with an angle greater than THMAX is considered to be removed from the sheet and amalgamated into the tip filament. The circulation, impulse, and kinetic energy of the original sheet are found. The new tip filament strength is found from conservation of circulation. The position of the tip filament is found from the conservation of impulse and the new core section radius of the tip filament is found from the conservation of kinetic energy. Before LUMPS is exited, Subroutine REDISC is called to rediscrctize the sheet and restore the number of vortex elements in the sheet to the value before the amalgamation.

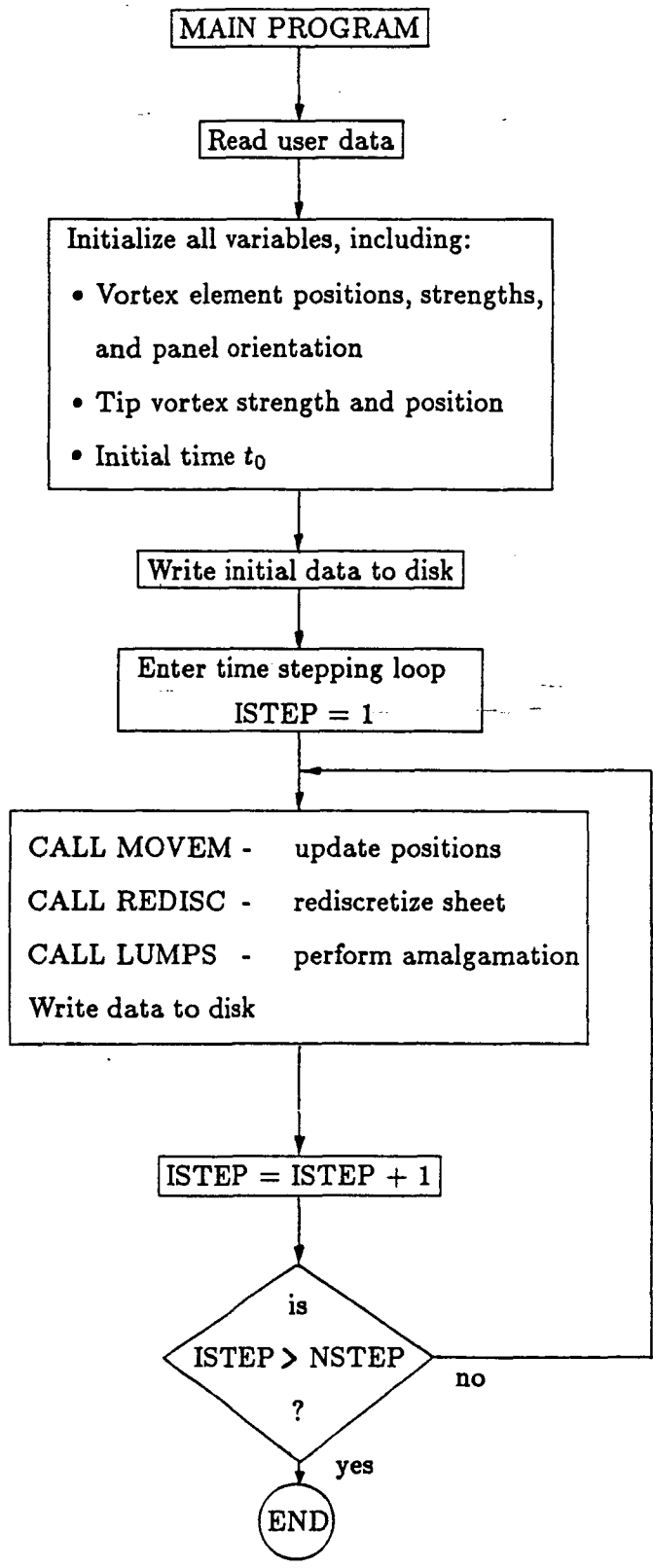


Figure B.1: Main Program of ROLLUP

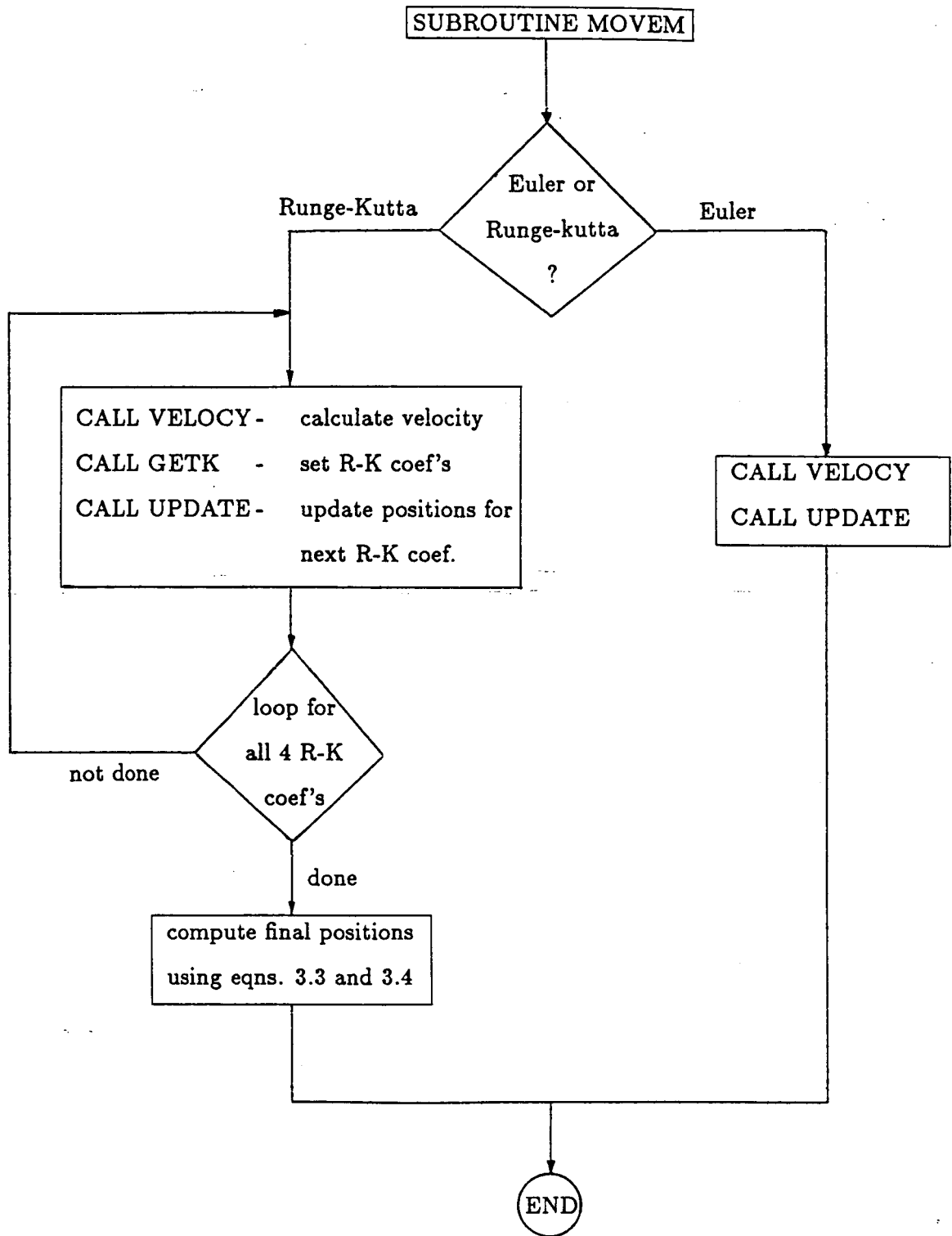


Figure B.2: Subroutine MOVEM

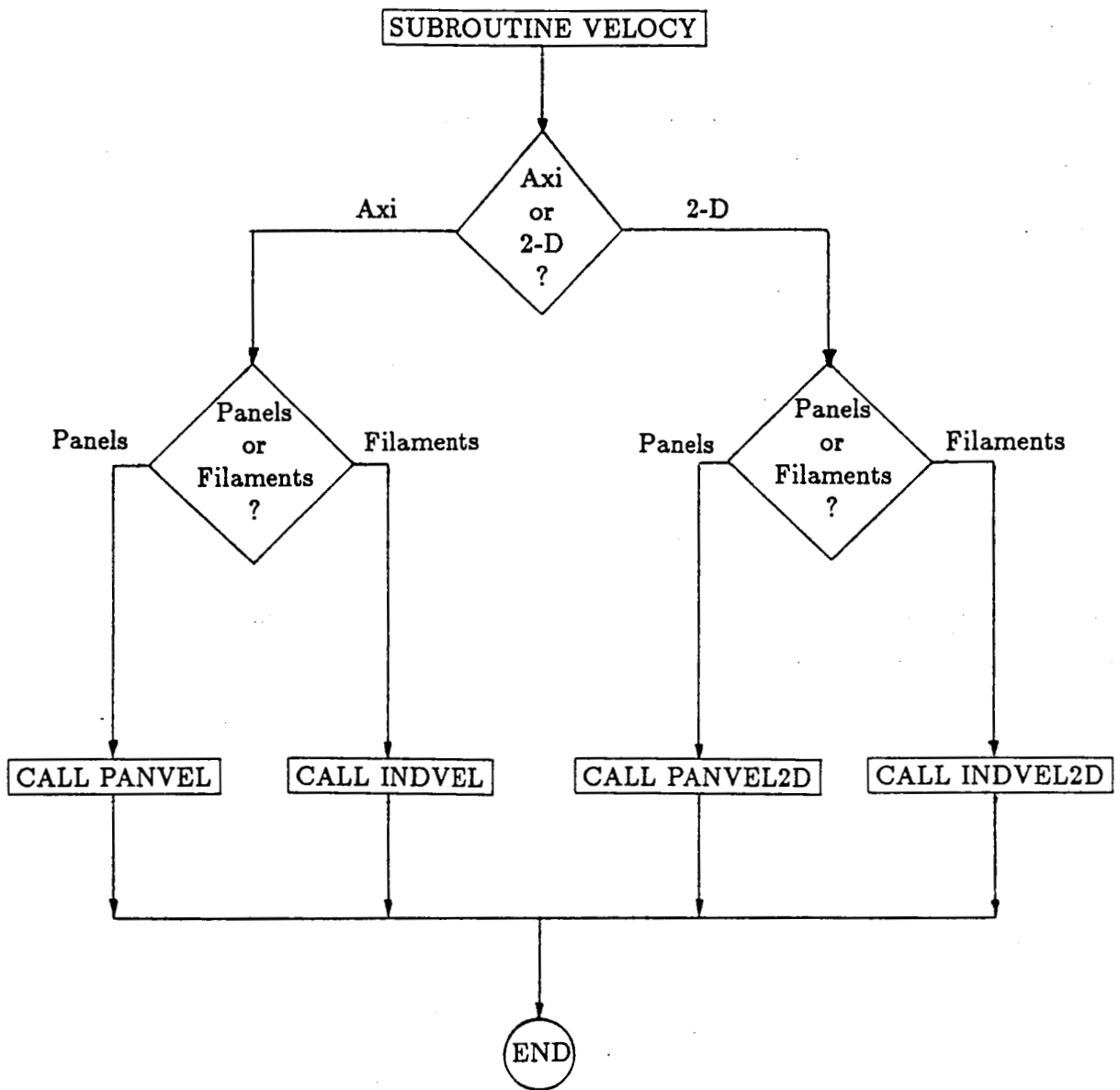


Figure B.3: Subroutine VELOCITY

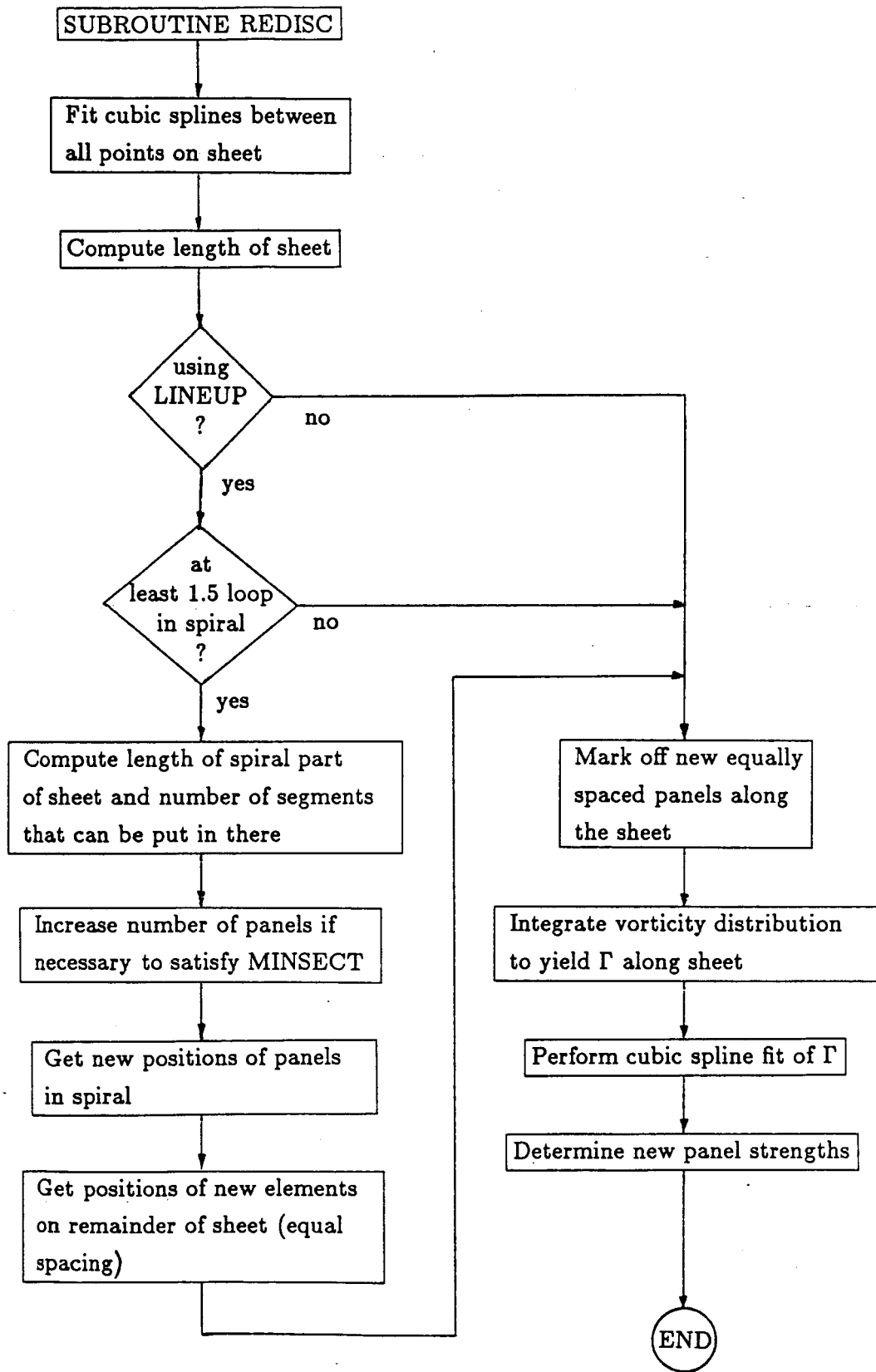


Figure B.4: Subroutine REDISC

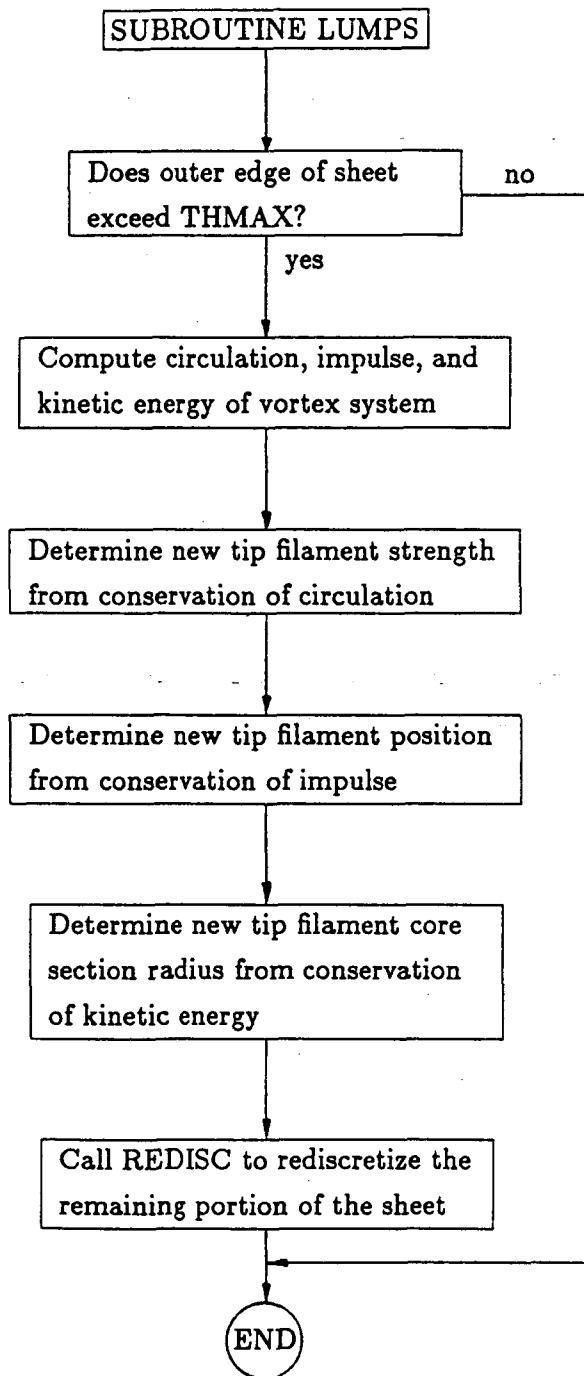


Figure B.5: Subroutine LUMPS

B.2 Program Listing

PROGRAM ROLLUP

C--This program calculates the trajectories of a group of vortex rings
C or panels which simulate a vorticity disk. The user has the option of
C using Euler or Runge-Kutta time integration. The curve fitting method
C allows for the inclusion of a concentrated tip core which is not part
C of the sheet. At any time step if the sheet rolls up by more than
C a certain amount (THMAX) the excess part of the sheet is
C chopped off and its vorticity lumped into the tip core. In
C doing this, conservation of impulse determines the location
C of the resulting core and conservation of kinetic energy
C determines the core radius.
C This version allows the simulation to start at some time $t > 0$ by
C lumping a fraction of the outer portion of the sheet into the
C concentrated tip vortex at the start.

```
C
COMMON /B1/ RADIUS(0:900),HEIGHT(0:900),WVEL(0:900),UVEL(0:900),
$          GAMMA(0:900),CORE(0:900),TIME(0:5000),TENERG(0:5000),
$          TIMPUL(0:5000)
COMMON /B2/ NRING,PI,DXMAX,INTKOD,NSMALL,VOLTIP,IAXI
C COMMON /B3/ DMIN(0:900)
COMMON /TH/ THETA(0:900),THMAX,DT(0:900)
COMMON /B9/ IWR
COMMON /PANEL/ IPANEL,DRPAN(0:900),DZPAN(0:900),WPAN(0:900)
COMMON /C1/ LINEUP,MAXSEGS,MINSECT
COMMON /D1/ DISTMX
COMMON /SEGS/ AXLSEG(0:900)
COMMON /F1/ ALPLAST,GMTO
COMMON /ZZ/ ZXO,ZYO
COMMON /G1/ TIPVAX
COMMON /E2/ DUM1,DUM2,DUM3,DUM4,DUM5,AE2
COMMON /NOW/ TIMENOW,BIGRREF
COMMON /E1/ TAUO,BDUM,CDUM,DDUM,TAU2LOOP
DIMENSION SGAM(0:900),DDGM(0:900)
REAL*4 LAMBDA,K
CHARACTER PLTITL*80,TITLE*80
```

```
C
C NRING = total number of rings (counting starts at 0)
C NSMALL = number of vortex rings which form the sheet, NSMALL=NRING-1
```

```
C Ring Indices -----
```

```
C
C Index      Meaning
C
C 0          Degenerate ring on the central axis of the ring system.
```



```

C           This ring has zero circulation and is used only to
C           define the inner boundary of the sheet.
C
C 1 - NSMALL These are the "real" vortex rings, i.e., they have non-
C (inclusive) zero circulation. These all lie on the sheet.
C
C NSMALL This ring forms the outer boundary of the sheet.
C
C NRING This is the index of the very last ring. It is the
C concentrated core tip ring. It does not lie on the sheet.
C Initially, this ring has circulation determined by FRAC.
C As the sheet rolls up, the circulation from the outer
C portions, which is chopped off, gets put into the core.
C
C
C PI=ACOS(-1.0)
C TIME(1)=0.0
C
C WRITE(6,*)' ENTER UNIT NUMBER FOR PRINTED OUTPUT'
C READ(5,*)IWR
C INEW=0
C WRITE(6,*)' ENTER: NRING, IAXI (1=AXI 0=2-D)'
C READ(5,*)NRING,IAXI
C ILOC=1
C WRITE(6,*)' ENTER: (1) FOR RUNGE-KUTTA OR (0) FOR EULER'
C READ(5,*)INTKOD
C WRITE(6,*)' ENTER: DXMAX, NSTEP (IF DXMAX .LT. 0, DT=DXMAX)'
C READ(5,*)DXMAX,NSTEP
C WRITE(6,*)' ENTER: THMAX (MAX ROLLUP ANGLE BEFORE CUT-OFF)'
C READ(5,*)THMAX
C WRITE(6,*)' ENTER: FRAC (OUTER PORTION TO BE LUMPED AT START)'
C READ(5,*)FRAC
946 WRITE(6,*)' ENTER: IWING (EXPONENT ON LOADING CURVE 0,2,4)'
C READ(5,*)IWING
C IF (IWING.NE.0.AND.IWING.NE.2.AND.IWING.NE.4) GO TO 946
C WRITE(6,*)' ENTER (1) FOR REDISCRETIZATION (0) FOR NONE'
C READ(5,*)IREDIS
C WRITE(6,*)' ENTER: NU2'
C READ(5,*)NU2
C NU2A=NU2
C TIMEAB=9.OE20
C WRITE(6,*)' ENTER: IPANEL (0)-RINGS (1)-PANELS'
C READ(5,*)IPANEL
C ISTART=0
C WRITE(6,*)' ENTER: LINEUP 0-NO SEGMENT LINEUP 1-LINEUP'
C READ(5,*)LINEUP
C WRITE(6,*)' ENTER: MINSECT (MIN # OF THETA SECT. IN SPIRAL)'
C READ(5,*)MINSECT

```

```

WRITE(6,*)' ENTER: MAXSEGS (MAX # OF RINGS OR PANELS)'
READ(5,*)MAXSEGS
DISTIN=9.OE5
DISTMX=DISTIN**2
C
NSMALL=NRING-1
LASTSTEP=1
C
C--Maximum circulation
C
IF (IAXI .EQ. 1) THEN !...3
  GCONST=4.O/PI
ELSE !...3
  GCONST=2.O
ENDIF !...3
C
C--Compute the initial location of the tip core
C
XO=FRAC
AO=0.520*XO
BO=0.825*XO
C
C--Set core size
C
CCORE=(1.O/NSMALL)/4.O
C
C--Compute radius, height, and ring circulation for constant spacing
C
CALL SETA
TIME(1)=((2.O*PI**2)/(9.O*AE2))*XO**(1.5)
TIMENOW=TIME(1)
DR=(1.O-FRAC)/NSMALL
IF (ISTART .EQ. 0) THEN
  EXPAND=(1.O-AO)/(1.O-FRAC)
ELSE
  EXPAND=1.O
ENDIF
DO 10 I=1,NSMALL
  HEIGHT(I)=0.O
  CORE(I)=CCORE
  R1=(I-1)*DR
  R2=I*DR
  RADIUS(I)=EXPAND*GETRAD(ILOC,R1,R2)
  IF (IWING .EQ. 0) THEN !...6
    CIRC1=-GCONST*(1.O-SQRT(1.O-R1**2))
    CIRC2=-GCONST*(1.O-SQRT(1.O-R2**2))
  ELSE !...6

```

```

        CIRC1=-GCONST*(1.0-(R1**IHING)*SQRT(1.0-R1**2))
        CIRC2=-GCONST*(1.0-(R2**IHING)*SQRT(1.0-R2**2))
        ENDIF !...6
        GAMMA(I)=CIRC2-CIRC1
10 CONTINUE
C
C--Initialize the arc length array, AXLSEG(I) is the total arc length
C to the end of segment I. (Note: segment I is the segment which
C contains ring or panel I)
C
        AXLSEG(0)=0.0
        DO 11 I=1,NSMALL-1
            AXLSEG(I)=AXLSEG(I-1)
            $           +SQRT( (RADIUS(I+1)-RADIUS(I))**2
            $           +(HEIGHT(I+1)-HEIGHT(I))**2 )
11 CONTINUE
        AXLSEG(NSMALL)=AXLSEG(NSMALL-1)
        $           +SQRT( (RADIUS(NSMALL)-RADIUS(NSMALL-1))**2
        $           +(HEIGHT(NSMALL)-HEIGHT(NSMALL-1))**2)
C
C--Initialize special tip vortex (Index=NRING)
C
        IF (FRAC .EQ. 0.0) THEN !...10
C
C--This section for no circulation in tip vortex initially
C
        HEIGHT(NRING)=0.0
        RADIUS(NRING)=1.0
        GAMMA(NRING)=0.0
        CORE(NRING)=0.0001
        VOLTIP=2.0*PI*PI*RADIUS(NRING)*CORE(NRING)**2
        ELSE !...10
C
        IF (IAXI .EQ. 1) THEN !...11           tip parameters for axi-flow
C
        HEIGHT(NRING)=BO
        REDG=1.0-FRAC
        GAMMA(NRING)=(-GCONST)-
        $           (-GCONST*(1.0-(REDG**IHING)*SQRT(1.0-REDG**2)))
        RADIUS(NRING)=1.0-AO
C
C--Now figure total K.E. and get core size
C
        SUM1=0.0
        SUM2=0.0
        DO 82 I=1,NRING
            W=RADIUS(I)

```

```

Z=HEIGHT(I)
DO 82 J=1,NRING
  IF (I .NE. J) THEN !...12
    WP=RADIUS(J)
    ZP=HEIGHT(J)
    R1=SQRT((Z-ZP)**2+(W-WP)**2)
    R2=SQRT((Z-ZP)**2+(W+WP)**2)
    LAMBDA=(R2-R1)/(R2+R1)
    CALL ELLIP(LAMBDA,K,E)
    SUM1=SUM1+GAMMA(I)*GAMMA(J)*(R1+R2)*(K-E)/2.0
  ENDIF !...12
82  CONTINUE
C
  IF (IHING .EQ. 0) THEN !...13
    TOTKE=4.0/3.0
  ELSE IF (IHING .EQ. 2) THEN !...13
    TOTKE=0.41
  ELSE IF (IHING .EQ. 4) THEN !...13
    TOTKE=0.245
  ENDIF !...13
DO 83 I=1,NSMALL
  W=RADIUS(I)
83  SUM2=SUM2+GAMMA(I)**2*W*(ALOG(8.0*W/CORE(I))-1.75)/2.0
  TNBAR=TOTKE-SUM2-SUM1
  XTEMP=EXP(2.0*TNBAR/(GAMMA(NRING)**2*RADIUS(NRING)))+1.75)
  CORE(NRING)=8.0*RADIUS(NRING)/XTEMP
C
C--Get volume of tip core
C
  VOLTIP=2.0*PI*PI*RADIUS(NRING)*CORE(NRING)**2
C
  ELSE !...11      tip parameters for 2-D flow
    HEIGHT(NRING)=BO
    REDG=1.0-FRAC
    GAMMA(NRING)=(-GCONST)-
    $      (-GCONST*(1.0-(REDG**IHING)*SQRT(1.0-REDG**2)))
    RADIUS(NRING)=1.0-AO
    CORE(NRING)=0.0
    VOLTIP=0.0
  ENDIF !...11
C
  ENDIF !...10
C
C--Center ring
C
  IF (IHING .EQ. 0) THEN !...15
    GMAX=-GCONST

```

```

ELSE !...15
  GMAX=0.0
ENDIF !...15
RADIUS(0)=0.0
HEIGHT(0)=0.0
C
C--If panel case, then calculate some more initial parameters
C
  IF (IPANEL .EQ. 1) THEN !...16
    DO 1920 I=1,NSMALL-1
      SL=-SQRT( (RADIUS(I)-RADIUS(I-1))**2
$           +(HEIGHT(I)-HEIGHT(I-1))**2 )
      SR= SQRT( (RADIUS(I)-RADIUS(I+1))**2
$           +(HEIGHT(I)-HEIGHT(I+1))**2 )
      A1=((SL*SR)/(SL-SR))*((RADIUS(I+1)-RADIUS(I))/SR**2
$           -(RADIUS(I-1)-RADIUS(I))/SL**2)
      B1=((SL*SR)/(SL-SR))*((HEIGHT(I+1)-HEIGHT(I))/SR**2
$           -(HEIGHT(I-1)-HEIGHT(I))/SL**2)
      DRPAN(I)=A1
      DZPAN(I)=B1
1920  CONTINUE
      A2=((RADIUS(I+1)-RADIUS(I))/SR-(RADIUS(I-1)-RADIUS(I))/SL)
$           /(SR-SL)
      B2=((HEIGHT(I+1)-HEIGHT(I))/SR-(HEIGHT(I-1)-HEIGHT(I))/SL)
$           /(SR-SL)
      DRPAN(NSMALL)=A1+A2*SR
      DZPAN(NSMALL)=B1+B2*SR
      DO 717 I=1,NSMALL
        WPAN(I)=(AXLSEG(I)-AXLSEG(I-1))/2.0 !WPAN is panel half-width
717  CONTINUE
      ENDIF !...16
C
    DO 8315 I=0,NRING
8315  HEIGHT(I)=HEIGHT(I)-1.0*TIME(1)
      GMTO=GAMMA(NRING)
C
C--Write out the input data
C
      WRITE(IWR,*)' NRING =' ,NRING
      WRITE(IWR,*)' FRAC =' ,FRAC
      WRITE(IWR,*)' INTKOD =' ,INTKOD
      WRITE(IWR,*)' DXMAX =' ,DXMAX
      WRITE(IWR,*)' NSTEP =' ,NSTEP
      WRITE(IWR,*)' THMAX =' ,THMAX
      WRITE(IWR,*)' IWING =' ,IWING
      WRITE(IWR,*)' IREDIS =' ,IREDIS
      WRITE(IWR,*)' NU2   =' ,NU2

```

```

WRITE(IWR,*)' IPANEL =' ,IPANEL
WRITE(IWR,*)' LINEUP =' ,LINEUP
WRITE(IWR,*)' MAXSEGS=' ,MAXSEGS
WRITE(IWR,*)' MINSECT=' ,MINSECT
WRITE(IWR,*)' IAXI  =' ,IAXI
WRITE(2) INEW
WRITE(2) NRING,CCORE, IDIST,FRAC,INTKOD,DXMAX,NSTEP,THMAX,
$      LINEUP,DISTIN,MAXSEGS,MINSECT,IAXI,IPANEL
CALL VELOCY
WRITE(IWR,*)' '
WRITE(IWR,*)' ----- INITIAL VALUES -----'
WRITE(IWR,*)' '
WRITE(IWR,3243)
3243  FORMAT('  I      RADIUS      HEIGHT      GAMMA      ' ,
$      '      CORE      UVEL      WVEL      AXLSEG      ' ,
$      '      DRPAN      DZPAN')
WRITE(IWR,3244)(I,RADIUS(I),HEIGHT(I),GAMMA(I),CORE(I),
$      UVEL(I),WVEL(I),AXLSEG(I),DRPAN(I),
$      DZPAN(I),I=0,NRING)
3244  FORMAT(1X,I3,9E14.6)
C
C--Initialize unit 2 plot data
C
WRITE(2) NRING,CORE(NRING),TIME(1)
WRITE(2) (RADIUS(I),HEIGHT(I),GAMMA(I),AXLSEG(I),I=0,NRING)
WRITE(2) TIPVAX
C
C-----
C----- MAIN TIME LOOP -----
C-----
C
DO 99 ISTEP=LASTSTEP,NSTEP+LASTSTEP-1
C
C--Compute velocities at step ISTEP which
C corresponds to time (ISTEP-1)*"DT" and also update positions
C
CALL MOVEM(ISTEP)
IF (IREDIS .EQ. 1) THEN
WVTIP=WVEL(NRING)
UVTIP=UVEL(NRING)
CTIP=CORE(NRING)
NIN=NSMALL
NOUT=NSMALL
GMM=GMAX-GAMMA(NRING)
CALL REDISC(RADIUS,HEIGHT,GAMMA,NIN,NOUT,GMM,SUML,DELTA,
$      TIME(ISTEP+1))
WVEL(NRING)=WVTIP

```

```

      UVEL(NRING)=UVTIP
      CORE(NRING)=CTIP
    ENDIF
    IF (IREDIS .EQ. 1) THEN
      WVTIP=WVEL(NRING)
      UVTIP=UVEL(NRING)
      CTIP=CORE(NRING)
      CALL LUMPS(TIME(ISTEP+1))
      WVEL(NRING)=WVTIP
      UVEL(NRING)=UVTIP
      CORE(NRING)=CTIP
    ENDIF
  C
  C--Now update the core size, since the sheet has stretched
  C
      IF (IAXI .EQ. 1) THEN
        DO 691 II=1,NSMALL
691   CORE(II)=WPAN(II)/2.0
      ENDIF
  C
  C--Write data to disk (unit 2) for plotting later
  C
      NU2=NU2C
      IF (TIME(ISTEP+1) .LT. TIMEBC) NU2=NU2B
      IF (TIME(ISTEP+1) .LT. TIMEAB) NU2=NU2A
  C
      IF((ISTEP/NU2)*NU2-ISTEP.EQ.0
  $      .OR. ISTEP.EQ.NSTEP+LASTSTEP-1)THEN
        WRITE(2)NRING,CORE(NRING),TIME(ISTEP+1)
        WRITE(2)(RADIUS(I),HEIGHT(I),GAMMA(I),AXLSEG(I),I=0,NRING)
        WRITE(2)TIPVAX
      ENDIF
  C
      NOWSTEP=ISTEP
      99 CONTINUE
  C
  C-----
  C----- END OF MAIN TIME LOOP -----
  C-----
  C
      STOP
      END
      FUNCTION GETRAD(ILOC,R1,R2)
  C
  C--This function determines the location of the vortex ring within
  C a segment, if ILOC=1 then the ring is centered, if ILOC=2 then the
  C ring is positioned such that the total impulse is maintained

```

```

C
IF (ILOC .EQ. 1) THEN
  GETRAD=(R1+R2)/2.0
ELSE
  F1=((SQRT(1.0-R1**2))**3-(SQRT(1.0-R2**2))**3)*8.0/3.0
  F2=4.0*R1**2*SQRT(1.0-R1**2)
  F3=4.0*R2**2*SQRT(1.0-R2**2)
  F4=4.0*(SQRT(1.0-R1**2)-SQRT(1.0-R2**2))
  GETRAD=SQRT((F1+F2-F3)/F4)
ENDIF
C
RETURN
END

SUBROUTINE MOVEM(ISTEP)
COMMON /B1/ RADIUS(0:900),HEIGHT(0:900),WVEL(0:900),UVEL(0:900),
$          GAMMA(0:900),CORE(0:900),TIME(0:5000),TENERG(0:5000),
$          TIMPUL(0:5000)
COMMON /B2/ NRING,PI,DXMAX,INTKOD,NSMALL,VOLTIP,IAXI
COMMON /RK/ RADO(0:900),HEIO(0:900),RK(0:900,4),HK(0:900,4)
COMMON /NOW/ TIMENOW,BIGRREF
COMMON /F1/ ALPLAST,GMTO
COMMON /G1/ TIPVAX
C
C--Computes velocities and new positions using either Euler or
C Runge-Kutta time stepping
C
C--First save original data
C
  ALPO=ALPLAST
  DO 20 I=0,NRING
    RADO(I)=RADIUS(I)
    HEIO(I)=HEIGHT(I)
  20 CONTINUE
C
C--Now check for time step method
C
  IF (INTKOD .EQ. 0) THEN !Euler time step
C
    TIMENOW=TIME(ISTEP)
    CALL VELOCY
    CALL GETDT(DT)
    CALL GETK(1)
    CALL UPDATE(DT,1)
    TIPVAX=WVEL(NRING)
C

```



```

ELSE                                !Runge-Kutta time step
C
  CALL PULANG(NRING-1,BEFORE) !angle at last panel center at start
  TIMENOW=TIME(ISTEP)
  CALL VELOCY
  CALL GETDT(DT)
  CALL GETK(1)
  CALL UPDATE(DT/2.0,1)
  TIPVAX=WVEL(NRING)
C
  CALL PULANG(NRING-1,ANOW) !get new angle and compute the change
  ALPLAST=ALPO+(ANOW-BEFORE) !and add it to the angle of the edge
  TIMENOW=TIME(ISTEP)+DT/2.0
  CALL VELOCY
  CALL GETK(2)
  CALL UPDATE(DT/2.0,2)
C
  CALL PULANG(NRING-1,ANOW)
  ALPLAST=ALPO+(ANOW-BEFORE)
  TIMENOW=TIME(ISTEP)+DT/2.0
  CALL VELOCY
  CALL GETK(3)
  CALL UPDATE(DT,3)
C
  CALL PULANG(NRING-1,ANOW)
  ALPLAST=ALPO+(ANOW-BEFORE)
  TIMENOW=TIME(ISTEP)+DT
  CALL VELOCY
  CALL GETK(4)
C
C--Update positions for Runge-Kutta
C
  DO 10 I=0,NRING
    RADIUS(I)=RADO(I)+(DT/6.0)*(RK(I,1)+2.0*RK(I,2)+
$      2.0*RK(I,3)+RK(I,4))
    HEIGHT(I)=HEIO(I)+(DT/6.0)*(HK(I,1)+2.0*HK(I,2)+
$      2.0*HK(I,3)+HK(I,4))
  10 CONTINUE
C
  ENDIF
C
C--Compute the new core radius for the tip ring and update time
C
  CORE(NRING)=SQRT(VOLTIP/(2.0*RADIUS(NRING)))/PI
  TIME(ISTEP+1)=TIME(ISTEP)+DT
C
  RETURN

```

```

END
SUBROUTINE GETK(N)
COMMON /B1/ RADIUS(O:900),HEIGHT(O:900),WVEL(O:900),UVEL(O:900),
$          GAMMA(O:900),CORE(O:900),TIME(O:5000),TENERG(O:5000),
$          TIMPUL(O:5000)
COMMON /B2/ NRING,PI,DXMAX,INTKOD,NSMALL,VOLTIP,IAXI
COMMON /RK/ RADO(O:900),HEIO(O:900),RK(O:900,4),HK(O:900,4)
C
C--Computes the 4 K parameters used in the Runge-Kutta routine.
C The K's are just the velocity components.
C
DO 10 I=0,NRING
  RK(I,N)=UVEL(I)
  HK(I,N)=WVEL(I)
10 CONTINUE
C
RETURN
END
SUBROUTINE UPDATE(H,N)
COMMON /B1/ RADIUS(O:900),HEIGHT(O:900),WVEL(O:900),UVEL(O:900),
$          GAMMA(O:900),CORE(O:900),TIME(O:5000),TENERG(O:5000),
$          TIMPUL(O:5000)
COMMON /B2/ NRING,PI,DXMAX,INTKOD,NSMALL,VOLTIP,IAXI
COMMON /RK/ RADO(O:900),HEIO(O:900),RK(O:900,4),HK(O:900,4)
COMMON /PANEL/ IPANEL,DRPAN(O:900),DZPAN(O:900),WPAN(O:900)
C
C--Computes new positions of the rings based on the time step H and
C the velocity contained in RK and HK.
C
DO 10 I=0,NRING
  RADIUS(I)=RADO(I)+H*RK(I,N)
  HEIGHT(I)=HEIO(I)+H*HK(I,N)
10 CONTINUE
C
C--Compute the new core radius for the tip ring
C
CORE(NRING)=SQRT(VOLTIP/(2.0*RADIUS(NRING)))/PI
C
C--If panel case, estimate inclinations
C
IF (IPANEL .EQ. 1) THEN
  DO 20 I=1,NSMALL-1
    SL=-SQRT( (RADIUS(I)-RADIUS(I-1))**2
$           +(HEIGHT(I)-HEIGHT(I-1))**2 )
    SR= SQRT( (RADIUS(I)-RADIUS(I+1))**2
$           +(HEIGHT(I)-HEIGHT(I+1))**2 )
    A1=((SL*SR)/(SL-SR))*((RADIUS(I+1)-RADIUS(I))/SR**2

```

```

$                                     -(RADIUS(I-1)-RADIUS(I))/SL**2)
B1=((SL*SR)/(SL-SR))*((HEIGHT(I+1)-HEIGHT(I))/SR**2
$                                     -(HEIGHT(I-1)-HEIGHT(I))/SL**2)
DRPAN(I)=A1
DZPAN(I)=B1
20 CONTINUE
A2=((RADIUS(I+1)-RADIUS(I))/SR-(RADIUS(I-1)-RADIUS(I))/SL)
$                                     /((SR-SL)
B2=((HEIGHT(I+1)-HEIGHT(I))/SR-(HEIGHT(I-1)-HEIGHT(I))/SL)
$                                     /((SR-SL)
DRPAN(NSMALL)=A1+A2*SR
DZPAN(NSMALL)=B1+B2*SR
ENDIF
C
RETURN
END
SUBROUTINE GETDT(DT)
COMMON /B1/ RADIUS(0:900),HEIGHT(0:900),WVEL(0:900),UVEL(0:900),
$          GAMMA(0:900),CORE(0:900),TIME(0:5000),TENERG(0:5000),
$          TIMPUL(0:5000)
COMMON /B2/ NRING,PI,DXMAX,INTKOD,NSMALL,VOLTIP,IAXI
COMMON /RK/ RADO(0:900),HEIO(0:900),RK(0:900,4),HK(0:900,4)
C
C--Find max velocity and DT, DT=(ABS(DXMAX) if DXMAX .LT. 0.0)
C
IF (DXMAX .LT. 0.0) THEN
DT=ABS(DXMAX)
ELSE
VMAX=UVEL(0)**2+WVEL(0)**2
DO 40 I=1,NRING
VRING=UVEL(I)**2+WVEL(I)**2
IF (VRING .GT. VMAX) VMAX=VRING
40 CONTINUE
VMAX=SQRT(VMAX)
DT=DXMAX/VMAX
ENDIF
C
RETURN
END
SUBROUTINE VELOCITY
C
C--Decide between routines for velocity from rings or panels, for
C axi or for 2-D
C
COMMON /B2/ NRING,PI,DXMAX,INTKOD,NSMALL,VOLTIP,IAXI
COMMON /PANEL/ IPANEL,DRPAN(0:900),DZPAN(0:900),WPAN(0:900)
C

```

```

IF (IAXI .EQ. 1) THEN                !Axi case
  IF (IPANEL .EQ. 0) THEN
    CALL INDVEL                        !Rings
  ELSE
    CALL PANVEL                        !Panels
  ENDIF
ELSE
  !2-D case
  IF (IPANEL .EQ. 0) THEN
    CALL INDVEL2D                      !Filaments
  ELSE
    CALL PANVEL2D                      !Panels
  ENDIF
ENDIF
C
RETURN
END
SUBROUTINE INDVEL
C
C AXISYMMETRIC FILAMENTS (RINGS)
C--This routine calculates the induced velocity at each ring position
C due to all the other rings and due to itself.
C
COMMON /B1/ RADIUS(0:900),HEIGHT(0:900),WVEL(0:900),UVEL(0:900),
$          GAMMA(0:900),CORE(0:900),TIME(0:5000),TENERG(0:5000),
$          TIMPUL(0:5000)
COMMON /B2/ NRING,PI,DXMAX,INTKOD,NSMALL,VOLTIP,IAXI
REAL*4 LAMBDA,K
DATA AO,A1,A2,A3,A4,BO,B1,B2,B3,B4/
$ 1.38629436112, .09666344259, .03590092383,
$ .03742563713, .01451196212, .5
$ .12498593597, .06880248576, .03328355346,
$ .00441787012/
DATA CO,C1,C2,C3,C4,DO,D1,D2,D3,D4/
$ 1.0, .44325141463, .06260601220,
$ .04757383546, .01736506451, .0
$ .24998368310, .09200180037, .04069697526,
$ .00526449639/
C
C--Loop over all rings, except center ring, get induced velocity at each
C
DO 10 I=1,NRING
  W=RADIUS(I)
  Z=HEIGHT(I)
  WVEL(I)=0.0
  UVEL(I)=0.0
C
C--Loop over all rings again (except control ring) and determine the

```

C contribution of each to the induced velocity at ring I.
C

```

IF (I .EQ. 1) GO TO 25
DO 20 J=1,I-1
  WP=RADIUS(J)
  ZP=HEIGHT(J)
  R1=SQRT((Z-ZP)**2+(W-WP)**2)
  R2=SQRT((Z-ZP)**2+(W+WP)**2)
  LAMBDA=(R2-R1)/(R2+R1)
  FK=1.0-LAMBDA**2
  K = AO+FK*(A1+FK*(A2+FK*(A3+FK*A4)))
  $      +(BO+FK*(B1+FK*(B2+FK*(B3+FK*B4))))*ALOG(1.0/FK)
  E = CO+FK*(C1+FK*(C2+FK*(C3+FK*C4)))
  $      +(DO+FK*(D1+FK*(D2+FK*(D3+FK*D4))))*ALOG(1.0/FK)
  F1=((W-WP)/R1+(W+WP)/R2)*(K-E)
  F2=2.0*E*LAMBDA/(1.0-LAMBDA**2)
  F3=(W*(R1**2-R2**2)+WP*(R1**2+R2**2))/(R1*R2*(R1+R2))
  WV=GAMMA(J)*(F1+F2*F3)/(2.0*PI*W)
  WVEL(I)=WVEL(I)+WV
  F4=(Z-ZP)*(R1+R2)/(R1*R2)
  F5=K-E*(1.0+LAMBDA**2)/(1.0-LAMBDA**2)
  UV=GAMMA(J)*F4*F5/(2.0*PI*W)
  UVEL(I)=UVEL(I)-UV
20 CONTINUE
25 IF (I .EQ. NRING) GO TO 40
DO 30 J=I+1,NRING
  WP=RADIUS(J)
  ZP=HEIGHT(J)
  R1=SQRT((Z-ZP)**2+(W-WP)**2)
  R2=SQRT((Z-ZP)**2+(W+WP)**2)
  LAMBDA=(R2-R1)/(R2+R1)
  FK=1.0-LAMBDA**2
  K = AO+FK*(A1+FK*(A2+FK*(A3+FK*A4)))
  $      +(BO+FK*(B1+FK*(B2+FK*(B3+FK*B4))))*ALOG(1.0/FK)
  E = CO+FK*(C1+FK*(C2+FK*(C3+FK*C4)))
  $      +(DO+FK*(D1+FK*(D2+FK*(D3+FK*D4))))*ALOG(1.0/FK)
  F1=((W-WP)/R1+(W+WP)/R2)*(K-E)
  F2=2.0*E*LAMBDA/(1.0-LAMBDA**2)
  F3=(W*(R1**2-R2**2)+WP*(R1**2+R2**2))/(R1*R2*(R1+R2))
  WV=GAMMA(J)*(F1+F2*F3)/(2.0*PI*W)
  WVEL(I)=WVEL(I)+WV
  F4=(Z-ZP)*(R1+R2)/(R1*R2)
  F5=K-E*(1.0+LAMBDA**2)/(1.0-LAMBDA**2)
  UV=GAMMA(J)*F4*F5/(2.0*PI*W)
  UVEL(I)=UVEL(I)-UV
30 CONTINUE
40 CONTINUE

```

```

C
C--Calculate final velocity including self-induced component
C
      WV=GAMMA(I)*(ALOG(8.0*W/CORE(I))-.25)/(4.0*PI*W)
      WVEL(I)=WVEL(I)+WV
C
C--get velocity of higher order terms in tip region, if not tip ring now
C
      IF (I .NE. NRING) THEN
        CALL DOUBLET(W,Z,VXPRM,VYPRM,VRPRM,VTHPRM)
        WVEL(I)=WVEL(I)+VYPRM
        UVEL(I)=UVEL(I)+VXPRM
      ENDIF
C
      10 CONTINUE
C
C--Get velocity contribution at tip due to inner spiral
C
      CALL CENSPIR(VXP,VYP)
      UVEL(NRING)=UVEL(NRING)+VXP
      WVEL(NRING)=WVEL(NRING)+VYP
C
C--Get induced velocity at center by extrapolating the velocities of
C points 1 and 2. Fit a parabola (for the velocity) through points
C 0, 1, and 2 by matching the values at points 1 and 2 and setting
C the slope=0 at r=0. Then the velocity at r=0 (i.e., the center
C point) is just the constant part of the parabola.
C
      UVEL(0)=0.0
      WVEL(0)=(WVEL(1)*RADIUS(2)**2-WVEL(2)*RADIUS(1)**2)
      $      /(RADIUS(2)**2-RADIUS(1)**2)
C
C--done
C
      RETURN
      END

      SUBROUTINE PANVEL
C
C AXISYMMETRIC PANELS
C--This routine calculates the induced velocity at each panel centroid
C and at the tip ring due to all the other panels and due to itself.
C
      COMMON /B1/ RADIUS(0:900),HEIGHT(0:900),WVEL(0:900),UVEL(0:900),
      $          GAMMA(0:900),CORE(0:900),TIME(0:5000),TENERG(0:5000),
      $          TIMPUL(0:5000)

```

```

COMMON /B2/ NRING,PI,DXMAX,INTKOD,NSMALL,VOLTIP,IAXI
COMMON /PANEL/ IPANEL,DRPAN(0:900),DZPAN(0:900),WPAN(0:900)
COMMON /VELO/ R,XX,YY,DXT,DYT,WW,G
COMMON /D1/ DISTMX
REAL*4 LAMBDA,K

```

C

C--Loop over all panels, except center ring, get induced velocity at each

C

```

DO 10 I=1,NSMALL
  WVEL(I)=0.0          !axial velocity
  UVEL(I)=0.0          !radial velocity

```

C

C--Loop over all panels again and determine the contribution of each to
C the induced velocity at panel I including the self-induced component.

C

```

DO 20 J=1,NSMALL
  R=RADIUS(J)
  G=GAMMA(J)/(2.0*WPAN(J))
  WW=WPAN(J)
  DXT=DRPAN(J)
  DYT=DZPAN(J)
  XX=RADIUS(I)-RADIUS(J)
  YY=HEIGHT(I)-HEIGHT(J)
  DISTSQ=XX*XX+YY*YY
  IF (DISTSQ .LT. DISTMX) THEN
    IF (I .EQ. J) THEN
      XX = -.1 * WW
      CALL VELIN ( UINA, VINA)
      CALL VELIO ( UIOA, VIOA)
      CALL VELOUT( UOUTA, VOUTA)
      XX = .1 * WW
      CALL VELIN ( UINB, VINB)
      CALL VELIO ( UIOB, VIOB)
      CALL VELOUT( UOUTB, VOUTB)
      UIN = (UINA + UINB) / 2.
      VIN = (VINA + VINB) / 2.
      UIO = (UIOA + UIOB) / 2.
      VIO = (VIOA + VIOB) / 2.
      UOUT = (UOUTA + UOUTB) / 2.
      VOUT = (VOUTA + VOUTB) / 2.
      XX=0.0
    ELSE
      CALL VELIN ( UIN, VIN)
      CALL VELIO ( UIO, VIO)
      CALL VELOUT( UOUT, VOUT)
    END IF
  ELSE

```

```

        UIN=0.0
        VIN=0.0
        UIO=0.0
        VIO=0.0
        CALL VELOUT(UOUT,VOUT)
    ENDIF
    UVEL(I)=UVEL(I)-(UIN+UOUT-UIO)
    WVEL(I)=WVEL(I)-(VIN+VOUT-VIO)
20  CONTINUE
C
C--Now get contribution of tip ring
C
    J=NRING
    W=RADIUS(I)
    Z=HEIGHT(I)
    WP=RADIUS(J)
    ZP=HEIGHT(J)
    R1=SQRT((Z-ZP)**2+(W-WP)**2)
    R2=SQRT((Z-ZP)**2+(W+WP)**2)
    LAMBDA=(R2-R1)/(R2+R1)
    CALL ELLIP(LAMBDA,K,E)
    F1=((W-WP)/R1+(W+WP)/R2)*(K-E)
    F2=2.0*E*LAMBDA/(1.0-LAMBDA**2)
    F3=(W*(R1**2-R2**2)+WP*(R1**2+R2**2))/(R1*R2*(R1+R2))
    WV=GAMMA(J)*(F1+F2*F3)/(2.0*PI*W)
    WVEL(I)=WVEL(I)+WV
    F4=(Z-ZP)*(R1+R2)/(R1*R2)
    F5=K-E*(1.0+LAMBDA**2)/(1.0-LAMBDA**2)
    UV=GAMMA(J)*F4*F5/(2.0*PI*W)
    UVEL(I)=UVEL(I)-UV
C
C--get velocity of higher order terms in tip region
C
    CALL DOUBLET(W,Z,VXPRM,VYPRM,VRPRM,VTHPRM)
    WVEL(I)=WVEL(I)+VYPRM
    UVEL(I)=UVEL(I)+VXPRM
C
10  CONTINUE
C
C--Get induced velocity at center by extrapolating the velocities of
C points 1 and 2. Fit a parabola (for the velocity) through points
C 0, 1, and 2 by matching the values at points 1 and 2 and setting
C the slope=0 at r=0. Then the velocity at r=0 (i.e., the center
C point) is just the constant part of the parabola.
C
    UVEL(0)=0.0
    WVEL(0)=(WVEL(1)*RADIUS(2)**2-WVEL(2)*RADIUS(1)**2)

```



```

$          /(RADIUS(2)**2-RADIUS(1)**2)
C
C--Get induced velocity at the tip ring
C
WVEL(NRING)=0.0
UVEL(NRING)=0.0
DO 40 J=1,NSMALL          !loop over all panels
  R=RADIUS(J)
  G=GAMMA(J)/(2.0*WPAN(J))
  WW=WPAN(J)
  DXT=DRPAN(J)
  DYT=DZPAN(J)
  XX=RADIUS(NRING)-RADIUS(J)
  YY=HEIGHT(NRING)-HEIGHT(J)
  CALL VELIN ( UIN, VIN)
  CALL VELIO ( UIO, VIO)
  CALL VELOUT( UOUT, VOUT)
  UVEL(NRING)=UVEL(NRING)-(UIN+UOUT-UIO)
  WVEL(NRING)=WVEL(NRING)-(VIN+VOUT-VIO)
40 CONTINUE
C
C--Get tip ring self-induced component
C
WV=GAMMA(NRING)*(ALOG(8.0*RADIUS(NRING)/CORE(NRING))-0.25)
$          /(4.0*PI*RADIUS(NRING))
WVEL(NRING)=WVEL(NRING)+WV
C
C--Get velocity contribution at tip due to inner spiral
C
CALL CENSPIR(VXP,VYP)
UVEL(NRING)=UVEL(NRING)+VXP
WVEL(NRING)=WVEL(NRING)+VYP
C
C--done
C
RETURN
END
SUBROUTINE INDVEL2D
C
C This routine is for the 2-D case, i.e., filaments
C It calculates the induced velocity at each filament position
C due to all the other filaments and due to itself.
C
COMMON /B1/ RADIUS(0:900),HEIGHT(0:900),WVEL(0:900),UVEL(0:900),
$          GAMMA(0:900),CORE(0:900),TIME(0:5000),TENERG(0:5000),
$          TIMPUL(0:5000)
COMMON /B2/ NRING,PI,DXMAX,INTKOD,NSMALL,VOLTIP,IAXI

```

```

COMMON /PANEL/ IPANEL,DRPAN(0:900),DZPAN(0:900),WPAN(0:900)
COMMON /VELO/ R,XX,YY,DXT,DYT,WW,G
COMMON /B9/ IWR
COMMON /SEGS/ AXLSEG(0:900)
COMMON /NOW/ TIMENOW,BIGRREF
COMMON /E1/ TAUO,BDUM,CDUM,DDUM,TAU2LOOP
COMMON /F1/ ALPLAST,GMTO
REAL*4 LAMBDA,K

```

C

```
TPIINV=1.0/(2.0*PI)
```

C

```

C--Loop over all filaments, except center filament,
C get induced velocity at each

```

C

```

DO 10 I=1,NRING                                !index of control point
  W=RADIUS(I)
  Z=HEIGHT(I)
  WVEL(I)=0.0      !axial component
  UVEL(I)=0.0      !radial component
  IF (IWR .EQ. 25 .AND. I .GE. 68) THEN
    WRITE(IWR,*) ' LOOP 10: I,W,Z',I,W,Z
    WRITE(IWR,*) ' LOOP 20: J,GAMMA(J),XX,YY,UIN,VIN,UINRF,VINRF'
  ENDIF

```

C

```

  IF (I .EQ. 1) GO TO 25
  DO 20 J=1,I-1                                !points before control point
    XX=W-RADIUS(J)
    YY=Z-HEIGHT(J)
    Q5Q5=XX*XX+YY*YY
    GCON=GAMMA(J)*TPIINV/Q5Q5
    UIN=GCON*YY
    VIN=-GCON*XX
    WVEL(I)=WVEL(I)+VIN
    UVEL(I)=UVEL(I)+UIN
20  CONTINUE
25  IF (I .EQ. NRING) GO TO 40
    DO 30 J=I+1,NRING                            !points after control point
      XX=W-RADIUS(J)
      YY=Z-HEIGHT(J)
      Q5Q5=XX*XX+YY*YY
      GCON=GAMMA(J)*TPIINV/Q5Q5
      UIN=GCON*YY
      VIN=-GCON*XX
      WVEL(I)=WVEL(I)+VIN
      UVEL(I)=UVEL(I)+UIN
30  CONTINUE
40  DO 45 J=1,NRING                            !contribution from reflection

```

```

        XX=W+RADIUS(J)
        YY=Z-HEIGHT(J)
        Q5Q5=XX*XX+YY*YY
        GCON=-GAMMA(J)*TPIINV/Q5Q5
        UIN=GCON*YY
        VIN=-GCON*XX
        WVEL(I)=WVEL(I)+VIN
        UVEL(I)=UVEL(I)+UIN
45    CONTINUE
C
C--Get velocity of higher order terms in tip region, if not tip ring
C
        IF (I .NE. NRING) THEN
            CALL DOUBLET(W,Z,VXPRM,VYPRM,VRPRM,VTHPRM)
            WVEL(I)=WVEL(I)+VYPRM
            UVEL(I)=UVEL(I)+VXPRM
        ENDIF
C
10    CONTINUE
C
C--Get velocity contribution at tip due to inner spiral
C
        CALL CENSPIR(VXP,VYP)
        UVEL(NRING)=UVEL(NRING)+VXP
        WVEL(NRING)=WVEL(NRING)+VYP
C
C--Get induced velocity at center by extrapolating the velocities of
C points 1 and 2. Fit a parabola (for the velocity) through points
C 0, 1, and 2 by matching the values at points 1 and 2 and setting
C the slope=0 at r=0. Then the velocity at r=0 (i.e., the center
C point) is just the constant part of the parabola.
C
        UVEL(0)=0.0
        WVEL(0)=(WVEL(1)*RADIUS(2)**2-WVEL(2)*RADIUS(1)**2)
        $      /(RADIUS(2)**2-RADIUS(1)**2)
C
C--done
C
        RETURN
        END
        SUBROUTINE PANVEL2D
C
C This is for 2-D flow, i.e., 2-D panels
C--This routine calculates the induced velocity at each panel centroid
C and at the tip ring due to all the other panels and due to itself.
C
        COMMON /B1/ RADIUS(0:900),HEIGHT(0:900),WVEL(0:900),UVEL(0:900),

```

```

$          GAMMA(0:900),CORE(0:900),TIME(0:5000),TENERG(0:5000),
$          TIMPUL(0:5000)
COMMON /B2/ NRING,PI,DXMAX,INTKOD,NSMALL,VOLTIP,IAXI
COMMON /PANEL/ IPANEL,DRPAN(0:900),DZPAN(0:900),WPAN(0:900)
COMMON /VELO/ R,XX,YY,DXT,DYT,WW,G
COMMON /D1/ DISTMX
REAL*4 LAMBDA,K

C
C--Loop over all panels, except center ring, get induced velocity at each
C
      DO 10 I=1,NSMALL
          WVEL(I)=0.0          !axial velocity
          UVEL(I)=0.0          !radial velocity

C
C--Loop over all panels again (except for the control panel which has
C no self-induced component) and determine the contribution of each to
C the induced velocity at panel I.
C
      DO 20 J=1,NSMALL
          R=RADIUS(J)
          G=GAMMA(J)/(2.0*WPAN(J))
          WW=WPAN(J)
          DXT=DRPAN(J)
          DYT=DZPAN(J)
          XX=RADIUS(I)-RADIUS(J)
          YY=HEIGHT(I)-HEIGHT(J)
          DISTSQ=XX*XX+YY*YY
          IF (I .NE. J) THEN
              IF (DISTSQ .LT. DISTMX) THEN
                  CALL VEL2D(UIN,VIN)
              ELSE
                  CALL VEL2DF(UIN,VIN)
              ENDIF
          ELSE
              UIN=0.0
              VIN=0.0
          ENDIF
          DXT=-DXT          !contribution from reflection
          G=-G
          XX=RADIUS(I)+RADIUS(J)
          DISTSQ=XX*XX+YY*YY
          IF (DISTSQ .LT. DISTMX) THEN
              CALL VEL2D(UINRF,VINRF)
          ELSE
              CALL VEL2DF(UINRF,VINRF)
          ENDIF
          UVEL(I)=UVEL(I)-UIN-UINRF
      
```

```

                WVEL(I)=WVEL(I)-VIN-VINRF
20  CONTINUE
C
C--Now get contribution of tip filament
C
        J=NRING
        WWPAN=1.0
        G=GAMMA(J)/(2.0*WWPAN)
        WW=WWPAN
        DXT=DRPAN(J)
        DYT=DZPAN(J)
        XX=RADIUS(I)-RADIUS(J)
        YY=HEIGHT(I)-HEIGHT(J)
        CALL VEL2DF(UIN,VIN)
        DXT=-DXT           !contribution from reflection
        G=-G
        XX=RADIUS(I)+RADIUS(J)
        CALL VEL2DF(UINRF,VINRF)
        WVEL(I)=WVEL(I)-VIN-VINRF
        UVEL(I)=UVEL(I)-UIN-UINRF
C
C--get velocity of higher order terms in tip region
C
        CALL DOUBLET(W,Z,VXPRM,VYPRM,VRPRM,VTHPRM)
        WVEL(I)=WVEL(I)+VYPRM
        UVEL(I)=UVEL(I)+VXPRM
C
10 CONTINUE
C
C--Get induced velocity at center by extrapolating the velocities of
C points 1 and 2. Fit a parabola (for the velocity) through points
C 0, 1, and 2 by matching the values at points 1 and 2 and setting
C the slope=0 at r=0. Then the velocity at r=0 (i.e., the center
C point) is just the constant part of the parabola.
C
        UVEL(0)=0.0
        WVEL(0)=(WVEL(1)*RADIUS(2)**2-WVEL(2)*RADIUS(1)**2)
        $      /(RADIUS(2)**2-RADIUS(1)**2)
C
C--Get induced velocity at the tip filament due to all of the panels
C
        WVEL(NRING)=0.0
        UVEL(NRING)=0.0
        DO 40 J=1,NSMALL           !loop over all panels
            R=RADIUS(J)
            G=GAMMA(J)/(2.0*WPAN(J))
            WW=WPAN(J)

```

```

DXT=DRPAN(J)
DYT=DZPAN(J)
XX=RADIUS(NRING)-RADIUS(J)
YY=HEIGHT(NRING)-HEIGHT(J)
CALL VEL2D(UIN,VIN)
DXT=-DXT                                !contribution from reflection
G=-G
XX=RADIUS(NRING)+RADIUS(J)
CALL VEL2D(UINRF,VINRF)
UVEL(NRING)=UVEL(NRING)-UIN-UINRF
WVEL(NRING)=WVEL(NRING)-VIN-VINRF
40 CONTINUE
C
C--Get the remaining contribution to the induced velocity at the tip
C from its reflection
C
WWPAN=1.0
G=-GAMMA(J)/(2.0*WWPAN)
WW=WWPAN
DXT=-DRPAN(J)
DYT= DZPAN(J)
XX=RADIUS(I)+RADIUS(J)
YY=HEIGHT(I)-HEIGHT(J)
CALL VEL2DF(UINRF,VINRF)
WVEL(NRING)=WVEL(NRING)-VINRF
UVEL(NRING)=UVEL(NRING)-UINRF
C
C--Get velocity contribution at tip due to inner spiral
C
CALL CENSPIR(VXP,VYP)
UVEL(NRING)=UVEL(NRING)+VXP
WVEL(NRING)=WVEL(NRING)+VYP
C
C--done
C
RETURN
END
SUBROUTINE IMPULS(TIM P)
C
C--Computes total impulse of the vortex filament system for
C either axi or 2-D. (Note: only computing the "x" or "radial"
C component of the 2-D impulse.
C
COMMON /B1/ RADIUS(0:900),HEIGHT(0:900),WVEL(0:900),UVEL(0:900),
$          GAMMA(0:900),CORE(0:900),TIME(0:5000),TENERG(0:5000),
$          TIMPUL(0:5000)
COMMON /B2/ NRING,PI,DXMAX,INTKOD,NSMALL,VOLTIP,IAXI

```

```

C
  IF (IAXI .EQ. 1) THEN
    TIMP=0.0
    DO 10 I=1,NRING
10  TIMP=TIMP+PI*GAMMA(I)*RADIUS(I)**2
    ELSE
      TIMP=0.0
      DO 20 I=1,NRING
20  TIMP=TIMP+GAMMA(I)*RADIUS(I)
    ENDIF
C
  RETURN
  END
  SUBROUTINE TOTENG(ENERG)
C
C--Computes total energy of the vortex ring system
C
  COMMON /B1/ RADIUS(0:900),HEIGHT(0:900),WVEL(0:900),UVEL(0:900),
$           GAMMA(0:900),CORE(0:900),TIME(0:5000),TENERG(0:5000),
$           TIMPUL(0:5000)
  COMMON /B2/ NRING,PI,DXMAX,INTKOD,NSMALL,VOLTIP,IAXI
  REAL*4 LAMBDA,K
C
  SUM1=0.0
  SUM2=0.0
  DO 20 I=1,NRING
    W=RADIUS(I)
    Z=HEIGHT(I)
    DO 20 J=1,NRING
      IF (I .NE. J) THEN
        WP=RADIUS(J)
        ZP=HEIGHT(J)
        R1=SQRT((Z-ZP)**2+(W-WP)**2)
        R2=SQRT((Z-ZP)**2+(W+WP)**2)
        LAMBDA=(R2-R1)/(R2+R1)
        CALL ELLIP(LAMBDA,K,E)
        SUM1=SUM1+GAMMA(I)*GAMMA(J)*(R1+R2)*(K-E)/(2.0*PI)
      ENDIF
20  CONTINUE
  SUM1=SUM1*PI
C
  DO 30 I=1,NRING
    W=RADIUS(I)
30  SUM2=SUM2+GAMMA(I)**2*W*(ALOG(8.0*W/CORE(I))-1.75)/(2.0*PI)
  SUM2=SUM2*PI
C
  ENERG=SUM2+SUM1

```

```

C
  RETURN
  END
  SUBROUTINE ELLIP(RK,SUMK,SUME)
C
C--Computes complete elliptic integrals, function of RK.
C Uses a four term series approximation.
C SUMK = K(RK) - FIRST KIND
C SUME = E(RK) - SECOND KIND
C
  DATA AO,A1,A2,A3,A4,BO,B1,B2,B3,B4/
  $ 1.38629436112, .09666344259, .03590092383,
  $ .03742563713, .01451196212, .5
  $ .12498593597, .06880248576, .03328355346,
  $ .00441787012/
  DATA CO,C1,C2,C3,C4,DO,D1,D2,D3,D4/
  $ 1.0, .44325141463, .06260601220,
  $ .04757383546, .01736506451, .0
  $ .24998368310, .09200180037, .04069697526,
  $ .00526449639/
C
  FK=1.0-RK**2
  SUMK = AO+FK*(A1+FK*(A2+FK*(A3+FK*A4)))
  $ +(BO+FK*(B1+FK*(B2+FK*(B3+FK*B4))))*ALOG(1.0/FK)
  SUME = CO+FK*(C1+FK*(C2+FK*(C3+FK*C4)))
  $ +(DO+FK*(D1+FK*(D2+FK*(D3+FK*D4))))*ALOG(1.0/FK)
C
  RETURN
  END
  SUBROUTINE SETA
  COMMON /B2/ NRING,PI,DXMAX,INTKOD,NSMALL,VOLTIP,IAXI
  COMMON /E2/ AO,A1,A2,A3,RHOSTAR,A
  COMMON /E1/ TAUO,BDUM,CDUM,DDUM,TAU2LOOP
  COMMON /F1/ ALPLAST,GMTO
  COMMON /NOW/ TIMENOW,BIGRREF
C
  ALPLAST=PI/2.0
  TAUO=0.045
  BIGRREF=0.0966063
  TAU2LOOP=1.4542
  IF (IAXI .EQ. 0) THEN
    A=SQRT(2.0)
  ELSE
    A=2.0*SQRT(2.0)/PI
  ENDIF
C
  RETURN

```


END

SUBROUTINE REDISC(R,Z,DGAM,NIN,NOUT,GMAX,SUML,DELTAL,TIMEY)

C

C--This does curve fitting using blended parabolas on R, Z, DGAM

C

COMMON /B2/ NRING,PI,DXMAX,INTKOD,NSMALL,VOLTIP,IAXI
COMMON /B9/ IWR
COMMON /C1/ LINEUP,MAXSEGS,MINSECT

C

DIMENSION R(0:900),Z(0:900),DGAM(0:900),S(0:900),QR(0:900),
\$ QZ(0:900),AO(0:900),A1(0:900),A2(0:900),A3(0:900),
\$ BO(0:900),B1(0:900),B2(0:900),B3(0:900),CO(0:900),
\$ C1(0:900),C2(0:900),C3(0:900),GMID(0:900),SMID(0:900),
\$ Q(0:900),RS(0:8100),ZS(0:8100),AL(0:8100),
\$ THSUB(0:8100),ARCG(0:900),GPL(0:900)
DIMENSION ROLD(0:900),ZOLD(0:900),DGAMOLD(0:900)
COMMON/STAR/ICIRC(10),FCIRC(10),SSTAR(10),GSTAR(10),NSTAR
COMMON /PANEL/ IPANEL,DRPAN(0:900),DZPAN(0:900),WPAN(0:900)
COMMON /SEGS/ AXLSEG(0:900)
COMMON /F1/ ALPLAST,GMTO
LOGICAL LINEAR !LINEAR = .TRUE. for linear circ. fit
DATA LINEAR/.FALSE./ !LINEAR = .FALSE. for cubic circ. fit
DATA NSUB/9/

C

ILOOPER=0

C

DO 1 I=0,NRING
ROLD(I)=R(I)
ZOLD(I)=Z(I)
1 DGAMOLD(I)=DGAM(I)

C

C--Get straight line distances between points, S(I) is the total
C distance along the straight lines to node I

C

S(0)=0.0
DO 20 I=1,NIN
20 S(I)=S(I-1)+SQRT((Z(I)-Z(I-1))**2+(R(I)-R(I-1))**2)

C

C--Get value of s for the trailing extended segment, this value
C of S is out at the presumed end of the sheet.

C

S(NIN+1)=S(NIN)+0.5*(S(NIN)-S(NIN-1))

C

C--Get slopes at each interior node, QR(I)=D(R)/DS at node I

C

```

DO 30 I=1,NIN-1
S1=(S(I+1)-S(I))/(S(I-1)-S(I))
S2=1.0/S1
S3=1.0/(S(I+1)-S(I-1))
QR(I)=((R(I-1)-R(I))*S1-(R(I+1)-R(I))*S2)*S3
30 QZ(I)=((Z(I-1)-Z(I))*S1-(Z(I+1)-Z(I))*S2)*S3

```

C

C--Coef's for interior segments

C

```

DO 40 I=1,NIN-2
S1=1.0/(S(I+1)-S(I))
AO(I)=R(I)
A1(I)=QR(I)
A2(I)=S1*(-QR(I+1)-2*QR(I)+3*S1*(R(I+1)-R(I)))
A3(I)=S1*S1*(QR(I+1)+QR(I)-2*S1*(R(I+1)-R(I)))
BO(I)=Z(I)
B1(I)=QZ(I)
B2(I)=S1*(-QZ(I+1)-2*QZ(I)+3*S1*(Z(I+1)-Z(I)))
40 B3(I)=S1*S1*(QZ(I+1)+QZ(I)-2*S1*(Z(I+1)-Z(I)))

```

C

C--Coef's for first segment

C

```

S1=S(1)-S(0)
S2=S(2)-S(0)
S3=1.0/(S(2)-S(1))
AO(0)=R(0)
A1(0)=((R(1)-R(0))*S2/S1-(R(2)-R(0))*S1/S2)*S3
A2(0)=((R(2)-R(0))/S2-(R(1)-R(0))/S1)*S3
A3(0)=0.0
BO(0)=Z(0)
B1(0)=((Z(1)-Z(0))*S2/S1-(Z(2)-Z(0))*S1/S2)*S3
B2(0)=((Z(2)-Z(0))/S2-(Z(1)-Z(0))/S1)*S3
B3(0)=0.0

```

C

C--Coef's for last segment

C

```

N=NIN
S1=S(N)-S(N-1)
S2=S(N-2)-S(N-1)
S3=1.0/(S(N-2)-S(N))
AO(N-1)=R(N-1)
A1(N-1)=((R(N)-R(N-1))*S2/S1-(R(N-2)-R(N-1))*S1/S2)*S3
A2(N-1)=((R(N-2)-R(N-1))/S2-(R(N)-R(N-1))/S1)*S3
A3(N-1)=0.0
BO(N-1)=Z(N-1)
B1(N-1)=((Z(N)-Z(N-1))*S2/S1-(Z(N-2)-Z(N-1))*S1/S2)*S3
B2(N-1)=((Z(N-2)-Z(N-1))/S2-(Z(N)-Z(N-1))/S1)*S3

```

```

      B3(N-1)=0.0
C
C--Get the angle of the ring with index NSMALL wrt the tip core
C
      CALL PULANG(NIN,THNIN)
C
C--Get the "A" coefficient for the Kadin spiral
C
      RNU=XNU(THNIN)
      IF (ABS(SIN(THNIN)) .GE. 0.5) THEN
        A=(Z(NRING)-Z(NIN))/(THNIN**(-RNU)*SIN(THNIN))
      ELSE
        A=(R(NRING)-R(NIN))/(THNIN**(-RNU)*COS(THNIN))
      ENDIF
C
C--Get array of R and Z at the subinterval locations, and compute
C the total length of the curve
C
C--First do the blended parabola segments
C
      RS(0)=AO(0)
      ZS(0)=BO(0)
      AL(0)=0.0
      DO 50 I=0,NIN-1
      DO 50 KSUB=1,NSUB
      J=I*NSUB+KSUB
      T=(S(I+1)-S(I))*FLOAT(KSUB)/FLOAT(NSUB)
      RS(J)=AO(I)+T*(A1(I)+T*(A2(I)+T*A3(I)))
      ZS(J)=BO(I)+T*(B1(I)+T*(B2(I)+T*B3(I)))
      50 AL(J)=AL(J-1)+SQRT((RS(J)-RS(J-1))**2+(ZS(J)-ZS(J-1))**2)
C
C--The next few sections find the value of theta at the end of the
C trailing extended segment, i.e., gets the theta corresponding
C to arclength S(NIN+1)
C
C--First, before doing the numerical integration, need to get a
C value to use for delta theta
C
      DS=S(NIN+1)-S(NIN)
      RNU=XNU(THNIN)
      DTG=DS/(SQRT(RNU**2+THNIN**2)*A*THNIN**(-RNU-1.0))
      DTG=DTG/2.0
C
C--Now have delta theta (i.e., DTG) which should yield several
C steps in the numerical integration from S(NIN) to S(NIN+1).
C
C--Now do the numerical integration and search for theta(NIN+1)

```

C

```
ITERS=0
SEND=S(NIN+1)-S(NIN)
STH=0.0
TH=THNIN
64 ITERS=ITERS+1
IF (ITERS .GT. 100) STOP 'ITERS .GT. 100 LOOP 63'
RNU=XNU(TH)
R1=R(NRING)-A*COS(TH)*TH**(-RNU)
Z1=Z(NRING)-A*SIN(TH)*TH**(-RNU)
RNU=XNU(TH+DTG)
R2=R(NRING)-A*COS(TH+DTG)*(TH+DTG)**(-RNU)
Z2=Z(NRING)-A*SIN(TH+DTG)*(TH+DTG)**(-RNU)
DS=SQRT((R2-R1)**2+(Z2-Z1)**2)
IF (STH+DS .GE. SEND) GO TO 63
STH=STH+DS
TH=TH+DTG
GO TO 64
63 FRAC=(SEND-STH)/DS
THNIN1=TH+FRAC*DTG
```

C

C--Now can get the sub-interval locations over the extended spiral
C segment.

C

```
DTH=(THNIN1-THNIN)/NSUB
DO 65 KSUB=1,NSUB
THETA=THNIN+KSUB*DTH
J=NIN*NSUB+KSUB
RNU=XNU(THETA)
RS(J)=R(NRING)-A*THETA**(-RNU)*COS(THETA)
ZS(J)=Z(NRING)-A*THETA**(-RNU)*SIN(THETA)
AL(J)=AL(J-1)+SQRT((RS(J)-RS(J-1))**2+(ZS(J)-ZS(J-1))**2)
65 CONTINUE
```

C

C--Total length of curve is SUML

C

```
SUML=AL((NIN+1)*NSUB)
```

C

689 CONTINUE

C

C--Check for lineup of spiral sheet segments

C

```
IF (LINEUP .EQ. 1) THEN
GO TO 2010           !line up the segments
ELSE
GO TO 2020           !for equal sized segments
ENDIF
```

```

C
C--This section for equal sized segments
C
C--Get new R and Z points at distance DELTAL apart, these are the
C centroids
C
2020 DELTAL=SUML/NOU
XLSEG=DELTAL/2.0
AXLSEG(O)=0.0
I=1
DO 60 J=1,NSUB*(NIN+1)
80 IF (XLSEG .LT. AL(J-1) .OR. XLSEG .GT. AL(J)) GO TO 60
FRAC=(XLSEG-AL(J-1))/(AL(J)-AL(J-1))
R(I)=FRAC*(RS(J)-RS(J-1))+RS(J-1)
Z(I)=FRAC*(ZS(J)-ZS(J-1))+ZS(J-1)
AXLSEG(I)=XLSEG+DELTAL/2.0 !running total of arc length to
! segment edge.
WPAN(I)=DELTAL/2.0 !panel half-width
I=I+1
XLSEG=XLSEG+DELTAL
IF (I .GT. NOU) GO TO 70
GO TO 80
60 CONTINUE
70 CONTINUE
GO TO 2030

C
C--This part is for lined up segments in the spiral region
C
2010 NOU1=NOU
NTOTSUB=NSUB*(NIN+1)
CALL ANGLES(RS,ZS,NTOTSUB,THSUB)
ALPLAST=THSUB(NTOTSUB) !save angle at edge of sheet for DOUBLET
IF (THSUB(NTOTSUB) .LE. 9.0*PI/2.0) THEN !ALFSPIR is the angle
ALFSPIR=THSUB(NTOTSUB)-3.0*PI/2.0 !at which the "spiral"
ELSE !part of the sheet begins
ALFSPIR=3.0*PI !(i.e., the equal angular
ENDIF !segments)
IF (THSUB(NTOTSUB) .LT. 7.0*PI/2.0) GO TO 2020 !check for at
!least 1.5 loop
STOTAL=SUML !total length of sheet
I=1 !find point on sheet where
3513 IF (THSUB(I) .GT. ALFSPIR) GO TO 3512 !the spiral section is
I=I+1 !assumed to start, at
GO TO 3513 !theta=ALFSPIR
3512 SFLAT=AL(I)
SSPIRAL=STOTAL-SFLAT !length of spiral part of sheet
R3PIQ2=SQRT((RS(I)-ROLD(NRING))**2+(ZS(I)-ZOLD(NRING))**2)

```

```

RAVERAGE=0.0
DO 3511 J=I,NTOTSUB
3511 RAVERAGE=RAVERAGE
$      +SQRT((RS(J)-ROLD(NRING))**2+(ZS(J)-ZOLD(NRING))**2)
RAVERAGE=RAVERAGE/(NTOTSUB-I+1)
7126 DENOM=1.0+(SSPIRAL*R3PIQ2)/(SFLAT*RAVERAGE)
NSEG=NOUT1                      !# of sheet segments to be output
NSEGFLAT=INT(NSEG/DENOM+0.5)    !estimate the # of segments on
NSEGSPIR=NSEG-NSEGFLAT         !the flat and spiral parts
RNLOOP=(THSUB(NTOTSUB)-ALFSPIR)/(2.0*PI) !# of loops in spiral
NTHSECT=INT((FLOAT(NSEGSPIR)/RNLOOP)+0.5) !# of theta sections
IF (NOUT1 .LT. MAXSEGS) THEN
  IF (NTHSECT .LT. MINSECT) THEN
    ILOOPER=ILOOPER+1
    IF (ILOOPER .GT. MAXSEGS) STOP ' ILOOPER .GT. MAXSEGS'
    NOUT1=NOUT1+1
    GO TO 7126
  ENDIF
ENDIF
DTHETA=2.0*PI/NTHSECT          !theta increment of a theta section
I=1                             !segment counter for spiral region
ISEG=NSEG+1-I                   !segment index, we are going backwards
THEDGE=THSUB(NTOTSUB)-DTHETA    !edge of current segment (small theta)
IF (THEDGE .LT. 7.0*PI/2.0) GO TO 2020 !check for at least 1.5 loop
THMID=THEDGE+DTHETA/2.0        !theta for centroid of current segment
AXLSEG(ISEG)=SUML
DO 3080 J=NTOTSUB,1,-1
3080 IF (THMID .GT. THSUB(J) .OR. THMID .LT. THSUB(J-1)) GO TO 3050
FRAC=(THMID-THSUB(J-1))/(THSUB(J)-THSUB(J-1))
R(ISEG)=FRAC*(RS(J)-RS(J-1))+RS(J-1)
Z(ISEG)=FRAC*(ZS(J)-ZS(J-1))+ZS(J-1)
THMID=THMID-DTHETA
3050 IF (THEDGE .GT. THSUB(J) .OR. THEDGE .LT. THSUB(J-1)) GO TO 3060
FRAC=(THEDGE-THSUB(J-1))/(THSUB(J)-THSUB(J-1))
AXLSEG(ISEG-1)=FRAC*(AL(J)-AL(J-1))+AL(J-1)
THEDGE=THEDGE-DTHETA
IF (THEDGE .LT. ALFSPIR) GO TO 3070          !done with spiral part
I=I+1
ISEG=NSEG+1-I
GO TO 3080
3060 CONTINUE
3070 CONTINUE      !I contains number of segments in the spiral region
NSEGSPIR=I        !exact value
NSEGFLAT=NSEG-NSEGSPIR
C
C now find segments on flat part of sheet
C

```

```

C--get segment stretching parameters
C
    SUMI=0.0
    DO 3761 I=1,NSEGFLAT-1
3761 SUMI=SUMI+I
    DSLAST=AXLSEG(ISEG)-AXLSEG(ISEG-1)
    HHH=(AXLSEG(ISEG-1)-NSEGFLAT*DSLAST)
    $ /((SUMI-NSEGFLAT*(NSEGFLAT-1))
    DSFIX=DSLAST-HHH*(NSEGFLAT-1)
C
    AXLSEG(0)=0.0
    I=1
    DSI=DSFIX+HHH*(I-1)
    XLSEG=DSI/2.0          !arc length to filament
    EDGE=DSI              !arc length to outboard edge of segment
    DO 3061 J=1,NTOTSUB
3081 IF (XLSEG .LT. AL(J-1) .OR. XLSEG .GT. AL(J)) GO TO 3061
    FRAC=(XLSEG-AL(J-1))/(AL(J)-AL(J-1))
    R(I)=FRAC*(RS(J)-RS(J-1))+RS(J-1)
    Z(I)=FRAC*(ZS(J)-ZS(J-1))+ZS(J-1)
    AXLSEG(I)=EDGE
    I=I+1
    DSI=DSFIX+HHH*(I-1)
    XLSEG=EDGE+DSI/2.0
    EDGE=EDGE+DSI
    IF (I .GT. NSEGFLAT) GO TO 3071
    GO TO 3081
3061 CONTINUE
3071 CONTINUE
C--set WPAN for all segments
    DO 3110 ISEG=1,NSEG
    WPAN(ISEG)=(AXLSEG(ISEG)-AXLSEG(ISEG-1))/2.0
3110 CONTINUE
    R(NOUT1+1)=ROLD(NRING)
    Z(NOUT1+1)=ZOLD(NRING)
    DGAM(NOUT1+1)=DGAMOLD(NRING)
    NOUT=NOUT1
    NRING=NOUT1+1
    NSMALL=NRING-1
    GO TO 2030
C
2030 CONTINUE
C
C--If panel case, estimate inclinations (only nec. for R-K)
C
    IF (IPANEL .EQ. 1) THEN
        DO 920 I=1,NSMALL-1

```

```

        SL=-SQRT((R(I)-R(I-1))**2+(Z(I)-Z(I-1))**2)
        SR= SQRT((R(I)-R(I+1))**2+(Z(I)-Z(I+1))**2)
        A1P=((SL*SR)/(SL-SR))
        $          *((R(I+1)-R(I))/SR**2-(R(I-1)-R(I))/SL**2)
        B1P=((SL*SR)/(SL-SR))
        $          *((Z(I+1)-Z(I))/SR**2-(Z(I-1)-Z(I))/SL**2)
        DRPAN(I)=A1P
        DZPAN(I)=B1P
920  CONTINUE
        A2P=((R(I+1)-R(I))/SR-(R(I-1)-R(I))/SL)/(SR-SL)
        B2P=((Z(I+1)-Z(I))/SR-(Z(I-1)-Z(I))/SL)/(SR-SL)
        DRPAN(NSMALL)=A1P+A2P*SR
        DZPAN(NSMALL)=B1P+B2P*SR
    ENDIF
C
C--Get values of S at the midpoints of the original ring locations
C
        SMID(0)=0.0
        SMID(NIN)=SUML
        DO 90 I=1,NIN-1
        90 SMID(I)=(AL(NSUB*(I+1))+AL(NSUB*I))/2.0
C
C--Get values of circulation at the midpoints of the original
C ring locations
C
        GMID(0)=GMAX
        DO 100 I=1,NIN
        100 GMID(I)=GMID(I-1)+DGAM(I)
C
C--Curve fit for circulation, test for linear or cubic fit
C
        IF (LINEAR) THEN
C
C--The following block is for a linear fit of circulation
C
        DO 411 I=0,NIN-1
        CO(I)=GMID(I)
        C1(I)=(GMID(I+1)-GMID(I))/(SMID(I+1)-SMID(I))
        C2(I)=0.0
        411 C3(I)=0.0
C
        ELSE
C
C--The following block is for a blended parabola fit of circulation
C
C--Get slopes at each interior point
C

```



```

DO 110 I=1,NIN-1
S1=(SMID(I+1)-SMID(I))/(SMID(I-1)-SMID(I))
110 Q(I)=$((GMID(I-1)-GMID(I))*S1-(GMID(I+1)-GMID(I))/S1)
$      /(SMID(I+1)-SMID(I-1))
C
C--Coef's for interior points
C
DO 120 I=1,NIN-2
S1=1.0/(SMID(I+1)-SMID(I))
G1=(GMID(I+1)-GMID(I))*S1
CO(I)=GMID(I)
C1(I)=Q(I)
C2(I)=S1*(-Q(I+1)-2*Q(I)+3*G1)
120 C3(I)=S1*S1*(Q(I+1)+Q(I)-2*G1)
C
C--Coef's for first segment
C
S1=SMID(1)-SMID(0)
S2=SMID(2)-SMID(0)
S3=1.0/(SMID(2)-SMID(1))
CO(0)=GMID(0)
C1(0)=S3*((GMID(1)-GMID(0))*S2/S1-(GMID(2)-GMID(0))*S1/S2)
C2(0)=S3*((GMID(2)-GMID(0))/S2-(GMID(1)-GMID(0))/S1)
C3(0)=0.0
C
C--Coef's for last segment
C
S1=SMID(NIN-2)-SMID(NIN-1)
S2=SMID(NIN)-SMID(NIN-1)
S3=1.0/(SMID(NIN-2)-SMID(NIN))
G1=GMID(NIN-2)-GMID(NIN-1)
G2=GMID(NIN)-GMID(NIN-1)
CO(NIN-1)=GMID(NIN-1)
C1(NIN-1)=S3*(G2*S1/S2-G1*S2/S1)
C2(NIN-1)=S3*(G1/S1-G2/S2)
C3(NIN-1)=0.0
C
ENDIF
C
651 CONTINUE
C
C--Interpolate for new delta circulation values.
C XLSEG will now be an array containing the arc length to the
C edge of segment I, call it AXLSEG(I)
C
I=1
GPREV=GMAX

```

```

DO 130 J=1,NIN
150 IF(AXLSEG(I) .LT. SMID(J-1) .OR. AXLSEG(I) .GT. SMID(J))GO TO 130
T=AXLSEG(I)-SMID(J-1)
GNEW=CO(J-1)+T*(C1(J-1)+T*(C2(J-1)+T*C3(J-1)))
DGAM(I)=GNEW-GPREV
GPREV=GNEW
I=I+1
IF (I .GT. NOUT-1) GO TO 140
GO TO 150
130 CONTINUE
140 CONTINUE
T=SMID(NIN)-SMID(NIN-1)
GNEW=CO(NIN-1)+T*(C1(NIN-1)+T*(C2(NIN-1)+T*C3(NIN-1)))
DGAM(NOUT)=GNEW-GPREV

```

C

C--Done

C

RETURN

END

SUBROUTINE ANGLES(RS,ZS,NTOTSUB,THSUB)

C

C--Get angles relative to tip for each subinterval

C

```

COMMON /B1/ R(0:900),Z(0:900),WVEL(0:900),UVEL(0:900),
$          GAMMA(0:900),CORE(0:900),TIME(0:5000),TENERG(0:5000),
$          TIMPUL(0:5000)
COMMON /B2/ NRING,PI,DXMAX,INTKOD,NSMALL,VOLTIP,IAXI
DIMENSION RS(0:8100),ZS(0:8100),THSUB(0:8100)
REAL*4 MAG

```

C

```

RT=R(NRING)      !tip values of radius
ZT=Z(NRING)      !           and height

```

C

```

A=-1.0
B=0.0
C=RS(0)-RT
D=ZS(0)-ZT
DOT=A*C+B*D
CROSS=A*D-B*C
MAG=SQRT((A*A+B*B)*(C*C+D*D))
ARG=DOT/MAG
IF (ABS(ARG) .GT. 1.0) ARG=SIGN(1.0,ARG)
THSUB(0)=SIGN(1.0,CROSS)*ACOS(ARG)

```

C

```

DO 100 I=1,NTOTSUB

```

```

A=RS(I-1)-RT
B=ZS(I-1)-ZT
C=RS(I)-RT
D=ZS(I)-ZT
DOT=A*C+B*D
CROSS=A*D-B*C
MAG=SQRT((A*A+B*B)*(C*C+D*D))
ARG=DOT/MAG
IF (ABS(ARG) .GT. 1.0) ARG=SIGN(1.0,ARG)
100 THSUB(I)=THSUB(I-1)+SIGN(1.0,CROSS)*ACOS(ARG)

```

C

```

RETURN
END
SUBROUTINE PULANG(NIN,THNIN)

```

C

```

COMMON /B1/ R(0:900),Z(0:900),WVEL(0:900),UVEL(0:900),
$          GAMMA(0:900),CORE(0:900),TIME(0:5000),TENERG(0:5000),
$          TIMPUL(0:5000)
COMMON /B2/ NRING,PI,DXMAX,INTKOD,NSMALL,VOLTIP,IAXI
COMMON /TEMP/ BETA(0:900)
REAL*4 MAG

```

C

```

RT=R(NRING)
ZT=Z(NRING)

```

C

```

A=-1.0
B=0.0
C=R(0)-RT
D=Z(0)-ZT
DOT=A*C+B*D
CROSS=A*D-B*C
MAG=SQRT((A*A+B*B)*(C*C+D*D))
ARG=DOT/MAG
IF (ABS(ARG) .GT. 1.0) ARG=SIGN(1.0,ARG)
BETA(0)=SIGN(1.0,CROSS)*ACOS(ARG)

```

C

```

DO 100 I=1,NIN
A=R(I-1)-RT
B=Z(I-1)-ZT
C=R(I)-RT
D=Z(I)-ZT
DOT=A*C+B*D
CROSS=A*D-B*C
MAG=SQRT((A*A+B*B)*(C*C+D*D))
ARG=DOT/MAG
IF (ABS(ARG) .GT. 1.0) ARG=SIGN(1.0,ARG)
100 BETA(I)=BETA(I-1)+SIGN(1.0,CROSS)*ACOS(ARG)

```

```

C      THNIN=BETA(NIN)
C
C      RETURN
C      END
C      FUNCTION XNU(THETA)
C      DATA PI/3.141592654/
C      XNU=2.0/3.0
C      IF (THETA .LT. 2.0*PI) THEN
C          XNU=(1.0/(2.0*PI-1.0))-(1.0/(THETA-1.0))+2.0/3.0
C      ENDIF
C
C      RETURN
C      END
C      SUBROUTINE LUMPS(TIMEY)
C
C      C--This subroutine looks at the rolled up part of the sheet and
C      C determines if part of it should be truncated and lumped into
C      C the tip vortex ring.
C
C
C      COMMON /B1/ RADIUS(0:900),HEIGHT(0:900),WVEL(0:900),UVEL(0:900),
C      $           GAMMA(0:900),CORE(0:900),TIME(0:5000),TENERG(0:5000),
C      $           TIMPUL(05000)
C      COMMON /B2/ NRING,PI,DXMAX,INTKOD,NSMALL,VOLTIP,IAXI
C      COMMON /TH/ THETA(0:900),THMAX
C      COMMON /B9/ IWR
C      REAL*4 LAMBDA,K
C
C      C-- Get segment angles relative to horizontal axis
C
C      CALL GETANG
C
C      C--See if any rings exceed the cut-off angle THMAX
C
C      M=0           ! M will contain the # of rings to be lumped
C      I=NSMALL-1    ! Highest segment number
C      20 IF (THETA(I) .LT. THMAX) GO TO 10
C      M=M+1
C      I=I-1
C      GO TO 20
C
C      C--Now M contains the # of rings to be lumped into the core
C
C      10 IF (M .EQ. 0) GO TO 999           !Return
C
C      C--Have M rings to lump, first find new position of tip by conserving
C      C impulse.

```

```

C
C GTIP = new tip circulation
C RTIP = new tip radius
C HTIP = new tip height
C
    GTIP=0.0
    DO 30 I=NSMALL-M+1,NRING
30 GTIP=GTIP+GAMMA(I)
C
    IF (IAXI .EQ. 1) THEN
        RT2=0.0
        DO 40 I=NSMALL-M+1,NRING
40 RT2=RT2+GAMMA(I)*RADIUS(I)**2
        RTIP=SQRT(RT2/GTIP)
        HTIP=0.0
        DO 50 I=NSMALL-M+1,NRING
50 HTIP=HTIP+GAMMA(I)*HEIGHT(I)*RADIUS(I)**2
        HTIP=HTIP/RT2
    ELSE
        RT2=0.0
        DO 41 I=NSMALL-M+1,NRING
41 RT2=RT2+GAMMA(I)*RADIUS(I)
        RTIP=RT2/GTIP
        HTIP=0.0
        DO 51 I=NSMALL-M+1,NRING
51 HTIP=HTIP+GAMMA(I)*HEIGHT(I)
        HTIP=HTIP/GTIP
    ENDIF
    CTIP=0.0
C
    IF (IAXI .EQ.1) THEN
C
C Only get new core size for the axi case
C--Get new tip core size by conserving kinetic energy.
C First compute total kinetic energy of system.
C
    CALL TOTENG(TKE)
C
C--Now get the various sums needed to compute TTBAR
C
    SUM1=0.0
    DO 60 I=1,NSMALL-M
        TIBAR=GAMMA(I)**2*RADIUS(I)*(ALOG(8.0*RADIUS(I)/CORE(I))
        $ -1.75)/2.0
60 SUM1=SUM1+TIBAR
C
    SUM2=0.0

```

```

DO 70 I=1,NSMALL-M
DO 70 J=1,NSMALL-M
  IF (I .NE. J) THEN
    R1=SQRT((HEIGHT(I)-HEIGHT(J))**2+(RADIUS(I)-RADIUS(J))**2)
    R2=SQRT((HEIGHT(I)-HEIGHT(J))**2+(RADIUS(I)+RADIUS(J))**2)
    LAMBDA=(R2-R1)/(R2+R1)
    CALL ELLIP(LAMBDA,K,E)
    SUM2=SUM2+GAMMA(I)*GAMMA(J)*(R1+R2)*(K-E)/2.0
  ENDIF
70 CONTINUE
C
SUM3=0.0
DO 80 I=1,NSMALL-M
  R1=SQRT((HEIGHT(I)-HTIP)**2+(RADIUS(I)-RTIP)**2)
  R2=SQRT((HEIGHT(I)-HTIP)**2+(RADIUS(I)+RTIP)**2)
  LAMBDA=(R2-R1)/(R2+R1)
  CALL ELLIP(LAMBDA,K,E)
  SUM3=SUM3+GAMMA(I)*GTIP*(R1+R2)*(K-E)/2.0
80 CONTINUE
C
SUM4=SUM3
C
C--Get energy contribution of tip.
C
TTBAR=TKE-SUM1-SUM2-SUM3-SUM4
C
C--Now get core size corresponding to this energy.
C
CZZZ=EXP(2.0*TTBAR/(GTIP**2*RTIP)+1.75)
CTIP=8.0*RTIP/CZZZ
C
ENDIF
C
C--Put tip variables into main arrays
C
RADIUS(NRING)=RTIP
HEIGHT(NRING)=HTIP
GAMMA(NRING)=GTIP
CORE(NRING)=CTIP
C
C--Compute new volume of tip ring
C
VOLTIP=2.0*PI*PI*RADIUS(NRING)*CORE(NRING)**2
C
C--Now rediscrctize remaining portion of sheet.
C
NIN=NSMALL-M

```

```

      NOUT=NSMALL
      GMM=GMAX-GAMMA(NRING)
      CALL REDISC(RADIUS,HEIGHT,GAMMA,NIN,NOUT,GMM,SUML,DELTAL,TIMEY)
C
C--done
C
      999 RETURN
      END
      SUBROUTINE GETANG
C
C--This routine computes the angles of the segments relative to
C the horizontal axis
C
C
      COMMON /B1/ RADIUS(0:900),HEIGHT(0:900),WVEL(0:900),UVEL(0:900),
      $           GAMMA(0:900),CORE(0:900),TIME(0:5000),TENERG(0:5000),
      $           TIMPUL(0:5000)
      COMMON /B2/ NRING,PI,DXMAX,INTKOD,NSMALL,VOLTIP,IAXI
C      COMMON /B3/ DMIN(0:900)
      COMMON /TH/ THETA(0:900),THMAX
      DIMENSION DT(0:900)
C
C--Get increment for first angle
C
      DT(0)=ATAN((HEIGHT(1)-HEIGHT(0))/(RADIUS(1)-RADIUS(0)))
      THETA(0)=DT(0)
C
C--Get THETA for the rest
C
      DO 10 I=1,NSMALL-1
      XM=RADIUS(I-1)
      XI=RADIUS(I)
      XP=RADIUS(I+1)
      YM=HEIGHT(I-1)
      YI=HEIGHT(I)
      YP=HEIGHT(I+1)
C
C--Get sign of cross product of Vi and Vi+1
C
      SCROSS=SIGN(1.0,(XI-XM)*(YP-YI)-(XP-XI)*(YI-YM))
      VMAGS=SQRT(((XI-XM)**2+(YI-YM)**2)*((XP-XI)**2+(YP-YI)**2))
      DOT=(XI-XM)*(XP-XI)+(YI-YM)*(YP-YI)
C
C--Watch out for numerical inaccuracy in argument of arccos
C
      DT(I)=0.0
      IF (ABS(DOT/VMAGS) .LE. 1.0) DT(I)=SCROSS*ACOS(DOT/VMAGS)

```

```

      THETA(I)=THETA(I-1)+DT(I)
10 CONTINUE
C
      RETURN
      END

      SUBROUTINE DOUBLET(W,Z,VXPRM,VYPRM,VRPRM,VTHPRM)
C
C--Calculates the higher order velocity components in the spiral region
C
C W      radius of control point
C Z      height of control point
C VXPRM  V sub x prime in the notes, radial velocity component
C VYPRM  V sub y prime in the notes, axial velocity component
C GMTO   strength of tip at start of run
C
      COMMON /B1/ RADIUS(0:900),HEIGHT(0:900),WVEL(0:900),UVEL(0:900),
$             GAMMA(0:900),CORE(0:900),TIME(0:5000),TENERG(0:5000),
$             TIMPUL(0:5000)
      COMMON /B2/ NRING,PI,DXMAX,INTKOD,NSMALL,VOLTIP,IAXI
      COMMON /E1/ TAUO,BDUM,CDUM,DDUM,TAU2LOOP
      COMMON /NOW/ TIMENOW,BIGRREF
      COMMON /E2/ AO,A1,A2,A3,RHOSTAR,A
      COMMON /F1/ ALPLAST,GMTO
      COMMON /ZZ/ ZXO,ZYO
      COMMON /B9/ IWR
      DIMENSION B(7,2),D(7,2)      !B(coef., exponent)
      DATA B /.0053006800, .0013100600, .000574976 , .000319442 ,
$           .0002020870, .0001387070, .000100337 ,
$           -1.38557 , -1.36294 , -1.34587 , -1.33015 ,
$           -1.31621 , -1.30109 , -1.28252
      DATA D /.0010074100, .0001546680, .0000656961, .0000312179,
$           .0000157322, .0000101938, .0000115224,
$           -2.37327 , -2.28212 , -2.40883 , -2.36051 ,
$           -2.17250 , -2.22138 , -2.80713
      BIGRREF=0.0966063
      NCOEF=7
C
      BIGRPRM=BIGRREF*(A*TIME(1))**(2.0/3.0) !constant in time
      RPRIME=SQRT((W-RADIUS(NRING))**2+(Z-HEIGHT(NRING))**2)
      R=RPRIME/BIGRPRM
      SINTST=(Z-HEIGHT(NRING))/RPRIME
      COSTST=(W-RADIUS(NRING))/RPRIME
      THETAST=ATAN2(SINTST,COSTST)
      VRPRM=0.0
      VTHPRM=0.0
      DO 10 N=1,NCOEF

```



```

RRR=GAMMA(NRING)/GMTO          !adjust for varying tip strength
TAUA=TAU2LOOP+ALPROT(TIMENOW)*(0.60702015)/(2.0*PI)
BN=B(N,1)*TAUA**B(N,2)
DN=D(N,1)*TAUA**D(N,2)
DDVR= (BN*COS(N*(THETAST+PI/2.0-ALPROT(TIMENOW)))
$     -DN*SIN(N*(THETAST+PI/2.0-ALPROT(TIMENOW))))
$     *(N/R**(N+1))*RRR*(A**(4.0/3.0)*TIMENOW**(1.0/3.0)/BIGRPRM)
DDVTH=(BN*SIN(N*(THETAST+PI/2.0-ALPROT(TIMENOW)))
$     +DN*COS(N*(THETAST+PI/2.0-ALPROT(TIMENOW))))
$     *(N/R**(N+1))*RRR*(A**(4.0/3.0)*TIMENOW**(1.0/3.0)/BIGRPRM)
VRPRM =VRPRM+DDVR
10 VTHPRM=VTHPRM+DDVTH
VXPRM=VRPRM*COSTST-VTHPRM*SINTST
VYPRM=VRPRM*SINTST+VTHPRM*COSTST
C
ALF=ALPROT(TIMENOW)
C
RETURN
END
FUNCTION ALPROT(TIMENOW)
COMMON /B1/ RADIUS(0:900),HEIGHT(0:900),WVEL(0:900),UVEL(0:900),
$         GAMMA(0:900),CORE(0:900),TIME(0:5000),TENERG(0:5000),
$         TIMPUL(0:5000)
COMMON /B2/ NRING,PI,DXMAX,INTKOD,NSMALL,VOLTIP,IAXI
COMMON /E1/ TAUO,B,C,D,TAU2LOOP
COMMON /F1/ ALPLAST,GMTO
C
ALPROT=ALPLAST-PI/2.0
C
RETURN
END
SUBROUTINE CENSPIR(VXP,VYP)
C--Calculates the velocity induced at the spiral center due to the
C inner spiral region
COMMON /B1/ RADIUS(0:900),HEIGHT(0:900),WVEL(0:900),UVEL(0:900),
$         GAMMA(0:900),CORE(0:900),TIME(0:5000),TENERG(0:5000),
$         TIMPUL(05000)
COMMON /B2/ NRING,PI,DXMAX,INTKOD,NSMALL,VOLTIP,IAXI
COMMON /E1/ TAUO,B,C,D,TAU2LOOP
COMMON /E2/ AO,A1,A2,A3,RHOSTAR,A
COMMON /NOW/ TIMENOW,BIGRREF
COMMON /ZZ/ ZXO,ZYO
C
TAUOLOOP=0.24016
BGROLOOP=0.32094
BIGRPRM=BGROLOOP*(A*TIME(1))**(2.0/3.0)
CC=A**(4.0/3.0)*TIMENOW**(1.0/3.0)/BIGRPRM

```

```
ALFR=ALPROT(TIMENOW)
TAUA=TAUOLOOP+ALFR*(0.60702015)/(2.0*PI)
```

C

```
ALF=ALPROT(TIMENOW)
```

C

```
VXTILD=-0.00029091*CC*TAUA**(-2.30525)
VYTILD=-0.00424515*CC*TAUA**(-1.45439)
VXP=VXTILD*COS(ALFR)-VYTILD*SIN(ALFR)
VYP=VXTILD*SIN(ALFR)+VYTILD*COS(ALFR)
```

C

```
RETURN
END
```

```
SUBROUTINE VELOUT (UO, VO)
COMMON /VELO/ R, X, Y, DX, DY, W, G
REAL M1, LAM, KO, K1, K2, KLO, KL1, KL2, K, KP
UO = 0.0
VO = 0.0
PI = 3.141592654
R1 = SQRT(X**2+Y**2)
R2 = SQRT((X+2.*R)**2+Y**2)
LAM = (R2-R1)/(R1+R2)
M1 = 1. - LAM**2
IF (R1.EQ.0) GO TO 730
IF (LAM.EQ.0) GO TO 730
DXR1 = X/R1
DYS1 = Y/R1
DXR2 = (X+2.*R)/R2
DYS2 = Y/R2
DXL = (DXR2-DXR1)/(R2+R1) - LAM/(R2+R1)*(DXR1+DXR2)
DYL = (DYS2-DYS1)/(R2+R1) - LAM/(R2+R1)*(DYS1+DYS2)
KO = 1.3862944
K1 = .1119723 * M1
E1 = .4630151 * M1
K2 = .0725296 * M1**2
E2 = .1077812 * M1**2
KLO = .5
KL1 = .1213478 * M1
EL1 = .2452727 * M1
KL2 = .0288729 * M1**2
EL2 = .0412496 * M1**2
K = KO + K1 + K2 - (KLO + KL1 + KL2)*LOG(M1)
E = 1. + E1 + E2 - (EL1 + EL2)*LOG(M1)
KP = E / LAM / M1 - K / LAM
EP = (E - K) / LAM
DXR = DXR1 + DXR2
DYS = DYS1 + DYS2
RR = R1 + R2
```

```

      UO = G*W/PI/(R+X) * (DYR*(K-E)+RR*(KP-EP)*DYL)
      VO = -G*W/PI/(R+X) * (DXR*(K-E)+RR*(KP-EP)*DXL)
730  RETURN
      END
      SUBROUTINE VELIN (UIN, VIN)
C
      COMMON /VELO/ R, X, Y, DX, DY, W, G
      PI = 3.141592654
C
      COST = DX / SQRT(DX**2+DY**2)
      SINT = DY / SQRT(DX**2+DY**2)
      Q5 = (X**2 + Y**2)/W**2
      Q4 = (Y*COST - X*SINT)/W
      Q3 = (X*COST + Y*SINT)/W
      Q2 = Q5 - 2.*Q3 + 1.
      Q1 = Q5 + 2.*Q3 + 1.
      IF (Q4.EQ.0) THEN
          ATN = 0.0
          GO TO 740
      END IF
      ATN = ATAN((1.-Q3)/Q4)+ATAN((1.+Q3)/Q4)
740  CONTINUE
      U1 = -SINT*LOG(Q2/Q1)+2.*COST*ATN
      V1 = -COST*LOG(Q2/Q1)-2.*SINT*ATN
      U2 = (X/2./R) * U1
      V2 = (X/2./R) * V1
      *      + .5*W/R      *( LOG(Q2*Q1)
      *                          -Q3*LOG(Q2/Q1)
      *                          +2.*Q4*ATN
      *                          -4.)
C
      UIN = -G / 4. / PI * (U1 + U2)
      VIN = G / 4. / PI * (V1 + V2)
C
750  RETURN
      END
      SUBROUTINE VELIO (UIO, VIO)
      COMMON /VELO/ R, X, Y, DX, DY, W, G
      PI = 2* ASIN(1.)
      COST = DX / SQRT(DX**2+DY**2)
      SINT = DY / SQRT(DX**2+DY**2)
      Q5 = (R**2 + Y**2)/W**2
      Q4 = (Y*COST + R*SINT)/W
      Q3 = (-R*COST + Y*SINT)/W
      Q2 = Q5 - 2*Q3 + 1.
      Q1 = Q5 + 2*Q3 + 1.
      UIO = 0.0

```

```

VIO = 0.0
C
R1 = SQRT(X**2+Y**2)
IF (R1.EQ.0.0) GO TO 720
UIO = -G*W/PI * ( 1. + X/R/2.) * Y/R1/R1
VIO = G*W/PI * (( 1. + X/R/2.) * X/R1/R1 + .5/R*LOG(R1/8/R))
720 VIO = G*W/PI * LOG( 8*R/W ) /2 /R
* + VIO
RETURN
C
END
SUBROUTINE VEL2D (UIN, VIN)
C
COMMON /VELO/ R, X, Y, DX, DY, W, G
PI = 2*ASIN(1.)
COST = DX / SQRT(DX**2+DY**2)
SINT = DY / SQRT(DX**2+DY**2)
Q5 = (X**2 + Y**2)/W**2
Q4 = (Y*COST - X*SINT)/W
Q3 = (X*COST + Y*SINT)/W
Q2 = Q5 - 2*Q3 + 1.
Q1 = Q5 + 2*Q3 + 1.
IF (Q4.EQ.0) THEN
    ATN = 0.0
    GO TO 740
END IF
740 ATN = ATAN((1.-Q3)/Q4)+ATAN((1.+Q3)/Q4)
CONTINUE
IF ((Q1.EQ.0).OR.(Q2.EQ.0)) THEN
    UIN = 0
    VIN = 0
    GO TO 750
END IF
750 U1 = -SINT*LOG(Q2/Q1)+2.*COST*ATN
V1 = -COST*LOG(Q2/Q1)-2.*SINT*ATN
UIN = -G / 4. / PI * U1
VIN = G / 4. / PI * V1
RETURN
END
SUBROUTINE VEL2DF (UIN, VIN)
C
COMMON /VELO/ R, X, Y, DX, DY, W, GG
G=GG*2.0*W
PI = 3.141592654
Q5 = SQRT(X**2 + Y**2)
IF (Q5.EQ.0) GO TO 750
COST = X / Q5

```

```
SINT = Y / Q5
U1 = SINT/Q5
V1 = COST/Q5
UIN = -G/2./PI * U1
VIN = G/2./PI * V1
750 RETURN
END
```